Cardiff University

Hydro-Environmental Modelling of the Arabian Gulf and Kuwait Bay

By

Yousef Al-Osairi

B-Eng Msc

Hydro-Environmental Research Centre

Cardiff School of Engineering

Cardiff University

February 2011

ProQuest LLC
789 East Eisenhower Parkway
P.O. Box 1346
Ann Arbor, MI 48106-1346

Abstract

Studying and understanding the hydro-environmental characteristics of the Arabian Gulf has received growing interest over the past few decades. This is mainly attributed to the strategic importance of the area, since it has been utilised to transport most of the oil production from the Gulf states. Over the last five decades, rapid industrial coastal development also has taken place around the Gulf. Development has brought desalination, power and petroleum refining plants. Coastal developments and industrial and domestic sewage discharges have contributed to the total nutrient levels in the Gulf, which have enhanced unwanted algal growth in various coastal areas. More recently, climate change has brought flooding to the Gulf states and frequent dust storms, which have increased various environmental issues, such as sediment transport and nutrient sorption processes, also in the shallow regions of the Gulf.

In the current study the geographic dispersion of numerical tracers and flushing characteristics, in terms of residence time, of the Gulf have been investigated. The study has revealed that dispersion of numerical tracers is chiefly controlled by tides in the Gulf, while winds had limited effects. The residence time in the Gulf was predicted to be almost 3 years using ELCOM. Kuwait Bay was also investigated in terms of the governing hydrodynamics using ELCOM. Similar to the Gulf, the study revealed that the Bay was chiefly driven by tides and to a lesser extent by winds. Detailed studies of temperature, using the same model, showed that temperatures varied seasonally in the Bay. In terms of salinity, investigations have shown that the Shatt Al Arab has an apparent effect on the Bay's salinity, particularly in the northern areas. The maximum residence time of the Bay was calculated to be 57 days near al Jahra using ELCOM.

The main model refinements were conducted on including the phosphorus source terms in TRIVAST, based on experimental investigations in a hydraulics flume channel. The refinements included the addition of new source terms accounting for the adsorption of phosphorus to suspended sediments and bed sediments. Model investigations have shown that the model refinements improved the model predictions of phosphorus levels, with

phosphorus being the limiting nutrient during high suspended sediment events in Kuwait Bay.

In general, good water quality predictions in Kuwait Bay were achieved using both ELCOM-CAEDYM and TRIVAST. Predictions have shown that the Shatt Al-Arab waterway has significant effects of the water quality of the Bay. Better hydrodynamic predictions were achieved using ELCOM than TRIVAST for the Gulf and the Bay. This was due to the additional mathematical terms included in ELCOM, including, in particular, the terms representing tidal forces that were calculated from the gravitational potential.

Acknowledgements

First of all I would like to thank Prof. Roger Falconer for all of his constant help, support, motivation and guidance throughout every academic stage at Cardiff University since undergraduate, masters and until the completion of this PhD research. I am also very appreciative of the massive help and support I have received from Prof Jorg Imberger, in particular for funding two precious visits to the Centre for Water Research in University of Western Australia, that have resulted in producing valuable publications. Also, I would like to thank Prof. Binliang Lin for the invaluable guidance encouragement and friendship.

I am truly grateful to, the Kuwait Ministry of Higher Education, Cardiff University and Halcrow Group, for the financial support that made it possible for me to maintain this research. I am grateful to Kuwait Institute for Scientific Research for providing important data for this study, in particular Dr. Faiza Al-Yammani. Also, I would like to say a word of gratitude to Dubai Meteorological Services and Kuwait Environmental Public Authority for supplying necessary data for this study.

My friends and fellow students who provided support and encouragement during all times; Dr. Reza Ahmadian, Dr. Rami Malki, Dr. Patricia Xavier, Dr. Shahid Akhtar, Dr. Phillip Vardon, Eqbal Al-Enezi, Teddy Tedjakusuma, Florian Schaefer, Xiaolin Wang, Olliver Wood. I am also very grateful to the staff at the research office of Cardiff School of Engineering, in particular Mrs Chris Lee for their continuous assistance. I would also like to thank everyone else who supported me throughout my study whom are too numerous to name.

Last but not least, I would like to express my deepest and sincere appreciation to my Mom (Sabah), and my Dad (Yacoub), and my brothers; Bashar, Bader, Ahmad, Abdul-Rahman, Ali, Omar and Abdul-Aziz and my sister Farah. They deserve considerable recognition and without their continuing support, patience, encouragement and true love this work would not be here today.

Table of Content

Chapter 1: Introduction and Overview

Chapter 2: Physical Characteristics and Environmental impacts of the Arabian Gulf and Kuwait Bay

Chapter 6: Hydrodynamic Modelling of Kuwait Bay

Chapter 7: Water Quality Modelling of Kuwait Bay

Chapter 8: General Numerical Model Comparisons for ELCOM-CAEDYM and TRIVAST

Chapter 9: Conclusions and Recommendations

List of Figures

List of Tables

List of Abbreviations

ADI	Alternative Direction Implicit
CAEDYM	Computational Aquatic Ecosystem DYnamics Model
CFL	Courant Friedrichs Lewy
DMS	Dubai Meteorological Services
DNS	Direct Numerical Simulation
ELCOM	Estuary, Lake and Coastal Ocean Model
EPC	Equilibrium Phosphorus Concentration
IOC	Intergovernmental Oceanographic Commission
KISR	Kuwait Institute for Scientific Research
K-EPA	Kuwait Environmental Public Authority
MATLAB	MATrix LABoratory
MBPD	Million Barrels of oil Per Day
MSF	Multi-Stage Flash distillation
NOAA	National Oceanic and Atmospheric Administration
OPEC	Organisation of Petroleum Exporting Countries
RANS	Reynolds Averaged Navier-Stokes equations
RMA	Resource Modelling Associates
RO	Reverse Osmosis
ROPME	Regional Organization for the Protection of the Marine Environment
TRIVAST	ThRee-dimensional layer Integrated Velocity And Solute Transport
TVD	Total Variation Diminishing
UAE	United Arab Emirates
ULTIMATE	Universal Limiter for Transient Interpolation Modelling of the Advective Transport Equation
QUICKEST	Quadratic Upstream Interpolation for Convective Kinematics with Estimated Streaming Terms

List of Publications

- Alosairi Y., Imberger J. and Falconer R. A.(2011), *Mixing and flushing in the Arabian/Persian Gulf*, Journal Geophysical Research,doi:10.1029/2010JC006769, (in press).

- Alosairi Y. , Al-Enezi E , Falconer R. A. and Imberger J. (2011), *Modelling Phosphorus Sorption Processes in Kuwait Bay: Effects of Sediment Grain Size,*34th IAHR World Congress, Brisbane, (in review).

- Alosairi Y., Falconer R. A., Imberger J. (2010), *Three-dimensional hydro-environmental modeling of the Arabian (or Persian) Gulf*, in Tao et al, Proceedings of the 9th international conference on hydroinformatics 2010, 1, 132-138.

- Al-Enezi E., Alosairi Y., Bockelmann-Evans B. N. and Falconer, R. A. (2010), Modelling of phosphorus adsorption in estuarine sediment, in Christodoulou G. C. et al. (Eds.), Proceedings of the 6th Internationa Symposium on Environmental Hydraulics, Athens, 2, 759-764.

- Alosairi Y., Al-Enezi E. and Falconer R. A. (2008), *Hydro-environmental Modelling of Kuwait Bay and the Arabian Gulf*, The Second Gulf Conference and Exhibition On Environment and Sustainability, Kuwait.

Chapter 1

Introduction and Overview

1. 1 Introduction:

Coastal waters have always been important for society because of their effective role in transportation and water supply, while also historically used as a means of disposal for treated or untreated effluent waste. During recent decades many scientists and engineers have been heavily involved in hydro-environmental research projects as a result of the increasing general awareness of public health and the growing public concern about the environmental and ecological pollution of coastal basins. In particular, over the past decade there has been a growing interest in the hydro-ecology of many estuaries worldwide, including concerns about the effects of climate change. These concerns have been primarily associated with the increasing greenhouse gases such as carbon dioxide, where there is strong evidence of them causing major disruption to aquatic life and water quality in many water bodies around the world [*Perry et al.*, 2005].

Studying and understanding the hydro-environmental conditions of the Arabian Gulf, hereafter called 'the Gulf', has received growing interest over the last few decades. This is mainly attributed to the strategic importance of the area, since it has been utilised to transport most of the oil production by the Gulf countries around the world. Over the last five decades, rapid industrial coastal development has also taken place around the Gulf. Development has brought desalination, power and petroleum refining plants [*Khan*, 2006]. Recently, the construction of desalination plants has escalated in the Gulf, due to increased public needs. In many-if not most-parts of the Gulf it is considered to be the sole source of fresh water, for human domestic, agricultural and industrial use. In addition to increasing solar radiation effects rising from climate change, the thermal pollution plume from industrial development has led

to rises in seawater temperatures as well, which has affected the marine ecosystems of the Gulf in many ways [*Al-Muzaini et al.,* 1997]. Oil spills are among the main pollutants to affect the marine environment in the Gulf [*Al-Muzaini et al.,* 1997]. Oil absorbs heat and, hence, has the capacity to increase seawater temperature [*Habib and Fakhral-Deen,* 2001]. This would normally lead to an increase in oxygen consumption via biodiversity respiration and the mineralisation processes of organic matter and therefore lead to what is frequently called 'Eutrophication' and algal blooms. In addition, coastal developments and industrial and domestic sewage discharges have also contributed to the total nutrient levels in the Gulf that have enhanced unwanted algal growth in various regions of the estuary, particularly in the northern shallow areas near Kuwait Bay. Unusually, climate change has also brought flooding to the Gulf countries and frequent dust storms, which have increased various environmental issues, such as sediment transport and nutrient sorption processes, as well as in the shallow regions of the Gulf. Politically, several military operations have taken place in the Gulf that have consequently affected the aquatic and marine environments, including three wars over the last 30 years.

Physical model studies have usually been the key means historically used for predicting flow fields and contaminant transport in hydro-environmental engineering and research projects for much of the past 80 years. With the rapid advances in computer technology over the past 40 years, computer models, based on numerical techniques, are now used widely for many hydro-environmental studies. With the rapid increase in the speed and memory capabilities of modern computers on the one hand, and with the fast developing numerical methods on the other hand, the scope of computer model applications has widened considerably. Numerical hydro-

environmental models have been proven to be efficient tools in predicting the flow fields in 1-D, 2-D and 3-D water basins and the corresponding water quality constituents and sediment transport levels are readily added to the hydro-dynamic predictions, particularly for estuarine and coastal water bodies.

1. 2 Objective of the study:

This research project aims to develop an effective understanding of the hydrodynamics, including dispersion mechanisms, and water quality processes in the Gulf and Kuwait Bay by utilising three dimensional numerical models. Special attention has been given to nutrient modelling, in particular phosphorus in the Bay, where further model refinements were made to include phosphorus sorption processes. In addition, this study focuses on the various numerical aspects of the models used and outlines the effectiveness of them. The main objectives and achievements of this research can be summarised as follows:

1) **Identify the geographic dispersion mechanism and the residence time of the Gulf:**

A three-dimensional model was used to investigate the dispersion processes in the Gulf. Data from 1992 was used to validate the model, and then numerical tracers were injected randomly over the basin. Spatial and temporal investigations were undertaken of the cloud of tracers by means of sensitivity analysis. This enabled the effectiveness of various physical forces in dispersing the tracers horizontally in the estuary to be quantified. The dispersion coefficients of the tracers were calculated at each point of injection. Also, the residence time was obtained for the

whole Gulf. This all led to a general understanding of the main hydrodynamic processes in the estuary.

2) Investigating the hydrodynamic processes of Kuwait Bay and identifying the residence time:

Hydrodynamics are the main drivers of effluents in the water body; therefore it is essential to understand such processes before conducting water quality investigations. The hydrodynamic processes of Kuwait Bay were investigated using a three dimensional model. The model was validated using the measured data of water levels, velocity speed and direction from 2005. The validated model was used to investigate the seasonal variations of temperature and salinity. In addition, other effects on temperature and salinity rising from the various boundaries were analysed. Numerical tracers were injected into the flow at the open boundary and the resultant cloud was analysed. This all contributed to the general understanding of the hydrodynamic processes in the Bay

3) Water quality modelling of Kuwait Bay:

Kuwait Bay is considered to be one of the most polluted water bodies in the Gulf and is subject to various algal blooms and red tide events. Previously, numerical modelling studies had only considered the hydrodynamics of the Bay but little was achieved in the modelling of water quality. In this study a three-dimensional model of the Bay was set and validated using data from 2005. The main water quality parameters considered in this study were dissolved oxygen, nitrate, ammonia and phosphorus. The model was utilised to investigate the seasonal

variations of each water quality parameter. This gave a very good understanding as to the water quality structure of the Bay.

4) Model refinements to include sediment effect on phosphorus sorption processes in Kuwait bay:

As a result of climate change, a number of major dust storms and flash flood events have occurred recently and these have become more frequent events. These extreme events have supplied the Gulfs water with fine polluted sediment particles, especially in the shallower regions. It is therefore important to estimate the impact of such processes in this region particularly with regards to the nutrient levels adsorbed onto the sediments and the corresponding inputs into the water column. Hence, in this study fundamental model refinements were conducted to include the sediment sorption processes of phosphorus. These refinements were achieved through extensive experimental work conducted on various sediments types in a flume channel, located in a hydraulics laboratory. Such effects were investigated for Kuwait Bay and were found to have a marked influence on the reduction of phosphorus levels.

5) Modelling phosphorus in Kuwait Bay:

In previous water quality studies in the Bay, it was been realised that phosphorus is in general the limiting factor of algal growth. Therefore, special attention was given to this parameter in the current study. Further investigations were conducted on various physical and chemical parameters, including the effects of sediment sorption processes, so as to identify the main contributors to the phosphorus level in the Bay.

6) **Compare hydrodynamic and water quality results of the three dimensional models and assess the numerical results and differences:**

Numerical models are widely used nowadays; however they can vary depending on the numerical background and the governing equations that are inherently included in; and solved, within the models. In terms of water quality, empirical equations representing source and sink terms in the numerical models may vary considerably from a simple diffusion equation to very sophisticated processes, such as chemical reactions. In this part of the research two three dimensional models, of different numerical background, were investigated in terms of both hydrodynamics and water quality in the Gulf and the Bay. This would give an understanding as to which physical or chemical processes are crucial when modelling this region and therefore determine the most suitable model that meets the purposes of the modelling.

1. 3 Outline of the thesis:

The details of this thesis are summarised as follows: Chapter 1 introduces the background to the environmental problems in the Gulf and the Bay, the numerical models and the objectives of this study. Chapter 2 reviews the environmental impacts of the Gulf and the Bay. Chapter 3 outlines the hydrodynamic and the solute transport governing equations, and discusses a number of terms within these equations. Chapter 4 presents the numerical models and methods utilised in this research, including the model developments associated with the inclusion of the phosphorus sorption processes, which were achieved by conducting experiments in a flume channel facility. In Chapter 5 the horizontal dispersion of numerical tracers is investigated in

the Gulf and the dispersion coefficients are determined. Chapter 6 considers the hydrodynamic modelling of Kuwait Bay and the circulation of the water column, discussed with the aid a sensitivity analysis on the various physical boundaries. In Chapter 7 water quality modelling of Kuwait Bay is analysed and the effects of the model boundary conditions are discussed with a special focus on phosphorus predictions. Chapter 8 brings together the numerical prediction differences of the models used in these studies and the effects of the various numerical aspects of each model. Finally, Chapter 9 draws conclusions from the developments and makes recommendations for further study and research.

Chapter 2

Physical Characteristics and Environmental Impacts of the Arabian Gulf and Kuwait Bay

2. 1 Introduction:

The Gulf is a shallow semi-enclosed water body. It is detached from the Gulf of Oman by the Strait of Hormuz, shown in Figure 2.1, which is only 56 km wide at its narrowest point. The channel near the Strait of Hormuz deepens to more than 100 m through the Strait and drops rapidly to more than 2,000 m within 200 km outside of the Strait. The maximum width of the Gulf is 338 km, and the length to its northern coast is nominally 1,000 km. The surface area of the Gulf is approximately 2.39 × 105 km^2, and with a mean depth of 36 m this implies an average volume of approximately 8.63 × 103 km^3. Unlike many estuaries, flooding and drying areas in the Gulf are limited.

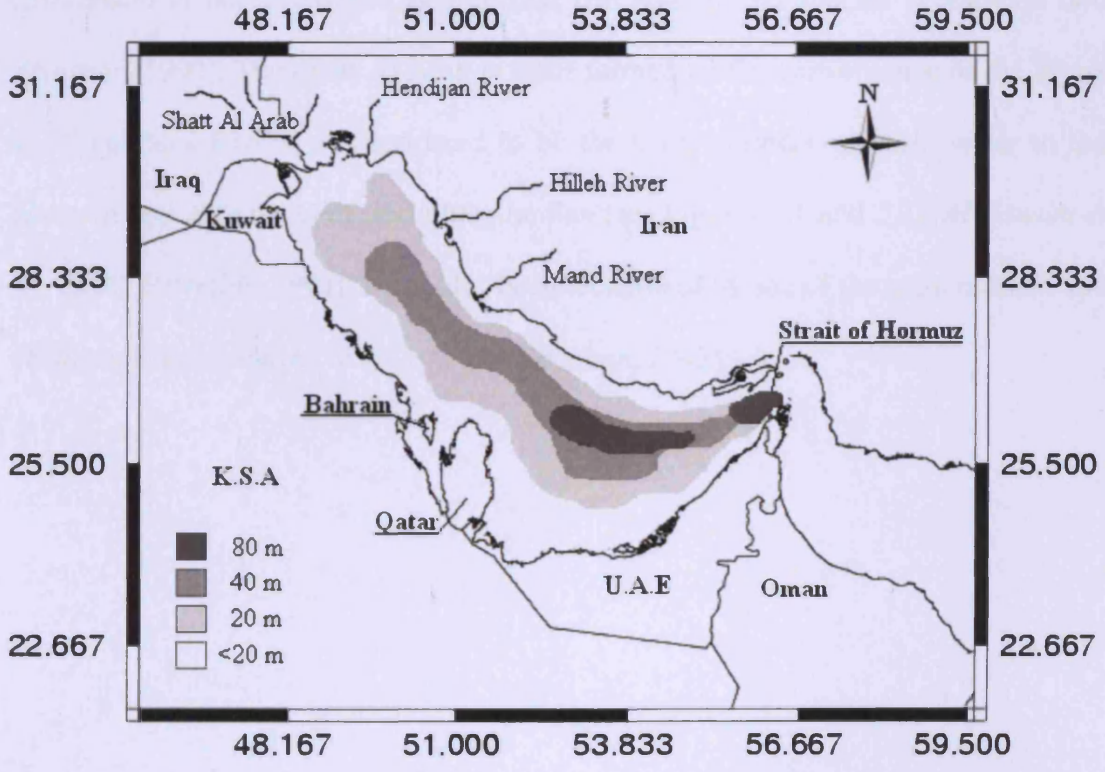

Figure 2.1: The Gulf, Strait of Hormuz and fresh water inflow sites [*National Geophysical Data Centre: http://www.ngdc.noaa.gov*]

The Gulf is located within the arid region of the Middle East, between latitudes 24° and 30°N and longitudes 48° and 56°E [*Al-Ghadban et al.*, 1998; *Elshorbagy*, 2005; *Robinson and Brink*, 2006]. The Gulf is bordered by a total of eight countries, including Iran and seven Arab countries, namely: Kuwait, Iraq, Saudi Arabia, Bahrain, Qatar, the United Arab Emirates and Oman (Figure 2.1).

Kuwait Bay, hereafter called 'the Bay', is an elliptically shaped embayment that extends in a westward direction from the extreme north of the Gulf (Figure 2.2). The Bay is characterised by relatively shallow water throughout. It covers an area of about 720 km^2 and has a boundary length of 20 km to the estuary. The extensive, intertidal mudflats in the Bay provide feeding grounds for a number of species of wading birds [*Al-Yamani et al.*, 2004] and also several fish and shrimp species [*Abouseida and Alsarawi*, 1990]. The Shatt Al Arab (a river formed by the convergence of the Tigris and Euphrates Rivers) is considered to be the main provider of fresh water to the northern region of the Gulf, including the Bay (see Figures 2.1 and 2.2) [*Al-Yamani et al.*, 2007; *Reynolds*, 1993]. It has also been recognised as one of the main nutrient and sediment supply sources to the Bay [*Al-Ghadban*, 2002].

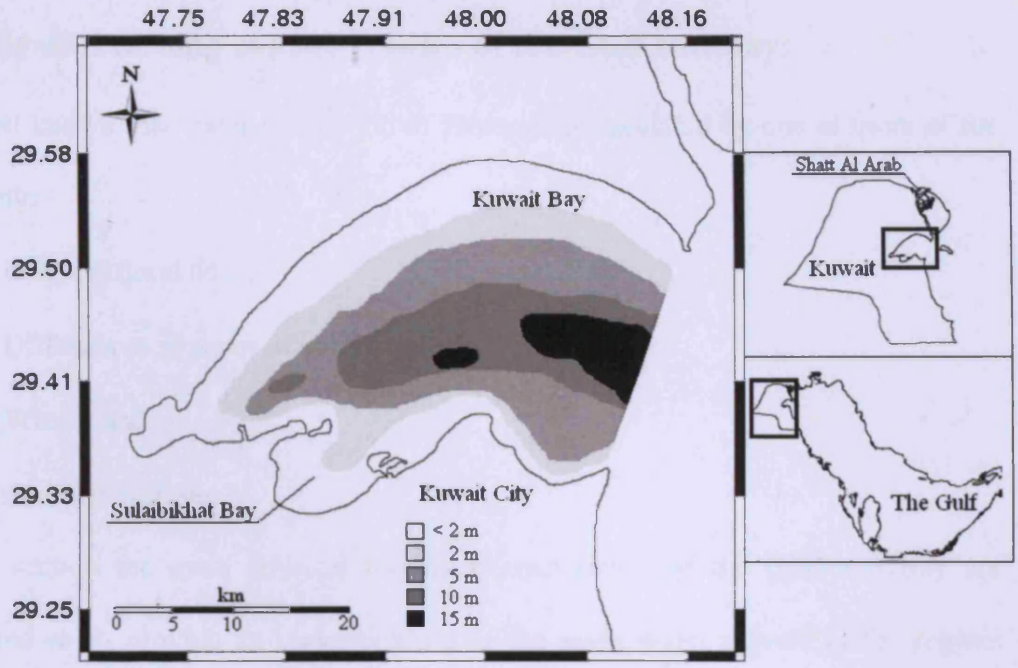

Figure 2.2: Kuwait Bay and Sulaibikhat Bay

It is worth mentioning that the geomorphological characteristics of the Gulf and its coastline formation were created by Plio-Pleistocone tectonic movements [*Robinson and Brink,* 2006]. Later tectonic activities were responsible for only minor adjustments to its present shape [*Al-Asfour,* 1981]. The Gulf is a sedimentary basin due to its enclosed topographic conditions and favours production of biogenic sediments, mainly by foraminifera and other micro-organisms [*Al-Ghadban*, 2002].

The primary aim of this chapter is to present the general physical force characteristics that mainly influence the water dynamics of the Gulf. Also, to address the main impacts on the marine environment resulting from anthropogenic activities and climate change.

2. 2 Physical forcing characteristics of the Gulf and Bay:

It is well known that water circulation in estuaries is regulated by one or more of the following:

- Ebb and flood tides;
- Differences in water densities;
- Winds; and
- Riverine inflows.

In this section the main physical forcing characteristics of the Gulf and Bay are illustrated as to provide an understanding of the main water drivers in the region. Such factors are essential to understand the dispersion and mixing processes in the region, as detailed in Chapter 5.

2. 2. 1 Tides:

The tides in the Gulf are complex standing waves and the dominant pattern varies from being mainly semidiurnal to diurnal. The tidal range is relatively large compared to the Gulf, with values greater than 1 m everywhere [*Lehr*, 1984], but small compared to U.K. coastal waters that has a range of typically 14 m in the Severn Estuary for example. *Rakha et al.*, [2007b] have estimated the tidal range to vary from 1 m (during neap tides) to approximately 4 m (during spring tides) in the north of the Gulf. The dimensions of the Gulf are such that resonance amplification of the tides can occur, resulting in semi-diurnal constituents that have two amphidromic points, in the northwest and southeast ends, and the diurnal constituents have a single amphidromic point in the centre, close to Bahrain [*Reynolds,* 1993]. Tides have often been considered to play a key role in stirring and mixing waters vertically and horizontally in the Gulf, at a scale of 10 km, but they do not make an important

contribution to the residual circulation of the Gulf [*Reynolds*, 1993]. The average velocity of both, surface and bottom, residual current in the Gulf is roughly 6 cm/s [*Abdelrahman and Ahmad*, 1995].

Due to the geological restrictions of the Gulf, tides normally experience an oscillation effect that intensifies tidal effects at the northern end of the estuary. Therefore, higher tidal range are generally observed in the Bay. Tides in the Bay are semidiurnal with two high tides and two low tides occurring within a lunar day. The mean tidal amplitude in the Bay is approximately 2 m, but tides may vary from 3.5 to about 4 m, depending largely on the lunar phase [*Al-Yamani et al.*, 2004]. The greatest tidal range occurred in the Bay during 2003 when it reached 4.45 m [*Al-Yamani et al.*, 2004].

2. 2. 2 Fresh water exchange:

Fresh water exchange in the Gulf is generally considered to be minor, due to high evaporation, low fresh water input and low precipitation. Evaporation in the Gulf is much higher than both river inflow and precipitation and so the net loss of water normally creates higher salinity in the estuary waters than at the coastal waters [*Reynolds*, 1993]. Thus giving rise to what is frequently called 'Reverse Estuary', in that the net circulation is in at the surface water (at the Strait) and out along the bottom similar to the Mediterranean water circulation [*El-Sabh et al.*, 1997].

Evaporation in the Gulf has been estimated through a number of studies. *Privett*, [1959] estimated the evaporation rate to be 144 cm/yr, and predominantly occurring during the winter. Such findings were related to the strong dominant north-westerly winds during this season. Meteorological data from Qatar and Bahrain for 1984 were

utilised by *Meshal and Hassan,* [1986], to approximate evaporation, who found it to be 202 cm/yr. However, *Ahmad and Sultan,* [1991] estimated the evaporation in the Gulf to be 228 cm/yr, while *Sultan and Ahmad,* [1994] obtained a value of 208 cm/yr for Kuwait's coastal waters. Most river inflow into the Gulf occurs at the northern end of the Gulf near Kuwait at Shatt Al Arab (see Figure 2.1 and 2.2).

The Shatt Al Arab is a nexus of three major rivers. The Tigris and Euphrates Rivers together provide an annual average inflow of 708 m^3/s, with the Karun adding a further inflow of 748 m^3/s. Thus, the total average outflow from Shatt Al Arab is roughly 1456 m^3/s [*Reynolds,* 1993]. Other main rivers are the Hendijan 203 m^3/s, the Hilleh 444 m^3/s, and the Mand 1387 m^3/s (see Figure 2.1). The total river runoff is 13 × 102 km^3/yr, corresponding to 46 cm/yr in depth. This approximation, from Iranian river measurement reports, is noticeably greater than formerly published estimates and ideally requires further verification, since *Al-Hajri,* [1990] estimated a value of 16 cm/yr. Industrial and agricultural developments, including dam construction, are having an obvious effect on the outflow from the Shatt A1-Arab, where annual runoff has reduced considerably over the past 20 years [*Jones et al.,* 2008a; *Al-Taiee,* 1990; *Altinbilek,* 2004]. Annual rainfall in the arid climate of the Gulf region is small, of the order of 7 cm/yr [*Reynolds,* 1993]. This leads to the fact that rainfall makes an almost negligible contribution to the fresh water budget of the Gulf.

2. 2. 3 Wind:

As mentioned earlier, the Gulf is situated between latitudes of 24 and 30 °N and between which most of the Earth's deserts are located. This region marks the boundary between tropical circulations and the synoptic weather systems of the mid-

latitudes. Descending dry air in these latitudes produces clear skies and arid conditions. Orographic effects are more evident in the north of the Gulf. The Taurus and Pontic mountains of Turkey, the Caucasus Mountains of Iran, and the Hejaz mountains of the Arabian Peninsula, together with the Tigris-Euphrates Valley, form a northwest-southeast axis that strongly influences the paths of extra tropical storms in a south-easterly direction [*Reynolds,* 1993]. The climate in the Gulf of Oman is markedly different to the climate in the Gulf. While the Gulf is essentially affected by the extra-tropical weather systems from the northwest, the Gulf of Oman is at the northern edge of the tropical weather schemes of the Arabian Sea and Indian Ocean [*Reynolds,* 1993]. This monsoon circulation generates southerly winds in the summer and strong northerlies in the winter. The Strait of Hormuz therefore approximates a boundary between the two systems.

The generally well-known weather phenomenon in the Gulf is the year round north-westerly wind [*Perrone*, 1981]. The winter north-westerly wind is a wind that sets in with massive shortness and force, and is associated with synoptic weather systems to the north-west, particularly affecting Kuwait. It infrequently exceeds 10 m/s, but lasts for a number of days. The summer north-westerly wind is almost continuous from early June through to the end of July. It is coupled with the relative forces of the Indian and Arabian thermal lows [*Sheppard*, 2000]. The winter wind carries some of the strongest winds and highest seas of the season into the Gulf area. Winds in the area ahead of an approaching cold front blow from the south-east. Due to the channelling of the low level air flow by the Zagros Mountains of western Iran, the strongest of the southerly winds occur in the eastern regions of the Gulf [*Reynolds,* 1993]. The north western wind normally develops first in the northwest and then

expands south. A strong sea breeze occurs along the whole coastline, principally along the Arabian Peninsula. Driven by the extreme temperature difference between the land and water surface, the sea breeze circulation adds a landward component to all winds [*Reynolds,* 1993]. The effect of these winds is to drive surface waters, including solutes and pollutants, towards the coastline much faster than they would move otherwise. According to KISR (Kuwait Institute of Scientific Research) data values of on-shore and, to a lesser extent, off-shore winds may reach 15 m/s during the winter; such observations have been recorded at coastal meteorological stations.

2. 3 Environmental impacts for the Gulf and Bay:

In recent decades, and especially during the last few years, coastal development in the Gulf countries have accelerated tremendously due to the major increase in oil related income and economic diversification schemes. The rapid expansion of industrial complexes, an exceptional rise in private real estate investment, tourism and service industries, including high birth rates and the entry of foreign labour, accompanied by prospering economies, have all resulted in a massive human population growth in the Gulfs coastal waters. This development has done much to further the well being of society in the region, however, it has also led to severe impacts on the terrestrial, coastal and marine environments. Such events have changed the environment and not always for the better [*Glibert* 2007, *Khordagui* 2002]. Large areas of the coastal zone, including important marine habitats, are presently threatened by increasing stress on the Gulf ecosystem, with pollution playing a major role in adversely affecting the marine ecology. Such effects have raised concern in the Gulf countries about the marine ecology, since the costal zone serves as a resource for fishing, recreation,

urban development, oil transportation and perhaps, most importantly, a major source of fresh water via desalination plants.

Global warming and related climate change issues are some of the most serious challenges facing the world. Unsurprisingly, the Gulf has first hand experience of these issues, where air temperatures of up to 54 °C have been recorded, leading to a very arid environment and high sea water temperatures during the summer months [*Al-Rashid and Al-Mikaimi* [2010]. Furthermore, other climatic issues related to climate change, such as frequent dust storms and flash floods have been recognised; this will be explained in section 2.3.2.1 and 2.3.2.2, respectively.

2. 3. 1 Human activity:

The Arabian countries of the Gulf have undergone an extraordinary process of development and social transformation. This has led to rising rates of transport and industrial development and increased consumption of food, water and goods that, in turn, have led to radically heightened rates of environmental pollution. Regional political conflicts have also taken their toll and contributed to air, land and water pollution. For example, the 1991 Gulf war oil spill, one of the biggest known marine pollution events in human history, occurred in the waters of the Gulf. Also, oil burnt during this war resulted in thick clouds of mainly carbon dioxide hanging over the region for several months. Furthermore, the Gulf is the busiest area in the world with regard to oil transportation, resulting in a number of daily oil spills along the estuary. Moreover, the Gulf waters have been and are increasingly utilised for desalination processes as well as for fishing and the tourism industry [*Bleninger and Jirka* 2010]. Waterfront developments, desalination plants and petrochemical activities and their

associated environmental impact in the Gulf will be reviewed next, in Sections 2.3.1.1, 2.3.1.2. and 2.3.1.3, respectively.

2. 3. 1. 1 Waterfront development:

The use of leisure and tourism to redesign and stimulate city growth has been interpreted as a mechanism for attracting capital and people to the capital. Waterfront developments across the Middle Eastern coast have become popular projects, creating entirely new urban communities. Although any development at the waters edge would, in theory, be recognised as 'waterfront', this Middle Eastern centred trend is particularly concerned with newly created and redesigned urban coastlines involving extensive 'land reclamation' as well as 'canalling' water channels inland, thereby creating new waterfronts, such as those found in Al-Khairan Pearl City in Kuwait, as shown in Table 2.1.

Urban developments, involving both land reclamation and canalling, have been carried out throughout modern metropolitan history, most noticeably in Washington DC, Singapore, Hong Kong, Macau, Monaco and Gibraltar. Even anthropogenic islands have been created from the sea, such as Kansai Airport in Osaka and Chek Lap Kok International Airport in Hong Kong. However, world attention is being attracted to the Middle East, and particularly Dubai, by the sheer scale of these projects, which are of the order of several million m^2 see Table 2.1, and with the number of such projects introducing a range of various environmental issues.

Project	General information	Picture
Al Khiran Pearl City (Kuwait)	• 25 years to complete • Serves facilities for 100,000 people. • Project area covers 6.4 million m^2	
The Pearl (Qatar)	• Consists of 13 islands • 8 private islands • Over 2 million m^2 of international retail, restaurants, cafes. • Three 5 star hotels • 4 million m^2	
Durrat Al Bahrain Islands (Bahrain)	• 13 large artificial islands • Several 5 star hotels, 18-hole golf course, 12 bridges, marina, flats etc. • 60 % completed. • Project area is roughly 20 million m^2	
The World (U.A.E)	• 5 star hotels, shopping malls, private flats etc. • 4 km off shore • 321 million m^3 of sand and 31 million tonnes of rock used for construction of islands • Project area is 21 million m^2	

Table 2.1: Waterfront development in the Gulf waters

There have been only a few studies undertaken to quantify the impact of waterfront developments in the Middle East and hardly any have been published. This is probably due to political reasons. Also, most projects are under construction and not ready to be environmentally evaluated. However, historically such projects show various environmental impacts on marine life, mainly as a result of poor mixing and

flushing characteristics. From an engineering point of view, Al Khairan Pearl City in Kuwait (see Table 2.1) shows a good example of possible marine impact arising from poor water flushing. While such projects involve an extensive number of artificial embayment and channels, poor water mixing and flushing can give rise to significant depletion of dissolved oxygen levels and, in turn, lead to unwanted algal growth locally [*Newton et al.,* 2003], and possible eutrophication events (see section 2.3.3). Broadly speaking, it may act as a point source of pollution in the estuary. In the Mediterranean, particularly in France, waterfront developments have been shown to have had two main impacts. Firstly, they have caused a direct and irreversible replacement of the natural environment. Secondly, a permanent alteration of the biological structure of the water column was observed [*Meinesz et al.,* 1991]. In the Red Sea in Egypt, waterfront recreational developments have caused environmental impacts including, changes to the depositional hydrodynamic regime, thereby creating down drift erosion and deterioration in the water quality and changes to the marine biota [*Frihy et al.,* 2006]. Other typical environmental issues that may arise due to land reclamation and canalling include:

- Transportation of sediments (erosion and deposition);
- Destruction of coral reefs that support marine life;
- Increase of turbidity; and
- Sediment sorption processes of nutrients, such as phosphorus (details of model development related to such process is detailed in Chapter 4) etc.

2. 3. 1. 2 Desalination plants:

The demand for freshwater resources is hastily risen on a worldwide scale, especially in coastal areas where approximately three quarters of the world population is expected to live by 2020 [*Lattemann and Hopner,* 2008]. Hence it is not surprising that desalination of seawater is receiving increasing global interest. Seawater is a seemingly unlimited resource and many coastal regions and islands have no other alternative than to utilise it for the production of drinking water. Desalination is a vastly favourable technology, but like many technologies, it has undesirable impacts on the environment that need to be investigated and managed regularly [*Lattemann and Hopner,* 2008].

Analogous to the worldwide trend, coastal areas in the Gulf are experiencing a tremendous industrial and urban expansion. Due to rapid developments, the Gulf is recognised for delivering three strategic fluids: desalinated water, gas and oil. Concerning seawater desalination, the supplies generated in the Gulf still remain unequalled to date, while capacities in other estuaries of the world, such as the Mediterranean, are growing swiftly [*Lattemann and Hopner,* 2008]. The Gulf with an installed seawater desalination capacity of roughly 11 million m^3/day, currently accounts for almost 50% of the world's capacity of 24 million m^3/day [IDA, 2006] (see Figure 2.3). Most of the plants are located along the shallow Arabian shoreline of the Gulf (see Figure 2.3) with varying capacities: Kuwait-1.7 million m^3/day, Saudi Arabia-2.3 million m^3/day, Bahrain-0.4 million m^3/day, Qatar-0.9 million m^3/day, and U.A.E-5.7 million m^3/day, whereas only a few can be found on the Iranian coast-0.1 million m^3/day.

Effluent Parameter	RO	MSF
Salinity	Typically 60-70 psu	Typically 50 psu
Temperature	Ambient seawater temperature	5-15 °C above ambient
Plume density	Negatively buoyant	Positively, neutrally or negatively buoyant
Oxygen	Decreased as a side-effect of chlorine neutralization	Very low by physical de-aeration and use of oxygen scavengers
Chlorine	Neutralized	10-25% of dosage
Heavy Metals (in varying concentrations)	Iron, chromium, nickel, molybdenum	Copper, nickel

Figure 2.3: Location of desalination plants, MSF 'Multi-Stage Flash distillation' (top-right) and RO 'Reverse Osmosis' (bottom-right), and effluent property of MSF and RO discharged to the receiving water (left table)

The number of potential environmental impacts relating to desalination plants is wide and in some respects, such as land use, air pollution and energy consumption is analogous to other development projects. Marine impacts relating to desalination plants specifically may be attributed to the intake of large quantities of seawater, including various sizes of organisms into the plant. Such intakes are often fatal for the organisms and may affect population and ecosystem dynamics [*Khordagui,* 2002]. The main worry with desalination plants, however, is the impact of the exceedingly saline waste stream on water and sediment quality, impairing marine life or the

functioning and intactness of the coastal ecosystem. Due to their waste discharges, desalination plants were identified as a main source of land-based marine pollution in the Gulf [*UNEP*, 1999]. For illustration, the installed capacity of multi-stage flash (MSF) plants in the Gulf is about 9.7 million m^3/day, which corresponds roughly to a freshwater production of 115 m^3/s and a waste water flow rate of more than 1,000 m^3/s, which is a substantial volume of water compared for example to the river runoff into the Gulf, i.e. Shatt Al Arab. In due course this effect may create a hyper-saline environment that many species may not withstand. The rejected effluent discharged from such a plant usually has different physical and chemical parameters to these of the receiving water, as shown in Figure 2.3.

In terms of water quality several studies have shown that the chlorine concentration near the outlet of a desalination plant may reach 25 μg/l, even when 90% of the total concentration is decomposed [*Shams El Din et al.*, 2000]. *Ali and Riley,* [1986] and *Abdel-Jawad and Al-Tabtabaei,* [1999] have observed chlorine levels of 30-100 μg/l and 50 μg/l approximately 1 km from the outlet, respectively. A number of toxicological studies have shown that chlorine is highly toxic to many aquatic species, even at low concentrations in the range of 100 μg/l or less [*Lattemann and Hopner,* 2008]. Studies have shown that the ecological impact of chlorine discharged from desalination plants is higher in the Gulf than the Red Sea and to lesser extent in the Mediterranean, due to both the number of desalination plants and the technology used [*Hoepner and Lattemann,* 2003].

2. 3. 1. 3 Petrochemical activities:

Over the past 85 years oil production in many countries around the world has grown to enormous proportions. The importance of the Gulf countries in generating such high levels of production is well known, since it is considered to be the main producer of oil in the world [*Facey,* 2008] (see Figure 2.4). In 2006 the countries bordering the Gulf produced 18.41 Million Barrels of oil Per Day (MBPD), out of a total OPEC (Organisation of Petroleum Exporting Countries) production of 34.20 MBPD, and a total world production of approximately 81.66 MBPD (source: http://www.bp.com/liveassets/bp, Statistical Review of World Energy pdf.). The countries bordering the Gulf therefore currently produce roughly 22.54% of the total world production. A production rate of 18.41 MBPD equates to roughly 1,180 million tonnes of oil per year, or 3.24 million tonnes of oil per day [*Facey,* 2008]. For illustration, if the average large tanker in the Gulf loads around 250,000 tonnes, then at least 10 large tankers will enter the Gulf in ballast, and leave the Gulf loaded with various types of oil daily.

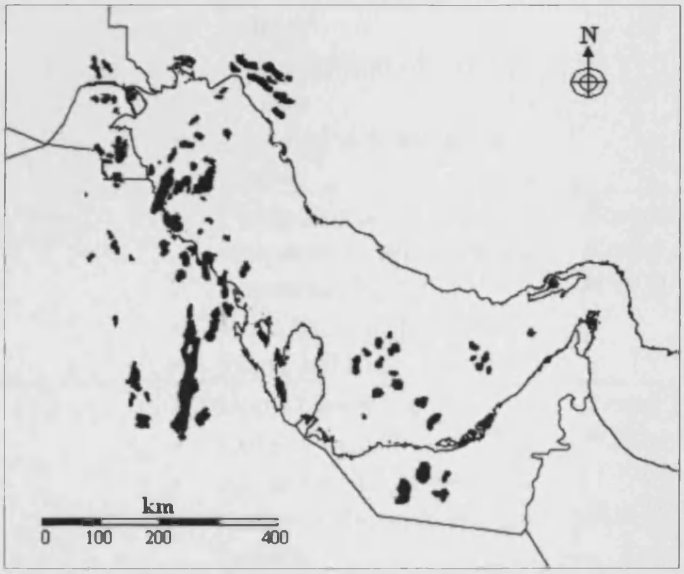

Figure 2.4: Main oil fields in the Gulf countries

Such activities normally involve oil spills that have hardly been quantified. Some are recognised as being operational spills, while others may arise due to political conflict, such as the Gulf war of 1990 [*Jones et al.,* 2008b]. In particular, the influx of oil from tankers and offshore oil operations is one of the major causes of pollution in the Gulf marine environment. Estimations of ballast water and other oily water discharged into the Gulf ranged from 400,000 to 750,000 tonnes in 1986 [*Harahsheh et al.,* 2004].

Due to the continuous large quantities of oil being spilled in the Gulf, various studies have been conducted to revise different biological impacts on the marine environment. Such impacts are summarised as shown in Table 2.2. Therefore, quantifying the dispersion and mixing in the Gulf is essential to understand the estuary dynamics, as detailed in Chapter 5.

Marine environment	Effects	Reference
Vertebrates (Sea birds and mammals)	• Stress and mortality • Oil ingestion leading to toxic effects • Disruption of nutrient uptake • Degeneration of liver tissues • Damage to respiration system.	*Burger and Gochfeld* [2002], *Krupp and Symens* [1994]
Inshore habitats and living marine resources	• Fluctuations of temperature and salinity that stress biota. • High fish mortalities. • Toxic habitat	*Basson et al.,* [1977], *Krupp and Anegay* [1993]
Coral reefs	• Coral bleaching • Coral mortality • Algae lost from the corals or die in their tissues.	*Krupp* [1998], *Wilkinson et al.,* [1999], *Fadlallah et al.,* [1995]

Table 2.2: Effect of oil activities in the Gulf on the marine environment

2. 3. 2 Effects of climate change:

The climate system is an interactive system consisting of the atmosphere, land surface, snow and ice, oceans, rivers, lakes and estuaries that interrelate with all forms of life on earth. Climate is frequently defined as the long-term mean and variability of temperature, precipitation and wind over different time scales, from decades to million of years (the classical period being 30 years) [*IPCC, Climate change 2007: The physical Science Basis*, 2007]. Climate change often refers to variations in each of the climate forms over a certain area, despite the reasons for the change. Although the extent and level at which climate change becomes intolerable is controversial, the fact that climate change is now occurring at a considerable rate is almost universally accepted.

The causes of climate change have been widely related to human activity on Earth, for example see Section 2.3.1.3. Other factors that may influence the climate include:

- Plate tectonics;
- Solar output;
- Orbital variations;
- Volcanism; and
- Ocean variability.

The effect of climate change on estuaries has been widely documented [*Purcell,* 2005; *Attrill and Power,* 2002]. Here we are concerned with two climatic phenomena that have been recently recognised in the Gulf as having apparent impact on the marine life in the estuary, namely dust storms and flooding.

2. 3. 2. 1 Dust storms:

Natural dust is a dynamic component of the climate system and plays multiple roles in mediating physical and biogeochemical exchanges between the atmosphere, land surface and ocean [*Harrison et al.,* 2001]. Dust storms are windstorms accompanied by suspended clay and silt material, usually-but not always-without precipitation. Presently, between 130 and 800 million tonnes of dust, with extremes as high as 5,000 million tonnes, are entrained by winds each year [*Bryant,* 2005]. The average annual amount of clay-sized particles moved is about 500 million tonnes [*Bryant,* 2005]. Dust storms are responsible for most of the terrigenous material found in ocean basins, contributing over 75 million tonnes of material per year to the Atlantic Ocean alone [*Simonson,* 1995]. At distances of 5,000 km out into the Atlantic Ocean, fallout from the Sahara is still deposited at a rate of 3,000 tonnes/km^2/yr [*Simonson,* 1995].

Dust storms generally form as a result of the passage of cold fronts linked to mobile polar highs across arid or drought-affected plains. The passage of these fronts can give rise to dust storms lasting for several days. In the northern Sahara region, dust storms are mainly produced by complex depressions linked with westerly winds. The depressions originate in the winter in the eastern Mediterranean Sea or the Atlantic Ocean. The seasonal movement of the monsoon into the Sudan region of the Sahara is responsible for dust in eastern Africa, while the Indian monsoon controls the timing of dust storms on the Arabian Peninsula [*Bryant,* 2005].

In terms of water quality, dust storms may carry heavy metals, fungi, bacteria, and viruses. In particular, nutrients such as phosphorus and nitrogen can be absorbed by sediment particles and transported to coastal areas (see Figure 2.5 for illustration).

The particles may then be deposited onto marine waters and for certain conditions, i.e. for suitable temperatures and chemical reactions, the nutrients may be released into the surrounding water. Therefore, in terms of sorption processes, this phenomenon may well be considered as a major source or sink of nutrients in a marine system (with more details related to model development being given in Chapter 4 and model application in Chapter 7). In addition, dust retention times in air and surface waters may limit algal growth in a marine system by blocking the light necessary for algal growth.

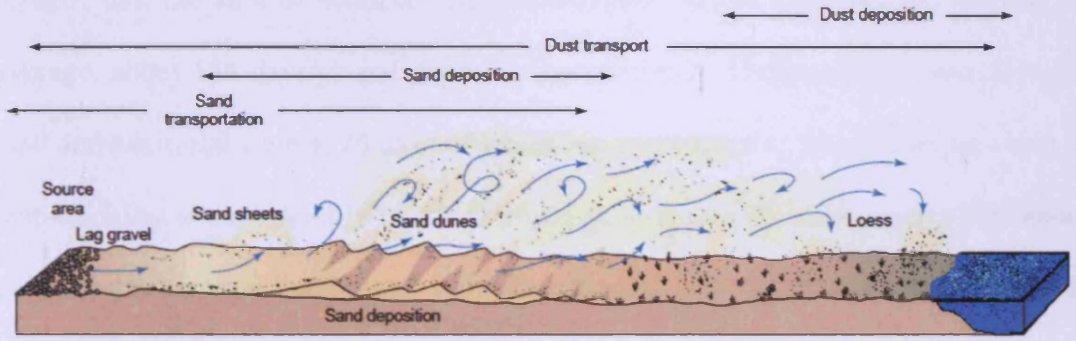

Figure 2.5: Flowing air erodes, transports, and deposits fine sediments on land or water [modified after http://earthds.info/]

Due to the effects of climate change and related global warming, the Gulf has been affected by dust storms in mainly two aspects. Firstly, high air temperatures: recent records have shown high temperatures in the northern region of the Gulf, particularly Kuwait, that have reached 50 °C [*Al-Gahtani and Maslehuddin*, 2002], while *Al-Rashid and Al-Mikaimi*, [2010] have recorded values of 55 °C in Kuwait City. Secondly, rainfall is very limited, but can occur in large quantities that occasionally results in flooding (see section 2.3.3.2). In addition to global effects, an area of about

9,000 km^2 (i.e. the southern marshes of Iraq) was drained, resulting in the occurrence of dry lands that were exposed to the dominant northwest and southeast winds [*Al-Ghadban et al.,* 1999]. This has all led to the fact that this region is very vulnerable to occasional dust storms as shown in Figure 2.6, in which even minor winds may attract sediment and displace sediments into the surrounding air streams. Such events have been widely recorded, particularly at the northern end of the Gulf. Dust storms have been occurring more frequently over the past few years and currently occur in over 25% of the year in Kuwait [*Alsharhan*, 2009]. In addition, *Al-Qabandi,* [2010] announced, with reference to a Kuwait Environmental Public Authority (K-EPA) reports, that the sum of sediment attraction related to this phenomenon occurs, on average, about 154 days/yr and deposits approximately 55 tonnes/km^2 over Kuwaiti land and territorial waters, 26 days of which are considered to be an extreme event in that visibility is considerably reduced. Thus, an approximate deposition of sediment particles can be roughly estimated to be 39,600 tonnes/yr over the whole Bay; most of these sediments deposits come from Iraq, in response to limited rainfall and increased desertification [*Al-Haddad*, 2009; *Khalaf et al.,* 1985].

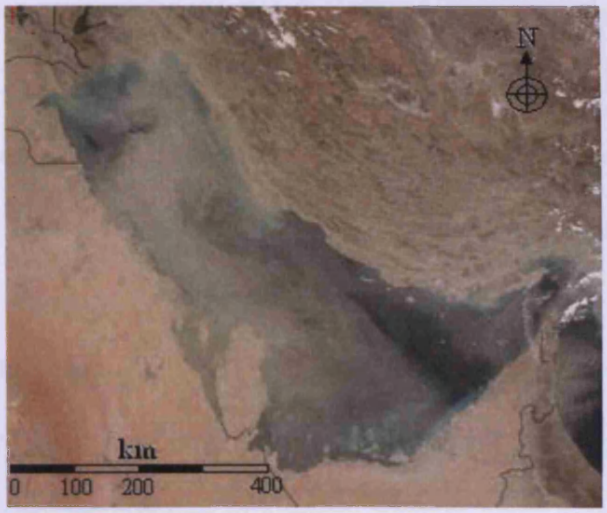

Figure 2.6: Dust storm in the Gulf occurred in March 2010, [Source: http://modis.gsfc.nasa.gov/index.php]

2. 3. 2. 2 Flooding:

With the increasing concerns of climate change in the Middle East, flash floods (see Figure 2.7) have received special interest in the Gulf countries. Although it has been considered to be a natural common phenomenon over the past few decades, there is increasing evidence in the region that climate change has accelerated such processes and caused them to occur more frequently. Flash floods in arid regions, such as the Gulf, can principally be harmful to the environment for several reasons. Firstly, storms in arid regions are occasional, but they can deliver an enormous amount of rain in a very short time interval, such as with the Jeddah flood of 2009 (see Figure 2.7). Secondly, these rains often fall on poorly absorbent land and often clay like soil that seriously increases the amount of runoff that rivers and other water channels have to handle. Thirdly, some regions do not have the infrastructure that wetter regions have to divert water from structures and roads, such as storm drains and retention basins, either due to the minor population and poverty in such regions or because of poor

planning that underestimates the risks of flash floods rising mostly from unpredictable climate change effects. Therefore, untreated water streams rising from such events would normally find their way to coastal areas and may likely cause disturbance to the receiving water by introducing different physical and chemical characteristics.

In terms of flood frequency, such events may have a major impact on the local biota. It has been shown that the frequency of disturbance by floods is a fundamental determinant of the spatial patterns in average benthic algal biomass among streams [*Biggs,* 1996], and it seems sensible to conclude that flood disturbance might also influence patterns in benthic algal taxonomic richness [*Biggs and Smith*, 2002]. For example, streams in regions of New Zealand with frequent floods appear to have larger mean monthly benthic algal richness than streams in regions with less frequent floods [*Clausen and Biggs,* 1997]. Other effects of flash floods on receiving waters can be summarised in the following:

- Increase of nutrients through sediment adsorption processes;
- Increase of turbidity;
- Local ecological effects;
- Bed erosion and sediment transport; and
- Increase of heavy metals.

Figure 2.7: Flash floods in Oman, cyclone Phet 2010: more than 360 mm of rain (left), Saudi Arabian flood (Jeddah) 2009 more than 90 mm of rain (middle), U.A.E flood (Dubai) 2008 reached 50 mm of rain (right)

2. 3. 3 Eutrophication:

Due to anthropogenic activities and related pollution, as mentioned in Section 2.3.1, and to lesser extent climate change (explained in section 2.3.2), the Gulf has experienced an increasing number of algal blooms and consequently 'eutrophication' events in various regions of the Gulf [*Glibert,* 2007]. Some of these events have been considered to be toxic to the marine life, while others have caused major fish kills and 'Red Tides', as experienced in the Bay (see Figure 2.8) [*Ismail et al.,* 2007, *Al-Yamani et al.,* 2006, *Glibert et al.,* 2002, *Heil et al.,* 2001, *Subba-Rao* and *Al-Yamani* 1998, *Richlen et al.,* 2010]. It is therefore important to review eutrophication in reasonable detail and the consequences of such events on the marine environment.

Figure 2.8: Major fish kill in Kuwait bay [*Glibert et al.*, 2002]

Eutrophication is often caused by an over-enrichment of a marine system with nutrients that enhance extensive growth, which can cause algal blooms. It has sometimes been defined as the biological response of a marine system to anthropogenic changes in rivers, lakes, and coastal waters [*Menesguen,* 1990]. Eutrophication is a natural process, but human activity can accelerate the process by increasing nutrient loadings into a water body. Natural eutrophication is a process that is measured in terms of thousands of years, whereas the on set of eutrophication due to human activity can take only a few decades or even years to develop. Eutrophication is one of the leading environmental problems which leads to excessive plant growth: algae in the open water, periphyton (attached to benthic algae) on the bottom of the water body, and macrophytes (large vascular rooted plants that are often called weeds) in the shallower water areas [*Glibert et al.*, 2002].

Based on its biological productivity and nutrient conditions, a water body can generally be categorised as oligotrophic, mesotrophic, and eutrophic as shown in Table 2.3.

Condition	Definition	Diagram
Oligotrophic	A water body with low biological activity and excellent water quality, since the water is low in nutrients and algae and both primary production and biomass are severely limited.	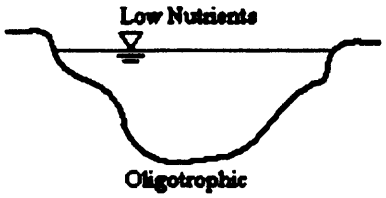
Mesotrophic	A water body with medium biological activity and good water quality.	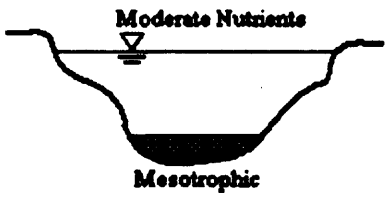
Eutrophic	A water body with excessive biological activity and poor water quality. The water has abundant nutrients and high rates of primary production, frequently resulting in oxygen depletion in the bottom layers	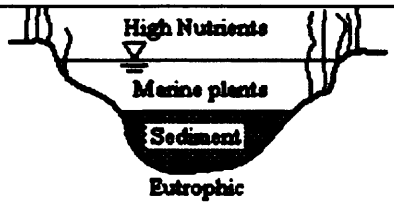

Table 2.3: Oligotrophic, Mesotrophic and Eutrophic condition of a marine system

As shown in the Table 2.3, an oligtrophic marine system is low in nutrients and is supplied with less nutrients, and therefore it is normally characterised with low biodiversity. Therefore, the water is normally clear with sufficient oxygen throughout the year. However, when the nutrient supply increases, the system can be well defined as a mestrophic system. As the nutrients increase slightly the production of both phytoplankton and zooplankton increase without extensive damage to the ecosystem. In such a state the system is normally well balanced in terms of both biological

growth and dissolved oxygen consumption, particularly in deep waters. Further supplies of nutrients can lead to over enrichment of the system and consequently large biological production and high dissolved oxygen consumption. Such effects lead to high turbidity levels, due to dense growth and therefore less light penetration. The bottom of an eutrophic system is often characterised by a thick sediment layer loaded with organic matter that often leads to changes in species composition. Trophic state is normally controlled by the following parameters:

- Nutrient loading from point and non-point sources, such as water treatment plant discharges, sewage discharges, industrial wastewater, agricultural and urban runoff;
- Meteorological conditions, such as solar radiation, air temperature and precipitation;
- Topographical and geometrical features of a marine system; and
- Horizontal and vertical dispersion mechanism (explained in Chapter 5).

Since the above feature varies dramatically from one system to another, there is no numerical criteria collectively applicable to measuring the trophic state of a marine system. Total phosphorus, total nitrogen, chlorophyll and secchi depth are normally used to represent the eutrophic state of a system. Since eutrophication is normally caused by high phosphorus and nitrogen level in a system, it is often related to these variables. On the other hand, chlorophyll and secchi depth are initial response variables. Other variables, such as dissolved oxygen are very helpful in identifying the eutrophication status of a water body. In practice, dissolved oxygen is used in the decomposition processes of algae, where nutrient enrichment would increase the algae production and accelerate the decomposition process until the dissolved oxygen is

mostly depleted. This would normally lead to larger fish kill and undesirable odours that would, in turn, be decomposed using dissolved oxygen and finally block light penetration leading to major retardation of photosynthesis processes throughout the water column, in particular near the seabed [*Ji,* 2008]. In general, the dissolved oxygen level is predominantly highest during the winter and lowest during the summer, when temperature and stratification are more appreciable. Noticeable modifications in the ecosystem may arise when a species dies due to eutoriphcation and is replaced by another species that can tolerate eutrophic conditions [*Ji,* 2008].

2. 3. 3. 1 Limiting nutrient and Redfield ratio:

In addition to nitrogen and phosphorus, algal growth is affected by light, water temperature and various trace nutrients, which in practice are hard to control in natural marine system. Since some control can be exerted over the concentration of nitrogen and phosphorus, considerable studies are conducted on how to make nitrogen or phosphorus a limiting nutrient, in which eutrophication can be controlled in a marine system.

Algae consume nutrients in a fixed stoichiometric ratio and this ratio is relatively constant and occasionally called the Redfield ratio named after Alferd Redfield. He found that the ratios of carbon to nitrogen to phosphorus remained the same from coastal to open ocean regions. The elemental ratios he found were; Carbon : Nitrogen : Phosphorus as 106 : 16 : 1. Disparity in the ratio of nutrients supplied often leads to depletion of one nutrient, while other remains available. This nutrient, which is least available for algal growth, is called limiting nutrient. When the limiting nutrient is depleted, according to the Liebig's Law of Minimum, the algal concentrations stop

increasing and the eutrophication process is retarded or in some cases reversed [*Ji,* 2008]. It is worth mentioning that in this research there was no attempt to identify the limiting nutrient in the Gulf region, instead physical processes affecting nutrient level were investigated such as phosphorus sorption processes (see Chapter 7).

Generally, seawater is most often limited by nitrogen, while freshwater are most often limited by phosphorus. Compared with phosphorus, nitrogen is frequently more complex to manage, because it is almost unattainable to control the nitrogen exchange between the atmosphere and water. In estuaries limiting nutrient may vary from being phosphorus, nitrogen or other physical parameters such as light due to its dynamic nature and the effect of human activities as mentioned previously. In the Gulf of Sarnique (Aegean Sea) *Becacos-Kontos* [1977] suggested that the factor limiting primary productivity in the waters were on occasion solely phosphorus and other times both phosphorus and nitrogen. Also, *MacIsaac and Dugdale* [1972] have conducted studies near Greece coastal water and reported enhancement of nitrate uptake after addition of phosphorus.

2. 4 Summary:

In this chapter an outline of the main physical forcing parameters (i.e. tide, freshwater input and wind) on the Gulf, including the Bay, has been discussed. Further details of such effects on the horizontal dispersion of numerical tracers will be investigated in Chapter 5. The main marine environmental impacts in the Gulf have been addressed in relation to human activity (such as: waterfront developments, desalination plants and petrochemical industry) and climate change, including the impacts arising from dust storms and flash floods. Such impacts have led to various problems in the Gulf,

in particular eutrophication events, which have been explained in some detail. It is therefore important to understand the fundamental dispersion mechanism of the Gulf; this will be studied in Chapter 5. The effects of sediment sorption processes of phosphorus arising from sediment deposition on the Bay waters will be addressed in Chapter 7.

Chapter 3

Governing Equations of Motion and Solute Transport

3. 1 Introduction:

During recent decades many scientists and engineers have been involved in hydro-environmental research projects as a result of the increasing general awareness of water quality and the growing public concern about environmental and ecological issues in the Gulf. Predicting the hydrodynamic processes and the distribution of contaminant quantities have generally been a major part of these projects. Analytical solutions are not options available for such predictions, because of the complex boundaries and natural geometry of practical studies.

Physical model studies have traditionally been a major means for predicting flow fields and contaminant transport in hydro-environmental research projects for much of the past 80 years. However, with the rapid advances in computer technology over the past 30 years, computer models, based on numerical techniques, have been used increasingly for such simulation studies. The rapid increase in the speed and memory capabilities of modern computers, on one hand, and the fast developing numerical methods, on the other hand, have widened the scope applications of the computer model applications.

The main aim of this chapter is to present the three-dimensional governing equations for the hydrodynamic processes and the advection diffusion equation for solutes that are commonly solved by numerical models, such as those detailed in Chapter 4.

3. 2 Hydrodynamic equations:

Prior to modelling the water quality and sediment transport processes in estuarine and coastal waters, the hydrodynamic characteristics of the flow fields, such as water

elevations and velocity components must be predicted. This is undertaken through the hydrodynamic model, which is used to solve the governing hydrodynamic equations.

The Navier-Stokes equations describe unsteady turbulent flow in coastal and estuarine waters, with the numerical procedures employed to solve these equations being called direct numerical simulation (DNS). Nevertheless, the storage capacity and speed of present day computers is, to some extent, still not satisfactory to permit a solution for any practically relevant turbulent flow [*Rodi*, 2000; *Tannehill et al.*, 1997]. Presently, the Navier-Stokes equations are averaged over time and these time-averaged equations are referred to as the Reynolds Averaged Navier-Stokes equations (RANS) that were first proposed by 'Osborne Reynolds'. This time-averaging process introduces new terms, known as the Reynolds stress or apparent stress terms into the equations, which require turbulent models to close the system of equations. Details about the different turbulence models and their application in hydraulics can be found in *Rodi,* [2000]. According to the number of transport equations used for the turbulence quantities to evaluate the eddy viscosity, a turbulence model can be classified into three main categories:

1) ***Zero-equation models***: which specify both a length and velocity scale using an algebraic relationship.
2) ***One-equation models***: which use an additional partial differential equation for the velocity scale and specify a length scale algebraically.
3) ***Two-equation models***: which use one partial differential equation for the velocity scale and one for the length scale.

Among these models, the zero-equation models (such as the mixing length model) and the two-equation models (such as the $k-\varepsilon$ model) are the most widely used [*Sotiropoulos,* 2005; *Rodi*, 2000].

In modelling estuarine and coastal waters, usually a hydrostatic pressure is assumed, which means that the pressure is balanced by the gravity [*Blumberg and Mellor*, 1987]. Hence, the vertical acceleration must be much smaller than the pressure gradient and gravitational acceleration [*Lin and Falconer,* 1997]. This can significantly simplify the equations and numerical solutions [*Vreugdenhil*, 1994]. Applying the kinematic boundary condition on the free surface, the hydrodynamic equations can be further simplified by integrating over the water column. The resulting depth-integrated equations are frequently called the shallow water equations (SWEs), which are widely used to prescribe the hydrodynamic processes in estuarine and coastal waters [*Liang et al.*, 2006].

Hydrodynamic models can be divided into: one-, two- and three-dimensional models. Normally for river modelling one dimensional models are used in water systems where vertical and lateral variations are minor e.g. [*Wondzell,* 2006]. Depth integrated two dimensional models are generally used for estuarine and near shore coastal waters and two dimensional laterally averaged models are generally used for narrow deep water bodies [*Crowder and Diplas,* 2006]. For deep and large water bodies, where stratification is significant, then a three-dimensional model should be used [*Chen and Sheng,* 2005]. In this study we are concerned with three-dimensional modelling.

In hydrodynamic modelling, the theory is now generally accepted and the quality of the numerical solution is the more critical aspect for discussion [*Falconer et al.*, 2001]. Therefore research efforts on numerical schemes and their performances have developed significantly in recent years, such as the TVD-MacCormack scheme refined by *Liang et al.*, [2006, 2007] to simulate rapid varying flooding flows.

3. 2. 1 Three-dimensional Reynolds averaged equations:

The numerical models commonly used to predict hydrodynamic, water quality and sediment transport processes in coastal, estuarine and river waters are based on first solving the governing hydrodynamic equations of motion. In a cartesian co-ordinate system, the corresponding three-dimensional Reynolds averaged equations for mass and momentum conservation in the x-direction can be respectively written in a general form as [*Falconer*, 1993]:

$$\frac{\partial u}{\partial x}+\frac{\partial v}{\partial y}+\frac{\partial w}{\partial z}=0 \tag{3.1}$$

$$\underbrace{\frac{\partial u}{\partial t}}_{1}+\underbrace{\frac{\partial u^2}{\partial x}+\frac{\partial uv}{\partial y}+\frac{\partial uw}{\partial z}}_{2}=\underbrace{X}_{3}-\underbrace{\frac{1}{\rho}\frac{\partial P_w}{\partial x}}_{4}+$$

$$\underbrace{\frac{1}{\rho}\left\{\frac{\partial}{\partial x}\left[\mu\frac{\partial u}{\partial x}-\rho\overline{u'u'}\right]+\frac{\partial}{\partial y}\left[\mu\frac{\partial u}{\partial y}-\rho\overline{u'v'}\right]+\frac{\partial}{\partial z}\left[\mu\frac{\partial u}{\partial z}-\rho\overline{u'w'}\right]\right\}}_{5} \tag{3.2}$$

where u,v and w are the time averaged velocity components in the x, y and z directions respectively,

t is the time,

X is the body force in the x-directions,

P_w is the pressure,

ρ is the water density,

μ is the viscosity and

u', v' and w' are the fluctuating velocity components in the x, y and z directions respectively.

The expressions $\rho\overline{u'u'}$, $\rho\overline{u'v'}$ and $\rho\overline{u'w'}$ are known as the Reynolds or apparent stresses in the x-direction, and on the x, y and z planes respectively (see Figure 3.1), with these terms existing due to the turbulence of the flow, in which for laminar flow they are zero. For the numbered terms in equation (3.2), these terms refer to, the local acceleration (term 1), the advective (or convective) acceleration (term 2), the body force (term 3), the pressure gradient (term 4) and the laminar and turbulent shear stresses (term 5) see [*Falconer,* 1993].

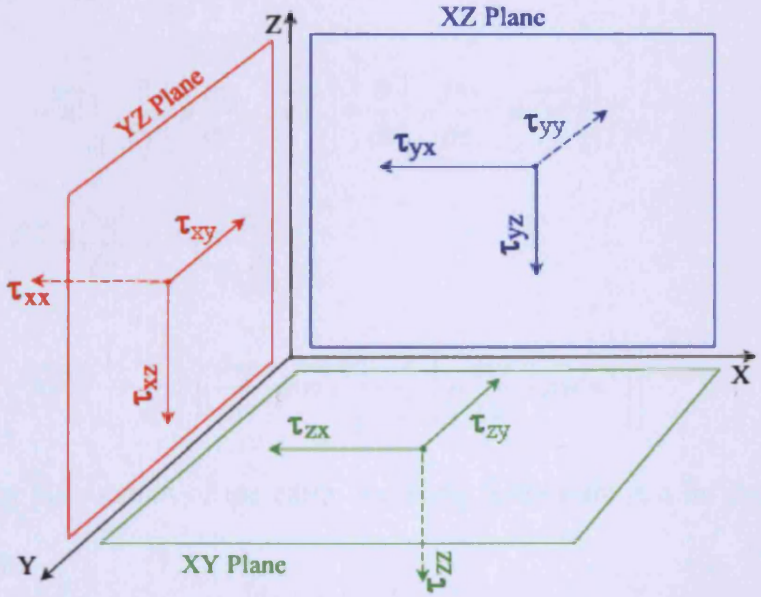

Figure 3.1: Co-ordinate system for the apparent stresses in the x, y and z planes

For the Reynolds stresses, Boussinesq [*Falconer*, 1993; *Goldstein*, 1938] proposed that they could be represented in a diffusive behaviour as follows:

$$-\rho\overline{u'u'} = \eta\left(\frac{\partial u}{\partial x}+\frac{\partial u}{\partial x}\right)$$

$$-\rho\overline{u'v'} = \eta\left(\frac{\partial u}{\partial y}+\frac{\partial v}{\partial x}\right) \qquad (3.3)$$

$$-\rho\overline{u'w'} = \eta\left(\frac{\partial u}{\partial z}+\frac{\partial w}{\partial x}\right)$$

where η is the absolute eddy viscosity,

ε is the kinematic eddy viscosity $= \eta / \rho$.

In general, $\eta >> \mu$, in the y and z directions similar equations can be obtained for the conservation of momentum giving respectively:

$$\frac{\partial v}{\partial t}+\frac{\partial vu}{\partial x}+\frac{\partial v^2}{\partial y}+\frac{\partial vw}{\partial z} = Y-\frac{1}{\rho}\frac{\partial P_w}{\partial y}+$$

$$\frac{1}{\rho}\left\{\frac{\partial}{\partial x}\left[\mu\frac{\partial v}{\partial x}-\rho\overline{v'u'}\right]+\frac{\partial}{\partial y}\left[\mu\frac{\partial v}{\partial y}-\rho\overline{v'v'}\right]+\frac{\partial}{\partial z}\left[\mu\frac{\partial v}{\partial z}-\rho\overline{v'w'}\right]\right\} \qquad (3.4)$$

$$\frac{\partial w}{\partial t}+\frac{\partial wu}{\partial x}+\frac{\partial wv}{\partial y}+\frac{\partial w^2}{\partial z} = Z-\frac{1}{\rho}\frac{\partial P_w}{\partial z}+$$

$$\frac{1}{\rho}\left\{\frac{\partial}{\partial x}\left[\mu\frac{\partial w}{\partial x}-\rho\overline{w'u'}\right]+\frac{\partial}{\partial y}\left[\mu\frac{\partial w}{\partial y}-\rho\overline{w'v'}\right]+\frac{\partial}{\partial z}\left[\mu\frac{\partial w}{\partial z}-\rho\overline{w'w'}\right]\right\} \qquad (3.5)$$

In considering the rotation of the earth, the body force term can be expressed in the following term:

$$X = fv$$

$$Y = -fu \qquad (3.6)$$

$$Z = -g$$

where f is the Coriolis coefficient= $2\omega \sin\theta_L$, ω is the angular speed of earth's rotation $\approx$ 7.3 x10^{-5} rads/s i.e. $2\pi/(24\times3600)$, θ_L is the latitude of the site and g is the acceleration due to gravity $\approx 9.807 m/s^2$.

For flows in estuarine and coastal waters usually a hydrostatic pressure distribution can be assumed, since the vertical acceleration of the fluid is small compared to that of gravity acceleration, and the Navier-Stokes equation in the vertical z-direction can be reduced to give:

$$\frac{\partial P_w}{\partial z} + \rho g = 0 \qquad (3.7)$$

At the free surface continuity of stress is assumed, i.e. the stresses in the water just below the free surface are assumed to be the same as those in the air just above, giving for pressure:

$$P_w = P_a \qquad (3.8)$$

where P_a is the atmospheric pressure.

Integrating down through the water column from the surface, using boundary condition in equation (3.8), and assuming a constant density gives:

$$P_w(z) = \rho g(\xi - z) + P_a \qquad (3.9)$$

where ξ is the water surface elevation above datum

From equation (3.9), the pressure gradients can be determined giving:

$$\frac{\partial P_w}{\partial x} \approx \rho g \frac{\partial \xi}{\partial x}$$

$$\frac{\partial P_w}{\partial y} \approx \rho g \frac{\partial \xi}{\partial y} \qquad (3.10)$$

3. 2. 2 Three-dimensional layer integrated equations:

For the three-dimensional layer integrated model, the water column was divided into several layers as illustrated in Figure 3.2.

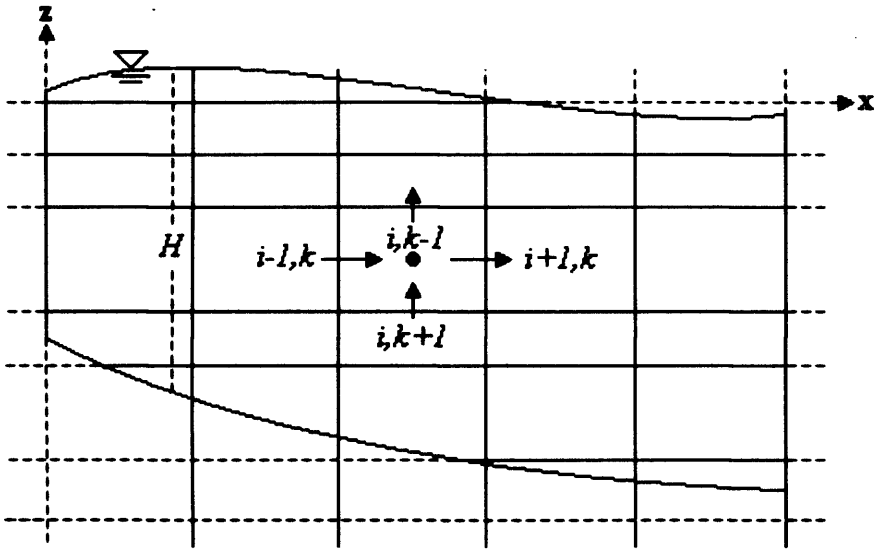

Figure 3.2: Co-ordinate system for layer integrated equations in the z(k) - x(i) plane: ↑ is the vertical velocity, → is the horizontal velocity and H is the total depth [*Lin and Falconer,* 1997]

For the three-dimensional layer integrated model, each layer has a different velocity from that in the neighbouring layers, with the governing equations for mass and momentum conservation being integrated over the layer thickness. As illustrated in Figure 3.2, there are three types of layers; including, a top layer ($k=1$), a bottom layer ($k=k_{max}$) and a middle layer. The top and bottom layer thicknesses are not

uniform and define both the free surface and bed topography respectively. In contrast the middle layers normally have a uniform thickness [*Lin and Falconer,* 1997].

3. 2. 2. 1 Continuity equation:

Integrating the continuity equation over the k_{th} layer gives:

$$\int_{k+\frac{1}{2}}^{k-\frac{1}{2}}\left(\frac{\partial u}{\partial x}+\frac{\partial v}{\partial y}+\frac{\partial w}{\partial z}\right)dz=0 \tag{3.11}$$

This leads to:

$$\int_{k+\frac{1}{2}}^{k-\frac{1}{2}}\left(\frac{\partial u}{\partial x}+\frac{\partial v}{\partial y}\right)dz+w_{k-\frac{1}{2}}-w_{k+\frac{1}{2}}=0 \tag{3.12}$$

where $k\pm 1/2$ refers to the vertical elevations of the interface between the $k+1$, k and $k-1$ layers. Expanding equation (3.12), using Leibnitz rule [*Hall,* 1987; *Lin and Falconer,* 1997] and simplifying the resulting equation, then the layer integrated continuity equation give the vertical velocity component w at the interface $k-1/2$:

$$w_{k-\frac{1}{2}}+\sum_{k=k}^{k_{max}}\left[\frac{\partial(h_k u_k)}{\partial x}+\frac{\partial(h_k v_k)}{\partial y}\right]=0 \tag{3.13}$$

At the water surface, the continuity equation reduces to:

$$\frac{\partial \xi}{\partial t}+\sum_{k=1}^{k_{max}}\left[\frac{\partial(h_k u_k)}{\partial x}+\frac{\partial(h_k v_k)}{\partial y}\right]=0 \tag{3.14}$$

Where h_k is the thickness of layer k.

3. 2. 2. 2 Momentum equations:

Integrating the momentum equation over the k_{th} layer gives:

$$\int_{k+\frac{1}{2}}^{k-\frac{1}{2}}\left(\frac{\partial u}{\partial t}+\frac{\partial uu}{\partial x}+\frac{\partial uv}{\partial y}\right)dz+\left(u_{k-\frac{1}{2}}w_{k-\frac{1}{2}}\right)-\left(u_{k+\frac{1}{2}}w_{k+\frac{1}{2}}\right)$$

$$=\int_{k+\frac{1}{2}}^{k-\frac{1}{2}}fvdz-\int_{k+\frac{1}{2}}^{k-\frac{1}{2}}\frac{1}{\rho}\frac{\partial P_w}{\partial x}dz+\int_{k+\frac{1}{2}}^{k-\frac{1}{2}}\frac{1}{\rho}\left(\frac{\partial \tau_{xx}}{\partial x}+\frac{\partial \tau_{xy}}{\partial y}\right)dz \qquad (3.15)$$

$$+\frac{1}{\rho}\left(\tau_{xz}\big|_{k-\frac{1}{2}}-\tau_{xz}\big|_{k+\frac{1}{2}}\right)$$

Where $\tau_{xx}=\rho\overline{u'u'}$ and $\tau_{xy}=\rho\overline{u'v'}$

$$\int_{k+\frac{1}{2}}^{k-\frac{1}{2}}\left(\frac{\partial v}{\partial t}+\frac{\partial uv}{\partial x}+\frac{\partial vv}{\partial y}\right)dz+\left(v_{k-\frac{1}{2}}w_{k-\frac{1}{2}}\right)-\left(v_{k+\frac{1}{2}}w_{k+\frac{1}{2}}\right)$$

$$=-\int_{k+\frac{1}{2}}^{k-\frac{1}{2}}fudz-\int_{k+\frac{1}{2}}^{k-\frac{1}{2}}\frac{1}{\rho}\frac{\partial P_w}{\partial y}dz+\int_{k+\frac{1}{2}}^{k-\frac{1}{2}}\frac{1}{\rho}\left(\frac{\partial \tau_{yx}}{\partial x}+\frac{\partial \tau_{yy}}{\partial y}\right)dz \qquad (3.16)$$

$$+\frac{1}{\rho}\left(\tau_{yz}\big|_{k-\frac{1}{2}}-\tau_{yz}\big|_{k+\frac{1}{2}}\right)$$

Where $\tau_{yx}=\rho\overline{v'u'}$ and $\tau_{yy}=\rho\overline{v'v'}$.From a hydrostatic pressure distribution assumption, the pressure gradient component can be expressed as given in equation (3.10), and applying the Boussinesq approximation of equation (3.3) for shear stress term, then the layer integrated momentum equations can be given as:

$$\frac{\partial(u_k h_k)}{\partial t}+\beta_k\left(\frac{\partial(u_k{}^2 h_k)}{\partial x}+\frac{\partial(u_k v_k h_k)}{\partial y}\right)=fv_k h_k-gh_k\frac{\partial \xi}{\partial x}\Big|_k$$

$$+\left[\frac{\partial}{\partial x}\varepsilon_h h_k\left(\frac{\partial u_k}{\partial x}+\frac{\partial u_k}{\partial x}\right)+\frac{\partial}{\partial y}\varepsilon_h h_k\left(\frac{\partial u_k}{\partial y}+\frac{\partial v_k}{\partial x}\right)\right] \qquad (3.17)$$

$$+(w_{k+\frac{1}{2}}u_{k+\frac{1}{2}})-(w_{k-\frac{1}{2}}u_{k-\frac{1}{2}})+\frac{1}{\rho}\left(\tau_{xz}\big|_{k-\frac{1}{2}}-\tau_{xz}\big|_{k+\frac{1}{2}}\right)$$

$$\frac{\partial(v_k h_k)}{\partial t}+\beta_k\left(\frac{\partial(u_k v_k h_k)}{\partial x}+\frac{\partial(v_k{}^2 h_k)}{\partial y}\right)=-fu_k h_k-gh_k\left.\frac{\partial\xi}{\partial y}\right|_k$$

$$+\left[\frac{\partial}{\partial x}\varepsilon_h h_k\left(\frac{\partial v_k}{\partial x}+\frac{\partial v_k}{\partial y}\right)+\frac{\partial}{\partial y}\varepsilon_h h_k\left(\frac{\partial v_k}{\partial y}+\frac{\partial v_k}{\partial y}\right)\right] \qquad (3.18)$$

$$+(w_{k+\frac{1}{2}}v_{k+\frac{1}{2}})-(w_{k-\frac{1}{2}}v_{k-\frac{1}{2}})+\frac{1}{\rho}\left(\tau_{yz}\Big|_{k-\frac{1}{2}}-\tau_{yz}\Big|_{k+\frac{1}{2}}\right)$$

where u_k, v_k and w_k are the velocity components for the layer k in the x, y and z directions respectively, h_k is the thickness of layer k, ε_h is the horizontal eddy viscosity in the layer k and β_k is the momentum correction factor for the layer k. For the surface layer (i.e. $k=1$), then $(w_{k-\frac{1}{2}}u_{k-\frac{1}{2}})$ and $(w_{k-\frac{1}{2}}v_{k-\frac{1}{2}})$ can be removed by applying the kinematic free surface boundary condition. At the bed boundary $(w_{k+\frac{1}{2}}u_{k+\frac{1}{2}})$ and $(w_{k+\frac{1}{2}}v_{k+\frac{1}{2}})$ are zero due to the no-slip boundary condition.

3. 2. 2. 3 Vertical and horizontal viscosity:

In modelling estuarine and coastal waters, the ratio of the vertical length scale to the horizontal length scale is generally very small. The eddy viscosity term in the vertical direction is generally more dominant than the corresponding viscosity terms in horizontal direction. In the current study, the horizontal eddy viscosity ε_h was assumed to be constant in the vertical, and its value was assumed to be equal to the depth-averaged eddy viscosity $\bar{\varepsilon}$. *Lin and Falconer,* [1997] represented the vertical eddy viscosity ε_v by using a two-layer mixing length model suggested by [*Rodi*, 2000] of the form:

$$\varepsilon_v = l^2\left[\left(\frac{\partial u}{\partial z}\right)^2 + \left(\frac{\partial v}{\partial z}\right)^2\right]^{\frac{1}{2}} \tag{3.19}$$

where l is mixing length, defined as :

$$l = k_{von} z \quad \text{for} \quad k_{von} z \le 0.1H$$

$$l = 0.1H \quad \text{for} \quad k_{von} z > 0.1H$$

and k_{von} is von Karman's constant.

3. 2. 2. 4 Surface wind shear stress:

At the water surface, the shear stress was equated directly to the wind shear stress giving:

$$\tau_{xz} = \gamma_w \rho_a W_y \sqrt{W_x^2 + W_y^2}$$

$$\tau_{yz} = \gamma_w \rho_a W_x \sqrt{W_x^2 + W_y^2} \tag{3.20}$$

where γ_w is the air-water resistance coefficient, generally ≈ 0.0026, ρ_a is the air density = 1.29 kg/m^3, and W_x, W_y is the wind velocity components in the in x, y directions, $W_s = \sqrt{W_x^2 + W_y^2}$ with the wind being measured at 10 m above water surface. *Wu,* [1969] has proposed a number of constants and expressions for the air-water resistance coefficient. They are the most broadly used expressions for the air-water resistance coefficient. The expressions are given in a piecewise formulation of the following form:

$$\gamma_w = 1.25\times10^{-3} W_s^{-0.2} \quad (W_s \le 1m/s)$$

$$\gamma_w = 0.5\times10^{-3} W_s^{-0.5} \quad (1m/s < W_s \le 15m/s)$$

$$\gamma_w = 2.6\times10^{-3} \qquad (W_s > 15m/s)$$

3. 2. 2. 5 Bed shear stress:

By assuming a logarithmic velocity profile within the bottom layer, *Lin and Falconer,* [1997] and *Hakimzadeh and Falconer,* [2007] represented the bed shear stress in the following form, as proposed by *French,* [1986]:

$$\frac{\tau_b}{\rho} = u\sqrt{u^2+v^2}\left[2.5\,ln\left(\frac{30d}{2.72k_s}\right)\right]^{-2} \tag{3.21}$$

Where τ_b is the flow induced bed shear stress, d is the thickness of the bottom layer and k_s is roughness length.

For a two-dimensional flow the bed shear stress can be represented in the form of a quadratic friction law, as given by *Henderson,* [1966], as follows:

$$\begin{aligned}\tau_{xb} &= \rho g U\sqrt{U^2+V^2}/C^2 \\ \tau_{yb} &= \rho g V\sqrt{U^2+V^2}/C^2\end{aligned} \tag{3.22}$$

where C is the Chezy roughness coefficient, typically $30m^{1/2}/s < C < 100m^{1/2}/s$. Alternatively, C can be evaluated from the Manning equation of the form:

$$C = \frac{H^{1/6}}{n} \tag{3.23}$$

where n is the Manning roughness coefficient and typically range from 0.012 for smooth lined rives to 0.05 for irregular and vegetated rivers [*Chanson,* 2004]. Even though the Manning's coefficient is mainly used for one-dimensional rivers, this

parameter has been extensively used in two-dimensional flow fields with high level of accuracy often being obtained for complex flow fields [*Falconer et al.*, 2005].

The Colebrook-White equation can be used to give:

$$C = \sqrt{\frac{8g}{f}} = -18\log_{10}\left[\frac{k_s}{12H} + \frac{2.5C}{R_e\sqrt{8g}}\right] \tag{3.24}$$

where f is the Darcy-Weisbach bed resistance coefficient, k_s is the equivalent sand grain roughness, and R_e is the Reynolds number for open channel flow ($\frac{4U_sH}{v}$), where U_s is the fluid speed. For fully rough flow this can be simplified to:

$$C = \sqrt{\frac{8g}{f}} = -18\log_{10}\left[\frac{k_s}{12H}\right]$$

The Colebrook-White equation is better for representing the bed roughness on shallow flood plains, such as wetland systems etc, since it includes Reynolds number flow effects at low Reynolds numbers and incorporates turbulent transitional flow as well as turbulent rough flow [*Falconer*, 1993; *Falconer and Owens*, 1987]. In contrast, the equations that use the Chezy C and Manning n coefficients assume turbulent rough flow only.

3. 3 Advective-Diffusion equation:

In modelling the flux of water quality parameters and suspended sediment concentrations within estuaries and coastal waters, the mass conversation equation can be written in general terms for any constituent introduced into the water column, as given by *Harleman* [1966] and *Falconer et al.* [2005]:

$$\underbrace{\frac{\partial \varphi}{\partial t}}_{1} + \underbrace{\frac{\partial u\varphi}{\partial x} + \frac{\partial v\varphi}{\partial y} + \frac{\partial w\varphi}{\partial z}}_{2} + \underbrace{\frac{\partial}{\partial x}\overline{u'\varphi'} + \frac{\partial}{\partial y}\overline{v'\varphi'} + \frac{\partial}{\partial z}\overline{w'\varphi'}}_{3} = \underbrace{\varphi_s + \varphi_d + \varphi_k}_{4} \qquad (3.25)$$

where u, v and w is the time averaged velocity component in x, y and z direction respectively, φ is the time averaged solute concentration, φ_s is the source or sink solute input (e.g. an outfall), φ_d is the solute decay or growth term, and φ_k is the total kinetic transformation rate for solute. Equation (3.25) is referred to as the advective-diffusion equation. Variable φ can represent a range of parameters, such as salinity, phosphorus, sediment concentration, or a wide range of other water quality parameters. In this section the general form of the advective-diffusion equation is discussed. The specific form of the advective-diffusion equation for phosphorus related to sediment adsorption-necessary for the current study-will be detailed in Chapter 4. The numbered terms in equation (3.25) refer to: (1) local effects; (2) transport by advection; (3) turbulence effects; and (4) source (or sink) terms, including decay (or growth); and kinetic transformation effects.

The cross product terms $\overline{u'\varphi'}, \overline{v'\varphi'}$ and $\overline{w'\varphi'}$ stand for the flux due to the turbulent fluctuations. By analogy with Fick's law of diffusion, which assumes that the mass flux is proportional to the gradient of the mean concentration and the flux is in the direction of decreasing concentration [*Harleman*, 1966], the turbulence diffusion effect can be expressed in following:

$$\left.\begin{aligned}\overline{u'\varphi'} &= -D_{tx}\frac{\partial\varphi}{\partial x}\\ \overline{v'\varphi'} &= -D_{ty}\frac{\partial\varphi}{\partial y}\\ \overline{w'\varphi'} &= -D_{tz}\frac{\partial\varphi}{\partial z}\end{aligned}\right\} \tag{3.26}$$

where D_{tx}, D_{ty}, D_{tz} is the turbulent diffusion coefficients in the x, y, and z directions. For well-mixed estuarine and river flows it is common to assume isotropic turbulence and to approximate the horizontal diffusion terms to the depth mean coefficients as given by *Fischer,* [1973]:

$$D_{tx} = D_{ty} = C_t u_* H \tag{3.27}$$

where C_t is the constant of diffusion, typically assumed to be 0.15, u_* shear velocity given by $u_* = \sqrt{\frac{\tau}{\rho}}$, H total depth of flow and τ is the shear stress.

For the vertical diffusion coefficient, it is common to assume a linear shear stress distribution and a logarithmic velocity profile, which gives [*Falconer et al.*, 2005] and [*Vieira,* 1993]:

$$D_{tz} = u_* \kappa_{von} z\left(1-\frac{z}{H}\right) \tag{3.28}$$

The turbulent diffusion coefficients are regularly related to the turbulent eddy viscosity by Schmidt numbers through the following equation:

$$D_{tx} = \varepsilon_x / \sigma_x, \quad D_{ty} = \varepsilon_y / \sigma_y, \quad D_{tz} = \varepsilon_z / \sigma_z \tag{3.29}$$

where $\sigma_x, \sigma_y, \sigma_z$ is the turbulent Schmidt number in the x, y and z direction respectively, and $\varepsilon_x, \varepsilon_y, \varepsilon_z$ is the eddy viscosity in the x, y and z direction respectively. Experiments have shown that the Schmidt number varies only little

across any flow field and also little from flow to flow [*Rodi*, 2000]. Therefore many models inherently assume that the Schmidt number is a constant, such as *Lin and Falconer*, [1996] with values ranging from 0.5 to 1.0.

3. 3. 1 Sediment transport modelling:

Sediment transport in estuarine and coastal water bodies is governed by the sediment particle properties, settling velocity and the hydrodynamic properties of the flow (including velocity or flow field). Suspended sediments in the water column are transported with the flow and will tend to settle out onto the bed due to gravity. The bottom sediments may also be entrained and suspended due to increased levels of turbulence and increased bed shear stresses. The main aim of this section is to introduce the key formulations used in modelling sediment transport, with these formulations then linked to phosphorus adsorption processes in Chapter 4. It is necessary to understand the phosphorus adsorption onto the sediments and the effects will be studied further in Chapter 7.

3. 3. 1. 1 Suspended sediment transport modelling:

Sediment transport formulations for predicting suspended sediment fluxes in a three-dimensional numerical model are usually based on solving the three-dimensional advective-diffusion equation. This equation for sediment transport processes can be written in a similar manner to equation (3.25) giving:

$$\frac{\partial s}{\partial t}+\frac{\partial us}{\partial x}+\frac{\partial vs}{\partial y}+\frac{\partial (w-w_s s)}{\partial z}-\frac{\partial}{\partial x}\left(D_{tx}\frac{\partial s}{\partial x}\right)-\frac{\partial}{\partial y}\left(D_{ty}\frac{\partial s}{\partial y}\right)-\frac{\partial}{\partial z}\left(D_{tz}\frac{\partial s}{\partial z}\right)=0 \quad (3.30)$$

where s is the suspended sediment concentration at a location x, y, z and w_s is the sediment settling velocity.

In solving the three-dimensional sediment transport equation (3.30), an operator splitting algorithm is used to split the three-dimensional advective-diffusion equation into a vertical one-dimensional equation and a horizontal two-dimensional formulation, as adopted by *Lin and Falconer,* [1996] and *Wu and Falconer*, [2000]. This approach will be discussed in more detail in Chapter 4.

The two-dimensional horizontal advective-diffusion equation for sediment transport can be obtained by integration of equation (3.30) to give:

$$\frac{\partial S}{\partial t}+\frac{\partial US}{\partial x}+\frac{\partial VS}{\partial y}-\frac{\partial}{\partial x}\left(D_{tx}\frac{\partial S}{\partial x}\right)-\frac{\partial}{\partial y}\left(D_{ty}\frac{\partial S}{\partial y}\right)=0 \qquad (3.31)$$

where U, V are the depth averaged velocity components in the x, y direction and S is the depth averaged concentration.

The one-dimensional vertical advective-diffusion equation for sediment transport can be written as:

$$\frac{\partial s}{\partial t}+\frac{\partial(w-w_s s)}{\partial z}-\frac{\partial}{\partial z}\left(D_{tz}\frac{\partial s}{\partial z}\right)=0 \qquad (3.32)$$

with the vertical boundary conditions being as the follows:

At the free surface the vertical sediment flux is zero given as:

$$-w_s S-D_{tz}\frac{\partial S}{\partial z}=0 \qquad (3.33)$$

while at the bed:

$$-w_s S-D_{tz}\frac{\partial S}{\partial z}=E-D \qquad (3.34)$$

where E is the erosion flux rate, D is the deposition flux rate, and E-D net sediment flux rate, which describes the exchange of sediment particles between the water and sediment bed.

The net sediment flux rate for non-cohesive sediment can be expressed in the form [*van Rijn*, 1993]:

$$E - D = w_s(S_{a,e} - S_a) \tag{3.35}$$

where S_a is the sediment concentration at a reference level (i.e. the concentration at an elevation 'a' above bed) and $S_{a,e}$ is the equilibrium sediment concentration at reference level 'a'. The equilibrium concentration is that value which occurs when the sediment flux vertically upwards from the bed due to turbulence is in equilibrium with the net sediment flux downwards attributable to the fall velocity (or gravity). The equilibrium reference concentration used in this study was proposed by *van Rijn*, [1993] and is given as:

$$S_{a,e} = 0.015\frac{D_{50}T^{1.5}}{aD_*^{0.3}} \tag{3.36}$$

where D_{50} is the sediment diameter of which 50% of the bed material is finer, T is the transport stage parameter [*van Rijn,* 1984a] and D_* is the particle parameter.

For cohesive sediment transport, the most widely used expression for the depositional flux is that originally proposed by *Krone,* [1962], see [*Winterwerp and Van Kesteren*, 2004]:

$$D = \begin{cases} w_s S_b \left[1 - \dfrac{\tau_b}{\tau_{c,d}} \right] & \tau_b \le \tau_{c,d} \\ 0 & \tau_b > \tau_{c,d} \end{cases} \tag{3.37}$$

where τ_b in the flow induced bed shear stress, $\tau_{c,d}$ is the critical shear stress for deposition and S_b is the near bed sediment concentration.

While the erosion flux rate can be calculated using the original formulation given by *Partheniades,* [1963], the equations have been recently generalised by *Winterwerp and Van Kesteren,* [2004] to give:

$$E = \begin{cases} M \left[\dfrac{\tau_b - \tau_{c,e}}{\tau_{c,e}} \right]^{n_0} & \tau_b > \tau_{c,e} \\ 0 & \tau_b \le \tau_{c,e} \end{cases} \tag{3.38}$$

where $\tau_{c,e}$ is the critical shear stress for erosion, M is the empirical erosion constant, with reported values being typically in the range of 0.00001 to 0.0005 for soft natural mud [*Falconer and Chen,* 1996] and the exponent n_0 being equated to unity.

Sediment transport formulations for predicting suspended sediment fluxes in depth integrated two-dimensional numerical models are based on solving the depth integrated form of equation (3.30), which can be shown to be of the form:

$$\frac{\partial SH}{\partial t} + \frac{\partial SUH}{\partial x} + \frac{\partial SVH}{\partial y} - \frac{\partial}{\partial x}\left(HD_{xx} \frac{\partial S}{\partial x} \right) - \frac{\partial}{\partial y}\left(HD_{yy} \frac{\partial S}{\partial y} \right) = E - D \tag{3.39}$$

where S is the depth-averaged suspended sediment concentration.

3. 3. 1. 2 Bed load transport:

The bed load sediment flux is calculated using the following equation [*van Rijn*, 1984a, b]:

$$q_b = s_b u_b \delta_b = s_a u_a a \qquad (3.40)$$

where s_b is the bed load concentration, u_b is the velocity of bed load particles, δ_b is the saltation height, and u_a is the effective particle velocity, the is given as $u_a = \alpha u_b$ where $u_b = \left[(1-s)gD_{50}\right]^{0.5} \times 1.5T^{0.6}$ and $\alpha = 2.3$.

3. 4 Summary:

The governing hydrodynamic and solute transport equations have been reviewed in this chapter. The two dimensional and three-dimensional hydrodynamic and solute transport equations have been presented for three-dimensional numerical model studies. Different terms and parameters of mass, momentum and sediment transport equations have been discussed and formulated. It is important to present the governing equations of the model in order to understand the main processes that are solved in any model. Also it is important to understand the sediment transport processes as these will be linked to the phosphorus adsorption processes to be discussed in Chapter 4.

Chapter 4

Numerical Model Details and Model Developments

4. 1 Introduction:

Flow and solute transport processes can be described by the sets of governing equations, as detailed in Chapter 3. These equations are based on the principles of conservation of mass and momentum and only have analytical solutions for idealised cases. Numerical methods provide a valuable tool to approximate the solution of these governing partial differential equations and such tools are increasingly important in environmental water management.

The main aim of this chapter is to give details of the numerical methods and procedures used to solve the governing equations, as mentioned in Chapter 3, in a three-dimensional model named TRIVAST (ThRee-dimensional layer Integrated Velocities And Solute Transport). Details are also given of the main developments made to the source and sink terms for phosphorus of the advection-diffusion equation (explained in Chapter 3), based on experimental work conducted in the Loughor Estuary (U.K.). The development was mainly focused on the sorption processes for phosphorus in the sediments. General details of another three-dimensional model, named ELCOM-CAEDYM (Estuary, Lake and Coastal Ocean Model linked to Computational Aquatic Ecosystem Dynamics Model), is also given and the main differences of both models i.e. (TRIVAST and ELCOM-CAEDYM) are outlined in this chapter, with the main differences between the model predictions between ELCOM-CAEDYM and TRIVAST being investigated in detail in Chapter 8, which are applied to the Arabian Gulf and Kuwait Bay.

4. 2 Numerical solution of the hydrodynamic equations (TRIVAST):

Since TRIVAST is a layer integrated model in which the depth integrated equations are first solved throughout the layer thickness (k), it is important to review the numerical solution of the depth integrated equations. Therefore, in this section the solutions to the depth integrated equations are first addressed, followed by the solution of the layer integrated equations.

4. 2. 1 Depth integrated equations:

In the two-dimensional depth integrated model a regular mesh is used. The discrete variables are represented in a space staggered grid system, as shown in Figure 4.1, where water elevations are defined at the centre of the grid cells and velocity and bed levels below datum are described at the centre of the sides of the grid cells. The Alternating Direction Implicit (ADI) method is used to solve the governing equations, as given in Chapter 3. Each time step is divided into two half time steps. For the first half time step, from time level n to $n+1/2$, values of water elevation and velocity are solved implicitly in the x direction, whereas velocity components in the y direction are expressed explicitly. For the second half time step, from time level $n+1/2$ to $n+1$, values of water elevation and velocity are solved implicitly in the y direction, while velocity components in the x direction are now expressed explicitly.

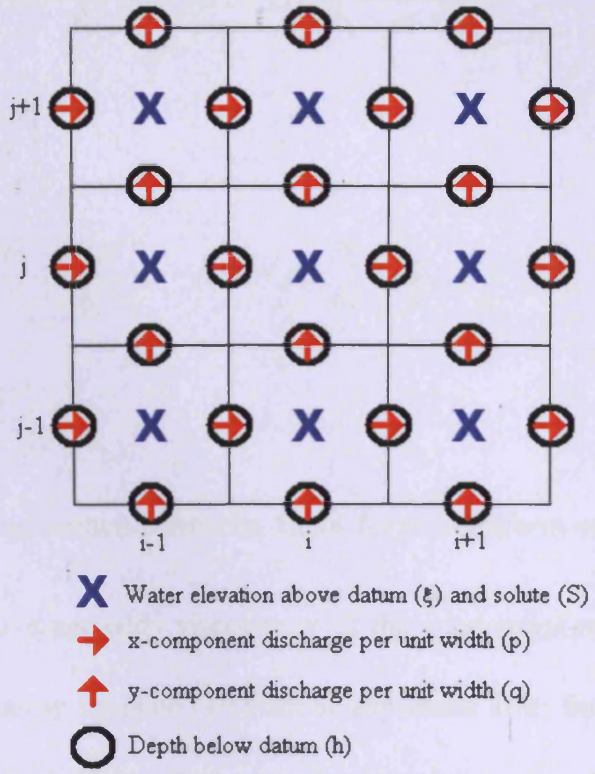

Figure 4.1: Description of the space staggered grid system

The continuity equation (3.1) can be integrated and expanded using Leibniz's rule, that gives the depth integrated continuity equation, as detailed in *Falconer*, [1993]:

$$\frac{\partial \xi}{\partial t} + \frac{\partial p}{\partial x} + \frac{\partial q}{\partial y} = q_m \qquad (4.1)$$

where $p = UH$, $q = VH$; with U, V being the depth averaged velocity components in the x and y directions respectively and H is the total depth of flow $(h+\xi)$ and q_m is the external source or sink discharge per unit area. Similarly, the momentum equations for an incompressible turbulent flow in a cartesian co-ordinate system can be integrated over the depth to give the depth integrated momentum equations, with the detailed derivation being found in *Falconer*, [1993]:

$$\frac{\partial UH}{\partial t}+\beta\left\{\frac{\partial U^2H}{\partial x}+\frac{\partial UVH}{\partial y}\right\}=fVH+gH\frac{\partial \xi}{\partial x}+\frac{\tau_{xw}}{\rho}-\frac{\tau_{xb}}{\rho}$$
$$+\bar{\varepsilon}H\left(\frac{\partial^2U}{\partial x^2}+\frac{\partial^2U}{\partial y^2}\right) \tag{4.2}$$

$$\frac{\partial VH}{\partial t}+\beta\left\{\frac{\partial UVH}{\partial x}+\frac{\partial V^2H}{\partial y}\right\}=-fUH+gH\frac{\partial \xi}{\partial y}+\frac{\tau_{yw}}{\rho}-\frac{\tau_{yb}}{\rho}$$
$$+\bar{\varepsilon}H\left(\frac{\partial^2V}{\partial x^2}+\frac{\partial^2V}{\partial y^2}\right) \tag{4.3}$$

where β is the momentum correction factor for non-uniform vertical velocity profile, $\bar{\varepsilon}$ is the depth average eddy viscosity, τ_w is the wind stress and τ_b is the bed shear stress. The continuity equation (4.1) can be expressed in its finite difference form for the first and second half time steps respectively as follows:

$$\frac{2}{\Delta t}\left(\xi_{i,j}^{n+\frac{1}{2}}-\xi_{i,j}^{n}\right)+\frac{1}{\Delta x}\left(p_{i+\frac{1}{2},j}^{n+\frac{1}{2}}-p_{i-\frac{1}{2},j}^{n+\frac{1}{2}}\right)+\frac{1}{\Delta y}\left(q_{i,j+\frac{1}{2}}^{n}-q_{i,j-\frac{1}{2}}^{n}\right)=q_m \tag{4.4}$$

$$\frac{2}{\Delta t}\left(\xi_{i,j}^{n+1}-\xi_{i,j}^{n+\frac{1}{2}}\right)+\frac{1}{\Delta x}\left(p_{i+\frac{1}{2},j}^{n+\frac{1}{2}}-p_{i-\frac{1}{2},j}^{n+\frac{1}{2}}\right)+\frac{1}{\Delta y}\left(q_{i,j+\frac{1}{2}}^{n+1}-q_{i,j-\frac{1}{2}}^{n+1}\right)=q_m \tag{4.5}$$

where i, j grid point location in the x and y directions respectively and superscripts n, $n+\frac{1}{2}$ and $n+1$ represent time levels at time $t=n\Delta t$, $t=(n+\frac{1}{2})\Delta t$ and $t=(n+1)\Delta t$ respectively, and Δt represents the time step for computations. It can be seen by summing the above two equations that the scheme is fully centred in both time and space over the whole time step, giving second order accuracy in both time and space. The x direction momentum equation (4.2) can be written in the following manner for the first half time step:

$$\frac{p^{n+\frac{1}{2}}_{i+\frac{1}{2},j} - p^{n-\frac{1}{2}}_{i+\frac{1}{2},j}}{\Delta t} + \beta\left[\frac{\left(\hat{U}\,\hat{p}\right)^{n}_{i+\frac{3}{2},j} - \left(\hat{U}\,\hat{p}\right)^{n}_{i-\frac{1}{2},j}}{2\Delta x} + \frac{\left(\overline{\hat{V}}\,\vec{\hat{p}}\right)^{n}_{i+\frac{1}{2},j+\frac{1}{2}} - \left(\overline{\hat{V}}\,\vec{\hat{p}}\right)^{n}_{i+\frac{1}{2},j-\frac{1}{2}}}{\Delta y}\right]$$

$$= fq^{n}_{i+\frac{1}{2},j} - \frac{gH^{n}_{i+\frac{1}{2},j}}{2\Delta x}\left(\xi^{n+\frac{1}{2}}_{i+1,j} + \xi^{n-\frac{1}{2}}_{i+1,j} - \xi^{n+\frac{1}{2}}_{i,j} - \xi^{n-\frac{1}{2}}_{i,j}\right) + \frac{\rho_a}{\rho}\gamma W_x W_s$$

$$- \frac{g\left(p^{n+\frac{1}{2}}_{i+\frac{1}{2},j} + p^{n-\frac{1}{2}}_{i+\frac{1}{2},j}\right)\sqrt{\left(\hat{p}^{n}_{i+\frac{1}{2},j}\right)^2 + \left(\overline{\hat{q}}^{n}_{i+\frac{1}{2},j}\right)^2}}{2\left(H^{n}_{i+\frac{1}{2},j}\,C^{n}_{i+\frac{1}{2},j}\right)^2}$$

$$+ \bar{\varepsilon}\,H\left[\frac{\hat{U}^{n}_{i+\frac{3}{2},j} - 2\cdot\hat{U}^{n}_{i+\frac{1}{2},j} + \hat{U}^{n}_{i-\frac{1}{2},j}}{\Delta x^2} + \frac{\hat{U}^{n}_{i+\frac{1}{2},j+1} - 2\cdot\hat{U}^{n}_{i+\frac{1}{2},j} + \hat{U}^{n}_{i+\frac{1}{2},j-1}}{\Delta y^2}\right] \qquad (4.6)$$

where $\hat{U}$ denotes a value corrected by iteration, by setting:

$$\hat{U}^{n} = \begin{cases} U^{n-\frac{1}{2}} \\ \frac{1}{2}\left(U^{n-\frac{1}{2}} + U^{n+\frac{1}{2}}\right) \end{cases} \qquad (4.7)$$

$\overline{\hat{V}}$ represents a value obtained by averaging the corresponding values for the surrounding grid points:

$$\overline{\hat{V}}^{n}_{i+\frac{1}{2},j+\frac{1}{2}} = \frac{1}{2}\left(V^{n}_{i,j+\frac{1}{2}} + V^{n}_{i+1,j+\frac{1}{2}}\right) \qquad (4.8)$$

and $\vec{\hat{p}}$ denotes a value obtained from the upwind algorithm where

$$\vec{\hat{p}}^{n}_{i+\frac{1}{2},j} = \begin{cases} p^{n}_{i+\frac{1}{2},j-1} & \text{if } V^{n}_{i+\frac{1}{2},j} > 0 \\ p_{i+\frac{1}{2},j+1} & \text{if } V^{n}_{i+\frac{1}{2},j} < 0 \end{cases} \qquad (4.9)$$

Similarly, the y direction momentum equation (4.3) can be written for the second half time step as:

$$\frac{q^{n+1}_{i,j+\frac{1}{2}} - q^{n}_{i,j+\frac{1}{2}}}{\Delta t} + \beta\left[\frac{\left(\hat{V}\hat{q}\right)^{n+\frac{1}{2}}_{i,j+\frac{3}{2}} - \left(\hat{V}\hat{q}\right)^{n+\frac{1}{2}}_{i,j-\frac{1}{2}}}{2\Delta y} + \frac{\left(\bar{U}\hat{\vec{q}}\right)^{n+\frac{1}{2}}_{i+\frac{1}{2},j+\frac{1}{2}} - \left(\bar{U}\hat{\vec{q}}\right)^{n+\frac{1}{2}}_{i-\frac{1}{2},j+\frac{1}{2}}}{\Delta x}\right]$$

$$= -f \cdot p^{n+\frac{1}{2}}_{i,j+\frac{1}{2}} - \frac{gH^{n+\frac{1}{2}}_{i+\frac{1}{2},j}}{2\Delta y}\left(\xi^{n+1}_{i,j+1} + \xi^{n}_{i,j+1} - \xi^{n+1}_{i,j} - \xi^{n}_{i,j}\right) + \frac{\rho_a}{\rho}\gamma W_y W_s$$

$$- \frac{g\left(q^{n+1}_{i,j+\frac{1}{2}} + q^{n}_{i,j+\frac{1}{2}}\right)\sqrt{\left(q^{n+\frac{1}{2}}_{i,j+\frac{1}{2}}\right)^2 + \left(\bar{p}^{n+\frac{1}{2}}_{i,j+\frac{1}{2}}\right)^2}}{2\left(H^{n+\frac{1}{2}}_{i,j+\frac{1}{2}} C^{n+\frac{1}{2}}_{i,j+\frac{1}{2}}\right)^2}$$

$$+ \bar{\varepsilon} H\left[\frac{\hat{V}^{n}_{i+1,j+\frac{1}{2}} - 2\cdot\hat{V}^{n}_{i,j+\frac{1}{2}} + \hat{V}^{n}_{i-1,j+\frac{1}{2}}}{\Delta x^2} + \frac{\hat{V}^{n}_{i,j+\frac{3}{2}} - 2\cdot\hat{V}^{n}_{i,j+\frac{1}{2}} + \hat{V}^{n}_{i,j-\frac{1}{2}}}{\Delta y^2}\right] \qquad (4.10)$$

Rearranging equation (4.4) gives:

$$a_{2i-1} p^{n+\frac{1}{2}}_{i-\frac{1}{2},j} + b_{2i-1}\xi^{n+\frac{1}{2}}_{i,j} + c_{2i-1} p^{n+\frac{1}{2}}_{i+\frac{1}{2},j} = d_{2i-1} \qquad (4.11)$$

where

$$a_{2i-1} = -\frac{\Delta t}{\Delta x}$$

$$b_{2i-1} = 2$$

$$c_{2i-1} = \frac{\Delta t}{\Delta x}$$

$$d_{2i-1} = 2\xi^{n}_{i,j} - \frac{\Delta t}{\Delta y}\left(q^{n}_{i,j+\frac{1}{2}} - q^{n}_{i,j-\frac{1}{2}}\right) + \Delta t q_m$$

Rearranging equation (4.6) gives:

$$a_{2i}\xi^{n+\frac{1}{2}}_{i,j} + b_{2i} p^{n+\frac{1}{2}}_{i+\frac{1}{2},j} + c_{2i}\xi^{n+\frac{1}{2}}_{i+1,j} = d_{2i} \qquad (4.12)$$

where

$$a_{2i} = -gH\frac{\Delta t}{\Delta x}$$

$$b_{2i} = 2 + \Delta t \frac{g\sqrt{\left(\hat{p}^{n}_{i+\frac{1}{2},j}\right)^2 + \left(\bar{q}^{n}_{i+\frac{1}{2},j}\right)^2}}{\left[(HC)^{n}_{i+\frac{1}{2},j}\right]^2}$$

$$c_{2i} = gH\frac{\Delta t}{\Delta x}$$

$$\begin{aligned} d_{2i} = & \left(2 - \Delta t \frac{g\sqrt{\left(\hat{p}^{n}_{i+\frac{1}{2},j}\right)^2 + \left(\bar{q}^{n}_{i+\frac{1}{2},j}\right)^2}}{\left[(HC)^{n}_{i+\frac{1}{2},j}\right]^2}\right) p^{n-\frac{1}{2}}_{i+\frac{1}{2}} \\ & - gH\frac{\Delta t}{\Delta x}\left(\xi^{n-\frac{1}{2}}_{i+1,j} - \xi^{n-\frac{1}{2}}_{i,j}\right) \\ & - \beta\left[\frac{\Delta t}{\Delta x}\left(\hat{(pU)}^{n}_{i+\frac{3}{2},j} - \hat{(pU)}^{n}_{i-\frac{1}{2},j}\right) + \frac{2\Delta t}{\Delta y}\left(\hat{(\vec{p}\bar{V})}^{n}_{i+\frac{1}{2},j+\frac{1}{2}} - \hat{(\vec{p}\bar{V})}^{n}_{i+\frac{1}{2},j-\frac{1}{2}}\right)\right] \\ & + 2\bar{\varepsilon} H\left[\frac{\Delta t}{\Delta x^2}\left(\hat{U}^{n}_{i+\frac{3}{2},j} - 2\hat{U}^{n}_{i+\frac{1}{2},j} + \hat{U}^{n}_{i-\frac{1}{2},j}\right) + \frac{\Delta t}{\Delta y^2}\left(\hat{U}^{n}_{i+\frac{1}{2},j+1} - 2\hat{U}^{n}_{i+\frac{1}{2},j} + \hat{U}^{n}_{i+\frac{1}{2},j-1}\right)\right] \\ & + 2\Delta t\frac{\rho_a}{\rho}\gamma W_x W_s + 2\Delta t \cdot f \cdot q^{n}_{i+\frac{1}{2},j} \end{aligned}$$

Similar rearranging can be made to equation (4.5) and (4.10) to give:

$$a_{2j-1}q^{n+1}_{i,j-\frac{1}{2}} + b_{2j-1}\xi^{n+1}_{i,j} + c_{2j-1}q^{n+1}_{i,j+\frac{1}{2}} = d_{2j-1} \qquad (4.13)$$

where

$$a_{2j-1} = -\frac{\Delta t}{\Delta y}$$

$$b_{2j-1} = 2$$

$$c_{2j-1} = \frac{\Delta t}{\Delta y}$$

$$d_{2j-1} = 2\xi_{i,j}^{n+\frac{1}{2}} - \frac{\Delta t}{\Delta x}\left(p_{i+\frac{1}{2},j}^{n+\frac{1}{2}} - p_{i-\frac{1}{2},j}^{n+\frac{1}{2}} \right) + \Delta t q_m$$

and

$$a_{2j}\xi_{i,j}^{n+1} + b_{2j}q_{i,j+\frac{1}{2}}^{n+1} + c_{2j}\xi_{i,j+1}^{n+1} = d_{2j} \qquad (4.14)$$

where

$$a_{2j} = -gH\frac{\Delta t}{\Delta y}$$

$$b_{2j} = 2 + \Delta t \frac{g\sqrt{\left(\bar{p}_{i,j+\frac{1}{2}}^{n+\frac{1}{2}}\right)^2 + \left(\hat{q}_{i,j+\frac{1}{2}}^{n+\frac{1}{2}}\right)^2}}{\left[(HC)_{i,j+\frac{1}{2}}^{n+\frac{1}{2}}\right]^2}$$

$$c_{2j} = gH\frac{\Delta t}{\Delta y}$$

$$d_{2j} = \left(2 - \Delta t \frac{g\sqrt{\left(\overline{p}^{\,n+\frac{1}{2}}_{i,j+\frac{1}{2}}\right)^2 + \left(\hat{q}^{\,n+\frac{1}{2}}_{i,j+\frac{1}{2}}\right)^2}}{\left[(HC)^{n+\frac{1}{2}}_{i,j+\frac{1}{2}}\right]^2} \right) q^n_{i,j+\frac{1}{2}}$$

$$- gH\frac{\Delta t}{\Delta y}\left(\xi^n_{i,j+1} - \xi^n_{i,j}\right)$$

$$- \beta\left[\frac{2\Delta t}{\Delta x}\left(\hat{\overline{pU}}^{\,n+\frac{1}{2}}_{i+\frac{1}{2},j+\frac{1}{2}} - \hat{\overline{pU}}^{\,n+\frac{1}{2}}_{i-\frac{1}{2},j+\frac{1}{2}}\right) + \frac{\Delta t}{\Delta y}\left(\hat{q}\hat{V}^{\,n+\frac{1}{2}}_{i,j+\frac{3}{2}} - \hat{q}\hat{V}^{\,n+\frac{1}{2}}_{i,j-\frac{1}{2}}\right)\right]$$

$$+ 2\overline{\varepsilon}\, H\left[\frac{\Delta t}{\Delta x^2}\left(\hat{V}^{\,n+\frac{1}{2}}_{i+1,j+\frac{1}{2}} - 2\hat{V}^{\,n+\frac{1}{2}}_{i,j+\frac{1}{2}} + \hat{V}^{\,n+\frac{1}{2}}_{i-1,j+\frac{1}{2}}\right) + \frac{\Delta t}{\Delta y^2}\left(\hat{V}^{\,n+\frac{1}{2}}_{i,j+\frac{3}{2}} - 2\hat{V}^{\,n+\frac{1}{2}}_{i,j+\frac{1}{2}} + \hat{V}^{\,n+\frac{1}{2}}_{i,j-\frac{1}{2}}\right)\right]$$

$$+ 2\Delta t\frac{\rho_a}{\rho}\gamma W_y W_s - 2\Delta t \cdot f \cdot p^{\,n+\frac{1}{2}}_{i,j+\frac{1}{2}}$$

These equations can be expressed in a matrix form as follows:

$$\begin{bmatrix} b_1 & c_1 & & & & & \\ a_2 & b_2 & c_2 & & & & \\ & a_3 & b_3 & c_3 & & & \\ & & \cdots & \cdots & \cdots & & \\ & & & \cdots & \cdots & \cdots & \\ & & & & a_{2i-1} & b_{2i-1} & c_{2i-1} \\ & & & & & a_{2i} & b_{2i} \end{bmatrix} \begin{bmatrix} \xi_{1,j} \\ p_{\frac{1}{2},j} \\ \xi_{2,j} \\ \cdots \\ \cdots \\ \xi_{i,j} \\ p_{i+\frac{1}{2},j} \end{bmatrix}^{\frac{1}{2}} = \begin{bmatrix} d_1 \\ d_2 \\ d_3 \\ \cdots \\ \cdots \\ d_{2i-1} \\ d_{2i} \end{bmatrix} \qquad (4.15)$$

This gives a tri-diagonal matrix that can be solved using the Thomas algorithm to give $\xi^{n+\frac{1}{2}}_{i,j}$ and $p^{n+\frac{1}{2}}_{i,j}$. A similar procedure can be used to obtain $\xi^{n+1}_{i,j}$ and $q^{n+1}_{i,j}$.

4. 2. 2 Layer-integrated equations:

In the three-dimensional layer integrated model, a regular square mesh is used in the horizontal plane, while an irregular mesh is used for the vertical layers. Figure 4.2

illustrates the location of the various variables for the three-dimensional finite difference mesh in the vertical plane.

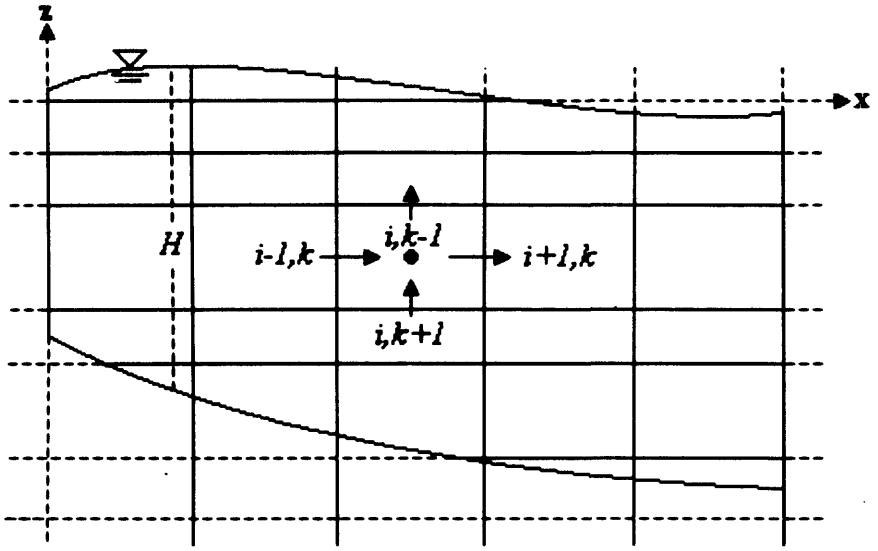

Figure 4.2: Vertical grid system

In the horizontal plane the discretised values for the variables are located in the same positions as for the two-dimensional depth integrated model (see Figure 4.1). The layer integrated governing equations are solved using a combined explicit and implicit scheme. The vertical diffusion terms were treated implicitly, whilst the remaining terms were treated explicitly [*Lin and Falconer*, 1997]. For the first half time step the depth integrated equations are first solved to obtain the water elevation field across the domain, as explained in section 4.2.1. The layer integrated equations in the x direction are solved using the water elevations obtained from solving the depth integrated equations. *Lin and Falconer* [1997] expressed the momentum equation in the x direction for the three-dimensional model as follows:

$$\frac{\partial(u_k h_k)}{\partial t} - \left[\left(\varepsilon_v \frac{\partial u}{\partial z}\right)_{k-\frac{1}{2}} - \left(\varepsilon_v \frac{\partial u}{\partial z}\right)_{k+\frac{1}{2}}\right] = S_{xo} \qquad (4.16)$$

where S_{xo} represents the terms treated explicitly. The following is the finite difference representation for equation (4.16):

$$\left((uh)_k^{n+\frac{1}{2}} - (uh)_k^{n-\frac{1}{2}}\right)$$
$$-\Delta t\left(\frac{\varepsilon_v}{h}\right)_{k-\frac{1}{2}}\left[\left(u_{k-1}^{n+\frac{1}{2}} - u_k^{n+\frac{1}{2}}\right)+\left(u_{k-1}^{n-\frac{1}{2}} - u_k^{n-\frac{1}{2}}\right)\right]/2 \qquad (4.17)$$
$$+\Delta t\left(\frac{\varepsilon_v}{h}\right)_{k+\frac{1}{2}}\left[\left(u_k^{n+\frac{1}{2}} - u_{k+1}^{n+\frac{1}{2}}\right)+\left(u_k^{n-\frac{1}{2}} - u_{k+1}^{n-\frac{1}{2}}\right)\right]/2 = S_x$$

where

$$S_x = ADV + COR + PRE + DIF + VTC$$

where

$$ADV = -\frac{\Delta t}{\Delta x}\left[u'q_x'\Big|_{i+1,j,k}^{n} - u'q_x'\Big|_{i,j,k}^{n} + q_y\Big|_{i+\frac{1}{2},j+\frac{1}{2},k}^{n} u'\Big|_{i+\frac{1}{2},j+\frac{1}{2},k}^{n} - q_y\Big|_{i+\frac{1}{2},j-\frac{1}{2},k}^{n} u'\Big|_{i+\frac{1}{2},j-\frac{1}{2},k}^{n}\right]$$

$$COR = \Delta t \cdot f \cdot q_y\Big|_{i+\frac{1}{2},j,k}^{n}$$

$$PRE = -\frac{g\Delta t}{2\Delta x} h^n_{i+\frac{1}{2},j,k}\left[\xi_{i+1,j}^{n+\frac{1}{2}} + \xi_{i+1,j}^{n-\frac{1}{2}} - \xi_{i,j}^{n+\frac{1}{2}} - \xi_{i,j}^{n+\frac{1}{2}}\right]$$

$$DIF = \frac{\Delta t}{(\Delta x)^2}\left\{\begin{aligned}&2\left[\varepsilon_h h^n_{i+1,j,k}\left(u'_{i+\frac{3}{2},j,k} - u'_{i+\frac{1}{2},j,k}\right) - \varepsilon_h h^n_{i,j,k}\left(u'_{i+\frac{1}{2},j,k} - u'_{i-\frac{1}{2},j,k}\right)\right]\\ &+\left[\varepsilon_h h^n_{i+\frac{1}{2},j+\frac{1}{2},k}\left(u'_{i+\frac{1}{2},j+1,k} - u'_{i+\frac{1}{2},j,k}\right) - \varepsilon_h h^n_{i+\frac{1}{2},j-\frac{1}{2},k}\left(u'_{i+\frac{1}{2},j,k} - u'_{i+\frac{1}{2},j-1,k}\right)\right]\\ &+\left[\varepsilon_h h^n_{i+1,j,k}\left(v_{i+\frac{3}{2},j,k} - v_{i+\frac{1}{2},j,k}\right) - \varepsilon_h h^n_{i,j,k}\left(v_{i+\frac{1}{2},j,k} - v_{i-\frac{1}{2},j,k}\right)\right]\end{aligned}\right\}$$

$$VTC = \Delta t\left[\left(wu'\right)_{i+\frac{1}{2},j,k+\frac{1}{2}} - \left(wu'\right)_{i+\frac{1}{2},j,k-\frac{1}{2}}\right]$$

Rearranging gives:

$$p_k u_{k-1}^{n+\frac{1}{2}} + q_k u_k^{n+\frac{1}{2}} + r_k u_{k+1}^{n+\frac{1}{2}} = s_k + S_x \qquad (4.18)$$

where

$$p_k = -\frac{\Delta t}{2}\left(\frac{\varepsilon_v}{h}\right)_{k-\frac{1}{2}}$$

$$q_k = h_k + \frac{\Delta t}{2}\left[\left(\frac{\varepsilon_v}{h}\right)_{k-\frac{1}{2}} + \left(\frac{\varepsilon_v}{h}\right)_{k+\frac{1}{2}}\right]$$

$$r_k = -\frac{\Delta t}{2}\left(\frac{\varepsilon_v}{h}\right)_{k+\frac{1}{2}}$$

$$s_k = h_k u_k^{n-\frac{1}{2}} + \frac{\Delta t}{2}\left\{\begin{array}{l}\left(\frac{\varepsilon_v}{h}\right)_{k-\frac{1}{2}} u_{k-1}^{n-\frac{1}{2}} \\ -\left[\left(\frac{\varepsilon_v}{h}\right)_{k-\frac{1}{2}} + \left(\frac{\varepsilon_v}{h}\right)_{k+\frac{1}{2}}\right] u_k^{n-\frac{1}{2}} \\ +\left(\frac{\varepsilon_v}{h}\right)_{k+\frac{1}{2}} u_{k+1}^{n-\frac{1}{2}}\end{array}\right\}$$

where $u^{n+\frac{1}{2}}{}_{i,j,k}$ is the velocity component in the x direction at the k_{th} layer. Equation (4.18) can be expressed in matrix form for the different layers, where $k = 1$ for the surface and $k = k_{max}$ for the bottom layer:

$$\begin{bmatrix} q_1 & r_1 & & & & \\ p_2 & q_2 & r_2 & & & \\ & \cdots & \cdots & \cdots & & \\ & & \cdots & \cdots & \cdots & \\ & & & p_{k-1} & q_{k-1} & r_{k-1} \\ & & & & p_k & q_k \end{bmatrix} \begin{Bmatrix} u_{i,j,1} \\ u_{i,j,2} \\ \cdots \\ \cdots \\ u_{i,j,k-1} \\ u_{i,j,k} \end{Bmatrix} = \begin{Bmatrix} s_1 \\ s_2 \\ \cdots \\ \cdots \\ s_{k-1} \\ s_k \end{Bmatrix} \qquad (4.19)$$

As before the Thomas algorithm has been used to solve this tri-diagonal matrix to obtain the velocity in the x direction. Once the water elevations and velocity component in the x direction have been solved, then the vertical velocity w can be determined everywhere for each layer across the computational domain by utilising

the continuity equation. The finite difference continuity equation used for the first half time step to obtain w can be obtained as follows:

$$w^{n+\frac{1}{2}}_{i,j,k-\frac{1}{2}} = w^{n+\frac{1}{2}}_{i,j,k+\frac{1}{2}} - \frac{h^{n+\frac{1}{2}}_{i,j,k+\frac{1}{2}} + h^{n+\frac{1}{2}}_{i,j,k-\frac{1}{2}}}{2\Delta x}\left[(uh)\Big|^{n+\frac{1}{2}}_{i+\frac{1}{2},j,k} - (uh)\Big|^{n+\frac{1}{2}}_{i-\frac{1}{2},j,k}\right] - \frac{h^{n}_{i,j,k+\frac{1}{2}} + h^{n}_{i,j,k-\frac{1}{2}}}{2\Delta y}\left[(vh)\Big|^{n}_{i+\frac{1}{2},j,k} - (vh)\Big|^{n}_{i-\frac{1}{2},j,k}\right] \tag{4.20}$$

For the bottom layer, where $k = k_{max}$, the vertical velocity is zero:

$$w^{n+\frac{1}{2}}_{i,j,k+\frac{1}{2}} = 0 \tag{4.21}$$

For the second half-time step, the same procedure is followed to calculate the velocity components in the y and z directions.

4. 3 Numerical solution of advection-diffusion equation (TRIVAST):

The three-dimensional advective-diffusion equation (3.25) in Chapter 3 is repeated here for completeness giving:

$$\frac{\partial \varphi}{\partial t} + \frac{\partial u\varphi}{\partial x} + \frac{\partial v\varphi}{\partial y} + \frac{\partial (w - w_s\varphi)}{\partial z} - \frac{\partial}{\partial x}\left(D_{tx}\frac{\partial \varphi}{\partial x}\right) - \frac{\partial}{\partial y}\left(D_{ty}\frac{\partial \varphi}{\partial y}\right) - \frac{\partial}{\partial z}\left(D_{tz}\frac{\partial \varphi}{\partial z}\right) = \varphi_o \tag{4.22}$$

This equation includes the three main terms of: advection, dispersion-diffusion and source or sink terms. In solving this three-dimensional equation, an operator splitting algorithm, as proposed by *Lin and Falconer*, [1996] and *Wu and Falconer*, [2000], has been used to split the three-dimensional advective-diffusion terms into a vertical one-dimensional and a horizontal two-dimensional set of equations. The three-dimensional equation is split into the following equations:

$$\frac{\partial \varphi}{\partial t}+\frac{\partial (w-w_s\varphi)}{\partial z}-\frac{\partial}{\partial z}\left(D_{tz}\frac{\partial \varphi}{\partial z}\right)=0 \qquad (4.23)$$

and

$$\frac{\partial \varphi \Delta z}{\partial t}+\frac{\partial u\Delta z}{\partial x}+\frac{\partial v\Delta z}{\partial y}-\frac{\partial}{\partial x}\left(\Delta z D_{tx}\frac{\partial \varphi}{\partial x}\right)-\frac{\partial}{\partial y}\left(\Delta z D_{ty}\frac{\partial \varphi}{\partial y}\right)=\Delta z\varphi_o \qquad (4.24)$$

The layer-integrated two-dimensional advective-diffusion equation (4.24) is first solved horizontally, and then the one-dimensional vertical advective-diffusion equation (4.23) is solved for the *z* direction.

For the layer-integrated equation, the ULTIMATE QUICKEST scheme is used for the advection term, the central difference scheme for the diffusion terms and the Euler method for the source and sink terms. For the vertical one-dimensional advective-diffusion equation, this equation is solved using a non-uniform grid in the vertical direction. Since the diffusion process is the key term in this equation, and also some of the grid sizes are very small near the sea bed and water surface, then this equation is solved using a centred implicit method to avoid the use of a very small time step. The discretised equation is then expressed in the following form:

$$-a_{T,k}\varphi_{k-1}^{n+1}+a_{p,k}\varphi_k^{n+1}-a_{B,k}\varphi_{k+1}^{n+1}=b_k \qquad (4.25)$$

where

$$a_{T,k}=D_{tz}^{T}A\left(|P_e^{T}|\right)+\left[F^{T},0\right],$$

$$a_{B,k}=D_{tz}^{B}A\left(|P_e^{B}|\right)+\left[-F^{B},0\right],$$

$$a_{p,k}=a_T+a_B+\frac{\Delta z}{\Delta t},$$

$$b_k=\frac{\Delta z}{\Delta t}\varphi_k^n$$

and

$$A(|P_e|) = \left[0,(1-0.1|P_e|)^5\right]$$

$$P_e = \frac{w - w_s}{D_{tz}} \Delta z$$

where the symbol $[a,b]$ is used to denote the greater of a and b, T and B denote the top and bottom control volume faces, P_e is the grid Peclet number and F is the mass flow rate. These finite difference equations are arranged in a matrix form, giving a tri-diagonal matrix, which is solved using the Thomas algorithm.

4. 4 Boundary conditions (TRIVAST):

In general, two types of boundary conditions exist, the first type being a closed boundary (also frequently known as a wall boundary condition) and the second type being an open boundary. For the three-dimensional modelling study, precise surface and bed boundary conditions also need to be specified.

4. 4. 1 Closed boundary condition:

For a closed boundary condition as shown in Figure 4.3, no flow is allowed to pass across the boundary, so for the closed boundary condition:

$$V_i = 0 \quad (i = 1,2,3,4) \tag{4.26}$$

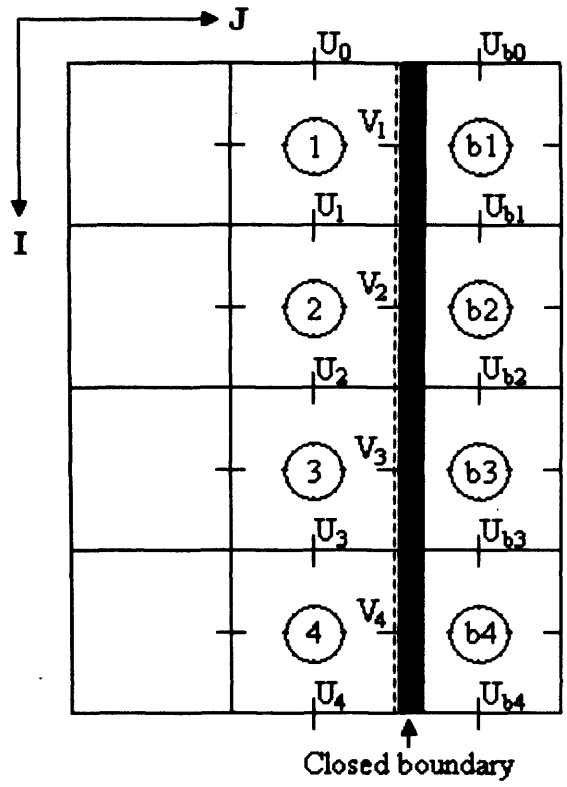

Figure 4.3: Closed boundary condition

For the velocity component parallel to the closed boundary, this can be expressed as follows:

$$U_{bi} = \lambda U_i \quad (i = 0,1,2,3,4) \tag{4.27}$$

where $\lambda = -1$ for a no-slip boundary, $\lambda = 1$ for a free-slip boundary, and $0 < \lambda < 1$ for a partial slip boundary. The closed boundary condition for a solute is:

$$\left.\frac{\partial \varphi}{\partial n}\right|_w = 0 \text{ and } \left.\frac{\partial \varphi^2}{\partial n^2}\right|_w = 0$$

This means that there is no solute flux across a wall boundary. The subscript w indicates that the value was taken from the wall boundary, while n indicates that the direction is perpendicular to the wall.

4. 4. 2 Open boundary condition:

For an open boundary condition both flow and solute fluxes were permitted across the boundaries. Thus suitable hydrodynamic and solute flux conditions needed to be satisfied, in the form of measured water surface levels, velocities and solute concentration values. If the open boundary was a flow boundary and the velocities at the boundary were defined, as indicated in Figure 4.4, then the following boundary condition could be obtained for the hydrodynamic conditions:

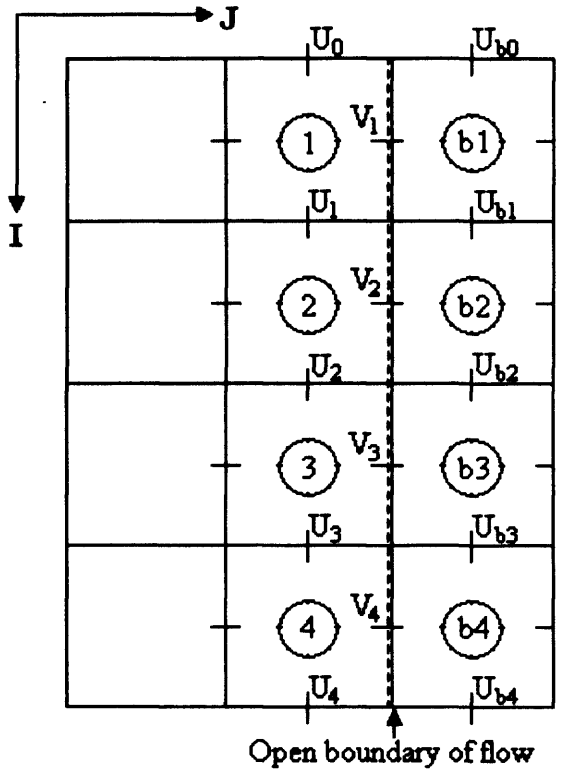

Figure 4.4: Flow boundary condition

$$\begin{cases} U_i = U_{bi} & (i=0,1,2,3,4) \\ V_i = V_{bi} & (i=1,2,3,4) \end{cases} \tag{4.28}$$

If the open boundary condition was a water elevation, as indicated in Figure 4.5, then the following condition could be obtained for the hydrodynamic conditions:

$$\begin{cases} V_i = V_{ai} & (i=1,2,3,4) \\ U_i = U_{ai} & (i=0,1,2,3,4) \\ \xi_i = \xi_{bi} & (i=1,2,3,4) \end{cases} \tag{4.29}$$

where ξ_{bi} is the known water level at the open boundary.

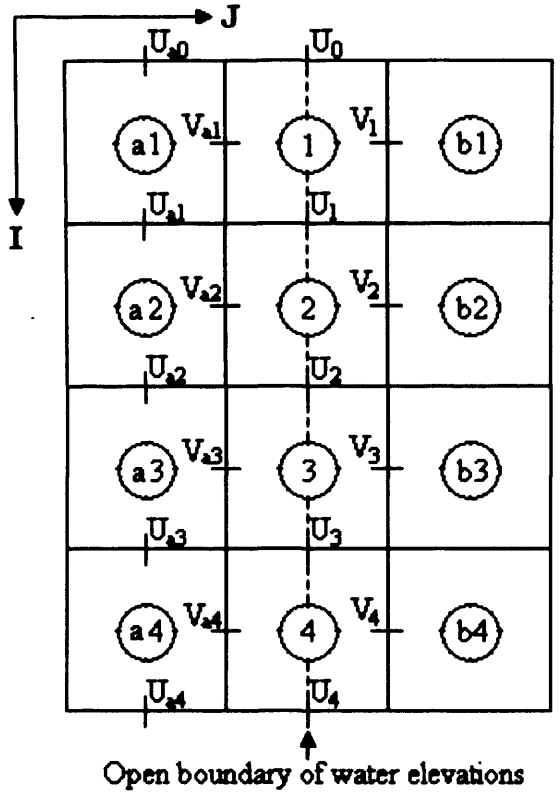

Figure 4.5: Water elevation boundary condition

Similarly, solute concentration values at the open boundary were described from known boundary value, φ_{bi} on the incoming tide as given below:

$$\varphi_i = \varphi_{bi} \quad (i=1,2,3,4) \tag{4.30}$$

and by extrapolation on the outgoing tide as given in *Falconer and Lin,* [1997].

4. 4. 3 Free surface boundary condition:

For the three-dimensional model, at the free surface boundary the shear stress is set to the wind shear stress, as given by:

$$\begin{aligned} \tau_{xz}\big|_{\xi} &= \rho_a \gamma_w W_x \sqrt{W_x^2 + W_y^2} \\ \tau_{yz}\big|_{\xi} &= \rho_a \gamma_w W_y \sqrt{W_x^2 + W_y^2} \end{aligned} \tag{4.31}$$

The surface boundary condition for the advective-diffusion terms is to set the solute flux across the free surface to zero, giving:

$$(w - w_s)\varphi - D_{tz}\frac{\partial \varphi}{\partial z} = 0 \tag{4.32}$$

4. 4. 4 Bed boundary condition:

For the bed boundary condition, a no-slip boundary is applied, with the corresponding velocity components at the bed being set to zero, giving:

$$\begin{cases} \overline{u}_{i,j,k_{max}+\frac{1}{2}} = 0 \\ \overline{v}_{i,j,k_{max}+\frac{1}{2}} = 0 \\ \overline{w}_{i,j,k_{max}+\frac{1}{2}} = 0 \end{cases} \tag{4.33}$$

For the bed shear stress a logarithmic velocity profile was assumed within the bottom layer, as suggested in *French,* [1986], representing the bed shear stress and as written in the following form, given by *Lin and Falconer*, [1997]:

$$\frac{\tau_b}{\rho} = \left| \frac{u_{k\,max}^{n+1/2} + u_{k\,max}^{n-1/2}}{2} \right| \left| \frac{u_{k\,max}^{n+1/2} + u_{k\,max}^{n-1/2}}{2} \right| \left[2.5 ln\left(\frac{30d}{2.72k_s} \right) \right]^{-2}$$

where d is the thickness of the bottom layer, and k_s is roughness height.

4. 5 Source and sink of solutes in TRIVAST based on QUAL2E:

QUAL2E is a comprehensive and adaptable stream water quality model used in TRIVAST. It represents the source and sink terms of various water quality parameters in the advection diffusion equation (3.25) for solutes. In the following sections a brief description of the source and sink terms will be given of dissolved oxygen (DO), nitrogen (N), including: ammonia (NH_4), nitrate (NO_3) and organic nitrogen (ON), and phosphorus (P) including: PO_4^{-3} in dissolved form and organic phosphorus (OP). Also, the development of PO_4^{-3} source and sink terms linked to the sediment transport model will be presented. This includes the effects of the sediment grain size on phosphorus sorption, based on experimental findings. Such effects will be incorporated into TRIVAST to model PO_4^{-3} levels in Kuwait Bay, with details of the model predictions being discussed in Chapter 7.

4. 5. 1 Dissolved oxygen (DO):

DO is a basic requirement for a healthy aquatic ecosystem and is one of the most important parameters of water quality that most marine species rely on heavily to survive. The DO balance in a stream system depends on the capacity of the stream to re-aerate itself. This capacity is a function of the advection and diffusion processes occurring within the system and the internal sources and sinks of DO. The main sources of DO, in addition to atmospheric re-aeration, are the oxygen produced by photosynthesis and the DO contained in the incoming flow. The sinks of DO include biochemical oxidation of carbonaceous and nitrogenous organic matter, benthic oxygen demand and the oxygen utilised by algae respiration [*Bowie et al.,* 1985]. The general DO cycle is summarised in Figure 4.6. The differential equation used in QUAL2E to describe the rate of change of DO is given as:

$$\frac{dDO}{dt} = K_2(DO^* - DO) + (\alpha_3\mu - \alpha_4\rho)A - K_1L - \frac{K_4}{d} - \alpha_5\beta_1 NH_4 - \alpha_6\beta_2 NO_3 \quad (4.34)$$

where DO is the dissolved oxygen concentration (mg/l), K_2 is the re-aeration rate (/day), DO^* is the saturation concentration of dissolved oxygen (mg/l), α_3 is the rate of oxygen production per unit of algal photosynthesis (mg O/mg A), μ is the algal growth rate, which is temperature dependant (/day), α_4 is the rate of oxygen uptake per unit of algae respired (mg O/mg A), ρ is the algal respiration rate, which is temperature dependant (/day), A is the algal biomass concentration (mg/l), K_1 is the carbonaceous biological oxygen demand (BOD) deoxygenation rate (/day), L is the concentration of ultimate carbonaceous biological oxygen demand BOD (mg/l), K_4 is the sediment oxygen demand rate (g/m^2 day), d is the mean stream depth (m), α_5 is the rate of oxygen uptake per unit of ammonia nitrogen (mg O/mg N), β_1 is the ammonia oxidation rate coefficient, which is temperature dependant (/day), NH_4 is the ammonia nitrogen concentration (mg/l), α_6 is the rate of oxygen uptake per unit of nitrite nitrogen (mg O/mg N), β_2 is the nitrite oxidation rate coefficient, which is temperature dependant (/day) and NO_3 is nitrate nitrogen concentration (mg/l).

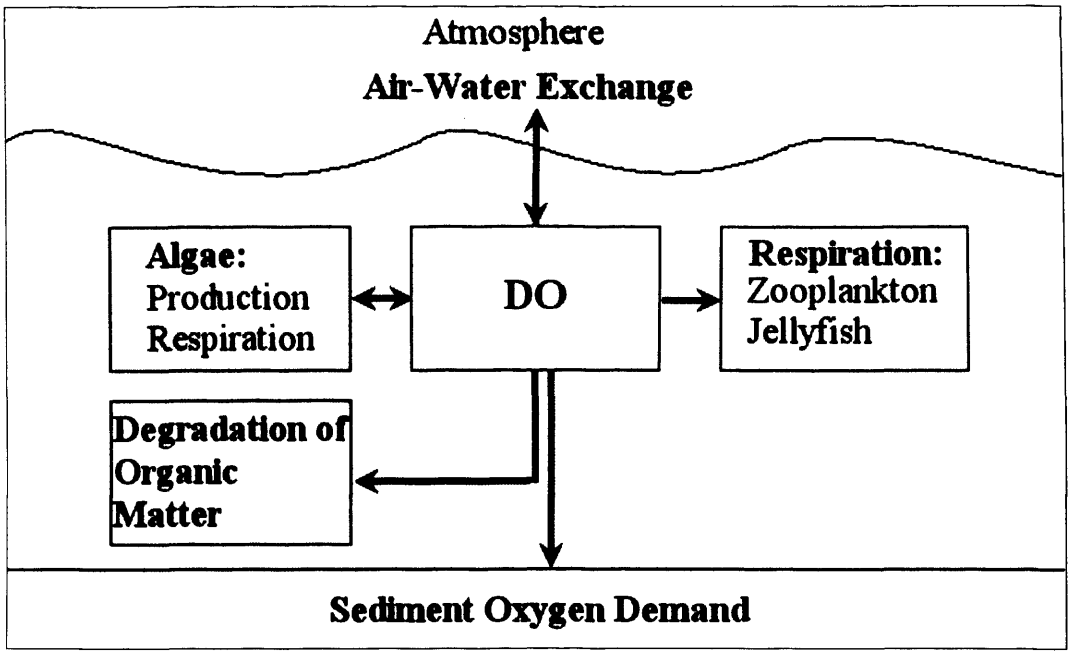

Figure 4.6: General DO cycle

4. 5. 2 Nitrogen (N):

N is the key component of proteins that is found in the cells of the entire living organisms, and is continually recycled by animals and plants [*Ji,* 2008]. N enters the marine system in numerous forms. In natural aerobic waters there is a stepwise transformation from ON to NH_4, to nitrite and finally to NO_3, generally the N cycle can be summarised as shown in Figure 4.7. The N cycle in QUAL2E contains all three of these components including: ON, NH_4 and NO_3 as given in equations (4.35), (4.36) and (4.37) respectively:

$$\frac{dON}{dt} = \alpha_1 \rho A - \beta_3 ON - \sigma_4 ON \qquad (4.35)$$

where ON is the concentration of organic nitrogen (mg/l), α_1 is the fraction of algal biomass consisting of nitrogen (mg N/mg A), β_3 is the rate constant for hydrolysis of organic nitrogen to ammonia nitrogen, which is temperature dependant (/day) and σ_4 is the rate of coefficient for organic nitrogen settling, which is temperature dependant (/day).

$$\frac{dNH_4}{dt} = \beta_3 ON - \beta_1 NH_4 + \frac{\sigma_3}{d} - F_1 \alpha_1 \mu A \qquad (4.36)$$

where $F_1 = P_N NH_4 / (P_N NH_4 + (1 - P_N) NO_3)$, β_3 is the organic nitrogen hydrolysis rate (/day), σ_3 is the benthos source rate for ammonia nitrogen (mg/m^2 day), F_1 is the fraction of algal nitrogen uptake from the ammonia pool and P_N is the preference factor for ammonia nitrogen.

$$\frac{dNO_3}{dt} = \beta_1 NH_4 - (1 - F)\alpha_1 \mu A \qquad (4.37)$$

where F is the fraction of algal nitrogen taken from the ammonia pool.

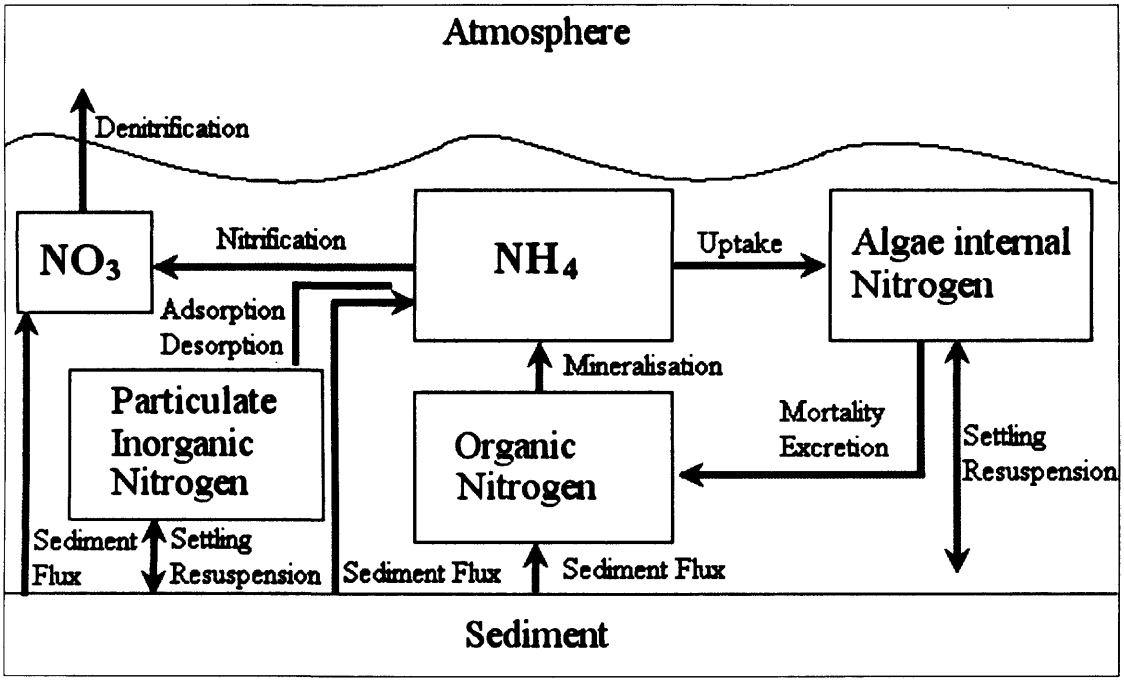

Figure 4.7: General N cycle

4. 5. 3 Phosphorus (P):

The P cycle operates like the N cycle in many respects, as shown in Figure 4.8. Organic forms of P (OP) are generated by the death of algae, which then convert into a dissolved inorganic state (PO_4^{-3}), it is considered as the only phosphorus compound readily available for algal uptake without further breakdown and provides a measure of the phosphorus immediately available for plant growth. Hereafter this has been

referred to as PO_4 for simplicity. Phosphorus discharged from sewage treatment plants is generally available in the dissolved inorganic form (PO_4) and is readily taken up by algae [*Bowie et al.*, 1985]. The differential equations representing organic and dissolved forms of P in QUAL2E are given as the following respectively:

$$\frac{dOP}{dt} = \alpha_2 \rho A - \beta_4 OP - \sigma_5 OP \tag{4.38}$$

where OP is the concentration of organic phosphorus (mg/l), α_2 is the phosphorus content of algae (mg *P*/mg *A*), β_4 is the organic phosphorus decay rate, which is temperature dependant (/day) and σ_5 is the organic phosphorus settling rate (/day) and for PO_4:

$$\frac{dPO_4}{dt} = \beta_4 OP + \frac{\sigma_2}{d} - \alpha_2 \mu A \tag{4.39}$$

where PO_4 is the concentration of inorganic or dissolved phosphorus (mg/l) and σ_2 is the benthos source rate for dissolved phosphorus (mg/m^2 day).

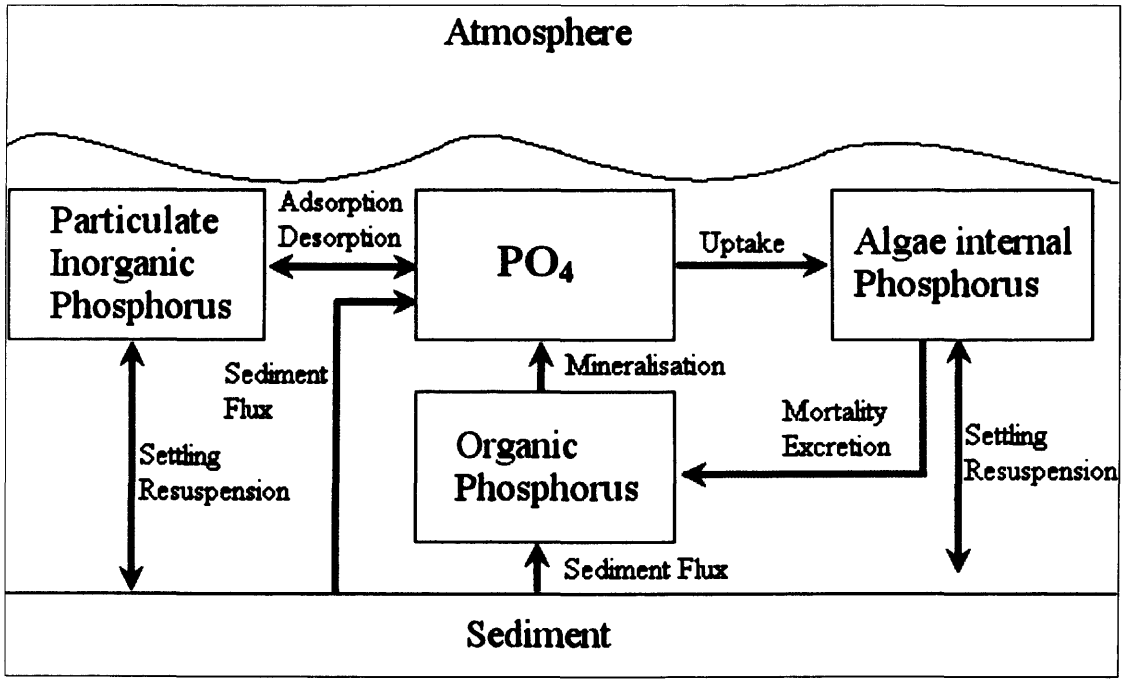

Figure 4.8: General P cycle

4. 5. 3. 1 Development of the model:

In recent years there has been a growing interest in the need to predict sediment transport fluxes in estuarine water more accurately. There has also been an increased interest directed towards how water pollutants and nutrients interact with solid matter, such as inorganic sediments [*Chapra*, 1997]. The high adsorption ability of fine suspended matter in the water column towards chemical constituents such as P and bacteria, enable fine sediments to act as a means of carrying or transferring contaminants along the flow field with substantial implications for related water quality problems [*Mehta et al.,* 1989].

Bed sediments can act as either a sink or source for PO_4 in the water column, depending on a number of physical processes that fundamentally influence stream sediment equilibrium phosphorus concentration (EPC). In well mixed systems, the availability of PO_4 in benthic sediments can possibly be estimated using an EPC of zero net sorption or desorption [*Froelich*, 1988; *Sharpley et al.*, 2002]. A quasi equilibrium for PO_4 concentration exists between marine sediments and the water column, where sorption and release rates of PO_4 are practically equal. Marine sediments may well have a key impact on PO_4 concentrations and P retention, in particular during normal flow conditions [*Klotz*, 1988]. Theoretically P will desorb from marine sediments if the water column's PO_4 concentration is below the sediment EPC, or otherwise P will adsorb to marine sediments if the water column's PO_4 concentration is greater than the sediment EPC [*Taylor and Kunishi*, 1971].In addition, However, the PO_4 concentration in streams is not exclusively controlled through sediment sorption and desorption processes, and the relative significance of

biological, chemical and physical processes may adjust this equilibrium concentration between the water column and the marine sediments.

In this section, a brief explanation will be given of the outcome of experimental work conducted on sediments collected from the Loughor Estuary, along the South Wales coast. This study was undertaken in parallel with a related PhD research project [*Al-Enezi,* 2010], in hydraulics laboratory of Hydro-Environmental Research Centre at Cardiff University. The main aim of the experiments was to investigate the sediment sorption processes of P, by means of sediment grain size. An empirical relationship was obtained and adapted for model predictions, with the model results being explained in detail in Chapter 7. More details can also be found in *Al-Enezi et al.,* [2010].

Experiment description: The main experimental work was conducted in a hydraulics flume facility which was 10 m in length, 1.2 m wide and 0.3 m deep, as shown in Figure 4.9. The channel had a steel bed and was enclosed with thick glass on either side of the channel. The water discharge along the channel was driven by an electric pump, which delivered the water from a reservoir, located underneath the channel, to the upstream end of the flume. The water passes through a honeycomb baffle in order to minimise the turbulence, before entering the flume channel. The discharge was controlled by a mechanical valve and was set at a constant rate of approximately 9.5 l/s. At the downstream end of the channel, a weir controlled the water level in the flume which was generally operated at a depth of approximately 16 cm.

Sediment samples of various sizes were collected from the Loughor estuary in order to assess the sorption processes in the sediments. The sediments were placed at approximately mid-length along the flume channel, in the form of a plug of 0.0045 m^3 (see Figure 4.9), and the water flow was then allowed to pass over the sediments at a low constant velocity of approximately 6 cm/s to minimise erosion. Samples of sediments were taken for adsorption analyses from the surface of the plug, at various time intervals, typically ranging from 5 minutes to 72 hours. The main technique used was the extracted method proposed by *Ruttenberg* [1992] to estimate the phosphorus levels adsorbed onto the grain surface of the sediments. Further details of the chemical aspect of this experiment can be found in *Al-Enezi* [2011].

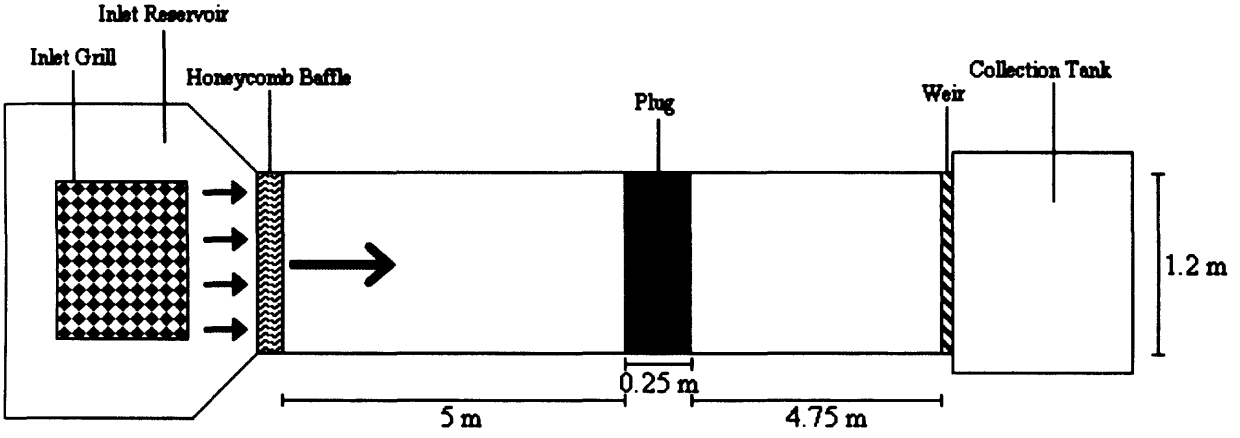

Figure 4.9: Flume channel dimensions including sediment plug in the middle of the channel

Experimental results: Sediment grain sizes, which varied spatially in the Loughor Estuary, have a relatively good correlation with PO_4 sorption processes with a R^2 value of 0.7654 (see Figures 4.10). Power relationships best explained the correlation between the sediment grain size and the P sediment flux as shown in Figure 4.10. This

may well be attributed to the fine grain sediment having a higher surface area to weight ratio and thus having a greater PO_4 adsorption capacity [*Jin et al.*, 2005].

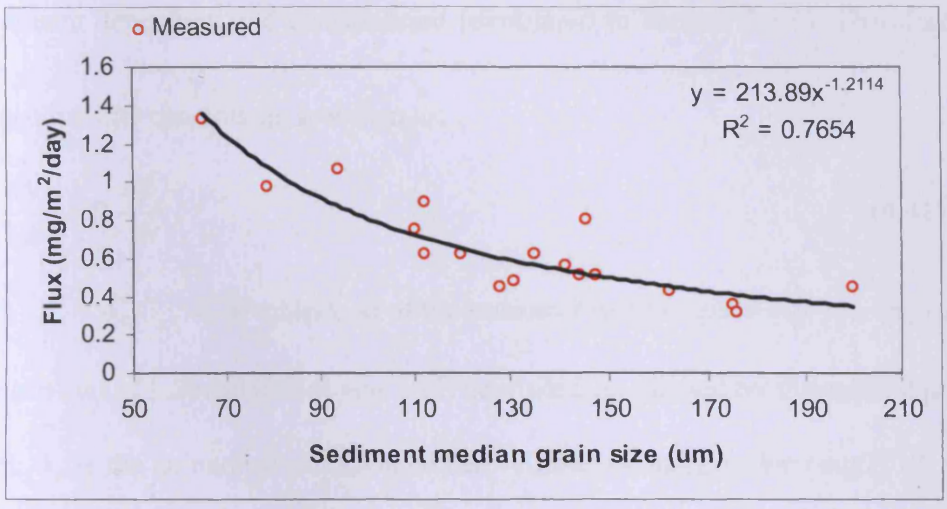

Figure 4.10: Phosphorus flux against sediment median grain size

Utilising Figure 4.10, the benthos source σ_2 in equation (4.39) can now be replaced by:

$$\sigma_2 = \frac{213.89}{D_{50}^{1.2114}} \tag{4.40}$$

where D_{50} is the bed sediments median grain size (μm).

Phosphorus (P) cycle refinement, linked with sediment transport: Since the PO_4 flux σ_2 only represents the benthos source, it is reasonable to link such a coefficient with the sediment transport processes (as explained in section 3.3.1), as the flux is not directly measured from the data acquired from the lab experiments, but it has been calculated from the PO_4 adsorption onto the bed sediments. Therefore, utilising PO_4 adsorption, rather than the flux, and linking it to the sediment transport processes is more reasonable to avoid errors in the transformation from PO_4 adsorption to PO_4 flux

(see Figure 4.11). A link to sediment transport can be achieved by considering PO_4 adsorption to bed P_b (mg/g) and P partition coefficient K_D (l/g), including the effects of sediment deposition and resuspension (explained in section 3.3.1). Therefore $\frac{\sigma_2}{d}$ in Equation 4.39 can now be rewritten as:

$$-P_w \frac{dS_d}{dt} + P_b \frac{dS_r}{dt} \tag{4.41}$$

where $P_w = K_D C_s$, P_b is a function of the sediment median grain size D_{50} (mg/g), S_d is the amount of suspended sediment (SS) deposited on the bed by the settling process (mg/l), S_r is the amount of resuspended bed sediment concentration (mg/l), P_w is the phosphorus adsorbed to the suspended sediment (mg/g) and C_s is the particulate phosphorus attached to the suspended sediment in the water column (mg/l). Therefore Equation 4.39 can be rewritten as:

$$\frac{dPO_4}{dt} = \beta_4 OP - \alpha_2 \mu A - P_w \frac{dS_d}{dt} + P_b \frac{dS_r}{dt} \tag{4.42}$$

Based on the experimental data (Figure 4.11), the sediment PO_4 adsorption can be written as:

$$P_b = \frac{2.4235}{D_{50}^{1.2119}} \tag{4.43}$$

$$K_D = 0.0076 \tag{4.44}$$

This is for Loughor Estuary case study, where a brief description will be given with regard to K_D for Kuwait Bay in Chapter 7.

For the particulate phosphorus attached to the suspended sediments in the water column we have:

$$C_s = \frac{K_D S}{1 + K_D S} C \tag{4.45}$$

where S is the SS concentration in the water column (mg/l) and C is the dissolved and particulate phosphorus concentration in the water column (mg/l).

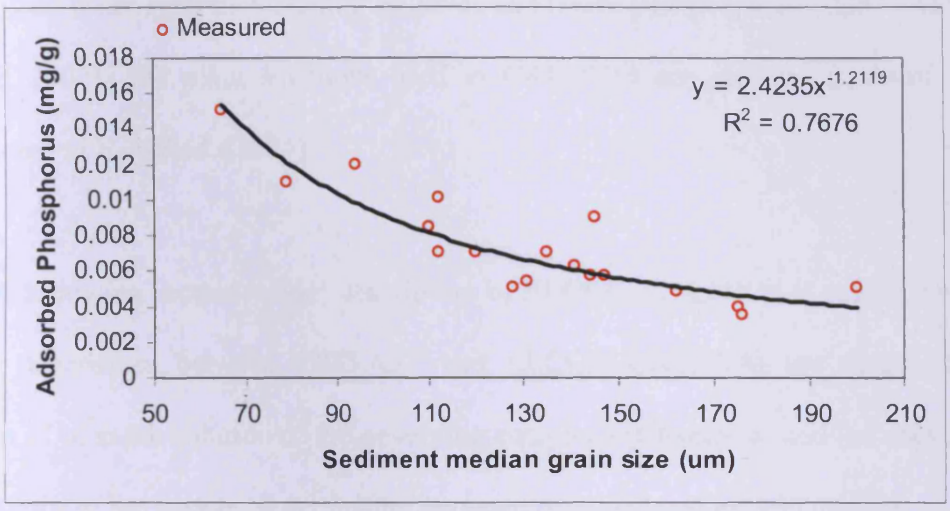

Figure 4.11: Phosphorus adsorption against sediment grain size

4. 6 Introduction to ELCOM-CAEDYM:

ELCOM (Estuary, Lake and Coastal Ocean Model) is a three-dimensional hydrodynamics model for lakes, reservoirs and estuaries. The model forms the three-dimensional hydrodynamics driver to the CAEDYM (Computational Aquatic Ecosystem Dynamics Model) water quality model (see Figure 4.12). Heat exchange through the water's surface is governed by standard bulk transfer models found in the literature (e.g., *Amorocho and Devries* [1980]; *Imberger and Patterson* [1981]; *Jacquet* [1983]). ELCOM and CAEDYM are coupled in that ELCOM simulates the physical parameters (such as salinity and temperature) that are necessary for the water quality variables included in CAEDYM. The advection and dispersion of a water quality variable is accounted for in CAEDYM by passing such a variable from CAEDYM to ELCOM as schematically illustrated in (Figure 4.12). The coupled

models present a powerful tool to study the spatial and temporal relationships between physical, biological, and chemical variables in lakes, rivers and estuaries. More details can be found in *Robson and Hamilton* [2004]. CAEDYM has previously been applied to various water systems including estuaries and rivers [*Romero et al.,* 2002 and *Chan et al.,* 2002]. The main equations used in CAEDYM are outlined in detail in by *Robson and Hamilton,* [2004].

In the following section a brief description of ELCOM-CAEDYM is given. Also the main differences between TRIVAST and ELCOM-CAEDYM are discussed, by means of both the solution of the governing equations (Chapter 3) and the source and sink terms of the various water quality parameters considered in both models.

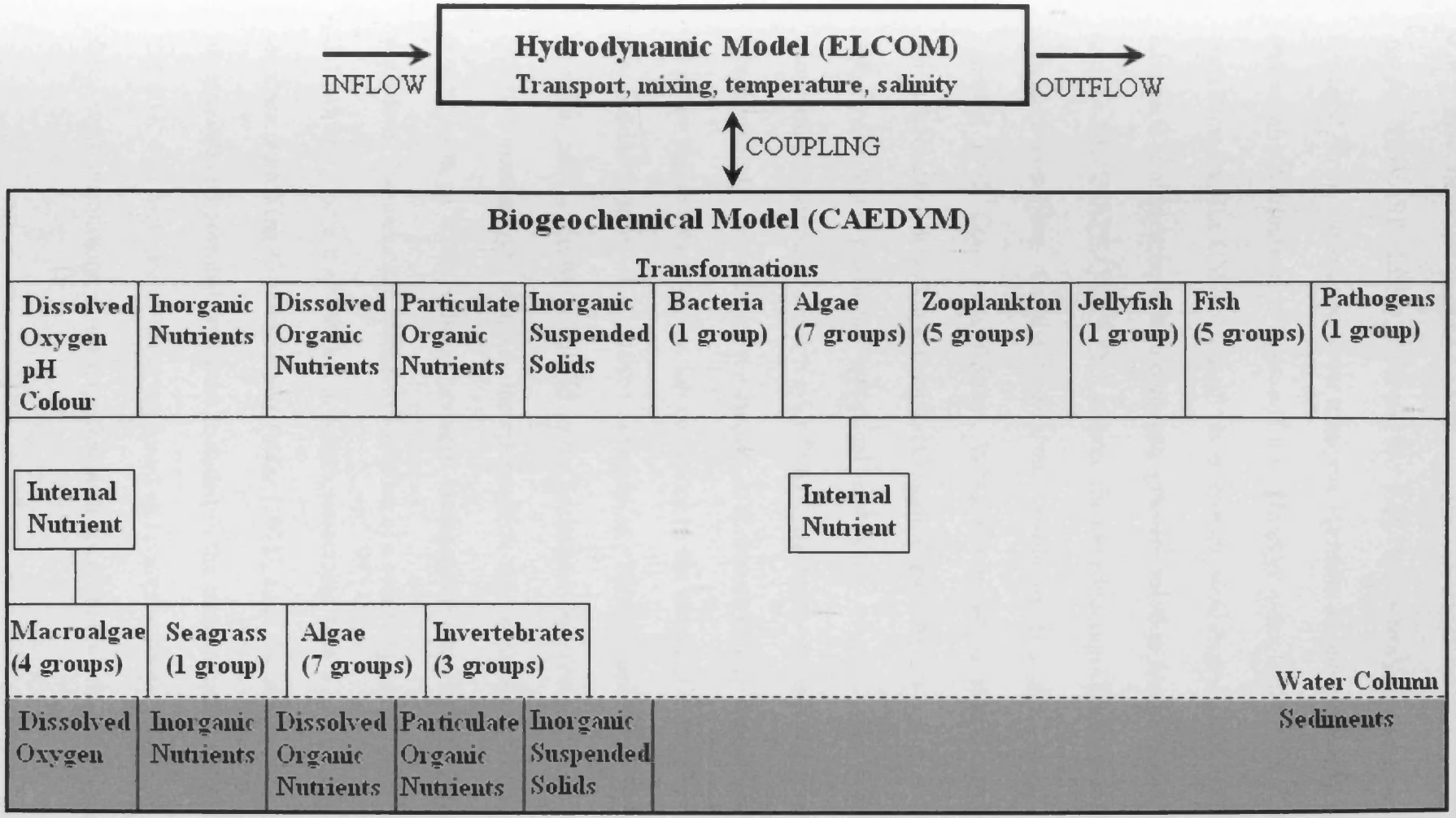

Figure 4.12: Schematic diagram of coupling ELCOM (hydrodynamic) and CAEDYM (Water Quality)

4. 6. 1 Brief description of ELCOM:

As for TRIVAST, ELCOM solves the 3-D, hydrostatic, Boussinesq, Reynolds-averaged Navier-Stokes and scalar transport equations to model velocity, temperature and salinity distributions in space and time [*Hodges et al.*, 2000]. The hydrodynamic algorithms in ELCOM are based on a proven semi-Lagrangian method for the advection of momentum with a conjugate gradient solution for the free surface height and the ULTIMATE-QUICKEST scheme for the advection of scalars and kinematic boundary conditions for the free surface evolution [*Casulli and Cheng*, 1992; *Leonard*, 1991; *Casulli and Cattani*, 1994]. For geophysical-scale simulations the time step can be allowed to exceed the Courant Friedrichs Lewy (CFL) condition for velocity, without producing numerical instability or requiring a fully-implicit numerical discretisation of the Navier-Stokes equations. Scalars and momentum are mixed vertically according to the amount of turbulent kinetic energy available from wind stirring and shear production compared to the potential energy of the ambient stratification [*Spigel et al.*, 1986; *Laval et al.*, 2003]. Similar to TRIVAST, the turbulent eddy viscosity is utilised in the horizontal direction, while in the vertical direction mixing layer model is incorporated. A new component to allow for tidal generation in an enclosed basin has been incorporated into ELCOM, examining the water level fluctuations in numerous locations of a relatively long estuary, such as the Gulf which is more than 900 km in length, associated with a lunar semidiurnal tidal response. Following *Cartwright and Tayler* [1971], tidal forces were calculated from the gravitational potential, and were included in the momentum-transport equation in ELCOM, with such effects being explained and compared with TRIVAST in Chapter 8. It is worth mentioning at this stage that such effects are not modelled in TRIVAST.

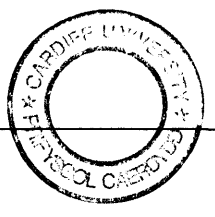

Unlike TRIVAST, ELCOM also takes into account the surface thermodynamics and mass fluxes for heat transfer across the free surface. The energy transfer across the free surface is separated into non-penetrative components of long-wave radiation, sensible heat transfer, and evaporative heat loss, complemented by penetrative shortwave radiation. Non-penetrative effects are introduced as sources of temperature in the surface-mixed layer, whereas penetrative effects are introduced as source terms in one or more grid layers on the basis of an exponential decay and an extinction coefficient based on 'Beer's law'. ELCOM computes a model time step in a staged approach consisting of:

1) Introduction of surface heating/ cooling in the surface layer;
2) Mixing of scalar concentrations and momentum using a mixed-layer model;
3) Introduction of wind energy as a momentum source in the wind-mixed layer;
4) Solution of the free-surface evolution and velocity field;
5) Horizontal diffusion of momentum;
6) Advection of scalars;
7) Horizontal diffusion of scalars.

4. 6. 2 Brief description of CAEDYM:

CAEDYM allows a flexible ecological configuration that could be modified for specific applications, though major elemental cycling and a minimum of one algal group is compulsory. Therefore, the model includes a comprehensive process illustration of the carbon (C), N, P, silica (SIO_3) and DO cycles (see Figures 4.6-4.8), a number of size classes of inorganic suspended solids and phytoplankton dynamics. Various optional biological and other state variables can also be configured. Consequently, CAEDYM is more advanced than traditional Nutrient-phytoplankton-zooplankton (N-P-Z) models, such as the one found in TRIVAST, as it is a general

biogeochemical model that can resolve species or group-specific ecological interactions. This often results in higher computational costs (see Chapter 8 for more details). CAEDYM operates on any sub-daily time step to determine algal processes, including diurnal photosynthesis and nocturnal respiration, and is generally run at the same time intervals as the hydrodynamic model (ELCOM). Algorithms for salinity reliance are included with the intention that a diverse range of aquatic settings can be simulated. With the condition of the nature of the water body being included (i.e. fresh, estuarine or marine), internal checks in the model are then activated to ensure that salinity reliance is maintained (e.g. for an estuarine case), or removed (e.g. for a freshwater or marine water case). Unlike TRIVAST, CAEDYM includes additional source and sink terms of DO, N and P as detailed in *Hipsey et al.,* [2006] and briefly described in Figure 4.12 and Table 4.1 (for further details see Chapter 8).

While sediment transport is essentially an issue of flow physics, the algorithms for the sediment transport processes are more suitably grouped with the water quality algorithms in CAEDYM. Settling of suspended matter is computed using 'Stokes law' to obtain settling velocities for the top and bottom of each affected grid cell. This permits the net settling flux in each cell to be computed. A two-layer sediment model has been developed that computes re-suspension, deposition, flocculation, and consolidation of sediment based on:

- The shear stress at the water-sediment interface;
- The type of sediment (cohesive and/or non-cohesive) and;
- The thickness of the sediment layer.

Parameter	Source and Sink
Dissolved Oxygen (DO)	• Exchange to and from the air/water interface • Utilisation of oxygen at the sediment/water interface. • Utilisation of oxygen as bacteria degrade organic matter. • Utilisation of oxygen in the process of nitrification. • Photosynthetic oxygen production and respiratory consumption by phytoplankton. • Utilisation of oxygen due to respiration by zooplankton. • Photosynthetic oxygen production and respiratory consumption by macroalgae and seagrasses/macrophytes. • Utilisation of dissolved oxygen due to respiration in jellyfish and higher organisms (macroinvertebrates, fish).
Nitrogen (N) DONL (Dissolved Organic Nitrogen Labile). DONR (Dissolved Organic Nitrogen Refractory). NH_4 (Ammonia). NO_3 (Nitrate). IN (Internal Nitrogen). PIN (Particulate Inorganic Nitrogen). PONL (Particulate Organic Nitrogen Labile). PONR (Particulate Organic Nitrogen Refractory).	• Mineralization of DONL and DONR to NH_4. • Biological uptake of NH_4 and NO_3 by phytoplankton and macroalgae into the IN pool. • Dissolved sediment fluxes of NH_4, NO_3, DONL, and DONR. • Adsorption/desorption of NH_4 onto inorganic suspended solids into PIN pool. • Decomposition of PONL to DONL and PONR to DONR. • Biological mortality and excretion into the DONL and PONL pools. • Settling of PONL, PONR, PIN and IN.
Phosphorus (P) DOPL (Dissolved Organic Phosphorus Labile). DOPR (Dissolved Organic Phosphorus Refractory). PO_4 (Dissolved Phosphorus) PIP (Particulate Inorganic Phosphorus). POPL (Particulate Organic Phosphorus Labile). POPR (Particulate Organic Phosphorus Refractory).	• Mineralization of DOPL and DOPR to FRP (directly or through bacteria). • Biological uptake of PO_4 by phytoplankton and macroalgae into the internal pools. • Dissolved sediment fluxes of PO4, DOPL, and DOPR. • Adsorption/desorption of PO_4 onto inorganic suspended solids into PIP pool. • Decomposition of POPL to DOPL and POPR to DOPR.

Table 4.1: General source and sink of DO, N and P incorporated in CAEDYM

4.7 Summary:

Details have been given herein of the numerical solution procedures for the two-dimensional and layer integrated three-dimensional flow and solute transport algorithms in TRIVAST. The three-dimensional layer integrated hydrodynamic equations were solved using a combined explicit and implicit finite difference method. The advective-diffusive equation was solved using an operator splitting scheme, where the equation was split into a set of both horizontal and vertical equations. The horizontal equations were solved using the ULTIMATE QUICKEST scheme and an implicit scheme was used to treat the vertical diffusive term, to avoid the use of a very small time step. It is important to understand the numerical solution of the governing equations as this would give an indication of how the model would behave according to the problem considered. The source and sink terms of DO, N and P were explained based on QUAL2E and the development of the PO_4 source and sink terms were included in TRIVAST based on lab experiments. A brief description and explanation was given of the ELCOM-CAEDYM model and the main differences between the two models were addressed, in which ELCOM-CAEDYM model was shown to have more sophisticated representations of the water quality processes than the TRIVAST model. Details of the differences between the ELCOM-CAEDYM and TRIVAST model predictions for the Gulf and Kuwait Bay are given in Chapter 8.

Chapter 5

Horizontal dispersion and Residence Time Studies of the Arabian Gulf

5. 1 Introduction:

For centuries native communities have made great use of the dispersive capacity of the Arabian Gulf to dilute and flush away waste products (see Chapter 2). Previously this practice worked well when the pollutant loading was much smaller than that of the receiving water's assimilative capacity. However, with the relatively acute expansion in anthropogenic activities in the region, the assimilative capacity of the coastal regions has been exceeded. This has led to a major impact on marine biodiversity and has become a threat to human wellbeing in the region. Furthermore, dispersion and mixing processes are of fundamental importance to marine life. For example, phosphorus excreted by fish would be toxic to aquatic life if it was not mixed and diluted with the surrounding waters. Generally, nutrients derived from the decay of dead organisms at the seabed would not be available to the plankton if, for example, there was no vertical mixing to disperse, and therefore spread the nutrients throughout the water column. Hence, identifying the horizontal dispersion coefficient of the marine system is of great importance in stressed regions such as the Gulf.

The term dispersion is sometimes applied to the spreading of immiscible substances that do not undergo any dilution. This can be misleading and a careful distinction must be made between dispersive spreading, in which there is no dilution, and that in which the mixing reduces the concentration of the material. Thus it is essential to define the physical transport processes of flow in natural waters that cause pollutants or solutes to be transported and mixed or exchanged with other mediums (see Table 5.1).

The main aim of this chapter is to highlight the dispersion and flushing characteristics across the Gulf, in terms of residence time, to provide a guide for new engineering developments, such as those shown in Chapter 2, and their environmental management. This will be first achieved by validating the three dimensional model (ELCOM) and showing that the model reproduces the dispersion of the salinity field originating from the Strait of Hormuz and the river inflows (see Figure 5.1). Once validated, the three dimensional model was then used to ascertain the degree of dispersion of numerical tracers as a function of geographic location.

Process	Definition
Advection	Transport by an imposed current system, as in a river or coastal waters
Convection	Vertical transport induced by hydrostatic instability
Molecular Diffusion	The scattering of particles by random molecular motions, which may be described by Ficks law and the classical diffusion equation
Turbulent Diffusion	The random scattering of particles by turbulent motion, considered roughly analogous to molecular diffusion, but with eddy diffusion coefficients (which is much larger than molecular diffusion coefficients)
Shear	The advection of fluid at different velocities at different positions
Dispersion	The scattering of particles or a cloud of contaminants by the combined effects of shear and transverse diffusion.
Mixing	Diffusion or dispersion as described above; turbulent diffusion in buoyant jets and plumes; any process which cause one parcel of water to be mingled with or diluted by another.
Evaporation	The transport of water vapour from a water or soil surface to the atmosphere.
Radiation	the flux of radiant energy, such as at a water surface
Particle Entrainment	The picking up of particles, such as sand or organic detritus, from the bed of water body by turbulent flow past the bed

Table 5.1: Definition of physical transport processes that are likely to occur in typical marine system

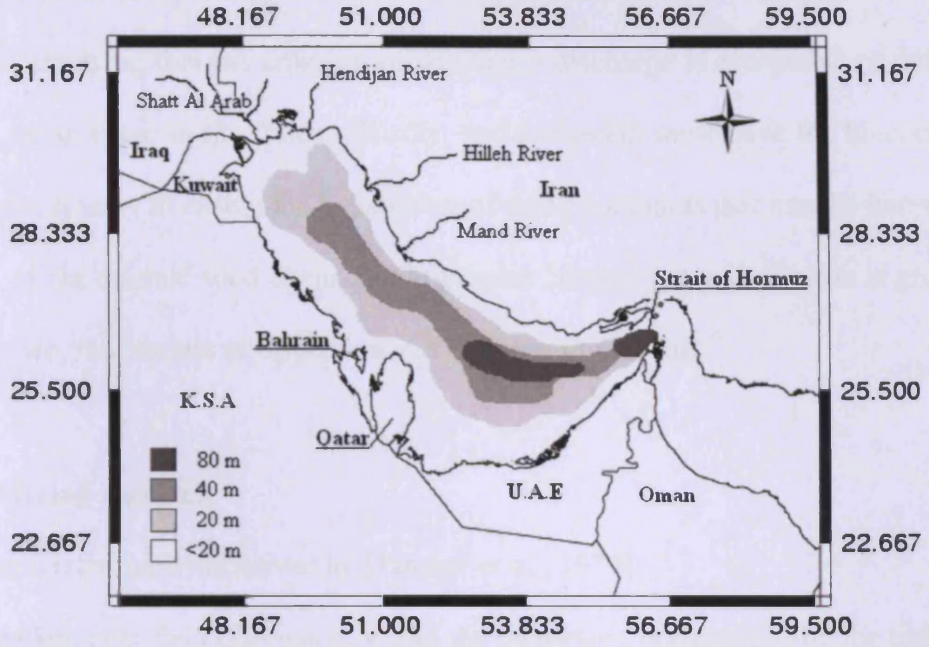

Figure 5.1: The Gulf including Strait of Hormuz and main river input

5. 2 Horizontal dispersion mechanism:

Traditionally, coastal communities have relied on dispersion of effluents once they entered coastal waters so that, once diluted, biological breakdown renders them harmless. Here the "assimilative capacity" is defined as that loading, which properly dispersed throughout the receiving domain, can be rendered harmless without jeopardizing the health of the ecosystem. Clearly, three distinct sets of processes combine to determine whether a domain has the assimilative capacity to accept an additional effluent loading. Firstly, the near and intermediate rates of dispersal must be sufficiently fast to dilute the effluent to a level that is sufficiently low, that when added to the background concentration, does not kill components of the ecosystem impacting on the functioning of the ecosystem [*Imberger et al.,* 2007]. Secondly, the transport or flushing must remove the by-products of the effluent breakdown processes rapidly enough not to cause a long-term build up in the domain as a whole,

in simple terms the flushing must prevent the domain from filling up with harmful products, implying that the criterion of whether a discharge is acceptable or not may depend on an event in the future. Thirdly, the ecosystem must have the biochemical capacity necessary to ensure the breakdown of those pollutants that may be harmful to the rest of the original food chain. In the present chapter special attention is given to the first two, the physics of dispersion and flushing in the Gulf.

5. 2. 1 Mixing regimes:

Dispersion is primarily achieved by [*Fischer et al.*, 1979]:

1) Turbulent near field dispersion, where the dispersion is energised by the turbulent kinetic energy from the discharge itself;

2) The region following the near field, called the intermediate field, where the mixing switches from being discharge energised to mixing energised by the turbulence of the ambient fluid flow; when the effluent density differs from that of the receiving water, the intermediate region can be quite significant in size because the added buoyancy must be overcome by the energy from the receiving water flow; and

3) The far field, where the pollutant is dispersed by mechanisms inherent to the ambient flow conditions.

The scale of such processes can be summarised as shown in Table 5.2.

Phase	Phenomenon	Length Scale[a] (m)	Time Scale[a] (sec)
Initial jet mixing	Rise of buoyant jets over an outfall diffuser in a stratified fluid	$< 10^2$	$< 10^3$
Establishment of sewage field or cloud	Travelling with the mean current, lateral gravitational spreading	10^1-10^3	10^2-10^3
Natural lateral diffusion and/or dispersion	Spread resulting in stretching	10^2-10^4	10^3-10^5
Advection	Due to currents (including scales of water motion too large compared to sewage plume to be called turbulence	10^3-10^5	10^3-10^6
Large scale flushing	Advection integrated over many tidal cycles, upwelling or down-welling, sedimentation	10^4-10^6	10^6-10^8

Table 5.2: Effluent flow from a typical outfall passes through a succession of physical processes at scales from small to large. [a] Approximate orders of magnitude [*Fischer et al.*, 1979]

5. 2. 2 Far field mixing:

5. 2. 2. 1 Turbulent dispersion:

After initial dispersion in the near field, effluents disperse by turbulent mixing until the effluent cloud has reached a size comparable to the scale of the velocity field. Once the cloud is as large as the scale of the shear, the mean background velocity field distorts the effluent cloud and shear and transverse mixing combine to yield an enhanced dispersion (see next section). For effluent clouds smaller than the scale of the background shear, turbulence disperses the effluent cloud and *Richardson,* [1926] showed that the dispersion may be modelled by the "4/3 law", which accounts for the rate of increase of dispersion as the effluent cloud intersects ever-increasing scales of turbulence as the cloud grows.

5. 2. 2. 2 Shear dispersion:

Longitudinal shear dispersion occurs when the distortion of a concentration field by a vertical or horizontal shear flow is balanced by vertical or transverse turbulent mixing [*Fischer et al.*, 1979]. Once this balance is achieved, the rate of dispersion may be modelled by a simple diffusion equation with a horizontal dispersion coefficient *Fischer et al.*, [1979]:

$$K_x = \phi \frac{U^2 l^2}{K_z}$$

Here ϕ is a constant dependent on the velocity and transverse diffusivity profile, l is the length scale of the velocity straining the concentration field, U is the velocity scale and K_z is the vertical diffusivity. As demonstrated by *Fischer et al.* [1979] for a simple plane flow with a vertical turbulent velocity profile, $l = h$, where h is the depth, U is the discharge velocity, and $K_z = 0.07hU^*$, where U^* is the bottom shear velocity. By contrast, in a wide river with a transverse velocity profile, l becomes the width of the channel and U is the discharge velocity. The coefficient ϕ depends on the vertical structure of the velocity and diffusivity. For a constant diffusivity, *Fischer et al.*, [1979] showed that $\phi = 0.008$ for a linear velocity profile and *Bowden,* [1965] showed that $\phi = 0.001$ for a logarithmic profile resulting from bottom friction, $\phi = 0.019$ for the density current profile, and $\phi = 0.005 - 0.008$ for wind drift profiles.

Clearly, dispersion due to the balance of transverse mixing and longitudinal straining will always be much larger than that due to vertical mixing in shallow estuaries. However, the validity of this statement depends on the time available for mixing. It is well known, see *Fischer et al.,* [1979], that a balance between distortion due to

velocity shear and that due to transverse mixing can be achieved only after there has been sufficient time for transverse mixing to take place, a time of $O\left(\frac{l^2}{K}\right)$ where K is the horizontal (or vertical) diffusion coefficient. Shear dispersion via vertical shear with, typically a depth of 10 m and a vertical diffusion coefficient of around 10^{-4} m^2/s, leads to a set up time $O(12)$ days and a horizontal dispersion coefficient of around 6 m^2/s, assuming a value of $\phi = 0.01$ and $U = 0.025$ m/s. If the water velocity is around 0.5 m/s, then shear dispersion would become relevant only after 500 km, which is already half of the studied domain. In contrast, if we assume a coastal current with a transverse scale of 1 km and a transverse diffusion coefficient of 1 m^2/s, then the horizontal dispersion coefficient for transverse mixing and longitudinal strain balance would be around 2,500 m^2/s and the time required to reach such a balance would again be $O(12)$ days. Hence the larger the length scale, the larger the horizontal dispersion. However, again the distance required for this estimate to become valid would be comparable to, or larger than, the dimensions of the Gulf itself [*Lewis*, 1997; *Dooley and Steele*, 1969; *Hughes*, 1956].

Dispersion of a coastal effluent discharge occurs in several stages. Firstly, in the near field the mean kinetic energy of the discharge generates turbulence that mixes or stirs the discharge into the receiving water. Secondly, in the absence of a buoyancy flux the diluted effluent is mixed with the receiving water turbulence until the cloud reaches a scale comparable to the scale of the ambient velocity field. Once this happens the mean velocity shear distorts the cloud, rather than simply transporting it, and this distortion may interact with the ambient turbulent mixing to produce shear dispersion and/or stagnation point dispersion as in *Okely et al.*, [2010], or it may

interact with particular kinematic flow forms to produce kinematic chaos or ghost rod dispersion [*Aref*, 1984; *Stocker and Imberger,* 2003; *Boyland et al.*, 2000; *Newhouse and Pignataro*, 1993]. Although the last three forms of dispersion were not specifically investigated in the present study, as this would require an extensive field survey to identify individual processes, it is likely that each contributes to the dispersion evaluated numerically with the three dimensional model.

ELCOM is first being validated for the Gulf by showing that the model reproduces the dispersion of the salinity field originating from the boundary values specified for the Strait of Hormuz and the river inflows. The salinity differences were low enough not to influence the buoyancy, with salinity acting simply as a tracer in the upper reaches of the Gulf. Once validated, ELCOM was used to ascertain the degree of dispersion of tracers as a function of geographic location, the processes sustaining the simulated dispersion and the net flushing or residence time resulting from this dispersion. Before proceeding to this stage it is useful to review the dispersion characteristics of estuaries as given in the following section.

5. 3 Dispersion in estuaries:

Estuaries vary in physical, chemical and biological properties, giving rise to a large variation of dispersion coefficients as shown in Table 5.3. Unlike rivers, estuaries are more complex systems since the flow is usually driven by the slope of the water surface, wind stresses and internal density variations. These may exist in rivers, however, oscillating flow adds complexity to the estuarine system. Hence, it is reasonable to classify estuaries in terms of the degree of stratification. *Bowden*, [1967]

and *Pritchard,* [1967] distinguished three main hydrodynamic groups shown in Table 5.4.

Estuary	Dispersion coefficient (m^2/s)	Comments	Source
Hundson	160		*Thatcher and Harleman* [1972]
Rotterdam Waterway	280		
Potomac	55		
Delaware	500-1500		
San Francisco Bay	200	Approximate value used in numerical model	*Cox and Macola* [1967]
Severn	10-100		*Stommel* [1953]
Potomac	20-100	From dye experiment	*Hetling and O'Connell* [1966]
Delaware	100		*Paulson* [1969]
Mersey	160-360		*Bowden* [1963]
Rio Guayas	760	Computed from data given by *Murray et al.,* [1975]	
Severn (summer)	54-122		*Bowden* [1963]
Severn (winter)	124-535		*Bowden* [1963]
Thames (low river flow)	53-84		*Bowden* [1963]
Thames (high river flow)	338		*Bowden* [1963]

Table 5.3: Typical values of dispersion coefficient in estuaries

Stratified and Partially Stratified Estuaries	
• Apparent difference in density. • Controlled by both temperature and salinity alterations. • Limited upward transport of turbulent kinetic energy generated by friction at the bed.	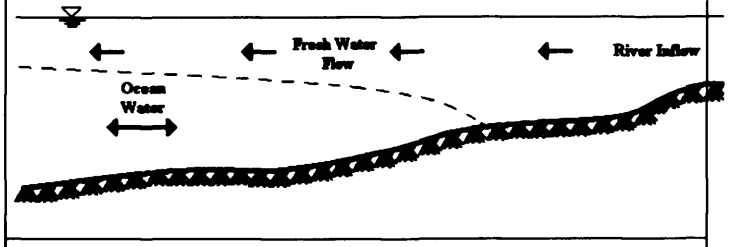 ***Example*** The Gulf (summer), Chesapeake Bay, Vellar River
Well Mixed Estuaries	
• Homogenous water vertically. • Strong tidal mixing and transport. • Wind and wave play an essential role for transferring kinetic energy.	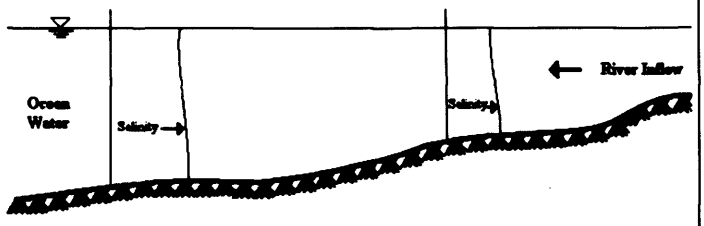 ***Example*** Delaware Bay, Kuwait Bay (see Chapter 6)

Table 5.4: General characteristics of stratified, partially stratified and well mixed estuaries

5. 4 Horizontal dispersion in the Gulf

The horizontal dispersion mechanism of the Gulf will be studied in the following sections by utilising ELCOM. It is worth mentioning that the results obtained in this study are mainly based on 1992 data, due to availability of data during this period.

5. 4. 1 Model setup:

The modelling approach adopted in this study involved a uniform grid of 5,000 m in both X and Y directions. Twenty layers in the Z direction at increments of 4 m for the first top 11 layers and 4.5 m for the remaining layers were adopted, leading to a total of 104,056 wet cells discretising the domain (see Figure 5.2). A computational time

step of 300 s was utilised in the model. The bathymetric information was obtained from a map digitiser at the Hydro-environmental Research Centre of Cardiff University that interpolated the depth at each grid point from a map obtained from the United Kingdom Hydrographic Office. The sea surface elevation due to semidiurnal tides was prescribed at the open boundary at the Strait of Hormuz using the KGULF model, developed by *Al-Salem* (Kuwait Institute of Scientific Research, 2009) for the 1992 period (available on Coastal Information System www.hceatkuwait.net). The salinity and temperature data acquired by the Mt Mitchell cruise [*Reynolds*, 1993] were used as initial conditions for the model. Also, temperature-salinity data gathered in a recent study in the southern part of the Gulf [*Elshorbagy et al.*, 2006] were used to define three main sub-domains for the model initial conditions, as shown in Figure 5.3. Discharges from the rivers were assumed to remain constant throughout the simulation period, based on the values given by *Reynolds,* [1993], and as explained in the introduction. Horizontal diffusivity, κ, is an input parameter in ELCOM representing turbulent sub-grid diffusion in the model transport equations, with more details being provided by *Hodges et al.,* [2000] and was set to 1 m^2/s. The effect of 5 and 10 m^2/s on the horizontal dispersion of numerical tracers was also investigated, as described in Section 5.4.4 and discussed in Section 5.4.6. A bottom drag coefficient of 0.005 was assigned across the whole domain to take account of bed friction. A light extinction coefficient of 0.25 was used for light attenuation. Meteorological forcing, shown in Figures 5.4 and 5.5, was applied at 8 m above sea level.

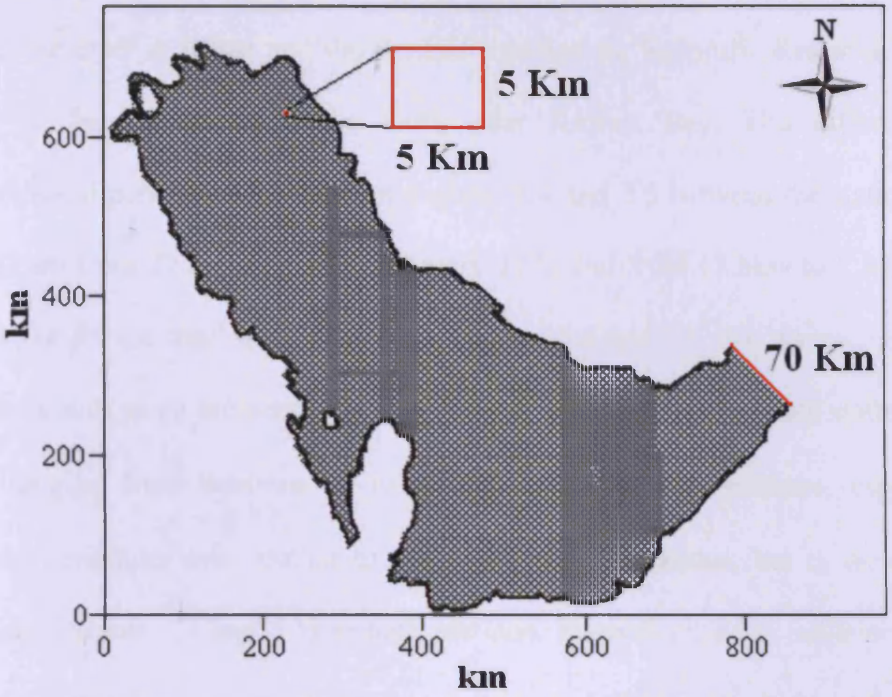

Figure 5.2: Grid size adopted in ELCOM and length of open boundary

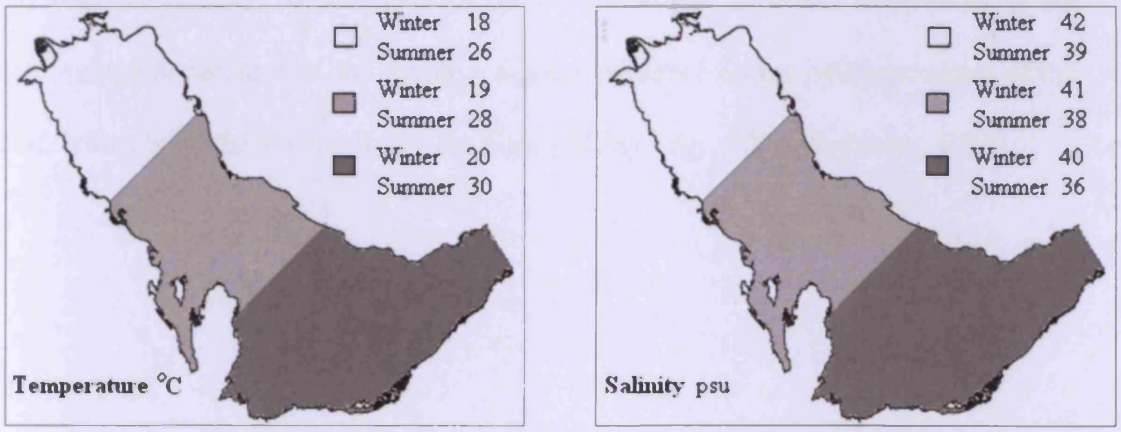

Figure 5.3: Initial condition configurations of temperature and salinity in ELCOM during winter and summer

5. 4. 1. 1 Meteorological effects:

Meteorological effects over the estuary during 1992 were included in the model and were obtained from the Dubai Meteorological Services (DMS), located at the far

south of the Gulf in Dubai and the Kuwait Institute for Scientific Research (KISR), located at the far north of the Gulf, near Kuwait Bay. The differences in meteorological parameters outlined in Figures 5.4 and 5.5 between the stations were insignificant from 27 January to 26 February 1992 and from 13 May to 7 June 1992, in particular for the wind speeds shown in Figures 5.6 and 5.7. Not surprisingly, other parameters such as air temperature were seen to vary seasonally at both stations, with values ranging from between 15 to 40 °C in winter and summer respectively. Humidity variations were similar to air temperature variations, but in the opposite sense (see Figures 5.4 and 5.5) at both stations. Records of solar radiation at both stations showed the same maximum mean values of 550 W/m^2 during January and February 1992, and 900 W/m^2 during May and June 1992, probably as a result of the similar geographic locations of the two stations. KISR data for 1992 (Figure 5.4 and 5.5) were assumed to be adequate for the current study, as minor differences in the meteorological parameters did not have a great influence on the hydrodynamics of the Gulf, which were driven chiefly by the tides [*Elshorbagy*, 2006; *Reynolds*, 1993].

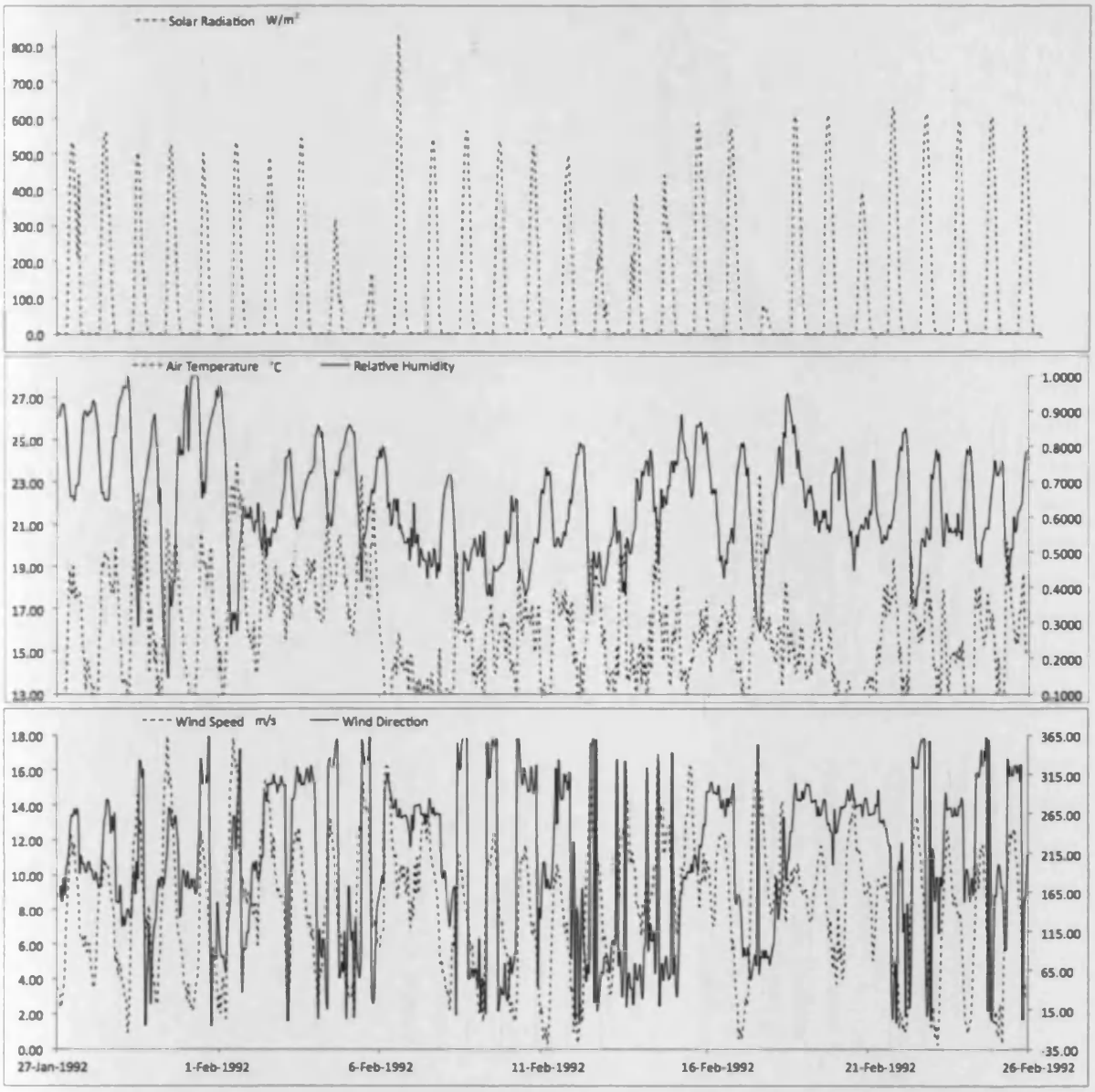

Figure 5.4: Winter meteorological conditions

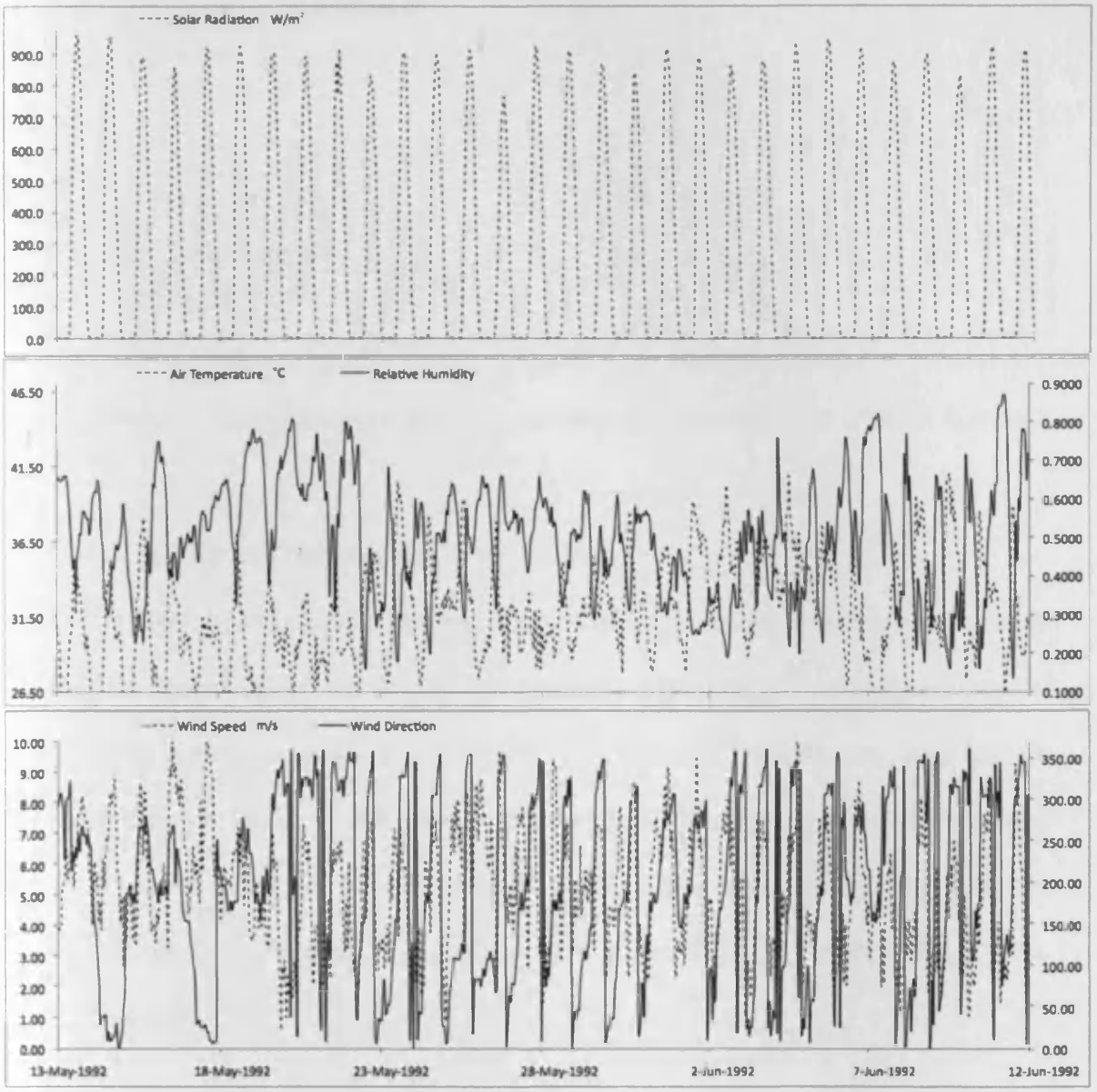

Figure 5.5: Summer meteorological conditions

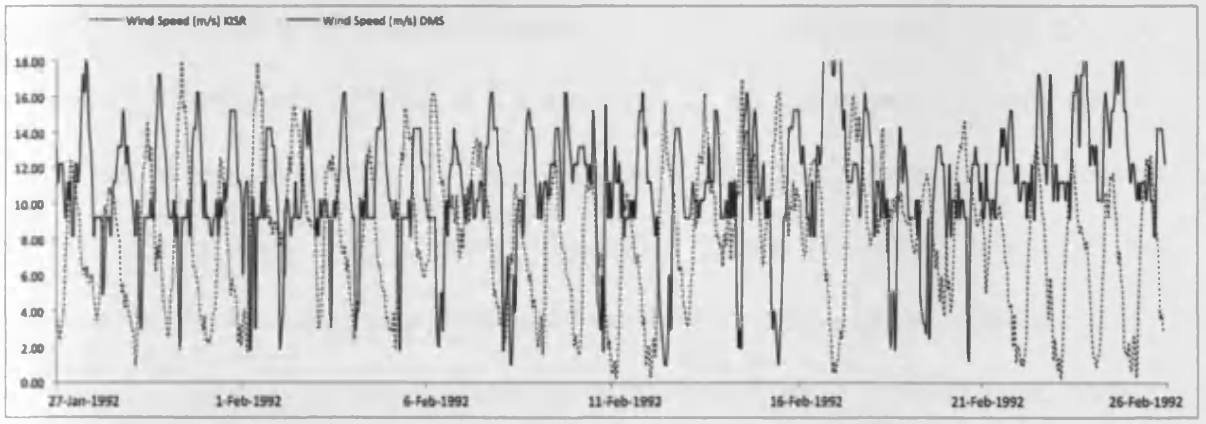

Figure 5.6: Comparison of wind speed between at KISR and DMS in winter

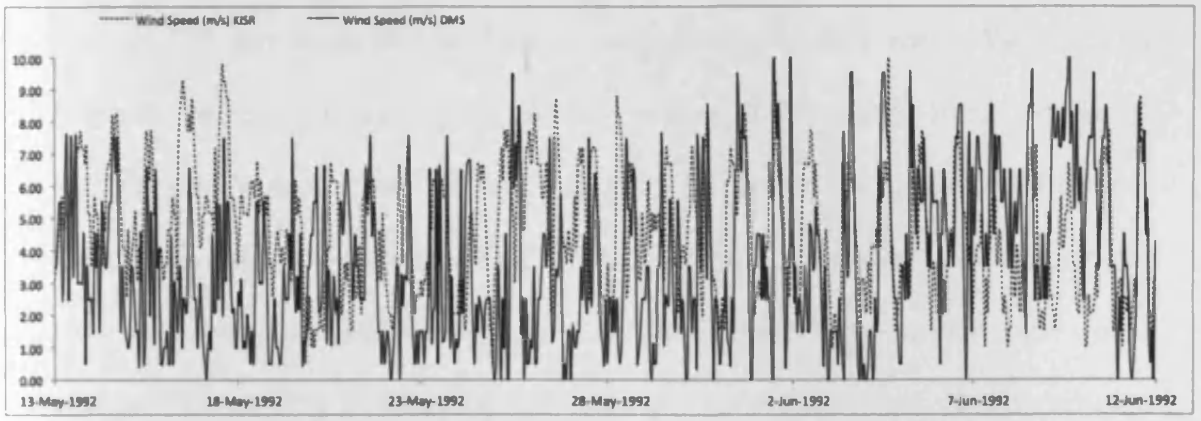

Figure 5.7: Comparison of wind speed between at KISR and DMS in summer

5. 4. 2 Salinity and temperature in the Gulf:

In late 1991 a joint monitoring programme was set up by the Regional Organization for the Protection of the Marine Environment (ROPME), the Intergovernmental Oceanographic Commission (IOC) and the National Oceanic and Atmospheric Administration (NOAA) with a vessel supplied by NOAA. A broad, multidisciplinary survey was carried out over six periods for 100 days between February and June 1992, with the relevant results being shown in Figures 5.8 and 5.9 [*Reynolds*, 1992 a, b; *Reynolds*, 1993].

During winter the water column was well mixed vertically to a depth of about 70 m (Figure 5.8 A) and both the temperature and salinity varied gradually along the Gulf between Kuwait and the Strait of Hormuz, in which the temperature increased and the salinity decreased towards the Strait. Together these variations resulted in a density difference of about 2 kg/m^3 over a distance of 500 km (Figure 5.8 A panel 3). In summer, the surface mixing penetrated to a depth of only about 30 m and the 25 °C isotherm (Figure 5.8 B panel 1) was almost horizontal over the whole domain. More saline and cooler water was observed (Figure 5.8 B panel 2), its location between 100

km and 700 km south east of Kuwait, suggesting an origin not in the Strait of Hormuz, as the salinity maximum lies over 100 km away from the Strait. Furthermore, as seen from Figure 5.8 B panel 3, the isopycnols showed a distinct slope downwards towards the Strait, with the origin of this water column therefore most likely being the Gulf perimeter, where evaporation over the shallow water would increase salinity. The Strait of Hormuz acts as a hydraulic control for the exchange between the Arabian Gulf and the Gulf of Oman, the upper layer of fresher water transferring from the Gulf of Oman to replace water lost by evaporation, and the lower, higher saline water exiting to complete the reverse-estuarine circulation [*Reynolds*, 1993]. More details of the temperature, salinity and density cross-sections across the estuary between Kuwait and Iran, Qatar and Iran, and across the Strait of Hormuz are given in *Reynolds,* [1993].

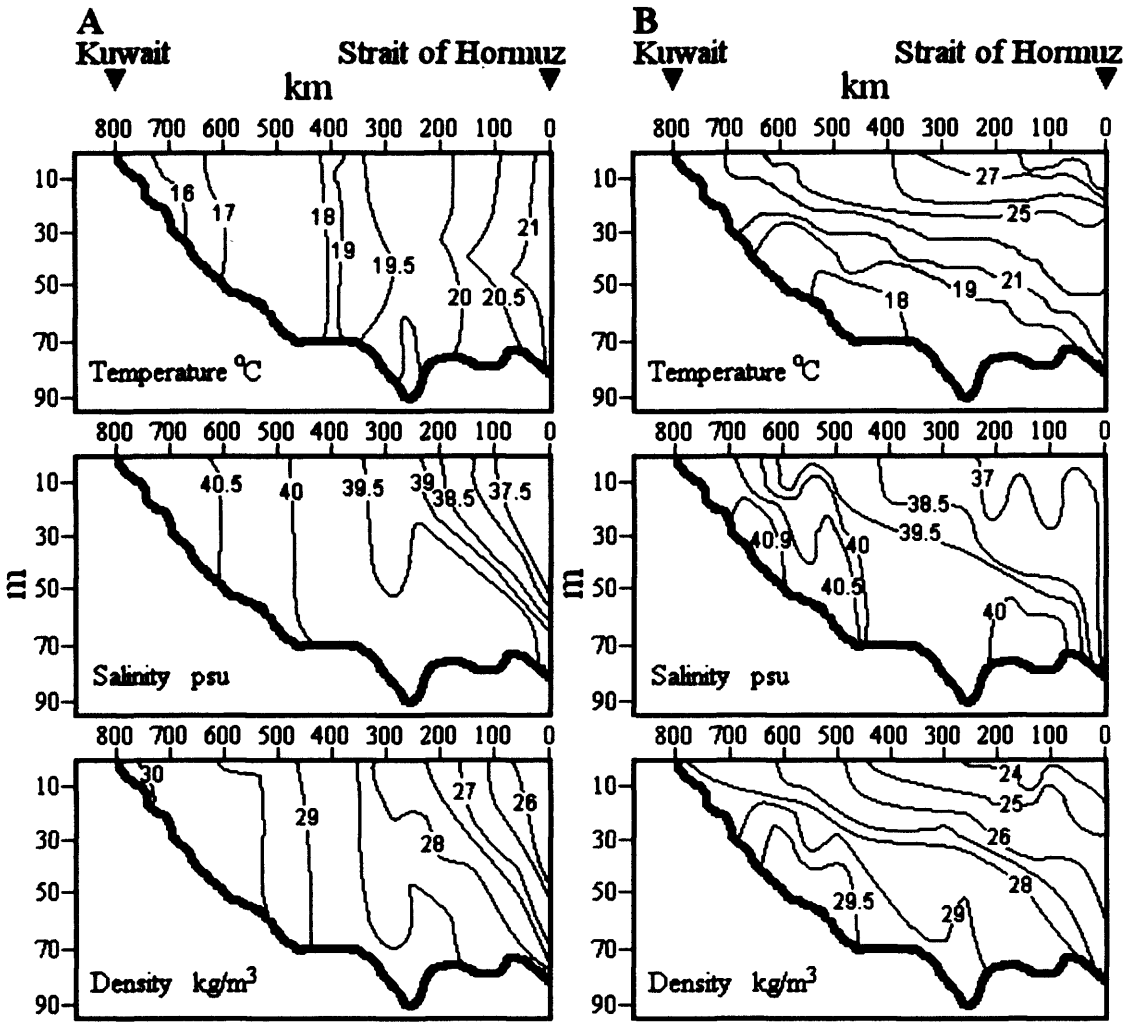

Figure 5.8: A. Vertical variation of temperature, salinity and density along the Gulf (from Strait of Hormuz to Kuwait) during winter; starting 26 February 1992 [Reynolds,1993]

B. Vertical variation of temperature, salinity and density along the Gulf (from Strait of Hormuz to Kuwait) during summer; starting 12 June 1992 [Reynolds, 1993]

The surface inflow from the Gulf of Oman into the Arabian Gulf occurs year round, but extends deeper along the northern boundary into the Gulf in the summer, as seen in Figures 5.8 and 5.9.

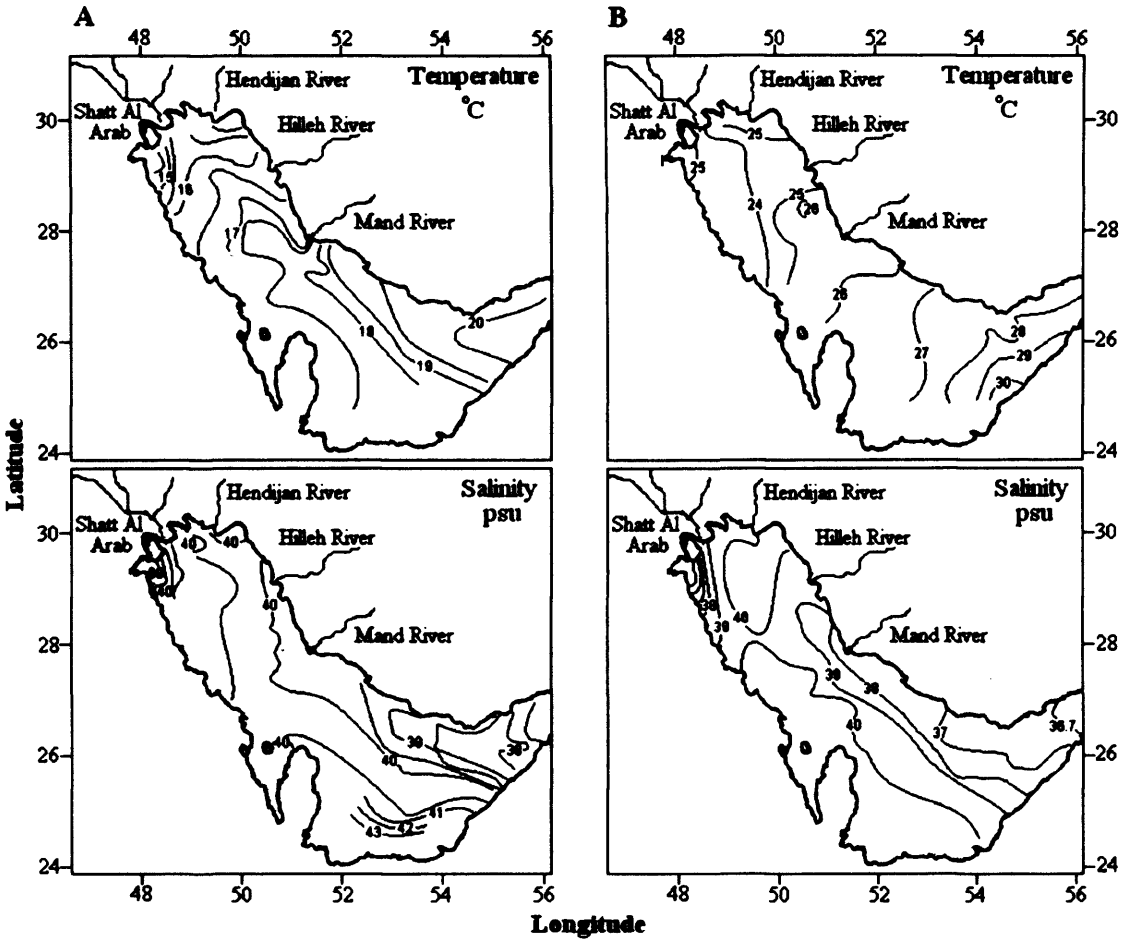

Figure 5.9: Surface field data variation of temperature and salinity of the Gulf during: **A.** winter, starting February 26 1992 [Reynolds, 1993]

B. summer, starting 12 June 1992 [Reynolds, 1993]

River inflows do not contribute significantly to the water structure in the Gulf, but local effects are apparent during both seasons, particularly during winter at Shatt Al Arab, north of the Gulf (Figure 5.9). In addition, records show that precipitation during 1992 was very low in the Gulf, so the relatively small fresh water inflow and the short period considered in this study (i.e. around 30 days each season) suggest that this is not likely to have had a significant impact on the dispersion mechanisms considered in this study.

5. 4. 3 Model validation using 1992 data and estimation of shear:

The above information provided an excellent data set for the validation of the model hydrodynamics and associated dispersion. To optimize the test a 30-day simulation was carried out for both winter and summer configurations, with initial values as stated in Figure 5.3 (i.e. 13 May to 12 June 1992 and 27 January to 26 February 1992). The simulations were required to model first the hydraulic control across the Strait of Hormuz and fresh water input from the rivers, and then the dispersal of the salinity across the Gulf, as observed in Figures 5.8 and 5.9. Evaluation of both temperature (mainly at the water surface) and salinity (mainly through the Strait and rivers) provided the validation.

The purpose of the validation simulations was to see whether ELCOM could reproduce the three dimensional summer and winter temperature and salinity structures when forced with the data shown in Figures 5.4 and 5.5 and initialized with uniform water columns having values given as shown in Figure 5.3. The results from these simulations are shown here for the winter (Figures 5.10 and 5.12) and summer (Figures 5.11 and 5.13) periods; the agreement between the simulation results and the field data are generally excellent as shown in Figures 5.10-5.13.

During winter, relatively fresh water entered the Gulf through the Strait of Hormuz, making its way to the comparatively deeper Iranian coast. In contrast, higher water densities were noticed all around the basin, particularly around the area surrounding Qatar and the UAE (Figure 5.10 A panel 3). These results support the predominant control of density by the salinity distribution (Figure 5.12 A). This pattern is consistent with the broad circulation in the Gulf where the Coriolis force deflects the

surface inflow towards Iran and the subsurface outflow towards the Arabian coastline [*Sultan et al.*, 1995]. The salinity increased from 36 psu near the Strait to 41 psu near Kuwait (Figures 5.10 A panel 2 and 5.12), while the temperature fell from 22 to approximately 14 °C, as shown in Figures 5.10 A panels 1 and 5.12, at the same location. In the shallower waters of the Gulf, higher salinity levels are obvious, reaching 44 psu near the UAE coastal waters (Figure 5.12), resulting in an increase in the surface density and consequent vertical sinking (Figure 5.10 A panel 3). This generally agreed with the findings of *Reynolds,* [1993]. The simulations revealed that the Gulf water is mostly mixed vertically along its main axis during 1992 winter conditions.

Summer simulations exposed a more stratified structure in the estuary but with horizontal trends of both temperature and salinity similar to those of winter (Figure 5.11 A panel 1 and 2). A significant rise in water temperature of the estuary was evident parallel to the coastal areas of the Gulf, as indicated in Figures 5.11 A panels 1 and 5.13, reaching 31 °C near the UAE. This sharp rise in temperature was due to the continuous heat input through the air-sea interface as indicated in Figure 5.5, leading to a rather lower surface water density than winter, ranging between 24 and 30 kg/m^3 (Figure 5.11 A panel 3). The contour plot in Figure 5.13 and the vertical plot in Figure 5.11 A imply that relatively cold, saline and dense Gulf water was found beneath the warmer, less saline and lighter surface inflow from the Gulf of Oman.

As for the collected data, fresh water inflow from the rivers did not significantly affect the flow characteristics of the basin as a whole for both seasons, but local effects were apparent, particularly at the far north of the Gulf near Kuwait, where the

Shatt Al Arab meets the hypersaline water (Figure 5.12 and 5.13). Also, during winter, at 650 km off the Strait predictions in Figure 5.10 A panel 2 show salinity values (41 psu) lower than the summer 42 psu (Figure 5.11 A panel 2), suggesting that the river buoyancy effect was apparent in this region of the Gulf.

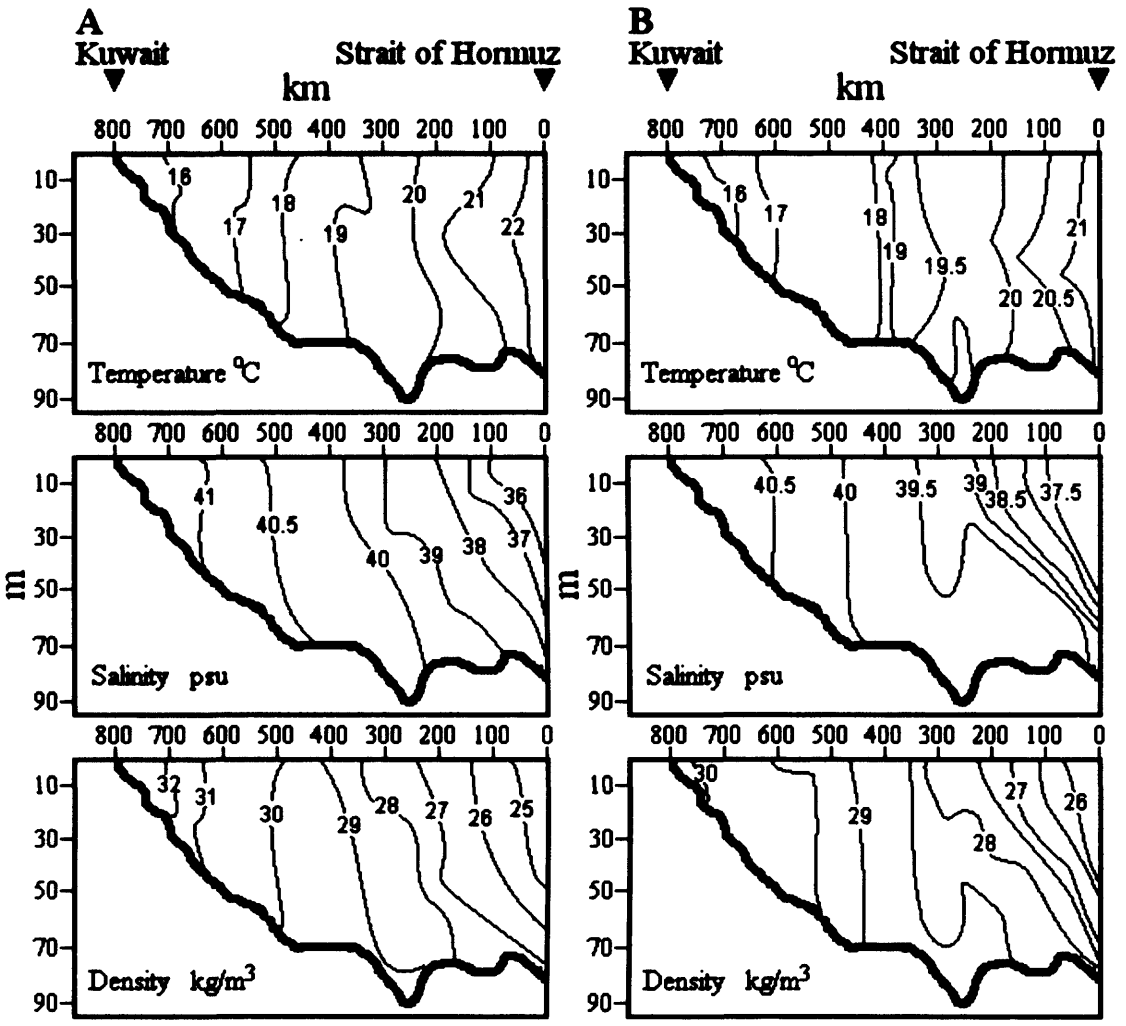

Figure 5.10: A. Simulated vertical variation of temperature, salinity and density along the Gulf (from the Strait of Hormuz to Kuwait) during winter (1992)

B. Field data variation of temperature, salinity and density along the Gulf (from the Strait of Hormuz to Kuwait Bay) during winter (1992)

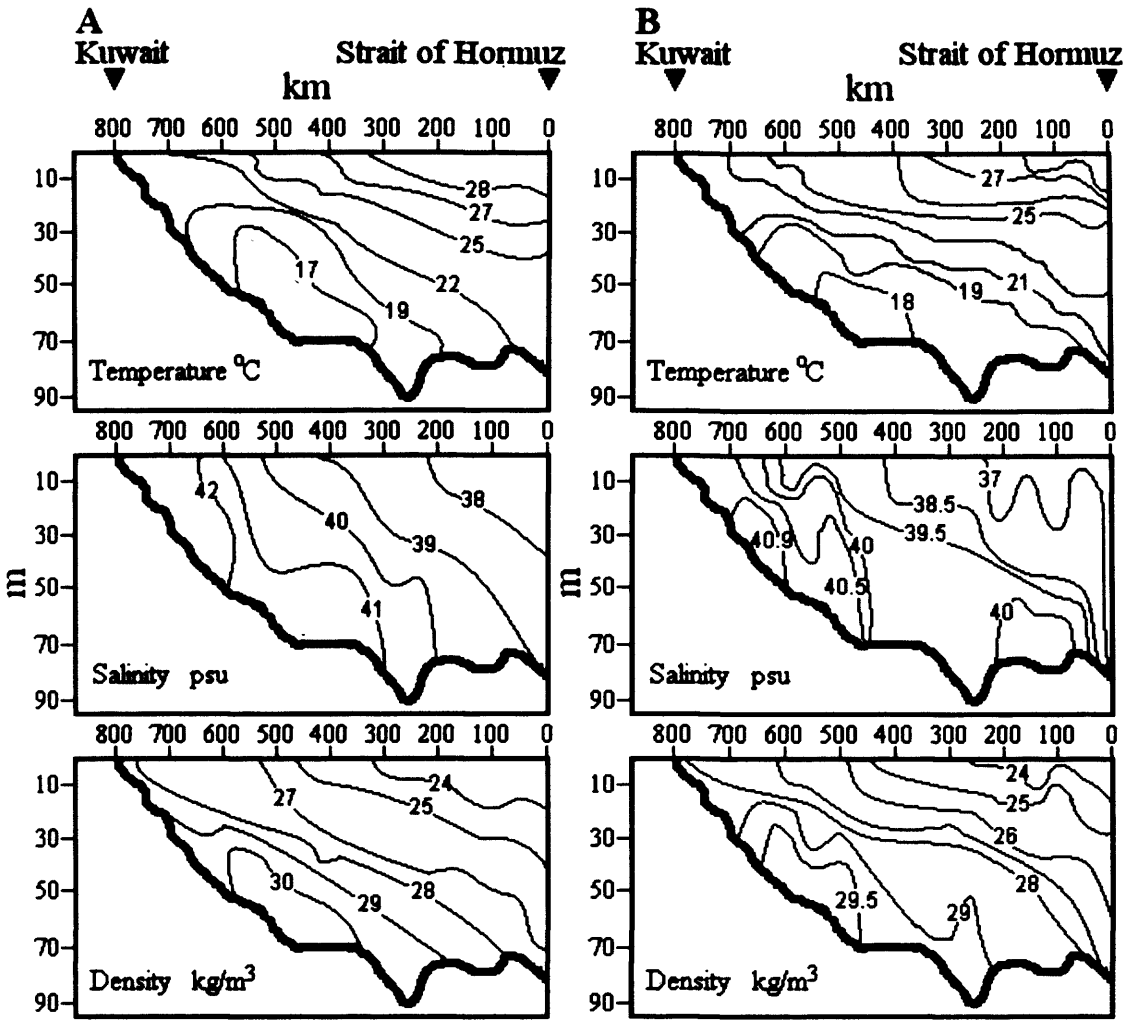

Figure 5.11: A. Simulated vertical variation of temperature, salinity and density along the Gulf (from the Strait of Hormuz to Kuwait) during summer (1992)

B. Field data variation of temperature, salinity and density along the Gulf (from the Strait of Hormuz to Kuwait Bay) during summer (1992)

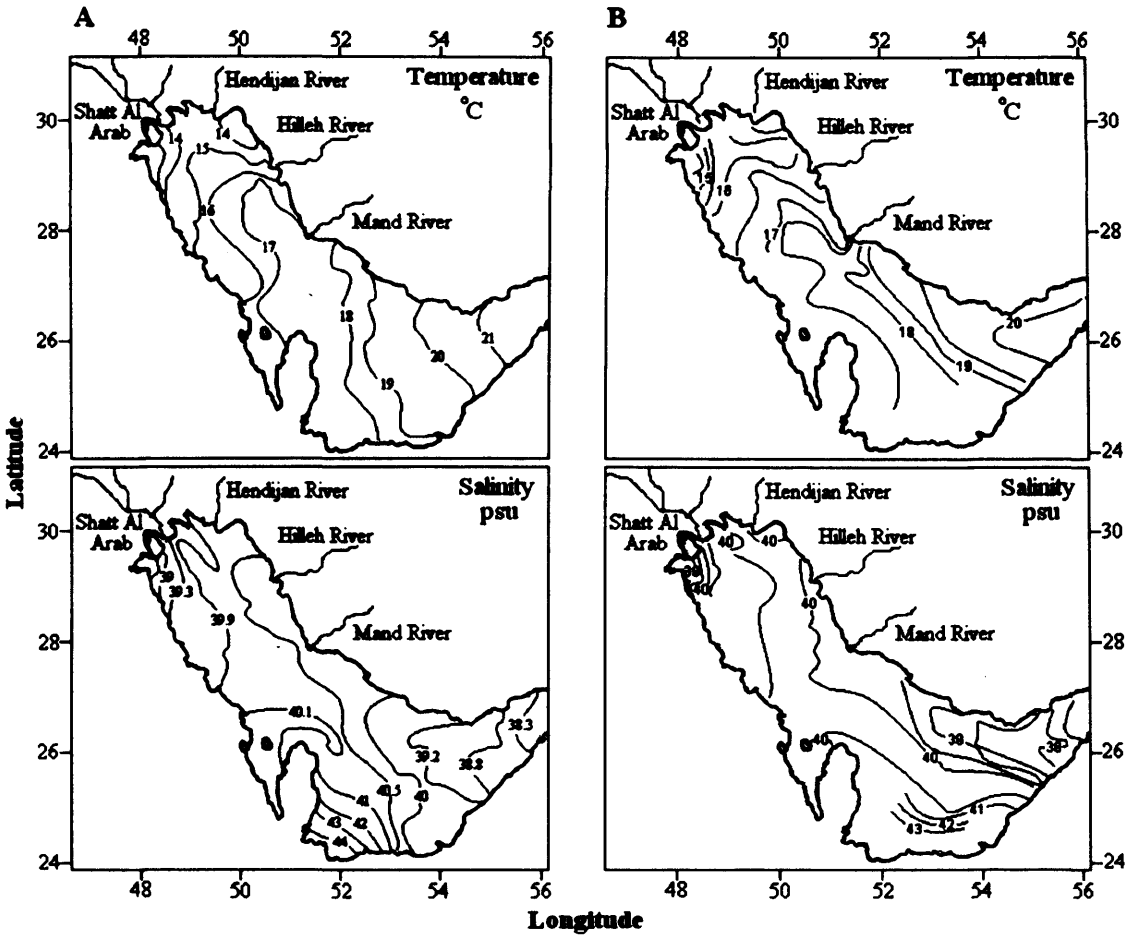

Figure 5.12: A. Simulated surface variation of temperature and salinity of the Gulf during winter

B. Field data of temperature and salinity of the Gulf during winter

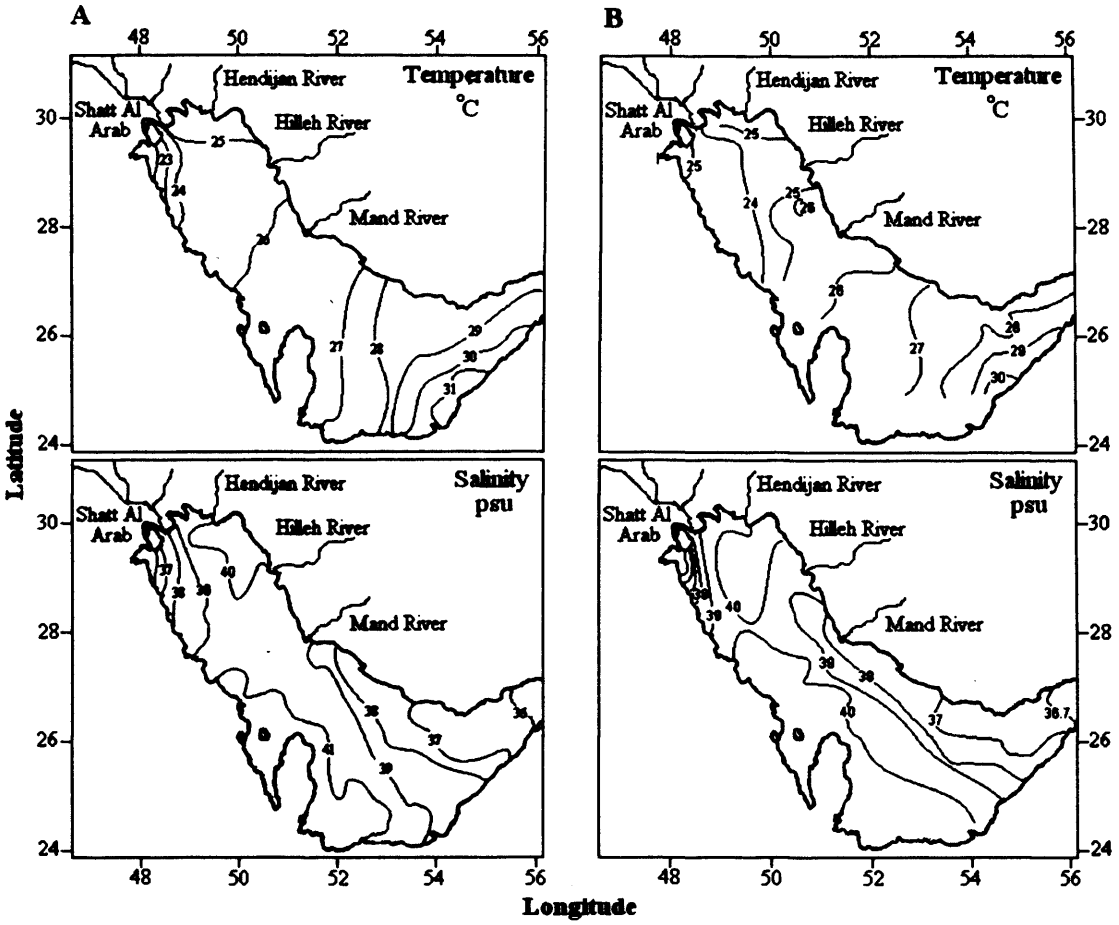

Figure 5.13: A. Simulated surface variation of temperature and salinity of the Gulf during summer

B. Field data of temperature and salinity of the Gulf during summer

The scale of motion in the domain is shown in Figure 5.14, where the depth-averaged velocity of the spring flood tide at the Strait of Hormuz is depicted. Clearly the scale of the velocity field is considerably larger than the grid resolution of 5,000 × 5,000 m.

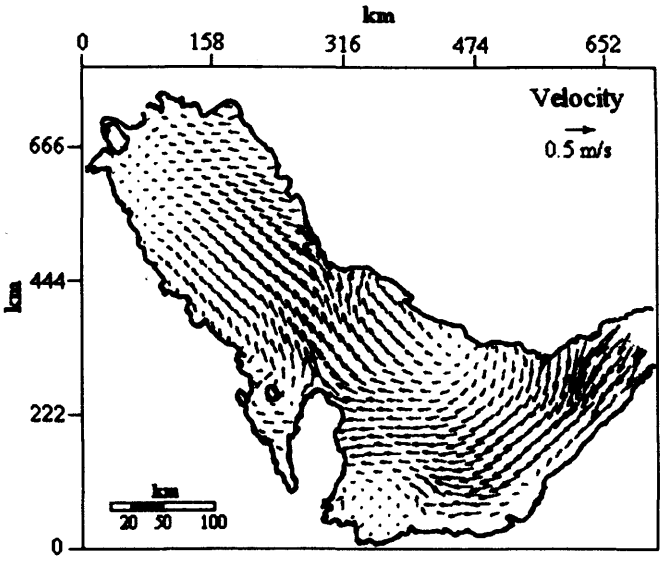

Figure 5.14: Depth-averaged velocity for spring flood tide during winter 1992 at the Strait of Hormuz

5. 4. 4 Geographic distribution of dispersion intensity:

Horizontal dispersion coefficients K_x were derived following *Taylor*, [1954], *Okubo*, [1971] and *Lawrence et al.*, [1995] using:

$$K_x = \frac{1}{4}\frac{\sigma^2}{t} \text{ and } \sigma^2 = \frac{A_{90}}{7.23}$$

where t is time (5 days, 20 days and 40 days) and A_{90} is the horizontal area containing 90% of the tracer mass. The time for vertical mixing t_v can be estimated by arranging the above equation to give:

$$t_v = \frac{\sigma_z^2}{4K_z}$$

It is usual to assume that vertical mixing is complete when the standard deviation equates to $0.8h$ [*Lewis*, 1997], where h is the total depth, and hence the mixing time is given by:

$$t_v = \frac{(0.8h)^2}{4K_z} = \frac{0.32h^2}{K_z}$$

For a well-mixed estuary, a typical value of K_z would be 0.01 m^2/s [*Lewis*, 1997], so that for a water depth of typically 36 m, such as the Gulf, the above equations imply that $t_v = 5.75$ hours for a completely mixed scenario over the depth. *Fischer et al.*, [1979] estimated the vertical mixing time scale to be:

$$t_v = \frac{h^2}{10K_z}$$

Using similar values of K_z in the above equation, t_v is estimated to be 3.6 hours.

Horizontal dispersion coefficients were determined by observing the horizontal spread of four numerical tracers and utilizing the above equations. The numerical tracers were introduced uniformly over the depth at various locations, as shown in Table 5.5, namely at stations T6, T7, T8 and T9. The initial size of the patch was 5,000 × 5,000 m, which equates to the size of a grid cell. The length scale was obtained by calculating $A_{90}/7.23$ using MATLAB, and the horizontal dispersion coefficient was calculated after 5, 20 and 40 days of continuous tracer release, starting from the validation period.

In general, higher values were apparent near the Arabian coast. The highest dispersion coefficient occurred during winter, with a value of 141 m^2/s at T9, during the early days of tracer release; similar values were achieved during summer. It is clear that even with higher horizontal diffusivities of 5 and 10 m^2/s, the dispersion coefficients remained almost the same as in Table 5.5. In the model validation the effects of the rivers were found significant only locally, and buoyancy related to fresh water inflows would only be substantial in the long run. Hence the effect of rivers may be neglected since all locations of injections were far enough away from the fresh water inputs.

Winter

5 Days			*20 Days*			*40 Days*		
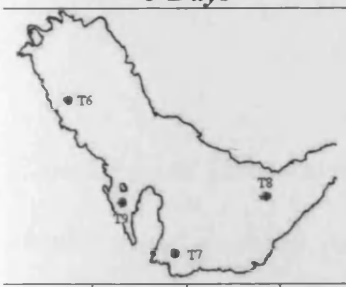						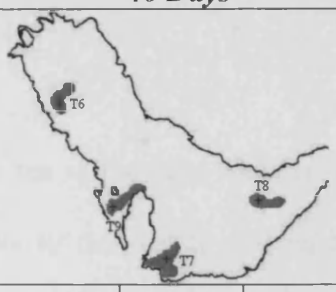		
κ	*1.0*	*5.0*	*10.0*	*1.0*	*5.0*	*10.0*	*1.0*	*5.0*	*10.0*
T6	103	103	104	73	73	73	77	78	78
T7	99	99	100	86	86	86	90	90	90
T8	127	128	128	61	62	62	80	80	80
T9	140	141	141	87	88	88	83	83	83

Summer

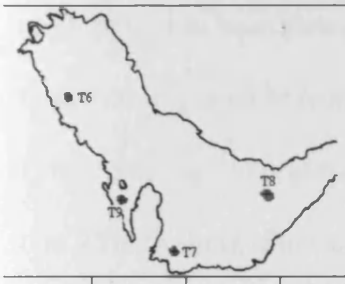						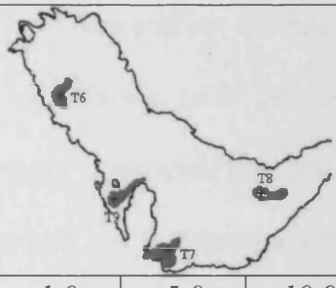		
κ	*1.0*	*5.0*	*10.0*	*1.0*	*5.0*	*10.0*	*1.0*	*5.0*	*10.0*
T6	100	100	100	70	71	71	75	75	76
T7	95	95	95	81	81	82	87	87	88
T8	126	127	127	60	61	61	83	83	83
T9	137	138	138	83	84	84	81	82	82

Table 5.5: Dispersion coefficients K_x (m^2/s) during summer and winter 1992, using meteorological effects from 18 January to 26 February for winter simulations and 8 May to 12 June for summer simulations, with κ=1, 5 and 10 m^2/s, + is the release point

5. 4. 5 Residence time:

Flushing times, age, and residence times are commonly used measures for calculating retention characteristics of water or scalar quantities transported by the flow. *Boynton et al.,* [1995] argued that the residence time is a vital element that should form the basis of comparative analyses of ecosystem nutrient budgets. In practice, different

approaches may lead to different time scales, even for the same domain [*Monsen et al.*, 2002].

Dronkers and Zimmerman, [1982] defined the residence time as the time taken for a whole water parcel to leave the lagoon through its outlet to the sea. In this study special attention was given to the residence time of the water in the whole estuary, since flushing time is an integrative system measure, whereas both residence time and age are local measures. In the case of the Gulf, the circulation in and out of the Strait of Hormuz has been poorly defined in the past, resulting in estimates of the residence times varying widely from between 2 to 5 years [*Hughes and Hunter*, 1979; *Hunter*, 1983]. *Sadrinasab and Kamp*, [2004] studied the flushing time of the Gulf and found that 95% flushing times of surface waters ranged from between 1 to 3 years along the Iranian coast, while larger values of more than 5 years were obtained along the Arabian coast.

In modelling the residence time of the Gulf using ELCOM, forcing model data of 1992 (January to December) were adopted and repeated for successive years. It was assumed that initially each cell contained water with a residence time of zero. The flushing time was defined as the residence time of the water as it left the domain (i.e. the time taken for the water to leave the domain). The model revealed that the residence time in the Gulf was almost 3 years, as shown in Figure 5.15, the residence time being the longest time for water packages to remain along the Arabian coast of the Gulf. In particular, near Kuwait Bay, Qatar and the UAE coast values reached 858 days. Obviously the residence time at the Strait of Hormuz was lowest (2 days), due to the open boundary effects in the region.

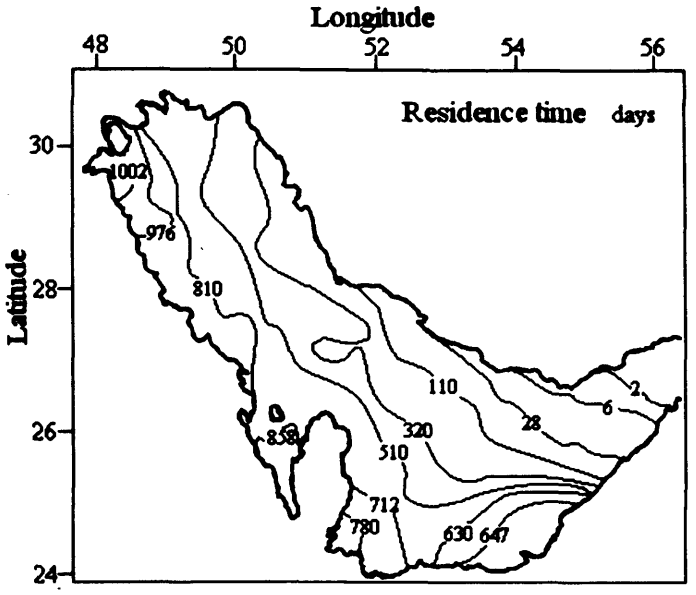

Figure 5.15: Residence time of the Gulf in days

5 .4 .6 Discussion:

To determine the main drivers of the horizontal dispersion of the tracers, various forcing scenarios were implemented for the sensitivity analysis. All the simulations were carried out using a selection of the above summer and winter forcing data from 1992, as detailed in Table 5.6.

Experiment	Season	Tide	Wind	T6 (K_x)	T7 (K_x)	T8 (K_x)	T9 (K_x)
ELCOM1	Winter	Yes	No	49	60	69	60
ELCOM2	Winter	No	Yes	24	27	10	20
ELCOM3	Summer	Yes	No	53	60	72	60
ELCOM4	Summer	No	Yes	20	25	8	19

Table 5.6: Diffusion Coefficients due to various effects after 40 days of release

These simulations enabled a sensitivity analysis to be undertaken for the various forcing mechanisms. As seen from Table 5.6, tidal forcing accounted for about two thirds of the total tracer dispersion at T6 and T7, almost 90% at T8 and 75% at T9, during summer and winter.

Justification for using a 5,000 m grid and the chosen horizontal diffusivity value is necessary before analysing the results obtained in this study. Previously, observations by *Lawrence et al.* [1995] suggested diffusivity values of $O(10^{-1})$ m^2/s for a length scale of 500 m; also *Stocker and Imberger* [2003] computed turbulent diffusivities of $O(10^{0})$ m^2/s in Lake Kinneret. *Okely et al.* [2010] for Victoria Lake revealed that a horizontal diffusivity in ELCOM of less than 1 m^2/s was appropriate. In this study, an initial horizontal diffusivity of 1 m^2/s was utilised in the model, selected on the basis of the findings of *Okubo,* [1974], in which a length scale of 5,000 m corresponded to 1 m^2/s (see Figure 5.16). By analogy, 1 m^2/s would take account of horizontal dispersion at scales smaller than the model grid resolution, as shown in Figure 5.17, in which this value was fixed throughout the simulation period. To ensure adequacy of the value chosen, the horizontal diffusivity was altered to 5 m^2/s and then to 10 m^2/s in the model, confirming that this did not significantly influence the horizontal dispersion of the tracers, as shown in Table 5.5. Therefore, Table 5.5 shows that as time progressed the tracer at each station formed a circular patch during the first days after injection, which eventually progressed into an oval shape along the mean flow direction due to turbulent diffusion, as shown in Figure 5.18 A and B. However, as the patch size evolved due to further injection the oval shape was distorted and stretched, forming a random shape dependent on the direction of shear force effects and, to a smaller extent, larger or smaller eddies. Shear effects played the main role in

expanding the patch size after 30 days, which will be explained in the following paragraphs. It is worth mentioning that by using the *Okubo,* [1974] K vs l graph to calculate K_x from the corresponding length scales of T6, T7, T8 and T9 during 20 days (shown in Table 5.5), values of 68, 78, 62 and 83 m^2/s were obtained (see Figure 5.16), with these values being similar to the respective computed values cited in Table 5.5.

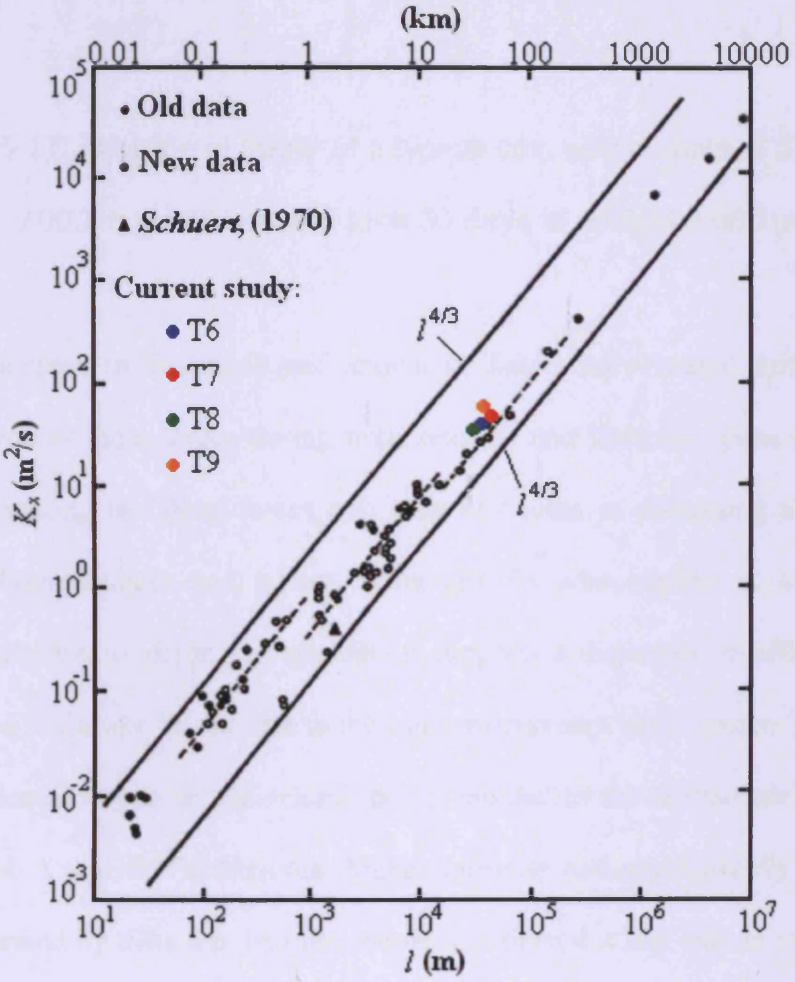

Figure 5.16: Separated ranges in plot of horizontal dispersion coefficient against length scale including typical dispersion coefficients obtained in the current study (modified after Okubo, [1974])

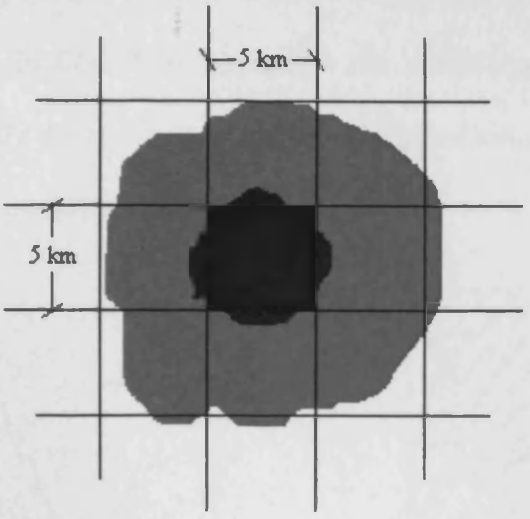

Figure 5.17: Injection of tracer at a typical cell, with a scale of 5,000 m × 5,000 m would typically take 30 days to spread 5,000 m

Scenarios adopted in this study and shown in Table 5.6 revealed that the Gulf is mainly driven by tidal forces during both seasons and therefore tides are the main drivers in creating the shear forces that play key roles in dispersing the numerical tracers in both summer and winter. Although T8 was located at a site with a comparatively greater depth, the simulation suggests a dispersion coefficient similar to that at the shallower T6 site due to the uniform currents, since tracers spread out in both directions away from the release point, similar to the spread shown at T7 in Figures 5.18 A and B. Furthermore, higher currents and consequently larger shear forces generated by tides are distinguishable and played a key role in dispersing the tracer at T8. Similarly, but to a smaller extent at T6, shear generated by wind speeds of approximately 15 m/s in a direction across the mean flow, combined with large eddies and Coriolis forces, enhanced dispersion by more than 15% along the estuary and deflected the patch in a seaward direction with dispersion coefficients comparable to values obtained at T8. Analogously, conditions at T9 are significantly affected by

wind shear, but the topography at this location caused dispersion coefficients to be increased due to bed friction. This elongated the patch towards the north Qatar coastline, and eventually it became vulnerable to large eddies (e.g. Figure 5.14) as it developed towards the estuary main channel.

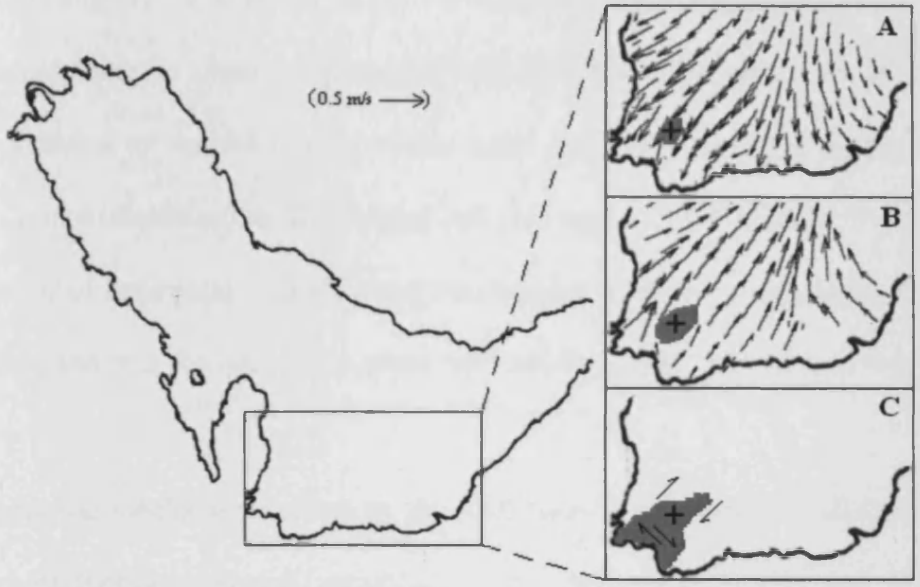

Figure 5.18 A: Flood tide effect at T7 (5 days), **B:** Ebb tide effect at T7 (10 days), **C:** Shear force effect in spreading the tracer at T7 (45 days)

At T7 the great contribution of tides in stretching the patch away from the release point towards the coast of the UAE and Qatar is indicated by its increase in size and developing a most random shape, as shown in Figure 5.18 C. This can be explained by the combination of wind, tides, an irregular topography and coastal interaction that enhanced shear forces. Moreover, as the patch evolved, it interacted with the coastline, comprising smaller bays and headlands that dramatically increased the dispersion coefficients after 40 days, giving rise to "Coastal Trapping" [*Inoue and Wiseman,* 2000] and making mixing efficient and chaotic (Figure 5.18 C). Although

the mixing processes appear to be considerable at T7, the residence time in Figure 5.15 suggests that the patch would prevail for about 750 days.

Horizontal turbulent diffusion played a minor role because dispersion coefficients varied only slightly for different horizontal diffusivities (shown in Table 5.5). Bottom and internal shear, as observed in the velocity profiles in the top centre of the Gulf, also contributed to vertical mixing of the water column particularly during summer due to minor stratification developing in the upper layer (Figure 5.11). Shear components of horizontal velocity along the Arabian coastline were greater, both near the surface and near the bed, due to wind drift and bottom friction respectively.

The dispersion mechanisms affecting the Gulf have a fundamental influence on the ecology. Furthermore, spatial variability in the horizontal mixing and dispersion coefficients has several implications for water quality within the Gulf. Due to the nature of the Gulf, high nutrient values normally result in high rates of oxygen consumption, particularly along the relatively shallow Arabian shoreline [*Brewer and Dyrssen*, 1985], so dispersion processes arising from the wind along this region would significantly influence the nutrient levels along the coast. *Brewer and Dyssen,* [1985] found high surface phosphorus levels that may be attributed to the vertical dispersion mechanism in such regions. Moreover, nutrient concentrations in the Gulf have often been concentrated in the north of the Gulf, in the Bay (see Chapter 7 for nutrient predictions in the Bay) and in the region around the outfall of Shatt Al Arab, and they have been cited as the cause of a number of eutrophication incidents, mostly during summer. For example, a major red tide and an associated fish kills occurred in 1999 [*Heil et al.*, 2001].

An estimate of the fluid residence time, i.e. the average time a water particle spends within a region [*Geyer and Signel*, 1992], is given as:

$$t_R = \frac{l^2}{K_x}$$

where $t_R \approx 200$ days for an average dispersion coefficient of 90 m^2/s and $l = 40$ km, an estimated length scale for the assemblage localities. This relatively long time scale allows the ecological niches to exist and promotes spatial heterogeneity of biochemical material, in particular in the northern part of the Gulf near the Bay (see Chapters 6 and 7).

5. 5 Summary:

Understanding and identifying the dispersion mechanisms of the Gulf is of great importance, since it has been used extensively for the mixing and spreading of various types of effluents. In this chapter, the general definition of horizontal dispersion has been given, including the dispersion coefficients for the Gulf which have been identified as a function of geographic location by using ELCOM. The model was first validated by means of temperature, salinity and density of the Gulf water, during the winter and summer of 1992. Then the validated model was used to calculate the dispersion coefficients of numerical tracers, distributed randomly in the basin and injected continuously throughout the simulation period (40 days). The analyses have shown that tides played a key role in the spreading of the tracers, while winds had a lesser effect. The highest dispersion coefficient obtained in this study occurred near Qatar, due to the shear effects produced by tides and the coastal geometry, which reached 141 m^2/s during the first 5 days of tracer injection. Other locations were shown to have similar dispersion coefficients that ranged from between 60 and 90

m^2/s. Also in this chapter, the residence time of the Gulf was calculated using ELCOM. The results showed that a higher residence time occurred along the Arabian coast, in particular near Kuwait and Qatar, which reached times of 1002 and 858 days respectively, while the lowest residence time occurred near the Iranian coast, with a typical period of 200 days. Such results have huge implementations in identifying the high-algal-production-zone in the basin.

Chapter 6

Hydrodynamic Modelling of

Kuwait Bay

6. 1 Introduction:

Every estuary is unique with respect to physical, chemical, and biological characteristics. Yet any estuary may share a number of features with any bays along its coastline. Therefore, it was important to understand the Gulf's water circulation and dispersion mechanisms (as discussed in Chapter 5) before studying the mechanisms of Kuwait Bay (see Figure 6.1). This analysis of the Gulf would provide some information about the behaviour of the Bay that could consequently help in understanding the various water quality processes within Kuwait Bay.

It is important to study the hydrodynamic processes of Kuwait Bay before conducting any water quality analyses. Here hydrodynamics is referred to as the study of the motion of the water and the major forces acting on it, such as those mentioned in Chapter 2. It is well recognised in the literature that hydrodynamics is the driving mechanism for the transport of nutrients, algal blooms and sediments and is also a major factor when considering the circulation of pollutants in a marine system. In addition, hydrodynamic modelling may supply essential information for other models, such as eutrophication models, including water level and velocity, circulation patterns, mixing and dispersion, water stratification and temperature variations.

The main aim of this chapter is to validate ELCOM and investigate the water circulation of the Bay using the validated model. This was achieved by conducting various sensitivity analyses on the domain boundaries and injecting numerical tracers at the open boundary. Also, the residence time of the Bay will be investigated in this chapter, so as to provide an understanding as to how effluents would, for example, accumulate within the Bay and then be flushed away to the Gulf water body.

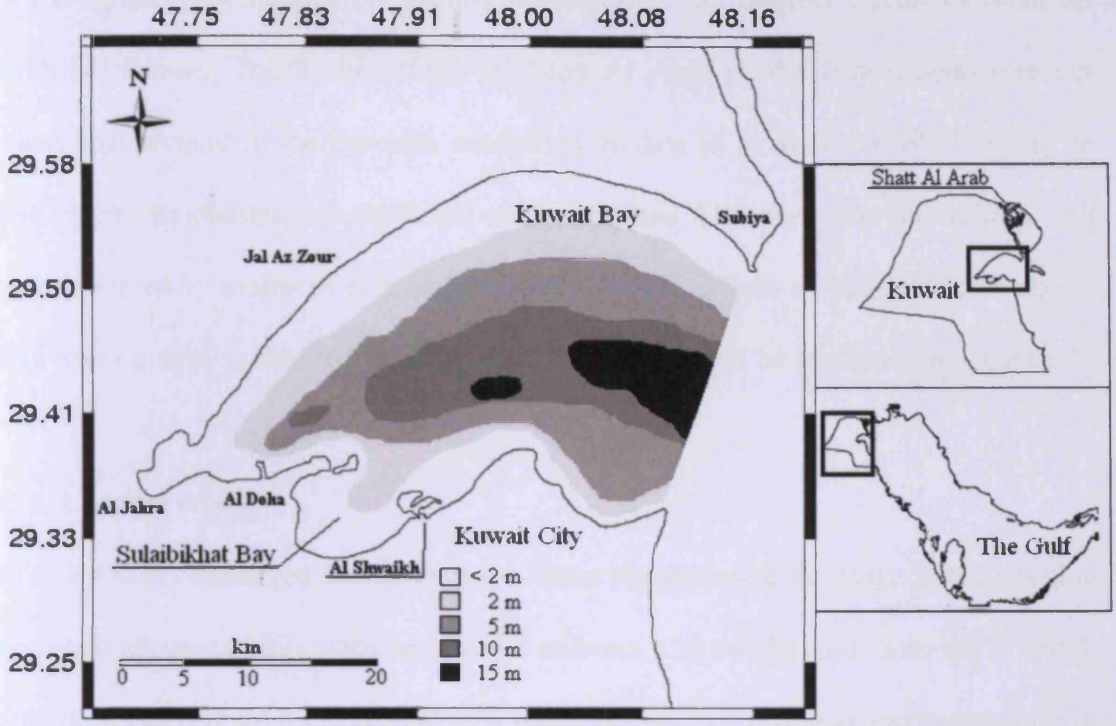

Figure 6.1: Kuwait Bay location in the Gulf and including Sulaibikhat Bay

6. 2 Hydrodynamic modelling of Kuwait Bay:

In studying the hydrodynamic processes in the Bay, special attention was given to temperature and salinity, as they were considered to have an apparent influence on water circulation in this region [*Reynolds,* 1993]. It is worth mentioning that direct fresh water input to the Bay can reasonably be considered negligible. Recently, temperature and salinity were recognised to have a fluctuative manner throughout the year in some parts of the Bay [*Al-Rashidi,* 2009]. In terms of fluctuations in water temperature this is due to the following three main reasons as explained by *Al-Rashidi,* [2009]:

- Global effects (climate change);
- Regional effects (anthropogenic activities in the Gulf); and
- Local effects (desalination plants in the Bay see Chapter 2).

While salinity fluctuations are mainly attributed to the indirect effects of Shatt Al Arab [*Al-Yamani,* 2008], the effects of Shatt Al Arab on the Bay waters were not taken into account in the previous modelling studies as in *Rakha et al.,* [2007a]. In this chapter an attempt to quantify the effects of Shatt Al Arab on the Bay salinity will be considered by means of a sensitivity analysis. The effects of Shatt Al Arab on the Bay water quality is detailed in *Al-Yamani,* [2008] and will be explained in Chapter 7.

6. 2. 1 Model setup:

ELCOM was considered in studying the water dynamics of the Bay. The modelling approach adopted in this study involved a uniform grid of 150 m in both the X and Y directions (see Figure 6.2). A total of 7 layers in the Z direction at increments of 5 m leading to a total of 115,095 wet cells discretising the domain and the open boundary was approximately 17.5 km in connection with the Gulf main channel (see Figure 6.2). A computational time step of 100 s was utilised in the model. The bathymetric information was obtained from a map digitiser at the Hydro-environmental Centre of Cardiff University that interpolated the depth at each grid point from a map obtained from the United Kingdom Hydrographic Office. The sea surface elevation, due to semidiurnal tide, was prescribed at the open boundary using the KTIDE model developed by *Al-Salem* (KISR, 2009) for the 2005 period (Available on Coastal Information System www.hceatkuwait.net). The salinity and temperature data necessary for initialising and running the model was obtained from the K-EPA and values were assigned based on previous data from 2004 as shown in Table 6.1. The typical values for desalination plant (MSF or RO, see Chapter 2 for more details) discharges were given at a rate of approximately 10 m^3/s through an outfall of approximately 60 m in width [*Bleninger and Jirka,* 2010]. However, in this study a

discharge of 4 m^3/s was utilised due to the relatively large grid size considered (150 m) to account for the desalination plant outflow. Two main desalination plant outfalls were considered in this study which are located at Al Doha (see Figure 6.3), with temperature and salinity values based on these cited in Figure 2.3 (in Chapter 2) and detailed in Table 6.1. To optimise the predictions, the model was allowed to run for 20 days before the actual intended simulation period (i.e. 20 days before 1st January 2005).

Boundary	Temperature (°C)	Salinity (psu)
Outfall	30	50
Open boundary	15-33	36-41
Domain	14	35

Table 6.1: Initialising values of temperature and salinity based on 2004 (K-EPA)

Horizontal diffusivity, κ, is an input parameter in ELCOM, representing turbulent sub grid diffusion. In the model transport equations (for more details see [*Hodges et al.*, 2000]) this was set to 1 m^2/s. Similar to *Rakha et al.*, [2007a] a bottom drag coefficient of 0.003 was assigned for the whole domain to take account for bed friction. A light extinction coefficient of 0.25 was used to take account of attenuation of light. The meteorological forcing adopted in this study is summarised in section 6.2.1.1 and was applied at 10 m above sea level.

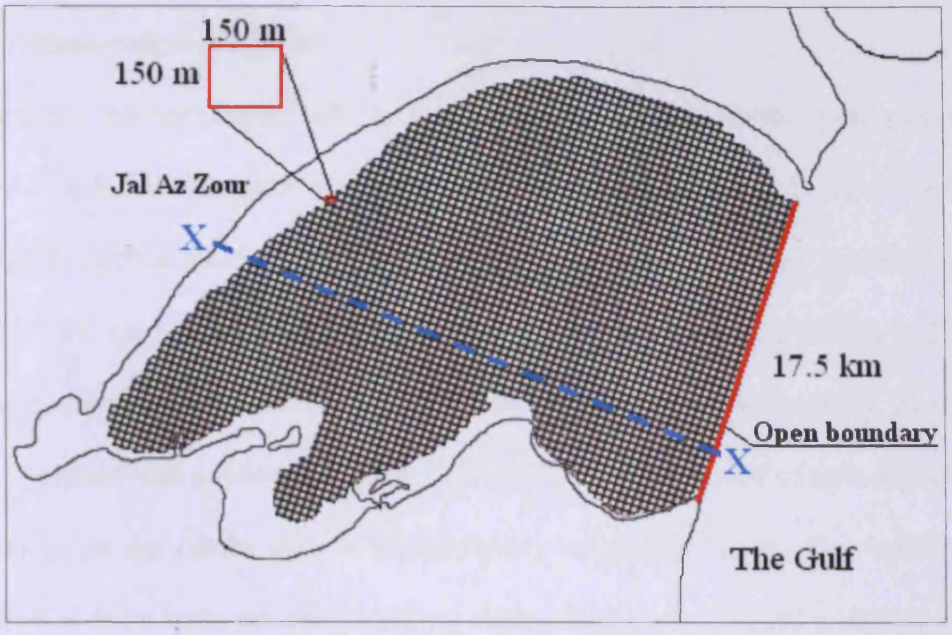

Figure 6.2: Discretisation of the Bay, showing the grids utilised in ELCOM and the length of the open boundary, also the cross section considered along 'X-X'

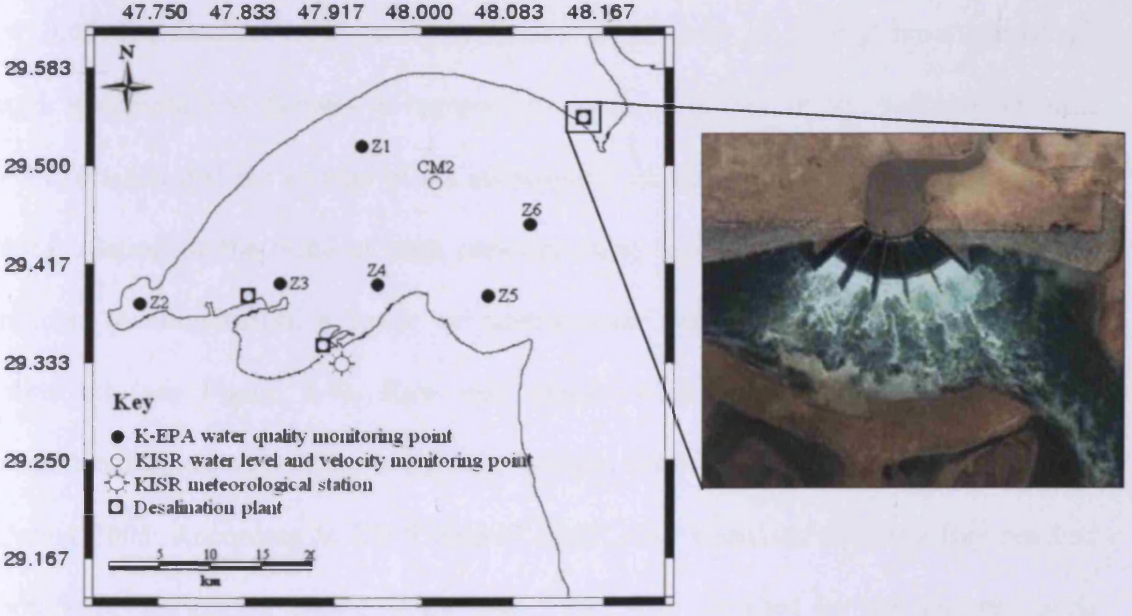

Figure 6.3: Location of sampling points in the Bay (left) and a discharge from the desalination plant at Sabiya (right)

6. 2. 1. 1 Meteorological effects:

The temporal meteorological effects necessary for the simulation purposes were obtained from KISR. The station that recorded the data on an hourly basis was located at the KISR campus south of the Bay, as shown in Figure 6.3. The meteorological parameters for the period 2005 were adopted in the model and are shown in Figure 6.4. These effects were considered to be applied over the entire water body, as a finer spatial resolution was not available; however this was not expected to have significant implications on the results due to the relatively small size of the Bay which was recognised to have been driven mainly by tides [*Rakha et al.,* 2007a; *Rakha et al.*, 2009]. As shown in Figure 6.4 the Bay is mostly affected by wind blowing from the northwest, particularly during winter with typical peak speeds of 12 m/s. Meanwhile, a less effective wind blows from the south, mostly during summer, reaching speeds of 5 m/s. In addition, a pronounced air temperature rise was observed during the summer of 2005 that reached 45°C during August. *Nasrallah et al.,* [2004] have related the high temperature to changes in regional circulation patterns of air to climate change. He explained that the change of the subtropical jet stream towards the north and the accumulation of the ridge of high pressure were mainly responsible for heat wave events. In comparison, a lower air temperature during the winter of 15°C was observed (see Figure 6.4). Rain and cloud cover effects were not taken into consideration, as records from the same station did not show any significant values during 2005. According to KISR data of 2005, solar radiation over the Bay reached 600 W/m^2 during the winter, while 900 W/m^2 was recorded for the summer; such effects were adapted in the model accordingly.

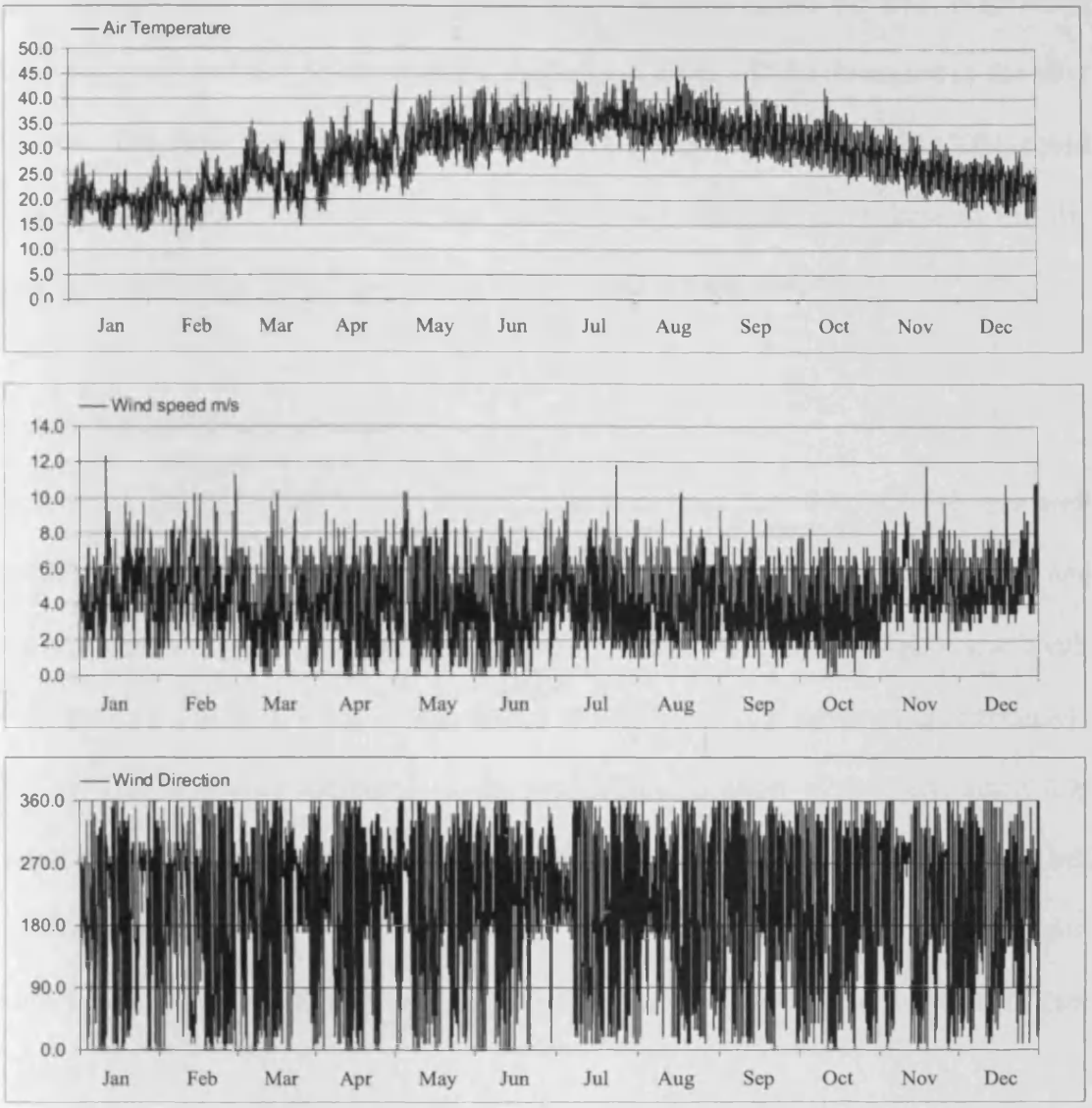

Figure 6.4: Meteorological data of 2005 adopted in the model, air temperature (top), wind speed (middle), wind direction (bottom)

6. 2. 2 Model validation and discussion:

The model was calibrated using data obtained from KISR at CM2, which is located approximately at middle of the Bay (see Figure 6.3). The main parameters used to validate the model were: water level, velocity magnitude and velocity direction. Due to limited data, the model validation period ran from 20th April 2005 to 10th May 2005 (see Figure 6.5). The simulations had to model first the hydraulic control across the

mouth of the Bay and then the dispersal of the salinity across the Bay, originating from both the Gulf and Shatt Al Arab. Such predictions will be discussed in the next section. The main aim of validating the model was to identify if ELCOM could represent the actual water levels and velocity, and therefore show how to use the model predictions to better understand the dynamics of the Bay.

6. 2. 2. 1 Water level and velocity:

In general, the water level and velocity magnitude and direction at CM2 was well predicted by ELCOM as shown in Figure 6.5, which had R^2 value of 0.850, 0.770 and 0.696, respectively. During the spring tide (24th April to 2nd May) high water levels were predicted, which reached more than 4 m and had a tidal range of approximately 3.5 m. This is mainly attributed to the geographic location of the Bay, since it is exposed to relatively high water levels compared to the southern part of the Gulf [*Rakha et al.,* 2007b]. Undoubtedly, this effect would make have an enormous contribution to the mixing processes of the Bay, in a similar manner to the Gulf (see Chapter 5).

Velocity magnitudes and direction predicted during 2005 followed an almost uniform pattern (see Figure 6.5). The highest velocity magnitude was predicted during the spring tides and the lowest during the neap tides at 95° and 275° during ebb and flood tides respectively. This uniformity can possibly be explained by the geographical location of CM2, which had minimal turbulence. In comparison, a more complex flow was apparent near the headlands e.g. Kuwait City and Sulaibikhat Bay (see Figure 6.6), with more explanations being given in Section 6.3. High velocity values were predicted at the mouth of the Bay reaching 1 m/s, while a relatively lower velocity

distribution was predicted in the northern part of the Bay. Due to the geophysical nature of the coastal areas of Kuwait City and Sulaibikhat Bay they can be classified as the least energetic waters, with velocity values reaching 0.1 m/s (see Figure 6.6), and therefore would occasionally be driven by winds, particularly during the winter (for more explanations see section 6.3).

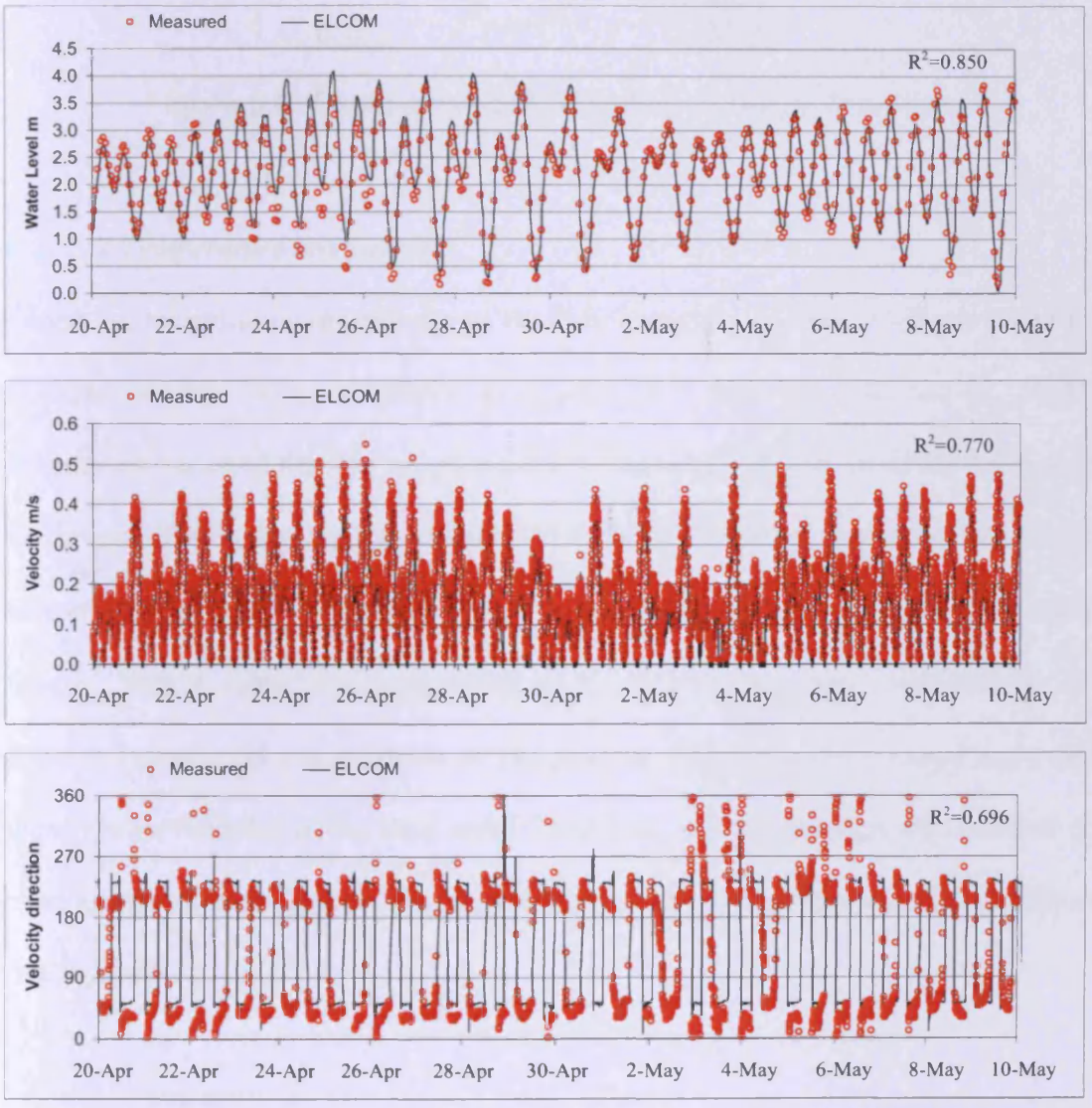

Figure 6.5: Model validation at CM2, Water Level (top), Velocity magnitude (middle), and Velocity direction (bottom)

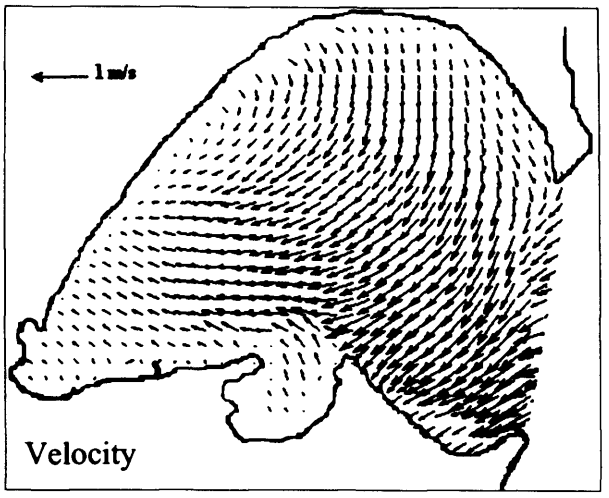

Figure 6.6: Depth-averaged velocities at typical flood tide

6. 2. 2. 2 Temperature and salinity:

Generally, temperature and salinity in the Bay at station Z1 were well predicted by ELCOM during 2005, as shown in Figures 6.7 and 6.8 respectively. Water temperature across of the Bay varied seasonally during 2005, similar to the findings of *Al-Yamani,* [2008]. The highest temperature level was predicted during August, which almost reached 34°C. While the lowest water temperature was predicted during January, with a value of approximately 15°C. In a recent study conducted by *Al-Rashidi,* [2009], the direct effects of desalination plants on water temperature and salinity were recorded in the local areas. Therefore, special attention was focused on areas near to stations Z3 and Z4 as they are located near two main desalination plants (see Figure 6.3).

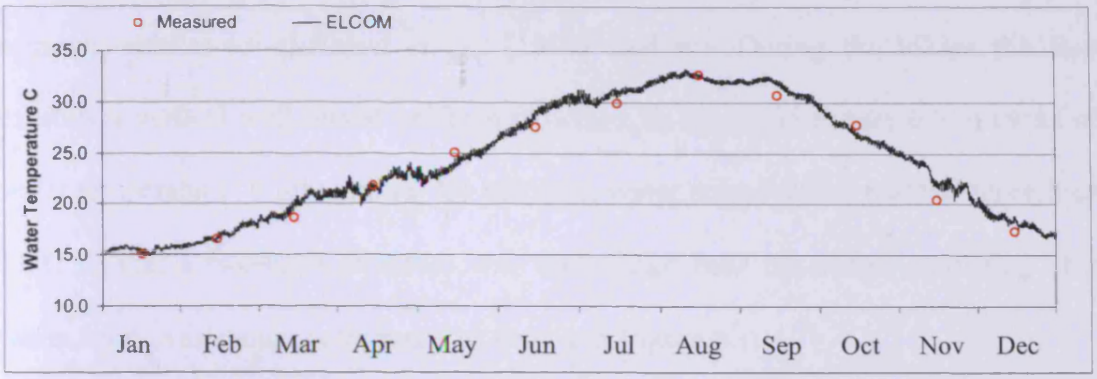

Figure 6.7: Comparison of predicted and measured water temperature at Z1 during 2005

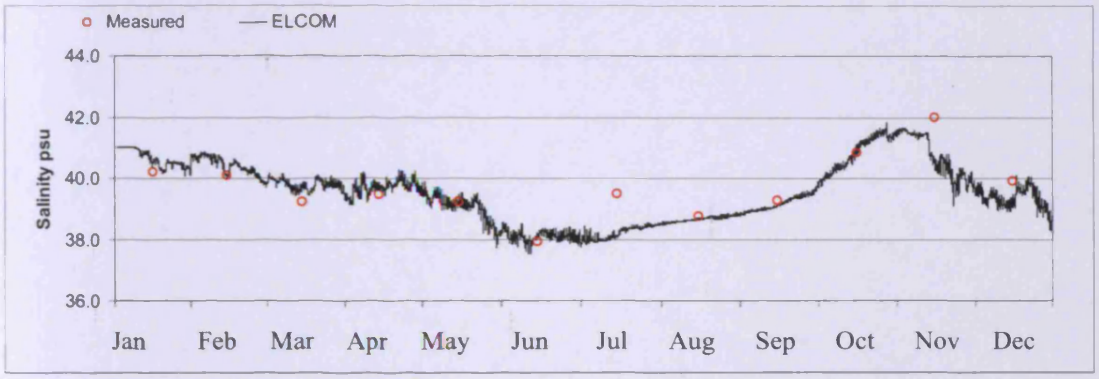

Figure 6.8: Comparison of predicted and measured salinity at Z1 during 2005

Broadly speaking, higher temperature levels are predicted at coastal areas, particularly near Kuwait city and Sulaibikhat Bay, rather than the deeper northern parts of the Bay, as shown in Figures 6.9 and 6.10, throughout all the seasons. This is similar to the findings of *Anderline et al.*, [1982], in which they explained that the northern areas are characterised by low salinity and temperature due to the relatively larger wind mixing and the minor anthropogenic activities in this region. Temperature is relatively higher at Z3 and Z4, as shown in Figures 6.9 and 6.10. This is mainly due to both the shallow nature of the Bay at these stations and the plume discharged from the desalination plants located nearby. Air temperature (see Figure 6.4) could be considered as the main source of heat to the surface water of the Bay during the

summer, similar to *Al-Fahed et al.,* [1997] findings. During the winter the Bay exhibits a vertical well-mixed uniform structure, as shown in Figure 6.9 in terms of water temperature. While, during the summer, water temperatures reached more than 31°C so that a two-layer structure was established near the shore, consisting of a warm layer overlaying cooler water as shown in Figure 6.10.

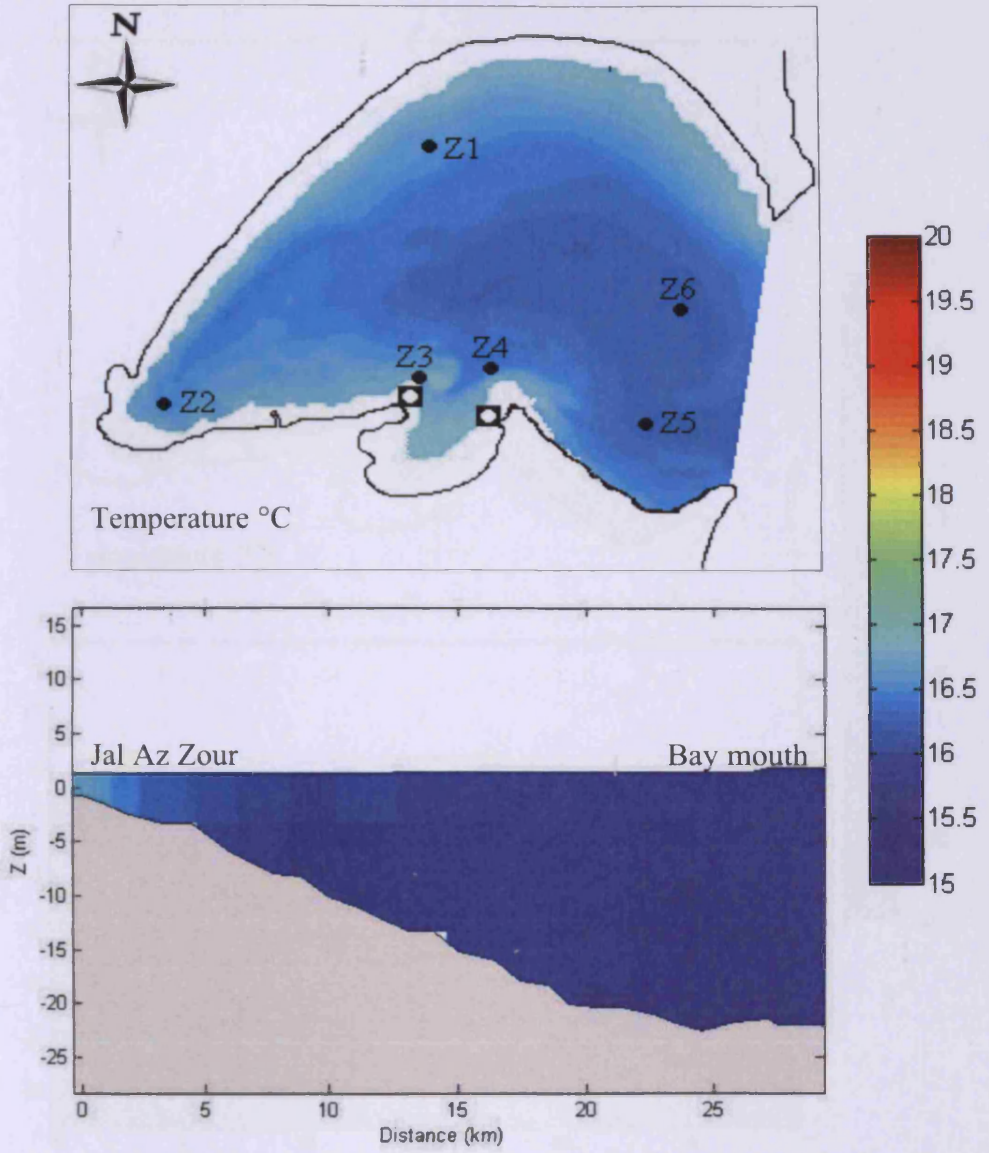

Figure 6.9: ELCOM predictions of surface temperature distribution in the Bay during the Winter (January 2005), including data collection stations and Al Doha desalination plants marked as '◘' (top graph) and a vertical temperature variation prediction during the winter (January 2005) between the Bay mouth and Jal Az Zour (bottom graph)

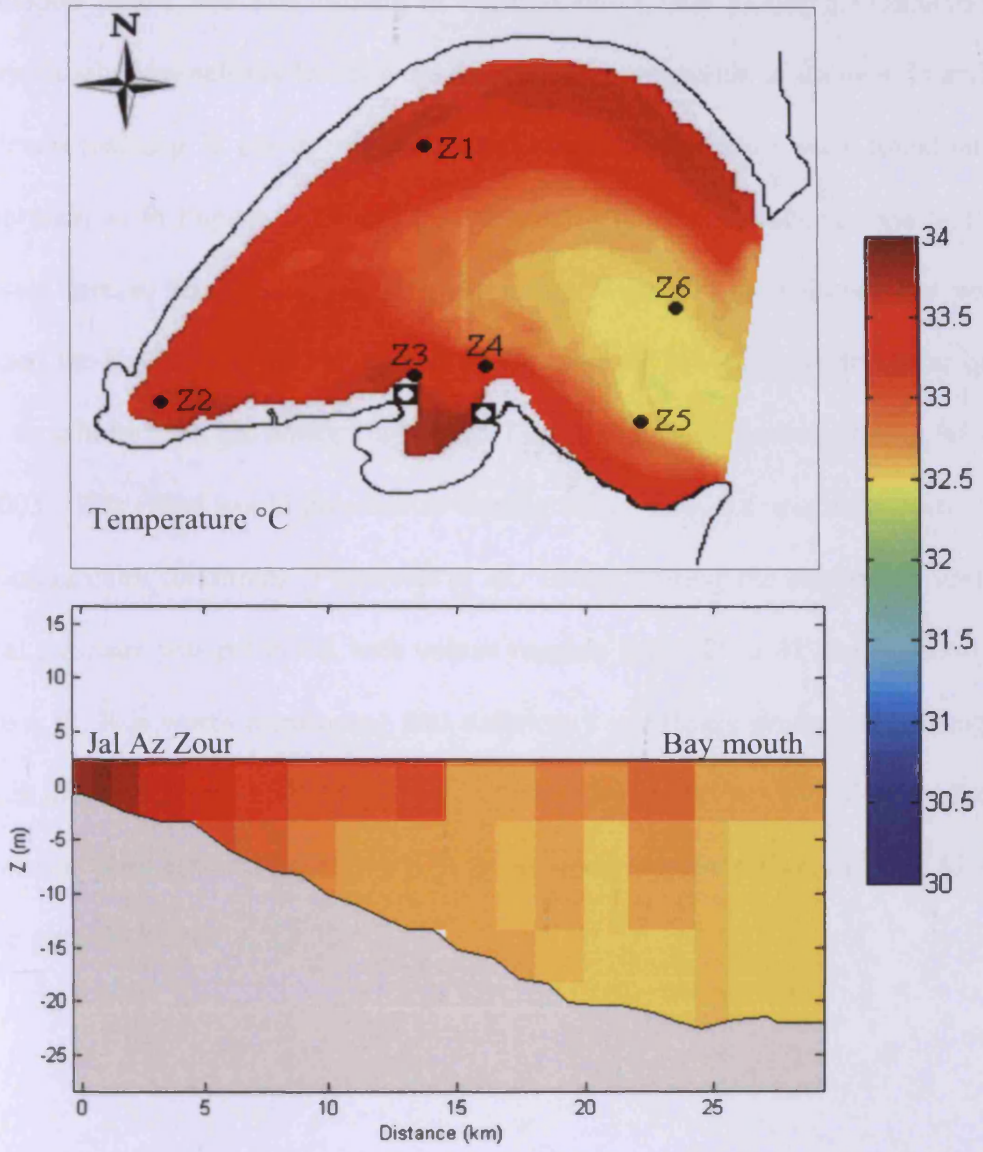

Figure 6.10: ELCOM predictions of surface temperature distribution in the Bay during the summer (July 2005), including data collection stations and Al Doha desalination plants marked as '◘' (top graph) and a vertical temperature variation prediction during the summer (July 2005) between the Bay mouth and Jal Az Zour (bottom graph)

Similar to temperature, salinity shows higher values near the coastal areas where they reached 41 psu at Z1, Z3 and Z4. This was mainly attributed to the discharge from the

desalination plants and low mixing at these stations (see Figure 6.11 and 6.12). Unsurprisingly, low salinity levels were marked near the mouth, at stations Z5 and Z6 with levels reaching 38 psu during the winter, while higher values were found during the summer, as in Figures 6.11 and 6.12 respectively. This supported the fact that relatively intense fresh water flowing from the Shatt Al Arab during the winter modified the Bay's water by creating a two layer water structure; the top layer being lower in salinity than the bottom layer (see Figure 6.12) [*Al-Yamani,* 2008; *Johns et al.,* 2003]. This effect would give rise to density driven currents near the mouth of the Bay during calm conditions [*Patterson et al.,* 1984]. During the summer, a uniform vertical structure was predicted with values ranging from 40 to 41 psu, as shown in Figure 6.12. It is worth mentioning that deficiency in salinity predictions during the summer may well rise from the exclusion, due to domain limitations, of the Al Sabiya desalination plant effects (see Figure 6.3). More details on the effects of Shatt Al Arab will be given in Section 6.2.2.3.

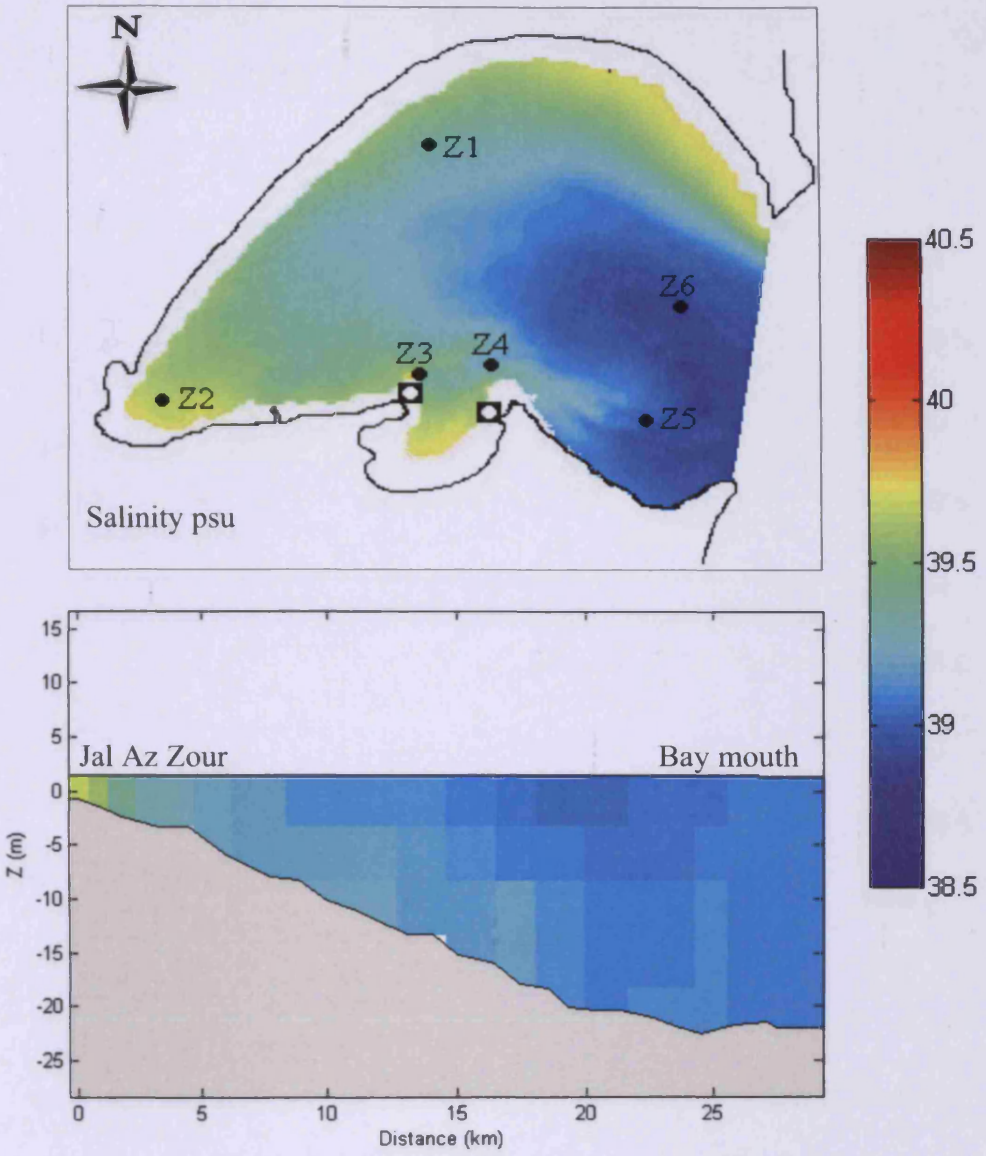

Figure 6.11: ELCOM predictions of surface salinity distribution in the Bay during the winter (January 2005), including data collection stations and Al Doha desalination plants marked as '◘' (top graph) and a vertical salinity variation prediction during the winter (January 2005) between the Bay mouth and Jal Az Zour (bottom graph)

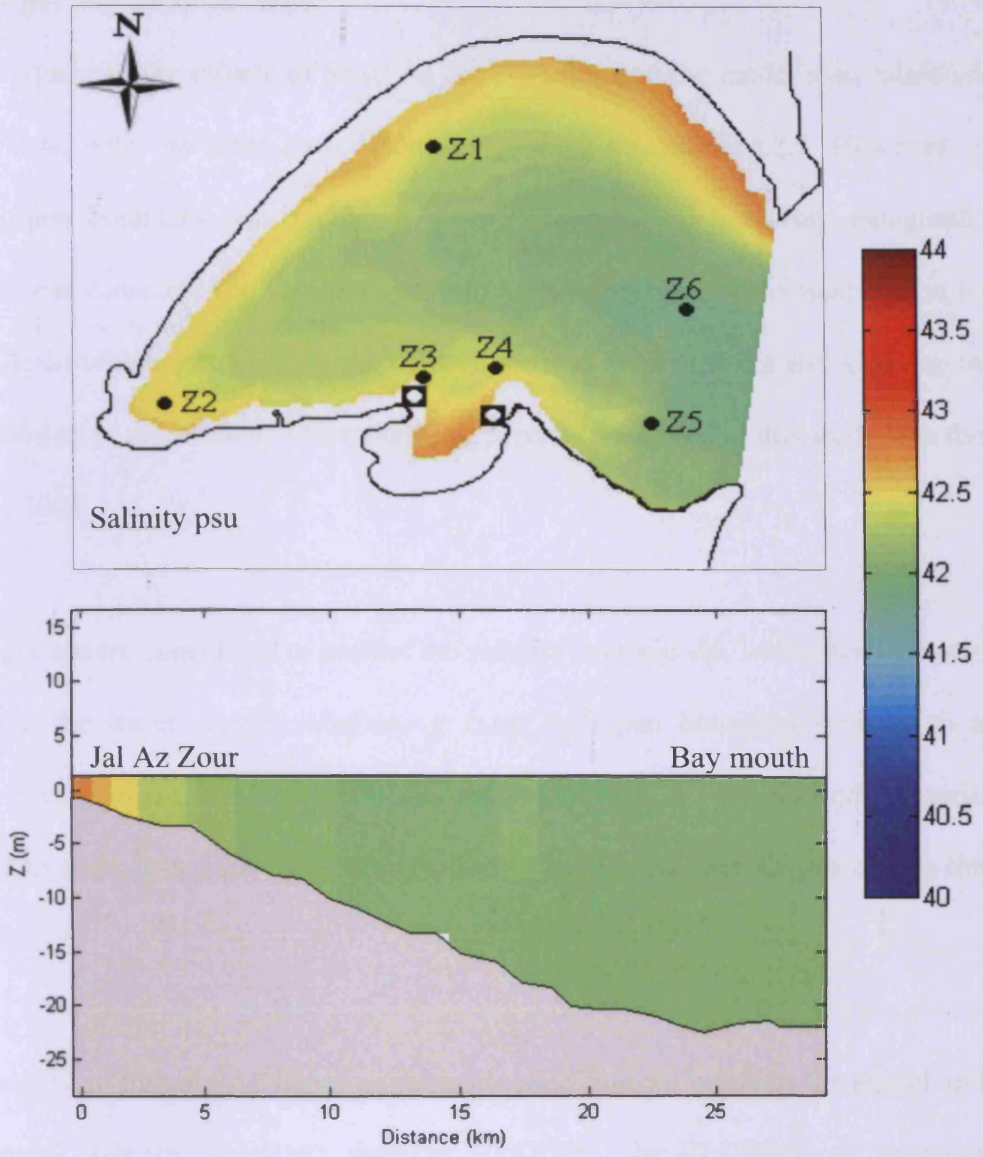

Figure 6.12: ELCOM predictions of surface salinity distribution in the Bay during the summer (July 2005), including data collection stations and Al Doha desalination plants marked as '◘' (top graph) and a vertical salinity variation prediction during the summer (July 2005) between the Bay mouth and Jal Az Zour (bottom graph)

6. 2. 2. 3 Effects of Shatt Al Arab:

In order to quantify the effects of Shatt Al Arab on the Bay the model was validated using Z6 data, with the same model settings as used in section 6.2.1. However, a modified open boundary was included, as explained in the following paragraph. Station Z6 was considered in this study due to the station location (closest station to Shatt Al Arab) which would show the effects of fresh water effects and also due to data availability at this station. The modelling period considered in this study was the entirety of 2005.

Two scenarios were considered to predict the salinity levels at Z6. In the first scenario (ELCOM1), the water salinity originating from the open boundary was set to a constant mean value of 41 psu. While water salinity in the second scenario (ELCOM2) varied seasonally with 38 psu during the winter and 43 psu during the summer.

As can be seen in Figure 6.13 better agreement was achieved between the model and the measured data in ELCOM2 than in ELCOM1. In ELCOM1 an apparent deficiency in model prediction occurred mainly during the winter (January, November and December 2005), with values of 20% more than the measured data. While the prediction in ELCOM2 showed that salinity at Z6 reached 36 psu during the winter and 44 psu during the summer (see Figure 6.13).

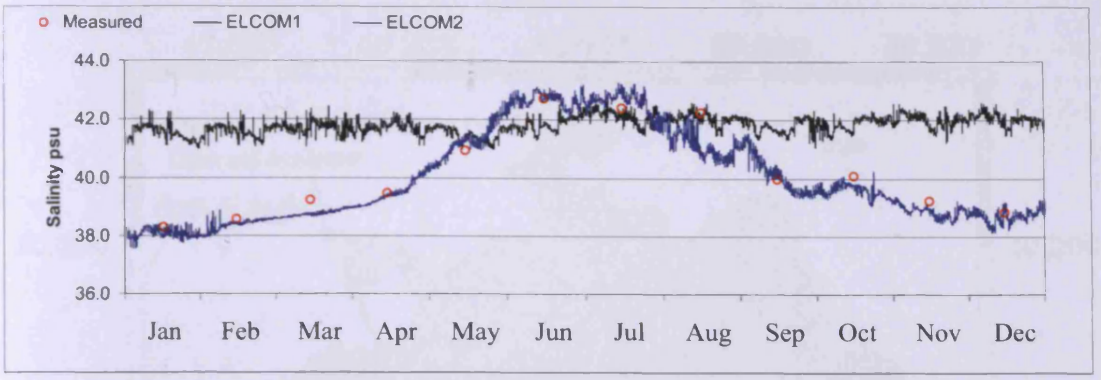

Figure 6.13: Comparison of predicted and measured salinity at Z6 during 2005

It is important that when modelling the Bay, the variation of salinity at the open boundary was taken into consideration due to the Shatt Al Arab fresh water effects. Otherwise, inclusion of fresh water input derived from the northern parts of the Gulf in the modelling domain was essential when modelling the Bay as suggested in Figure 6.14. Such grid configurations were not considered in this study due to a lack of data. Even though, the desalination outfalls were considered in this investigation, they had gradual effects on raising the salinity at Z6 during 2005. Such findings confirm *Al-Rashidi,* [2009] the main conclusion in which desalination plants only have local effects in the Bay (see section 6.2.2.4). For completeness, water salinity originating from the southern areas of the Gulf, near Saudi Arabia, may be reasonably considered to be constant and have a minimal role in modifying the structure of the Bay's waters. Other water quality parameters such as nutrients associated with the Shatt Al Arab input would defiantly have a pronounced influence on the water quality of the Bay, this will be addressed in Chapter 7.

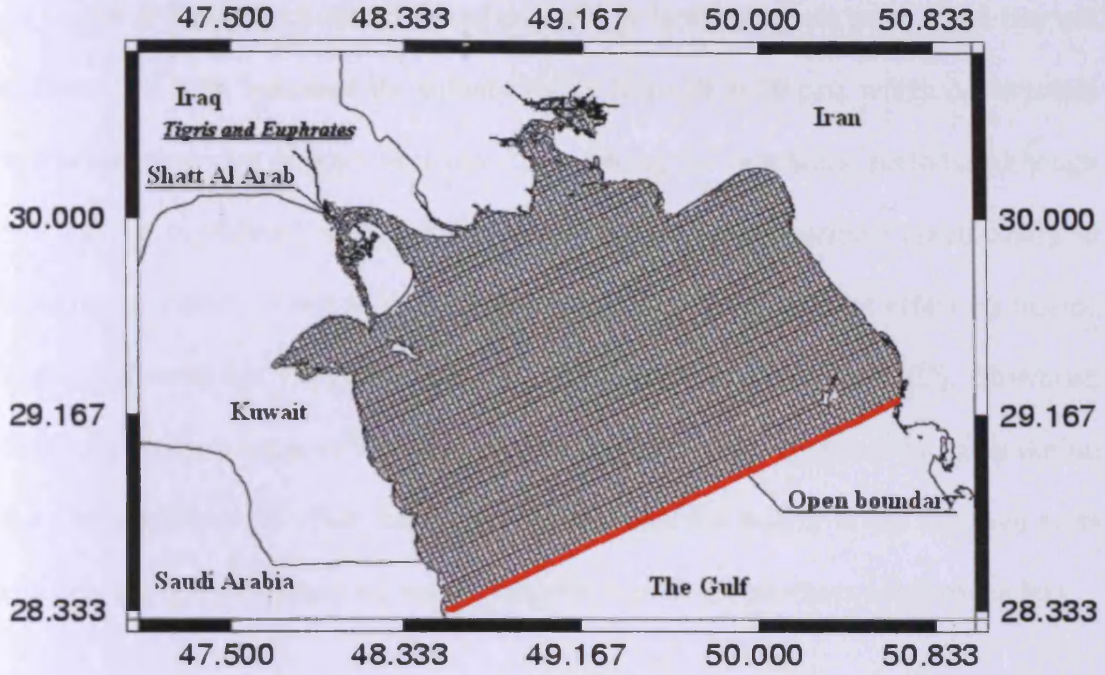

Figure 6.14: Inclusion of Shatt al Arab and other fresh water input (from Iran) in the modelling domain

6. 2. 2. 4 Effects of outfalls to the southern parts of the Bay:

As mentioned earlier in Chapter 2, desalination plants have had a major effect on increasing the salinity of the receiving waters. Here, the model was used to quantify the effects of the desalination plants located in the southern areas of the Bay, especially at Al Doha, (see Figure 6.3), on the surrounding water salinity. This was achieved by running the model using the same settings as mentioned in Table 6.1 and considering two key scenarios. Firstly, the model was run without outfalls. Secondly, the model was run with outfalls in the same locations as shown in Figure 6.3, with the Al Sabiya desalination plant excluded. Summer conditions were considered in the simulations, since the discharges were considered to be constant at a rate of 4 m^3/s throughout the simulation period.

As shown in Figure 6.15 the effects of the outfalls in the southern parts of the Bay are apparent and have increased the salinity levels from 39 to 40 psu, which corresponds to a salinity increase of approximately 2.5% during the simulation periods. Although this may be considered to be a small increase, it would contribute significantly in building up salinity levels in those regions that may have a direct effect on marine biology [*Borowitska,* 1981; *Bouvier and del Giorgio and Bouvier,* 2002]. However, in the far northern areas of the Bay, salinity concentration remained the same during the simulation periods. This reinforces the fact that the waters in the northern parts and near the open boundary are more energetic than in the southern areas of the Bay.

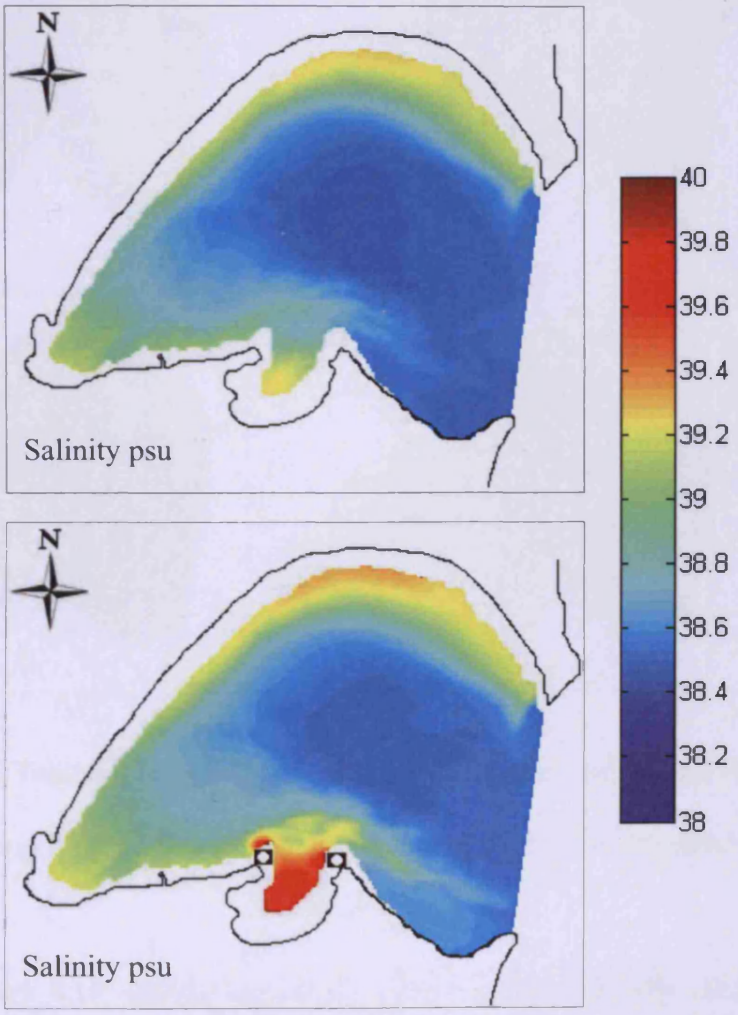

Figure 6.15: Salinity distribution in the Bay, excluding desalination outfall (top) and including desalination outfall marked as '◘' (bottom)

6. 3 Water circulation of the Bay:

The water circulation of the Bay was investigated by injecting tracer within the open boundary water flow. Meteorological and tidal forcing of 1 January 2005 to 10 February 2005 was considered in this study. The circulation of the Bay was investigated by analysing the concentration of the tracers resulting from continuous injection after 3, 10, 30 and 40 days (see Figure 6.16).

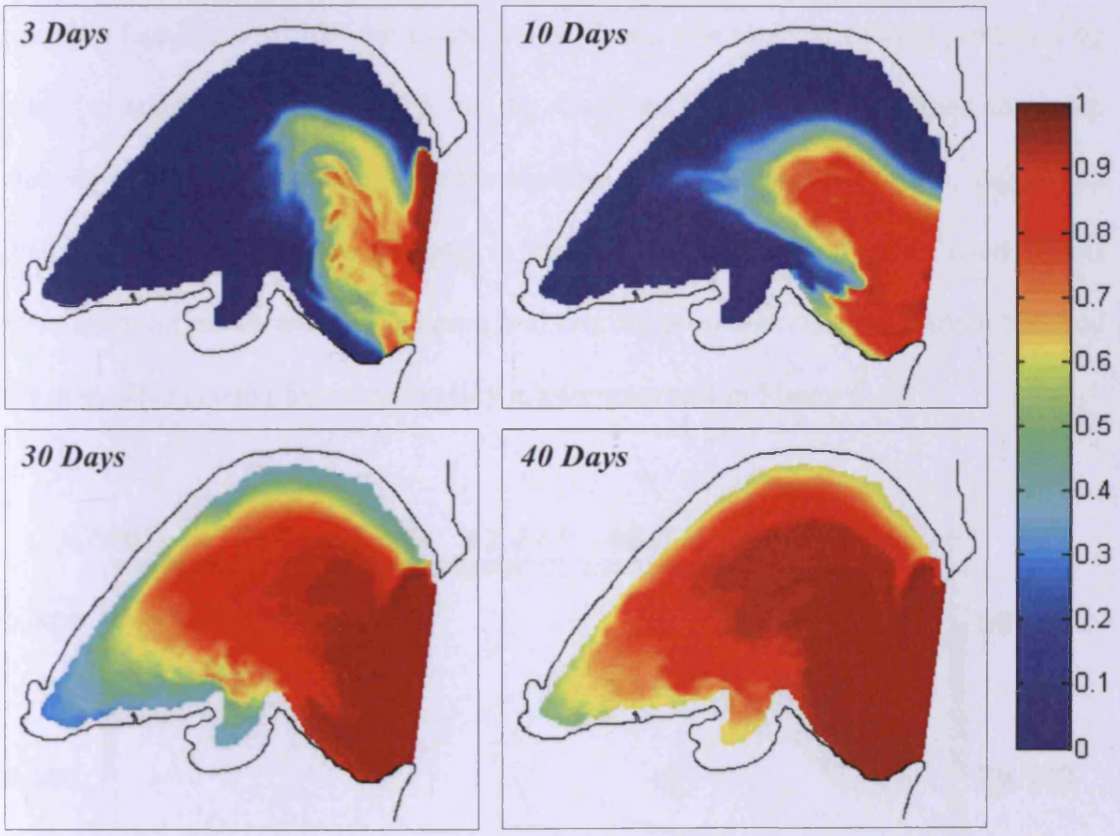

Figure 6.16: Tracer injection at the open boundary; progress of tracer spreading after 3, 10, 30 and 40 days of continues injection

As shown in Figure 6.16, during the first 3 days the tracer mostly made its way towards the middle and northern area of the Bay and away from the mouth with a number of small eddies apparent near coastal areas. This was mainly attributed to the

headlands on the coastal areas of Kuwait city. As the time develops (see Figure 6.16 after 10 days), the tracer started to split to form two larger eddy shape, first towards the northern part of the Bay in a clockwise direction (see Figure 6.6), while the second was relatively smaller in a counter clockwise direction towards Al Jahra, allowing for further stretching of the tracer cloud. Such processes can be explained due to both the irregular coastline restrictions and the dominant north westerly wind effects during this period of the year (January and February). After 30 days of further injection (see Figure 6.16), the tracer was widened due to shear mixing produced by tides (as addressed in Chapter 5 for the Gulf) and has mostly occupied the main channel of the Bay, apart from the far northern parts and the lower parts, suggesting that tidal force effects were minimal in those regions. In those regions wind effects were apparent in the water circulation and mixing processes. General circulation and the associated driving forces of the Bay are summarised in Figure 6.17.

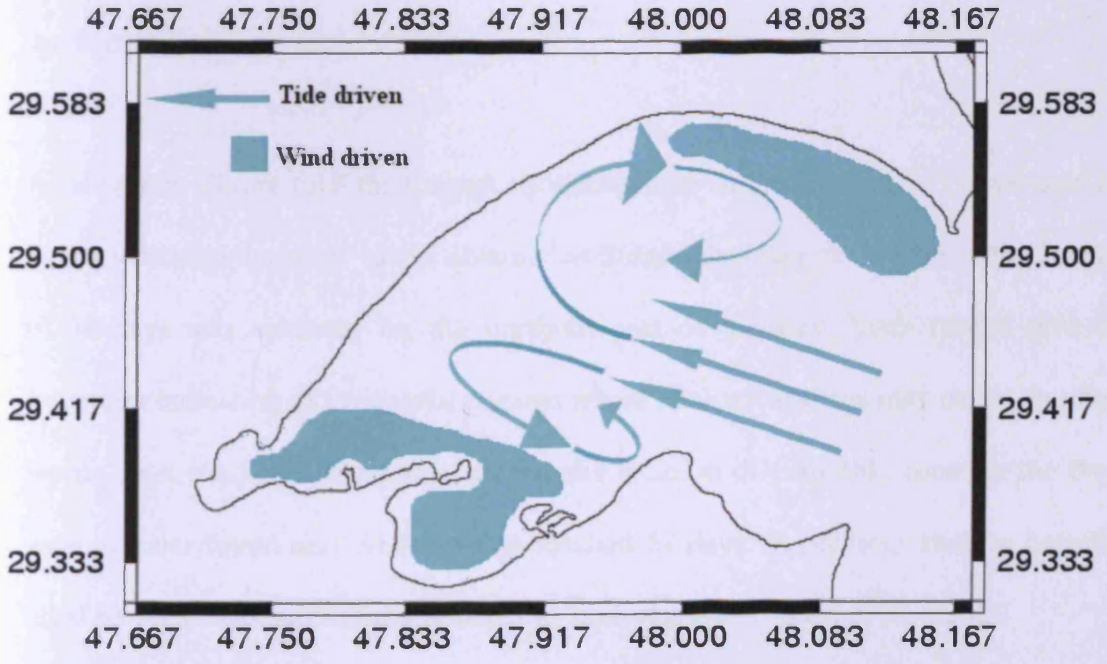

Figure 6.17: Water circulation of the Bay due to tides and winds effects

6. 4 Residence time of the Bay:

In a similar manner to calculating the residence time of the Gulf in Chapter 5, the residence time of the Bay is estimated in this section using ELCOM. Previously the flushing of the Bay was estimated to take two months using a simple box type model based on the residual flow [*Gopalakrishnan and Muralidhar*,1989]. However, *Rakha et al.*, [2009] estimated the flushing time of the inner parts of the Bay to take more than 2 years for a complete flush using RMA-10 (Resource Modelling Associates), which is three dimensional finite element HD model [*King*, 1988], using an unstructured grid.

In modelling the residence time of the Bay using ELCOM, the forcing data of 2005 (from January to December) was adopted. It was assumed that initially each cell contained water with a residence time of zero. The flushing time was defined as the residence time of the water as it left the domain (i.e. time taken for the water to leave the domain).

As shown in Figure 6.18 the longest residence time in the Bay was 57 days near Al Doha, with slightly lesser values obtained at Sulaibikhat Bay of 36 days. Also a value of 30 days was achieved for the northern part of the Bay. Such results give an important indication of the crucial regions where ecological stress may occur. In other words, high residence time values define the location of eutrophic zones in the Bay, such as those found near Al Jahra that reached 57 days. In previous studies, harmful algal bloom events were found to occur in such regions [*Glibert et al.*, 2002].

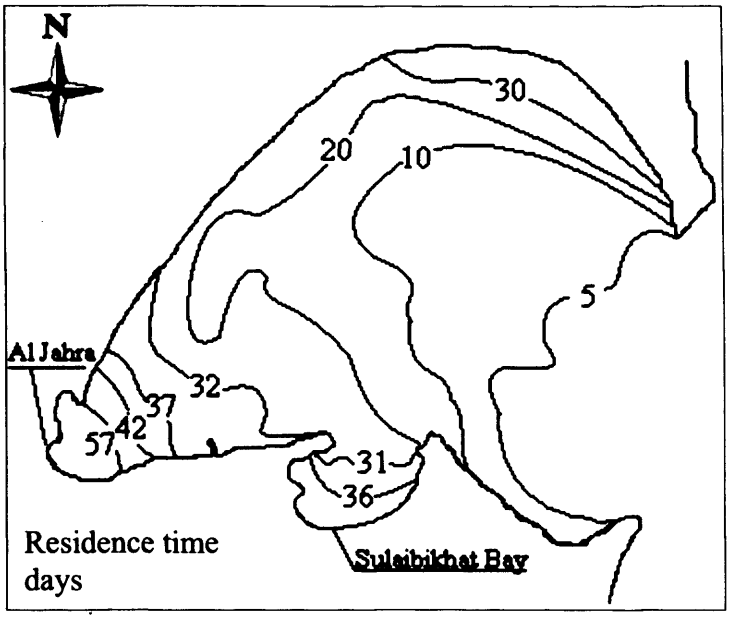

Figure 6.18: Residence time of the Bay

6. 5 Summary:

Details of the hydrodynamic modelling of Kuwait Bay are given in this chapter. The investigations were carried out using ELCOM and the data used were for 2005. The model was first validated using data obtained from KISR, comprising water levels and current speed and direction in the northern area of the Gulf. The model showed good agreement with the measured data. As for the Arabian Gulf, the hydrodynamic model results showed that the Bay has mainly driven by tides and high water velocities were predicted at the mouth of the Bay (almost 1 m/s), as opposed to the relatively low velocities near Sulaibikhat Bay (0.1 m/s).

Temperature and salinity levels were investigated in the Bay using the same model. The model showed that the water temperature had a seasonal variation of 34 °C in the summer and 15 °C in the winter, while salinity concentrations were affected by Shatt Al Arab and desalination plants. Further investigations were undertaken to estimate

the effects of the Shatt Al Arab and the desalination plants using the model. The investigation revealed that the Shatt Al Arab had pronounced effects on the salinity in the northern areas of the Bay, particularly during the winter when fresh water input was a maximum. In comparison, desalination plants were shown to have predominantly local effects only.

In order to investigate the water circulation in the Bay a tracer was injected along with the water inflow at the open boundary. The investigations revealed that tides were the main drivers of hydrodynamics in the Bay and produced variously complex eddies near the coastal zones and along the Bay's main channel. Hence tides are mainly responsible for dispersion and mixing in those regions. Winds are important in circulating the water in the shallow areas of the Bay, particularly in the southern regions. This has all provided crucial information to the understanding of the water quality processes in this region.

Chapter 7

Water Quality Modelling of

Kuwait Bay

7. 1 Introduction:

Water quality includes the physical, chemical, and biological characteristics of water and measures the capability of a marine system to sustain beneficial use to society [*Ji,* 2008]. Estuaries are in general considered to be a highly productive system, as they normally contain a reasonable amount of biomass made up of algae, phytoplankton and sea grass, thus supporting large bird and fish populations. This high population of living plants and animals implies that biota and seabed sediments embody important nutrient pools. Due to the geological, meteorological and biochemical variability of estuaries, quantification of eutrophication and the source of nutrients, or any other algal-growth limiting factor, is very complex (see Table 7.1).

Estuary/Lake/Harbour	Eutrophication and algal growth limitation factor	Reference
Peel-Harvey Estuary	Nutrient supply from agriculture land	[*McComb et al.,* 1993]
Tuggerah Lakes	Nutrient urban runoff	[*King and Hodgson,* 1995]
Pearl River Estuary	Turbidity and PO_4 from domestic sewage and industrial wastewater	[*Huang et al.*, 2003]
Tolo Harbour	Solar radiation	[*Lee and Arega,* 1999]
Ems Estuary	Retention time of PO_4 and N	[*Beusekom and Jonge,* 1998]

Table 7.1: Limitation factors of eutrophication and algal growth in various estuaries, lakes and harbours

One of the most critical water quality issues in Kuwait Bay is eutrophication (see Chapter 2) and red tides. Similar to many estuaries (see Table7.1), algal growth is mainly controlled by nutrients, such as N and P in the Bay [*Subba Rao and Al-Yamani,* 1999]. The resultant product of eutrophication and red tides (i.e. algae, including high nutrients levels such as N and P), are significantly affected by hydrodynamic processes, such as those explained in Chapters 5 and 6, in that they

controls their distribution in a marine system. Therefore, when considering the water quality of Kuwait Bay, it is first important to understand the hydrodynamic characteristics of the marine system as detailed in Chapter 6. This gives an indication as to the location of the most vulnerable sites to eutrophication in the Bay and also has huge implications in understanding the sediment adsorption processes relating to nutrients such as phosphorus.

The main aim of this chapter is to model the water quality parameters (including DO, N and P) in the Bay and explain the seasonal variations of each parameter, using same hydrodynamic settings as in Chapter 6. This has been undertaken by utilising ELCOM-CAEDYM and the developed TRIVAST model (see Chapter 4). Special attention has been given to PO_4 predictions in both models, since it is thought that algal growth is limited to PO_4 availability, in particular in the northern area of the Bay [*Subba Rao and Al-Yamani,* 1999]. In ELCOM-CAEDYM an attempt to quantify PO_4 rising from different sources has been achieved, in order to understand PO_4 management strategies. While in TRIVAST the effects of adsorption and desorption processes relating to sediment grain size have been investigated (based on TRIVAST developments in Chapter 4).

7. 2 Water quality modelling of the Bay:

Rapid coastal developments in the Bay (see Figure 7.1) have caused considerable ecological stress [*Bou-Olyan and Al-Sarawi,* 1993]. Major sources of pollution include the effluents from oil production, exploration, transportation and the municipal and petrochemical industries, including three major power plants (as

explained in Chapter 2). As a result, algal blooms and consequently red tides have been noted along various parts of the Bay [*Glibert et al.*, 2002].

Two major fish kill events were reported in 1999 and 2001 in the Bay. Significant natural and aquacultural fish deaths in the Bay occurred from September to October in 1999 and were attributed to a bloom of the dinoflagellate [*Heil et al.*, 2001] (Dinoflagellate: known as saltwater plankton, are important in marine biodiversity food chains). A scenario of the bloom event suggests that a period of low winds and a steady water column structure preceded the bloom. High cell concentrations of dinoglagellates were also immediately preceded by more than a 20-fold increase in the mean NH_4 and NO_3 concentrations that promoted PO_4 concentrations [*Heil et al.*, 2001]. This incident, with elevated inorganic and organic nutrient concentrations within the bloom, suggests that coastal nutrient eutrophication, including DO reduction, were likely to have contributed significantly to bloom development and support (more details can be found in *Heil et al.*, [2001]).

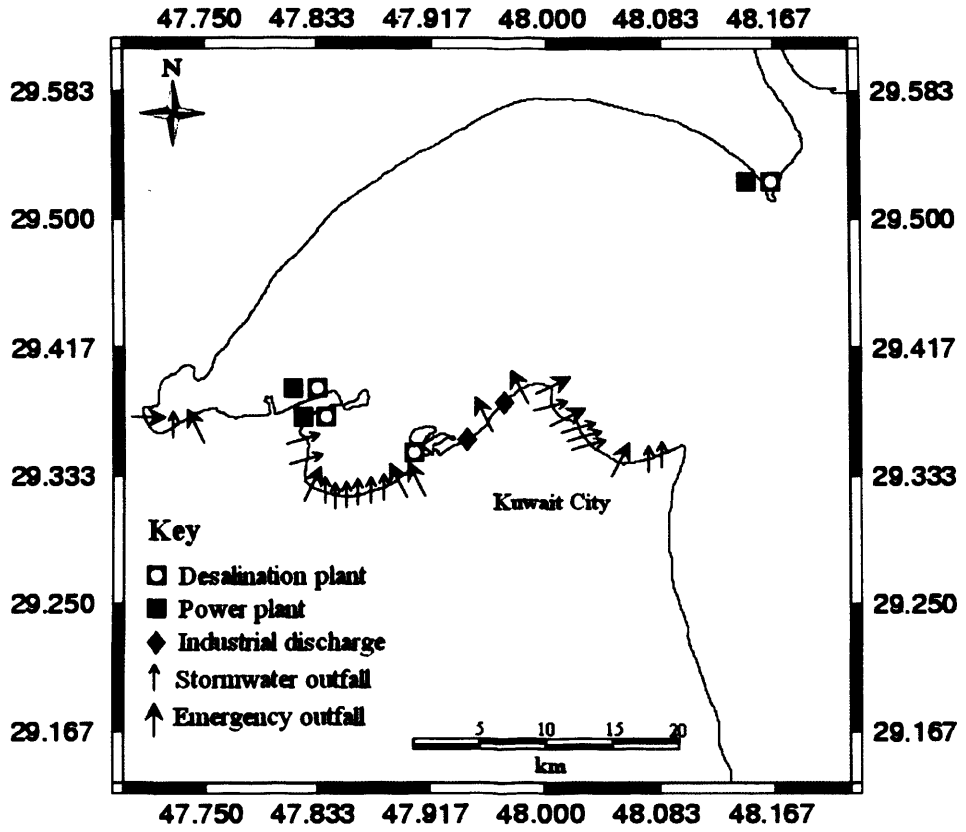

Figure 7.1: Main activities in the Bay

In the following sections details are given of the DO and N levels predicted using ELCOM-CAEDYM. Special focus is then given to PO_4 predictions using both ELCOM-CAEDYM and TRIVAST. In ELCOM-CAEDYM, the effects of an open boundary, outfalls, decomposition rates of organic matter and sediment flux on PO_4 levels have been investigated (see section 7.3.1.1), whereas TRIVAST has been used to study the effects of sorption processes on PO_4 levels (see Section 7.3.2).

7. 2. 1 Field data and model setup (ELCOM-CAEDYM):

DO data was obtained from (K-EPA) and includes nutrient data for 2004 and 2005. The data were collected on a monthly basis from six sites that were spread randomly over the Bay, as shown in Figure 7.2. DO levels had spatial and temporal variations

during 2004 and 2005, with similar variations for both years. Higher DO levels were observed during the winter and near the open boundary, while lower DO levels were observed during the summer and near the coastal areas of the Bay. Stations Z1 and Z6 (see Figure 7.2) had the highest level throughout the seasons, varying from 10 down to 6 mg/l during the winter and the summer respectively. However, stations Z2, Z3, and Z4 had comparatively lower values, ranging from 8.5 to 5 mg/l respectively for the same seasons.

In general, the data showed that there was a slight increase in all nutrients from 2004 to 2005. In coastal areas, near stations Z2, Z3, Z4 and Z5, higher nutrient values were observed compared to the middle of the Bay at Z1 (see Figure 7.2), particularly during the summer months. Inorganic N levels in general had higher values compared to PO_4 levels, particularly during the winter months, when levels reached more than 0.08 and 0.4 mg/l for NH_4 and NO_3 respectively at Z3. This was possibly due to the Shatt Al Arab fresh water effects [*Al-Yamani,* 2008]. However, during the warm seasons NH_4 and NO_3 levels ranged from 0.01 to 0.05 mg/l and 0.01 to 0.06 mg/l respectively, at most stations.

PO_4 levels at Z2 were found to have the highest values among the other stations reaching levels of 0.08 mg/l during the warmer seasons, while the rest of the stations fell with levels in the range of 0.03 to 0.009 mg/l during the winter. *Bou-Olyan and Al-Sarawi,* [1993] related such increases to anthropogenic activities near the coastline (see Figure 7.1), and added that PO_4 concentrations do not vary temporally, but spatially.

An abundance of SIO_3 was noticeable throughout the year in the Bay, with maximum values obtained during the winter and mostly in the coastal areas of the Bay with concentrations varying from 0.2 to more than 2 mg/l [*Al-Yamani et al.,* 2004]. Therefore, SIO_3 was not investigated in this study as it would not act as a limiting factor of algal growth in the Bay. According to the K-EPA, suspended sediment (SS) data were incomplete and less frequently recorded than nutrient data; however the data were set to a mean value of 10 mg/l during the winter and 18 mg/l during the summer.

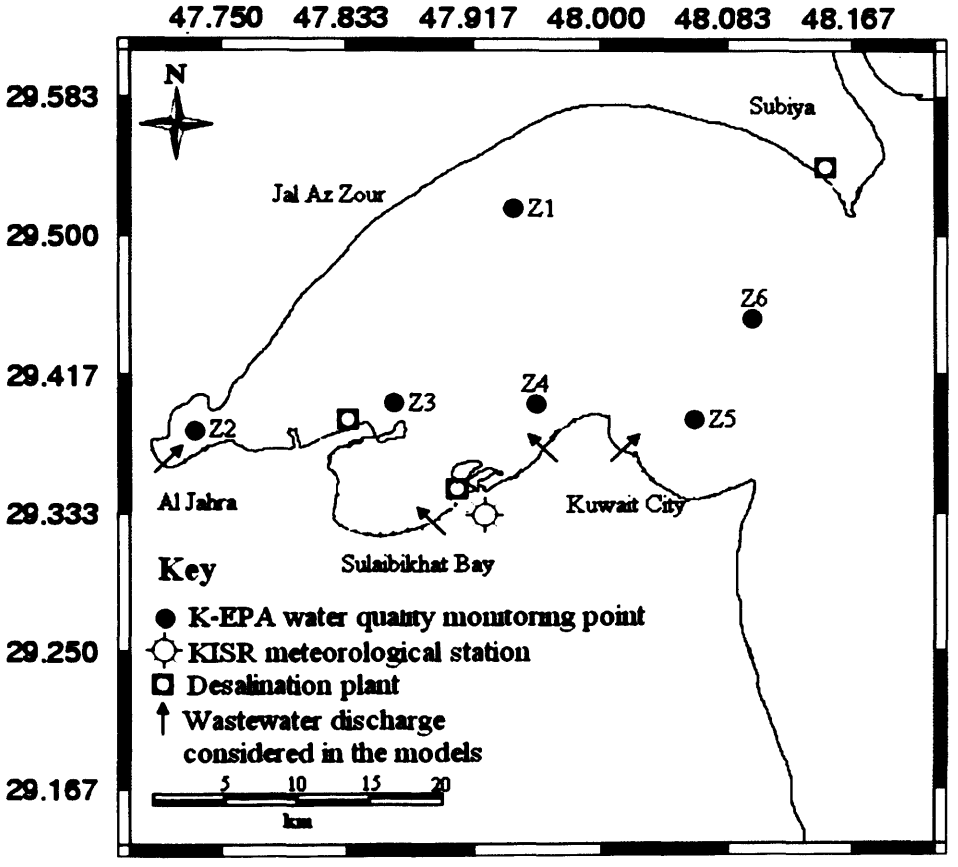

Figure 7.2: Water quality data collection sites and outfalls considered in modelling studies

The data for 2004 were incorporated to initialise and calibrate CAEDYM to give predictions for 2005. For water flowing from the open boundary, the data from Z6

were initially used to define the concentrations of water parameters, that varied to include the summer and winter effects as described previously (see Table 7.2). Due to a lack of wastewater outfall data, it was deemed reasonable to group the outfalls in Figure 7.1 into a single outfall to represent each region as shown in Figure 7.2, and treat the outfalls as a calibration factor in the model. The water quality parameters for the outfalls were initially assigned according to the data from Z2 (see Table 7.2) and the findings of *Al-Muzaini et al.,* [1997]. This was done at Z2, which is located very near to the Al Jahra wastewater outfall and would likely represent the water quality parameter concentrations (see Figure 7.2). The outfalls had a typical flow rate of 4 m^3/s throughout the simulation periods [*Bou-Olyan and Al-Sarawi,* 1993]. All data obtained from K-EPA were assumed to be depth averaged values. Other parameters, such as the mineralisation rate of organic matter, the sediment nutrient flux rate and the pH values were treated as calibration factors (see Table 7.3), as direct data for such parameters were not available.

In CAEDYM all measurements of water quality parameters were interpolated linearly in time to provide forcing data at the 100 s timestep. It is worth mentioning that other physical effects, such as tides, meteorological forcing, salinity and temperature, were set as shown in Chapter 6 for the 2005 predictions.

Parameter	Initial	Open boundary	Outfall
DO	9.0	8.5-10.0	5.0
NH_4	0.11	0.09-0.11	0.09
NO_3	0.10	0.01-0.08	0.017
PO_4	0.03	0.010-0.023	0.015
SIO_3	0.02	0.02-0.16	0.04

Table 7.2: Calibrated values of dissolved oxygen and nutrients, adopted in CAEDYM (all values in mg/l)

Parameter	Value	unit
Maximum mineralisation rate of organic matter to PO_4	0.02	/day
Maximum mineralisation rate of organic matter to NH_4	0.0035	/day
Sediment flux rate of PO_4	0.0031	$g/m^2/day$
Sediment flux rate of NH_4 and NO_3	0.015	$g/m^2/day$
pH	7.00	Neutral

Table 7.3: Calibrated values of other water quality parameters adopted in CAEDYM based on [*Abdel Aziz, 1997*]

7. 2. 1. 1 Phytoplankton setup:

As mentioned earlier, dinoflagellate was observed to be the main phytoplankton produced before major algal bloom events occurred in the [*Heil et al.,* 2001]. Thus, in this study dinoflagellate was considered, for two main reasons. Firstly, the lack of any other phytoplankton data, secondly phytoplankton primary production transforms energy and inorganic material into organic material, with significant implications, not only for phytoplankton biomass, but also for cycling of DO, nutrients, trace elements and suspended matter [*Cloern,* 2001] (see Chapter 4 for more details). Hence the consideration of phytoplankton is essential in order to represent the source and sink terms to nutrients. It is worth mentioning that zooplankton grazing was considered to be of secondary importance to nutrient increases in the Bay, as the main supply was derived from anthropogenic activities and opened boundaries [*Bou-Olyan and Al-Sarawi,* 1993; *Al-Yamani,* 2008; *Al-Yamani et al.,* 2004]. Higher biological groups, such as jellyfish, pathogens and fish, were not considered in this study. For completeness, modelling equations of phytoplankton (dinoflagellate) in CAEDYM consider various processes as shown in Table 7.4. Other phytoplankton (dinoflagellate) parameters were used to calibrate the model, as given in Table 7.5.

Parameters	Description
Rate of change of phytoplankton concentration	Increases with growth rate, decreases with respiration rate and also changes according to the net flux of phytoplankton due to settling (vertically) and due to advection and mixing.
Phytoplankton growth rate	Changes as a function of the maximum growth rate under ideal conditions and limitation functions for temperature, salinity, light and nutrients.
Phytoplankton respiration and mortality rate	Concatenates respiration, natural mortality and excretion. It is a function of the respiration rate coefficient and a temperature function, and also increases with more severe salinity limitations
Temperature limitation	Allows for inhibition above optimal temperatures. Limitation value is 1 at standard temperature, increases up to an optimum temperature and then decreases at a defined maximum temperature.
Light limitation	Exponentially decreasing curve according to incoming photosynthetically active radiation and the defined initial slope of the photosynthesis irradiance curve.
N limitation	Formulated to give a limitation curve dependent on the internal nutrient store relative to defined maximum and minimum internal N levels.
P limitation	Formulated to give a limitation curve dependent on the internal nutrient store relative to defined maximum and minimum internal P levels

Table 7.4: Explanation of phytoplankton (dinoflagellate) modelling equations in CAEDYM [*Hipsey et al.*, 2006]

Parameter	Calibrated value	Units
Dinoflagellate mean concentration	70	µg chl a/l
Maximum growth rate	0.8	/day
Respiration rate coefficient	0.06	/day
Temperature multiplier for respiration	1.08	dimensionless
Minimum internal N	4.5	mg N/mg chl a
Minimum internal P	0.27	mg PO_4/mg chl a
Maximum internal N	9.3	mg N/mg chl a
Maximum internal P	0.6	mg PO_4/mg chl a
Maximum rate of N uptake	1.7	mg N/mg chl a/day
Maximum rate of P uptake	0.06	mg PO_4/mg chl a/day
Half saturation constant for N uptake	0.052	mg/l
Half saturation constant for P uptake	0.005	mg/l
Light saturation for maximum production	180	µE /m^2/s
Maximum optimum salinity tolerance	41	psu
Minimum optimum salinity tolerance	34	psu
Multiplier for temperature limitation	1.1	dimensionless
Chlorophyll a per cell	0.000005	mg chl a/cell

Table 7.5: Calibrated phytoplankton (dinoflagellate) parameters in CAEDYM based on typical values given by *Hipsey et al.*, [2006]; *Hipsey et al.*, [2008]; *Subba Rao and Al Yamani*, [1999]; *Heil et al.*, [2001]

7. 2. 2 Model validation and discussion:

As mentioned earlier the model was calibrated using the values given in Tables 7.2, 7.3 and 7.5, based on the K-EPA 2004 data and was validated using the 2005 K-EPA data at station Z1. Water quality parameters, such as DO, were relatively uncomplicated for calibration purposes. However, other water quality parameters, such as nutrients, were more complex for calibration, particularly when sophisticated modelling terms were involved, such as those found in CAEDYM (as outlined in Chapter 4). A key consequence of so many water quality parameters was that it takes much more effort to tune the parameters and to calibrate the model, such as those shown in Tables 7.3 and 7.5. It is always desirable to attain actual measurements of water quality parameters, but in practise a number of these parameter values are not

measured or difficult to measure [*Smith et al.,* 1997], e.g. organic matter mineralisation rate, nutrient phytoplankton uptake etc [*Hecky and Kilham,* 1988], and so these are often determined via model calibration. For illustrative purposes, cultural studies have recognised that internal cellular concentrations of nutrients determine phytoplankton growth rates, and these studies have shown that it is often complex to relate growth rate to external nutrient concentrations [*Hecky and Kilham,* 1988]. Since water quality processes are interrelated, adjusting one parameter may affect several processes. Therefore, it is vital to understand the processes being modelled and the controlling factors of the system, in order to obtain acceptable model predictions and interpretations.

In the Bay it is thought that the main controlling factor of algal growth is nutrients, in particular PO_4 [*Al-Yamani et al.,* 2006]. Other limiting factors such as solar radiation and temperature (typically 20 °C) are frequently available for algal growth in the Bay [*Subba Rao and Al-Yamani,* 1999]. It was therefore deemed important to model nutrients in the Bay and understand the fundamental water quality processes that contributed significantly to nutrient levels.

7. 2. 2. 1 Dissolved oxygen (DO):

In general, good agreement was achieved between the model and measured DO levels as shown in Figure 7.3. At Z1 the lowest DO levels were predicted during the summer with 5.6 mg/l, while the highest levels reached almost 9 mg/l during the winter. Broadly speaking predictions of DO levels in the Bay had higher values in the northern areas than in the southern areas, as shown in Figure 7.4. In comparing station

Z1 with stations Z2-Z5, it was clear that Z1 had consistently higher DO levels throughout the year by at least 1 mg/l, this was mainly due to the following reasons:

- Fresh water input effects from the open boundary (see Chapter 6);
- Lower anthropogenic activities near Z1 (see Figures 7.1 and 7.2);
- Lower DO utilisation for organic matter mineralisation processes at Z1 (see section 7.3.1.1 and explained later in Figure 7.12); and
- Better mixing processes at Z1 (see Chapter 6).

During the winter, the model had slightly underestimated DO levels by about 10%. Such a deficiency may well have arisen from the DO representation at the open boundary of the domain. It was therefore important to investigate the DO levels beyond the Bay as higher DO could arise from the Shatt Al Arab [*Al-Hassan and Hussain,* 1985] similar to salinity explanations in Chapter 6. Not surprisingly, DO levels in Sulaibikhat Bay had the lowest value with approximately 5.0 mg/l during the summer.

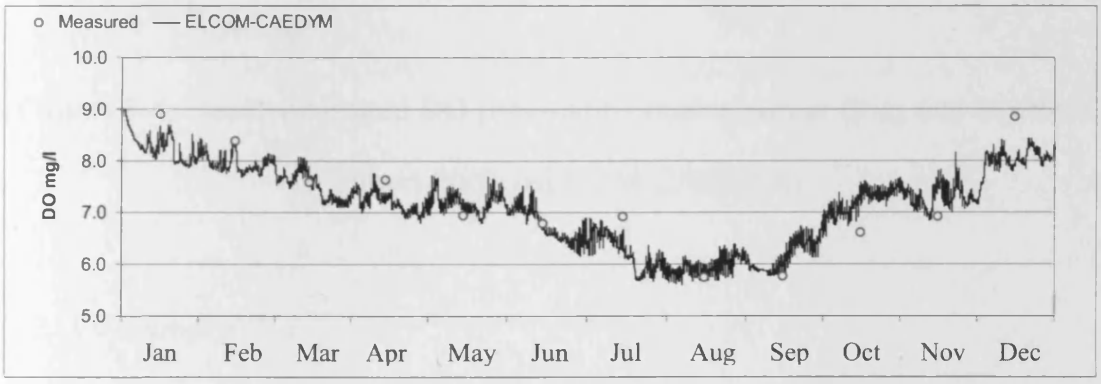

Figure 7.3: Model validation of DO at Z1 during 2005 (ELCOM-CAEDYM)

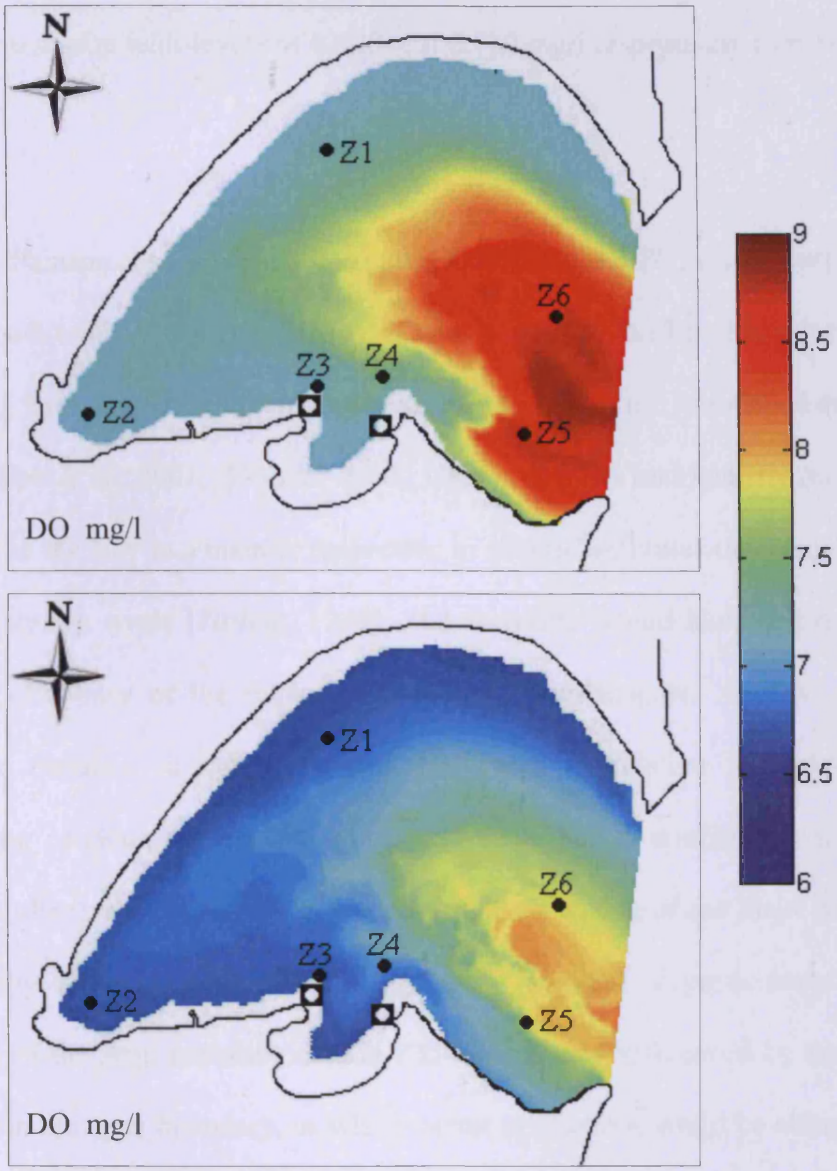

Figure 7.4: Depth-averaged DO predictions during winter (top) and summer (bottom) 2005 (ELCOM-CAEDYM)

7. 2. 2. 2 Nitrogen (N):

Although good predictions of NH_4 and NO_3 were apparent during the summer season, CAEDYM underestimated the levels by approximately 5% and 10% during the winter respectively (see Figures 7.5 and 7.6). NH_4 and NO_3 levels were predicted to be at their highest concentration during the wet season, with 0.11 and 0.12 mg/l, and lowest

during the warm season with levels of 0.025 and 0.020 mg/l respectively (see Figures 7.5 and 7.6).

Due to a large drainage channel constructed after the Gulf war 1991, whose purpose is to drain the southwest Al-Ahwar wetlands of coastal Iraq at the Iraq-Kuwait border (Shatt al Arab), large, nutrient rich and reduced salinity waters are introduced directly into the Bay [*Heil et al.,* 2001; *Al-Saadi et al.,* 1989]. This has undoubtedly modified nutrient levels in the Bay in a manner respective to various activities upstream of the Tigris and Euphrates rivers [*Talling,* 1980], and therefore would have had a direct effect on the efficiency of the model's predictions. Furthermore, *Abaychi et al.,* [1988] studied nutrients in the Tigris and Euphrates in relation to agricultural activities in the catchment areas and suggested that the most abundant nutrient introduced into the river is nitrogen. In a similar manner to that of the Shatt Al Arab effect on salinity levels (as explained in Chapter 6), levels of N, particularly in the northern areas of the Bay, including station Z1, were highly influenced by nutrients originating from the open boundary, in which better predictions could be achieved if detailed data were available. Better model predictions were achieved for NH_4 than NO_3 in the Bay. Again, this is probably attributed to the N representations at the open boundary, in which the additional input may have arisen from other sources outside the modelling boundaries. Unlike DO, depth averaged distributions of both NH_4 and NO_3 showed higher values in the southern areas than in the northern areas (see Figures 7.7 and 7.8). This is mainly attributed to the anthropogenic activities, presented by outfalls in the model, and high temperatures that enhance nutrient release from the sediments in the southern shallower regions (see Chapter 6).

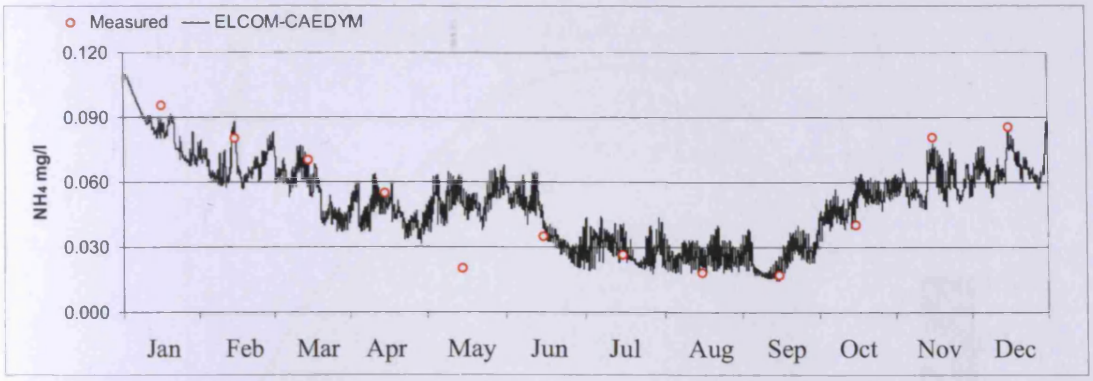

Figure 7.5: Model validation of NH_4 at Z1 during 2005 (ELCOM-CAEDYM)

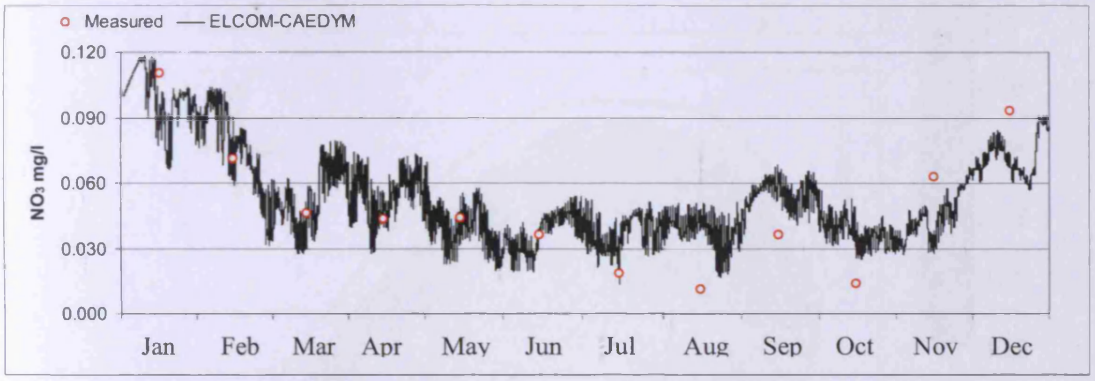

Figure 7.6: Model validation of NO_3 at Z1 during 2005 (ELCOM-CAEDYM)

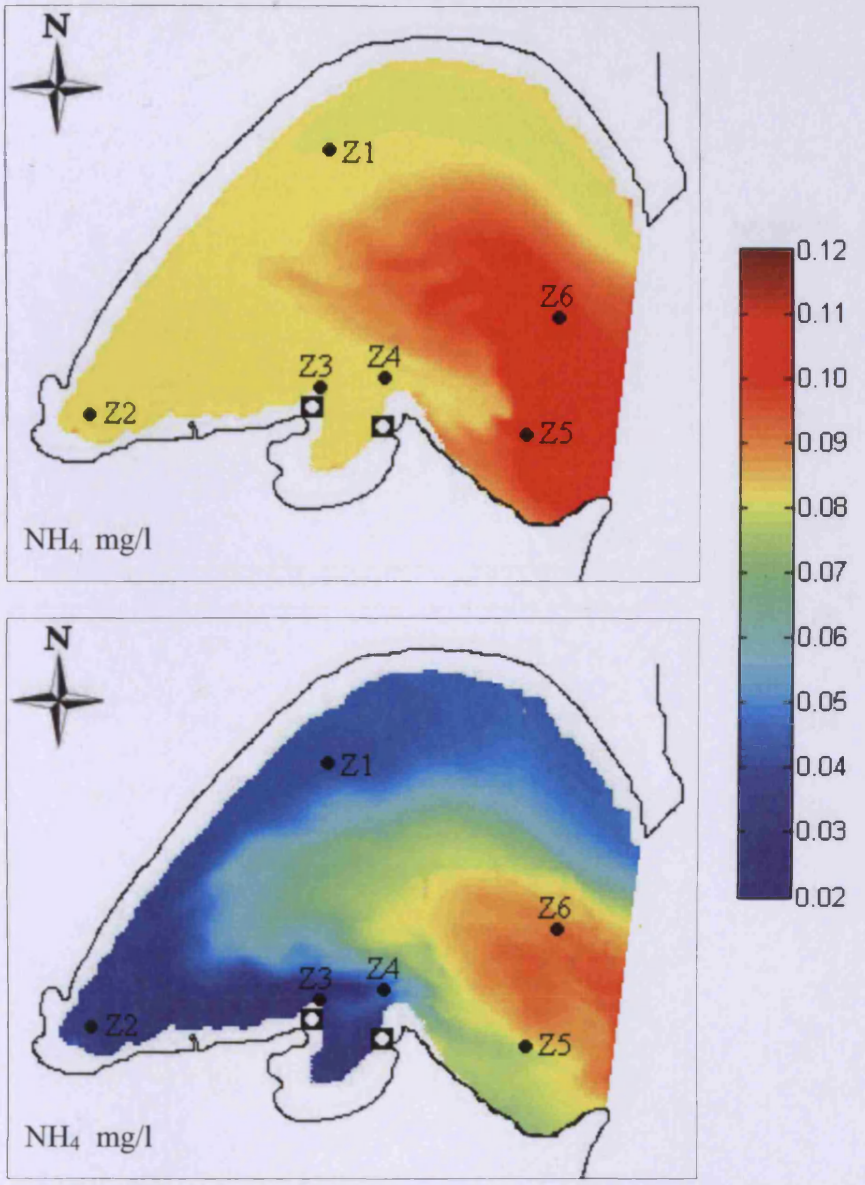

Figure 7.7: Depth-averaged NH_4 predictions during the winter (top) and the summer (bottom) 2005 (ELCOM-CAEDYM)

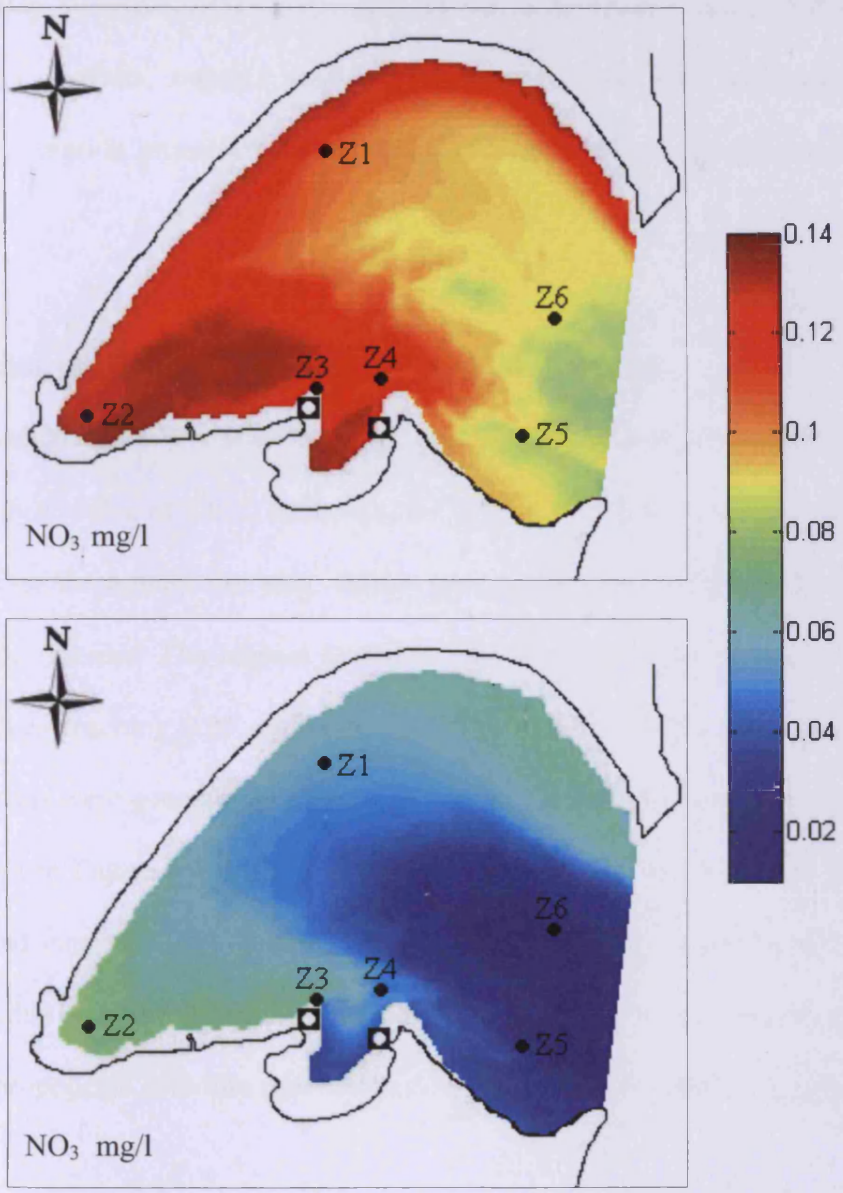

Figure 7.8: Depth-averaged NO_3 predictions during the winter (top) and the summer (bottom) 2005 (ELCOM-CAEDYM)

7. 3 Modelling phosphorus (PO_4) using ELCOM-CAEDYM and TRIVAST:

As mentioned earlier, in the following section a special focus will be given to PO_4 predictions. Firstly, ELCOM-CAEDYM was used to produce annual predictions of PO_4. Subsequently, the same model was used to study the main contributors of PO_4

levels in the Bay by means of a sensitivity analysis to the main sources of PO_4 (i.e. open boundary, outfalls, organic matter mineralisation rate and sediment flux). Secondly, PO_4 sorption processes, as detailed in Chapter 4, were investigated using TRIVAST.

7. 3. 1 Modelling phosphorus (PO_4) using ELCOM-CAEDYM:

In general, predictions of PO_4 at Z1 showed good agreement with the collected data from 2005 with R^2 value of 0.652, as shown in Figure 7.9, in which PO_4 did not show a large variation throughout the year. Better predictions were achieved during the winter than the summer. The highest levels were predicted during the winter, with maximum values reaching 0.03 mg/l during January 2005. On the other hand, the lowest PO_4 levels were generally predicted during the summer season reaching 0.023 mg/l, as shown in Figure 7.9. Similar to the findings of *Bou-Olyan and Al-Sarawi*, [1993] PO_4 had more apparent spatial than temporal variations, as shown in Figures 7.9 and 7.10, this will be investigated further in section 7.3.1.1. This was thought to be due to anthropogenic activities predominantly in the southern shallow regions (see Figure 7.2).

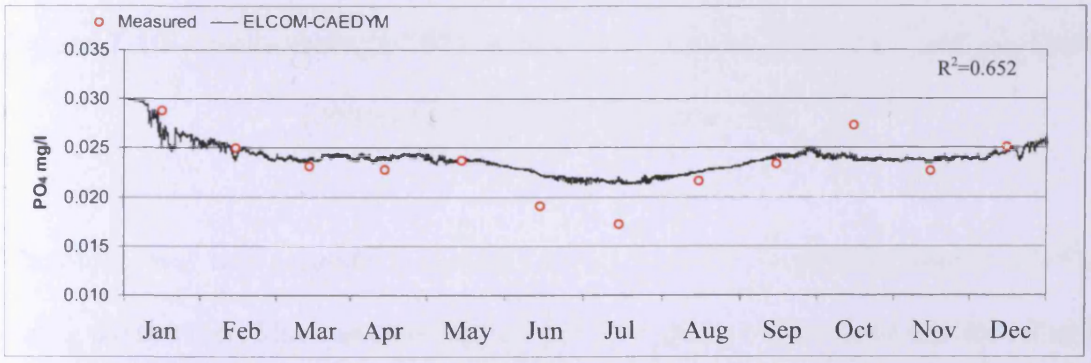

Figure 7.9: Model validation of PO_4 at Z1 during 2005 (ELCOM-CAEDYM)

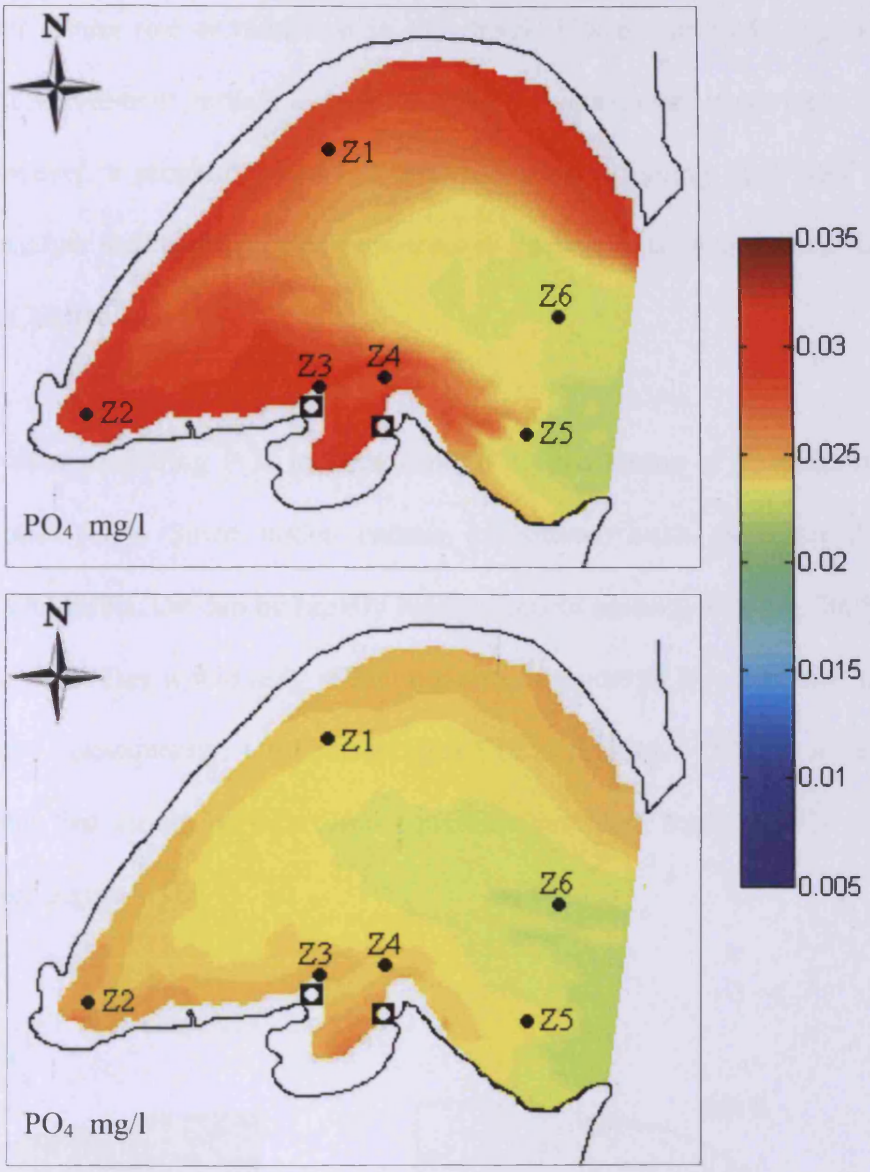

Figure 7.10: Depth-averaged PO_4 predictions during winter (top) and summer (bottom) 2005 (ELCOM-CAEDYM)

The model was less accurate in predicting the measured fluctuating manner of PO_4 during the summer. This was possibly thought to be due to dust storms and the related sorption processes of PO_4 (see Chapter 2). Unlike N, PO_4 has a higher tendency to be adsorbed onto sediment particles due to the negatively charged ions, or in certain

conditions (e.g. suitable temperature and DO) PO_4 may be released into the surrounding water giving rise or reduction in PO_4 levels [*Paytan and McLaughlin,* 2007]. In CAEDYM sediment particle deposition from the atmosphere is not included in the model, however, a sensitivity analysis will be conducted using TRIVAST in section 7.3.2 to analyse sediment sorption processes in relation to sediment grain size (as developed in Chapter 4).

It is important when modelling PO_4 to be aware of all the forms of P, including organic phosphorus (OP). Since under certain conditions, such as reasonable temperature and DO levels, OP can be rapidly mineralised to produce PO_4 [*Ji,* 2008]. Hence PO_4 levels in the Bay would only reflect the direct amount of PO_4 available for biological activity. Consequently, total phosphorus (TP) ($TP=PO_4 + OP$) is a very important indicator that should be taken into consideration when studying PO_4 in a marine system (see Figure 7.11).

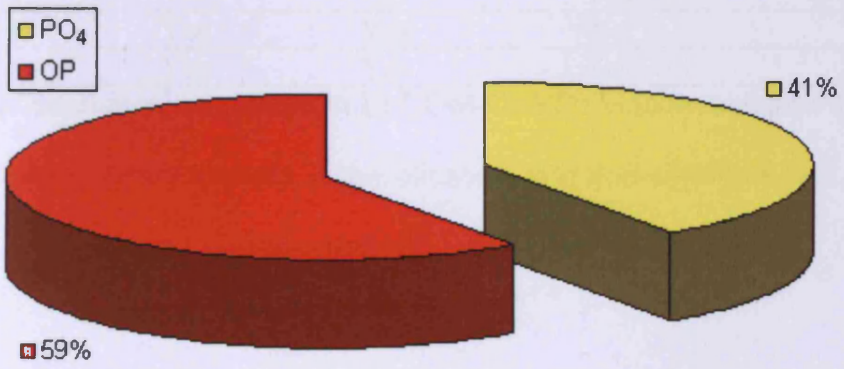

Figure 7.11: Percentage of PO_4 and OP representing total amount of P in the Bay during the summer at station Z3

As can be seen in Figure 7.11, most P in the Bay at Z3 during the summer is in organic form. Hence, parameters affecting mineralisation rate should be heavily investigated when considering PO_4 modelling in the Bay. However, this is beyond the scope of this study. In the current study the effects of the mineralisation rate will be investigated in the following section.

7. 3. 1. 1 Effect of open boundary, outfalls, mineralisation rate of OP and sediment flux:

In order to quantify the effects of the open boundary, outfalls, mineralisation rate of OP and sediment flux on PO_4 levels in the Bay, various sensitivity analyses were conducted on each parameter, as summarised in Table 7.6. Two main stations were considered for this investigation, analysing the spatial distribution of PO_4 in the Bay.

Scenario	Open Boundary	Outfalls	Mineralisation rate	Sediment flux
CAEDYM 1	Yes	Yes	Yes	Yes
CAEDYM 2	No	Yes	Yes	Yes
CAEDYM 3	Yes	No	Yes	Yes
CAEDYM 4	Yes	Yes	No	Yes
CAEDYM 5	Yes	Yes	Yes	No

Table 7.6: Scenarios conducted in ELCOM-CAEDYM to investigate the effect of the open boundary, outfalls, mineralisation rate and sediment flux on PO_4 concentration in the Bay

It is important to note that 'Yes' in Table 7.6 corresponds to the values of PO_4 assigned as shown in Tables 7.2 and 7.3, while 'No' corresponds to a zero value for each parameter. The results of the investigation shown in Table 7.6 can be summarised as shown in Figure 7.12.

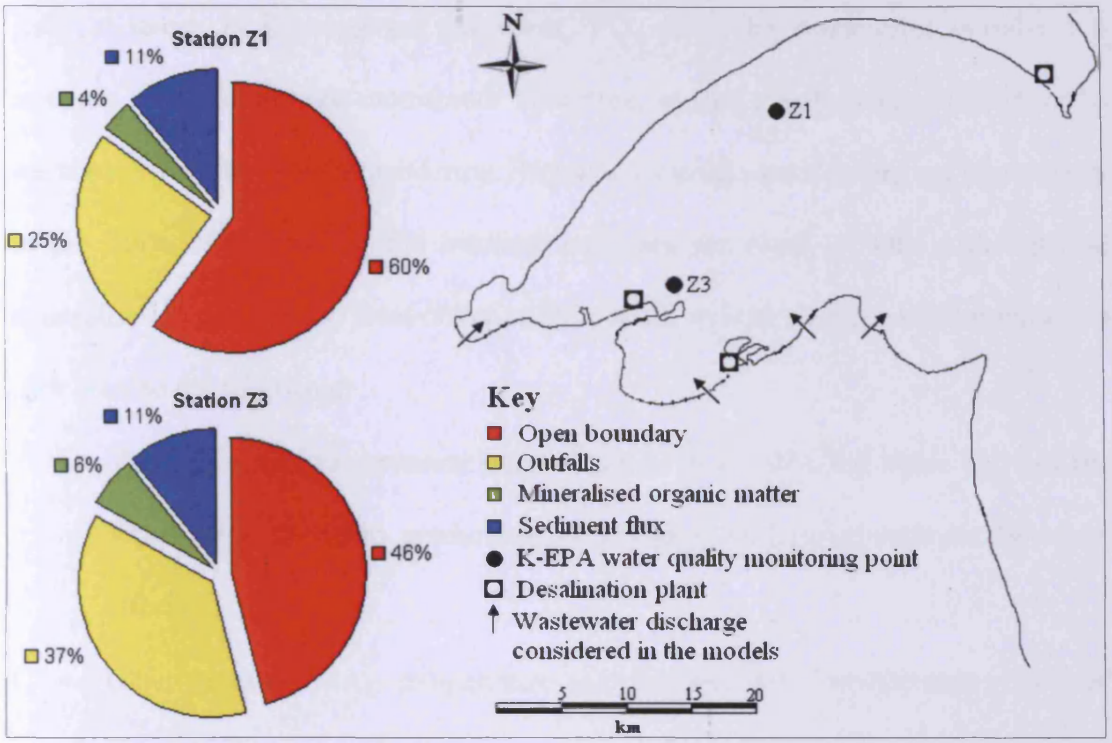

Figure 7.12: Percentages of open boundary, outfalls, mineralisation organic matter and sediment flux contributions to PO_4 at stations Z1 and Z3 during winter

As shown in Figure 7.12 most PO_4 is delivered from the open boundary of the Bay, in particular at Station Z1. Not surprising, it was established that outfalls at Z3 were responsible for more than 35% of the PO_4 at this location, while at Z1 this impact dropped to 25%. The sediment flux had a stable influence at both stations where it accounted for 11% of the PO_4 level. The mineralisation rate had the least effect on the other parameters, where it accounted for 4% of the PO_4 at Z1 and just a little more at Z3.

In terms of marine water management, PO_4 from sediment flux and the open boundary were almost incontrollable parameters; in particular with regard to real sources associated with the Shatt Al Arab water flow entering the Bay, and the current

political issues in this regions. However, PO_4 from the wastewater outfalls can certainly be controlled and monitored. Therefore, special attention should be given to wastewater outfalls when considering Bay water management strategies, particularly in the sense of controlling the limiting nutrients for algal growth. Although the mineralisation rate had the least effect on PO_4 levels at both stations, it is important to bare in mind the following:

- The value used to represent mineralisation is a calibrated value and not the actual value; therefore, predictions may slightly under/over-estimate the actual effects;
- Other parameters (e.g. temperature and pH) may have considerable effects on mineralisation rates; these were not investigated since it is beyond the scope of this study (see Chapter 9); and
- OP is higher than PO_4 (see Figure 7.11) and therefore mineralised OP may be a large source for PO_4 when considering large time scales.

7. 3. 2 Modelling phosphorus (PO_4) using TRIVAST:

During the last few decades, Kuwait's coastline, including the Bay, has undergone various waterfront developments, such as the Al-Kairan Pearl (for more details see Chapter 2). Such projects, and the associated dredging and land reclamation, have introduced large amounts of suspended sediments (SS) to the coastal waters [*Al-Ghadban and El-Sammak*, 2005]. In addition to human activity, it has recently been established that occasional natural dust storms (detailed in Chapter 2) are one of the main sources of fine sediment inputs into the Bay (see Figure 7.13). These source inputs in turn, lead to various environmental impacts that are related to nutrient increases/decreases via sorption processes [*Aqrawi,* 1994*; Stutter and Lumsdon,*

2008]. In addition to dust storms, the Shatt Al Arab was also considered through several studies to be the main input of SS in the northern region of the Gulf, and subsequently in the Bay, as shown in Figure 7.13 [*Aqrawi, 1994; Al-Ghadban and El-Sammak*, 2005; *Anderlini et al.*, 1982; *Elsayed and Albakri,* 1994; *Saad and Al-Azmi*, 2002]. In these studies the sedimentation rate at the mouth of the Shatt Al Arab was estimated to be approximately 0.05 m/year and the net annual sediment discharge entering the Gulf was estimated to be approximately 0.93 million tons [*Karim and Salman*, 1987].

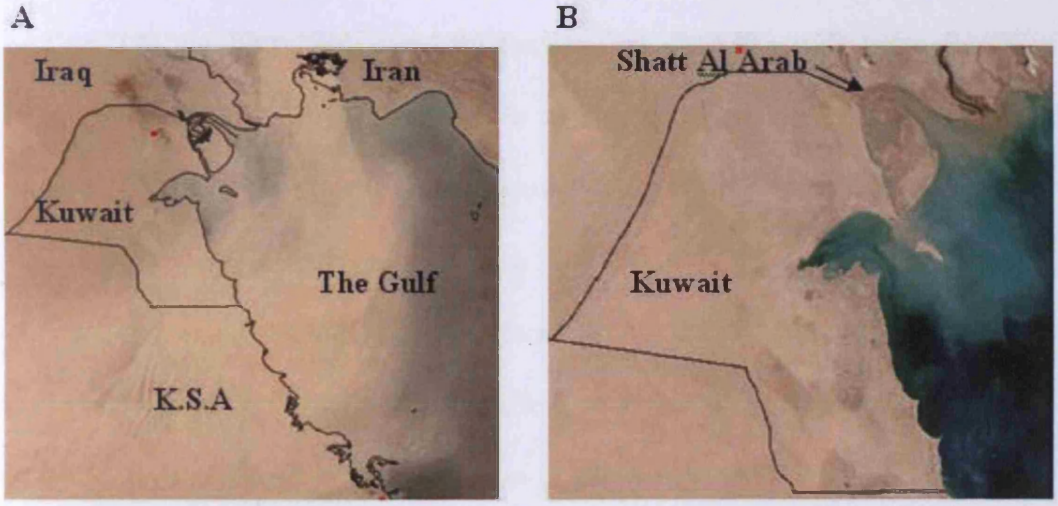

Figure 7.13: A. Typical dust storm during the summer affecting the northern region of the Gulf. **B.** Shatt Al Arab sediment effects on the Bay, Source: http://modis.gsfc.nasa.gov/.

Based on the relationship detailed in Chapter 4, PO_4 sorption processes were investigated by means of sediment adsorption effects using the developed TRIVAST model. Two main periods were considered in this study; winter (January, February and March) and summer (June, July and August) 2005, with these periods being

recognised as to have apparent differences in SS concentrations according to K-EPA data.

7. 3. 2. 1 Model set up:

The TRIVAST settings were similar to the ELCOM-CAEDYM settings in terms of both physical parameters (i.e. tides, wind effects, salinity, temperature etc.) and water quality parameters (e.g. DO, NH_4, NO_3, PO_4 etc.) as summarised in Table 7.7. The partition coefficient (K_D) is a site specific parameter [*EPA,* 1999], and special attention should be given when assigning it. According to [*Abdil Aziz,* 1997] a value of K_D= 0.01 can be suitably used for the Bay's conditions, with more details of K_D being given in [*EPA,* 1999]. In order to represent the SS levels during the summer months (i.e. dusty events), the concentration was initially set to 55 mg/l for the entire Bay waters, while the levels ranged from 30 to 64 mg/l at the open boundaries. These values were considered to reflect the effects of dust storms which occurred during this period of the year (i.e. summer) according to K-EPA meteorological data, and the Shatt Al Arab sediment input, which can reach as high as 125 mg/l [*Hartmann et al.,* 1971]. The bed sediments median grain size D_{50} was typically set to 110 μm.

Parameter	Initial		Open boundary		Outfall
	Winter	Summer	Winter	Summer	
DO	9.0	8.0	10.0	8.0	5.0
NH_4	0.11	0.027	0.10	0.07	0.09
NO_3	0.10	0.025	0.01	0.01	0.01
PO_4	0.03	0.023	0.27	0.019	0.015
SS	6	55	6-10	30-64	15

Table 7.7: Water quality set up parameters used in TRIVAST

Unlike ELCOM-CAEDYM, heat transfer through surface waters is not considered in TRIVAST (see Chapter 4) and therefore there will be a slight difference in the prediction of water dynamics, particularly during the summer months when there is a slight stratification rise during the warm season. Broadly speaking, such effects would not significantly modify the water circulations; since the Bay is chiefly driven by tides [*Rakha et al.,* 2007a] (explained in Chapter 6). The differences in model predictions between TRIVAST and ELCOM-CAEDYM will be investigated in Chapter 8.

7. 3. 2. 2 Results and discussion:

To assess the effects of the adsorption processes derived in Chapter 4, the TRIVAST model was run with the PO_4 benthos term σ_2 being included as given in equation 4.39 and with the corresponding results for the simulation being given in Figures 7.14 and 7.15 as TRIVAST 1. Then, using the same settings, the adsorption term in equation 4.42 was included instead of the benthos source term σ_2, with the corresponding simulation results being shown in Figures 7.14 and 7.15 as TRIVAST 2. As can be seen in Figure 7.14, good agreement was achieved between the model and the K-EPA data during the winter, while less accurate predictions were found during the summer months for TRIVAST 1, as shown in Figure 7.15). However, when applying equation 4.42, good predictions were achieved for both seasons, as shown in Figure 7.15.

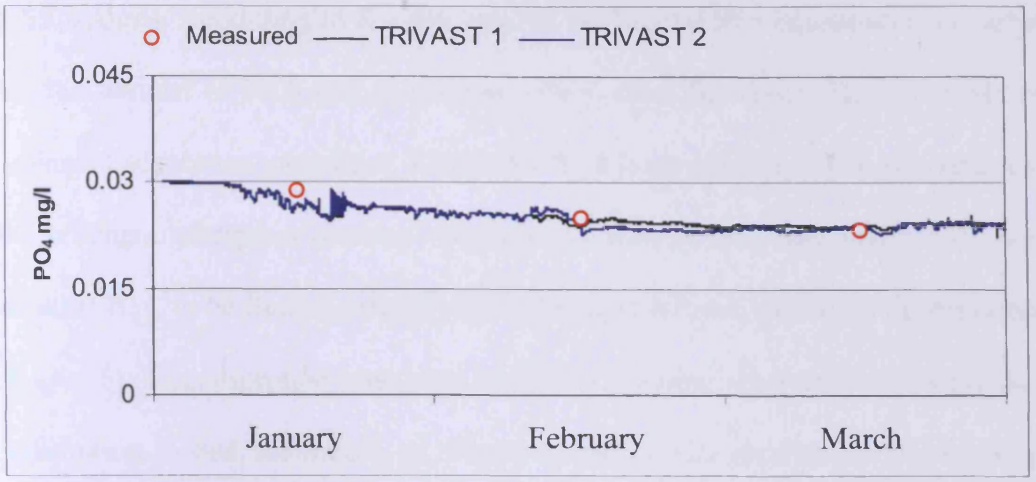

Figure 7.14: TRIVAST predictions validated with measured data at Z1 during winter 2005, TRIVAST 1 including equation 4.39, TRIVAST 2 including equation 4.42

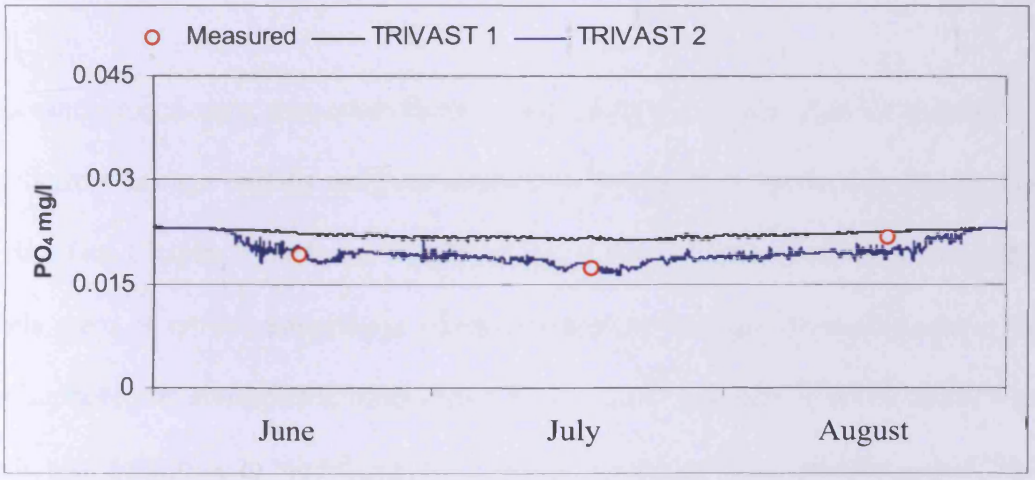

Figure 7.15: TRIVAST predictions validated with measured data at Z1 during summer 2005, TRIVAST 1 including equation 4.39, TRIVAST 2 including equation 4.42 (sediment grain size effects only)

It is thought that the deficiency in predicting the PO_4 levels with the benthos model, σ_2, was mainly due to the lack of PO_4 representations being included for the

high SS seasons. According to K-EPA records the highest SS concentration occurred during the summer of 2005 and, to a lesser extent, over the winter. Thus, in applying the sediment adsorption model (i.e. TRIVAST 2), a large amount of PO_4 was removed by the sediment adsorption process, which would then either settle, particularly near Sulaibikhat Bay, or be flushed away by the tidal currents near the mouth (as explained in Chapter 6). The adsorption processes of PO_4 to SS were comparatively larger than the adsorption to bed sediments, as shown in the model predictions illustrated in Figures 7.14 and 7.15. This was mainly attributed to the dynamics of the Bay (explained in Chapter 6), in which lower residence times, allowing minor sediment settling, persisted near the Bay main channel than in the coastal areas of the Bay. Such findings are crucial when defining the limiting nutrient of algal growth in the Bay, as adsorption process could lead to PO_4 becoming the limiting factor in the Bay.

It is worth mentioning that other factors may affect the predictions for example, SS levels from sewage outfalls were not efficiently presented in the model, due to a lack of data (see Chapter 9 for future work and recommendations). Therefore, detailed SS levels were of crucial importance when considering sorption processes in the Bay. Furthermore, the atmospheric input of dry PO_4 was not considered in this study which could also contribute to modifying PO_4 concentrations as in the Mediterranean [*Herut et al.,* 2002]. Hence, an additional mathematical representation would need to be included to represent the amount of dry PO_4 in the sediments, together with the rate of deposition from the air to the surface water (see Chapter 9 for future work and recommendations).

7. 4 Summary

In this chapter general water quality parameters were investigated using ELCOM-CAEDYM and TRIVAST. First ELCOM-CAEDYM was used to predict DO, NH_4, NO_3 and PO_4 during 2005. The model showed good agreement with the measured data. DO predictions were shown to vary seasonally, with the highest values of 8.5 mg/l being achieved during the winter and the lowest values of 5.8 mg/l occurring during the summer. High DO is attributed to the fresh water input from the open boundary (mainly from the Shatt Al Arab). While low DO concentrations during the summer are mainly due to biological respiration and decomposition processes, predictions of NH_4 and NO_3 showed good agreement with the measured data from 2005. N levels in the Bay are mainly supplied from the open boundary and it has been shown that the levels are sufficient for biological activity. NH_4 concentrations generally ranged from 0.02 to 0.12 mg/l throughout 2005, with the highest values occurring during the winter. Similarly, NO_3 ranged from 0.02 to 0.14 mg/l. Model predictions of PO_4 agreed reasonably well with the measured data from winter, but less so with the measured data from the summer. Unlike N, PO_4 concentrations did not vary greatly throughout 2005, ranging from 0.023 to 0.03 mg/l. Further investigations were undertaken using the same model on the main contributors to PO_4. It was found that most of the PO_4 entered the Bay from the open boundary, while anthropogenic activities made similar contributions. OP was found to have larger concentrations than PO_4 where special attention should be given to mineralisation processes in the Bay.

TRIVAST predictions were shown to have better results when considering adsorption processes during the summer. Therefore, in modelling the seasonal variation of PO_4 in

the Bay it is essential to consider the adsorption processes in the Bay, particularly during the high SS level seasons, when PO_4 sorption processes are significant. Such processes have encouraged PO_4 to be the limiting factor of algal growth in the Bay. Hence, this leads to the finding that any processes related to sediment sorption and grain size should also be given special attention when considering any environmental issues in the Bay.

Chapter 8

General Numerical Model Comparisons for ELCOM-CAEDYM and TRIVAST

8. 1 Introduction:

Numerical models, such as ELCOM-CAEDYM and TRIVAST, are based upon fundamental physical, chemical, and biological principles that aim to simulate the spatial and temporal variations of a marine system. Numerical models do not generally assert to represent all of the complex features of the marine environment, but simply attempt to integrate only those aspects of the problem that are most relevant. The parameters of the model can be adjusted so that it can logically represent certain characteristics of the marine system. However, in some cases where unique water characteristics are involved, new parameterisations or mechanisms may be required to represent the water system appropriately (e.g. the development of the model in Chapter 4). Numerical models are often a set of coupled, nonlinear, partial differential equations (see Chapters 3 and 4), and they can be classified according to the numerical methods, grid types, time differencing schemes and spatial differencing schemes (see Chapters 3 and 4). Three-dimensional models such as ELCOM-CAEDYM and TRIVAST, normally offer the closest approximation to reality by simulating gradients along three spatial dimensions, i.e. X, Y and Z. Although these models all solve the same three-dimensional Navier-Stockes equations, they can be significantly different in terms of their turbulence schemes, numerical methods, grid types and solution algorithms, which would give rise to different model predictions.

The aim of this chapter is to investigate the main differences between ELCOM-CAEDYM and TRIVAST predictions in terms of hydrodynamics and water quality (PO_4). This will be achieved by modelling the Gulf and Bay dynamics using similar model settings as described in Chapters 5 and 6. For water quality investigations, PO_4 will be studied in both models in the Bay.

8. 2 Hydrodynamic predictions in ELCOM and TRIVAST:

In this section the main differences in the hydrodynamic predictions of both models will be studied. First, both models were set up for the Gulf, and then the Bay. It is obvious that the Gulf and the Bay have different domain sizes (the Gulf is roughly 900 km × 300 km whereas the Bay is around 40 km × 20 km), enabling us to understand the major forces which may arise due to domain orientations in both models. In order to investigate the differences between the models special attention was given to the model set up stage. Both models should have identical boundaries and forcing boundary conditions, i.e. the same tides at the open boundary and the same meteorological effects etc, to achieve valid comparisons and conclusions.

8. 2. 1 Model setup and prediction results for the Gulf:

In this section the hydrodynamics of the Gulf was investigated in terms of water levels and velocity using data from the summer of 1992 only, due to limited availability (obtained from KISR). The models were set up in a similar manner as to those described in Chapter 5, which can be summarised as shown in Table 8.1. River discharge settings are as described in Chapter 5, for both models. The meteorological effects in the summer of 1992 were considered in this study as shown in Figure 5.5 (Chapter 5). The location of measured data considered for this investigation is shown in Figure 8.1. To optimise the test, a 30 day simulation was allowed prior to the validation period in both models.

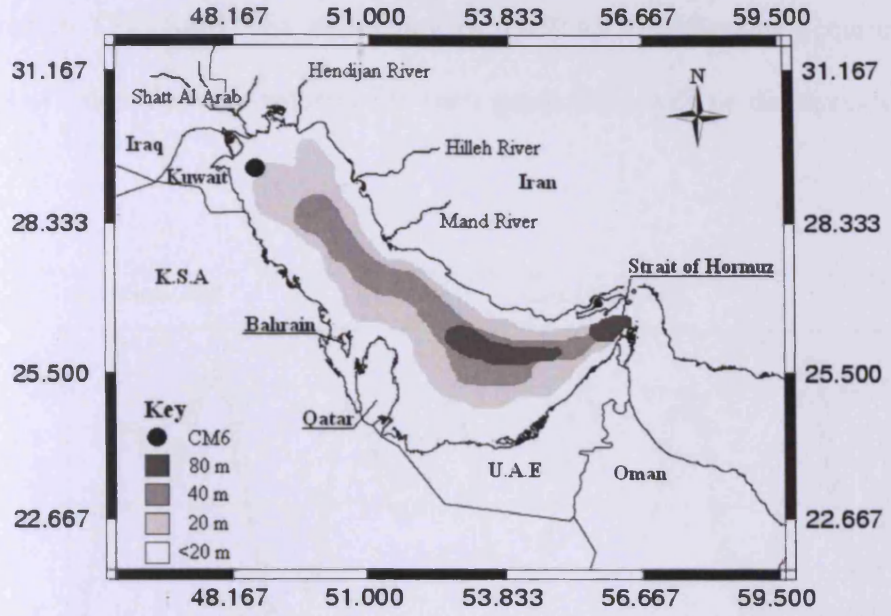

Figure 8.1: Location measured data in the Gulf (CM6), including water level and velocity

Parameter	ELCOM	TRIVAST
Grid size (m)	5000	5000
Layers number	18	18
Layers thickness (m)	5	5
Time step (s)	100	*50
Tides at open boundary	KGULF model	KGULF model
Initial temperature (℃)	28	28
Temperature at open boundary (℃)	28	28
Initial salinity (psu)	38	38
Salinity at open boundary (psu)	38	38
Bottom drag	0.005	0.005
Light extinction coefficient	0.25	-
Horizontal diffusivity (m^2/s)	1	1

Table 8.1: Model settings of ELCOM and TRIVAST, (*) represent the half time step for TRIVAST

8. 2. 1. 1 Water levels:

As shown in Figure 8.2 both models followed the same pattern in predicting the water levels at CM6 in the Gulf. However, better predictions were achieved by ELCOM

compared to TRIVSAT. The deficiency in TRIVAST predictions occurred mostly during low tides. Possible reasons for such predictions will be discussed in section 8.2.3.

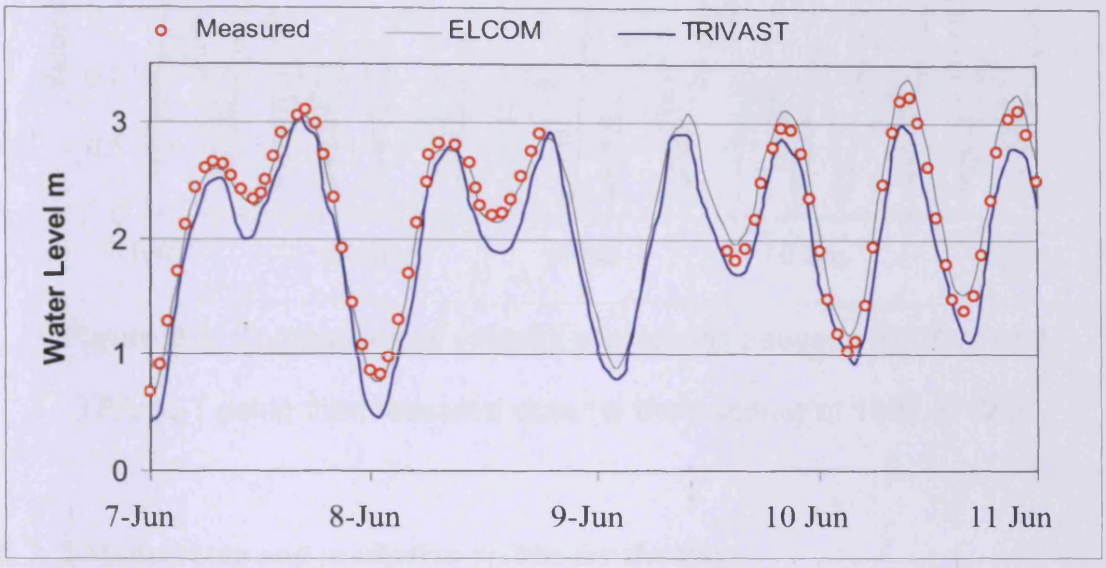

Figure 8.2: Comparisons of water level predictions between ELCOM and TRIVAST using the measured data for the summer of 1992 at CM6

8. 2. 1. 2 Velocity:

As with the water levels, the velocities in both models were satisfactorily predicted, however again better predictions were achieved by ELCOM. According to the measured data, the velocity at CM6 ranged from 0.05 to almost 0.5 m/s. Neither of the models showed accurate prediction at low velocities.

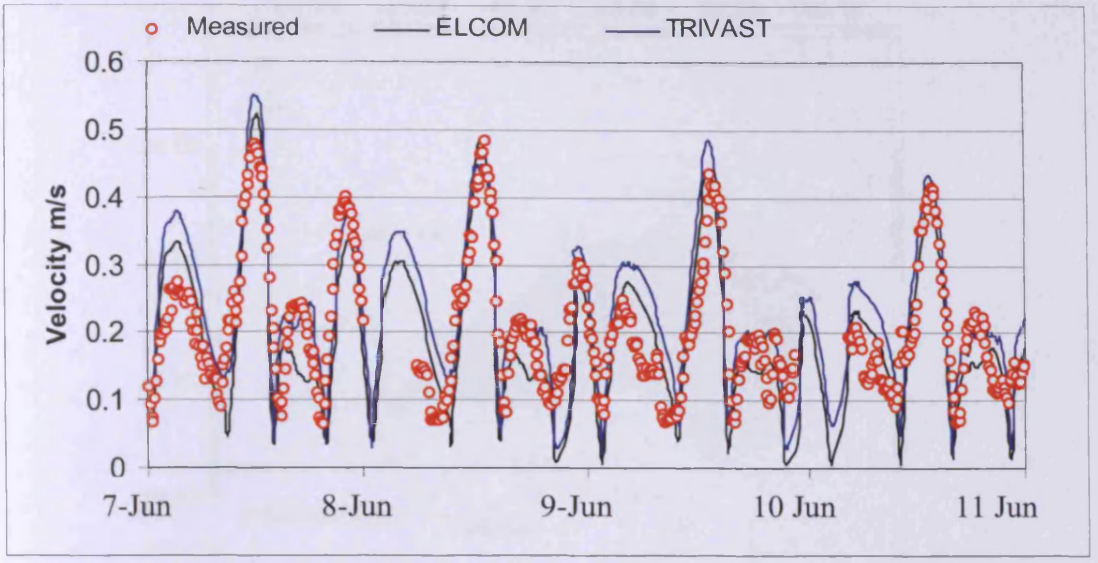

Figure 8.3: Comparison of velocity predictions between ELCOM and TRIVAST using the measured data for the summer of 1992 at CM6

8. 2. 2 Model setup and prediction results for the Bay:

In a similar manner to the Gulf predictions in the previous section, the hydrodynamics of the Bay was investigated in terms of water levels and velocity using data from the summer of 2005 only, due to limited availability (obtained from KISR). The models were set up in a similar manner as to those described in Chapter 6, which can be summarised as shown in Table 8.2. The outfalls were set to the same values as shown in Chapter 6. The meteorological effects in the summer of 2005 were considered in this study as shown in Figure 6.4 in Chapter 6. The location of the measured data considered for this investigation is shown in Figure 8.4. To optimise the test, a 10 day simulation was undertaken prior to the validation period.

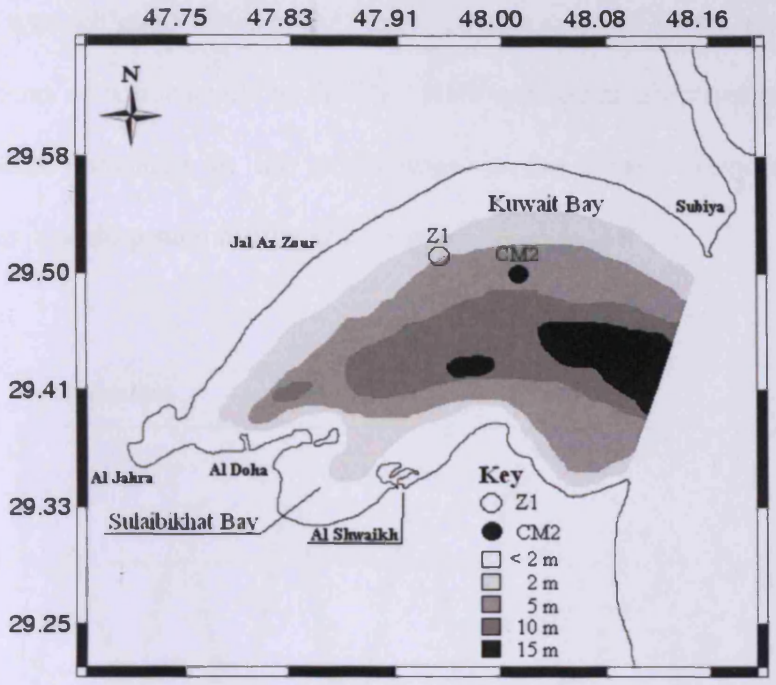

Figure 8.4: Location measured data in the Bay (CM2), including water level and velocity

Parameter	ELCOM	TRIVAST
Grid size (m)	150	150
Layers number	7	7
Layers thickness (m)	5	5
Time step (s)	30	*15
Tides at open boundary	KTIDE model	KTIDE model
Initial temperature (℃)	33	33
Temperature at open boundary (℃)	34	34
Initial salinity (psu)	41	41
Salinity at open boundary (psu)	41	41
Bottom drag	0.003	0.003
Light extinction coefficient	0.25	-
Horizontal diffusivity (m^2/s)	1	1

Table 8.2: The Bay model settings of ELCOM and TRIVAST, (*) represents the half time step for TRIVAST

8. 2. 2. 1 Water levels:

In general good agreement was achieved between the measured and predicted results by both models in the Bay, as shown in Figure 8.5. In particular, slightly better

agreement was achieved between the measured data and ELCOM. Generally speaking the predictions of water levels in the Bay were comparatively more accurate in both models when compared to the predictions of the Gulf's water levels. Further explanation regarding such results will be given in section 8.2.3.

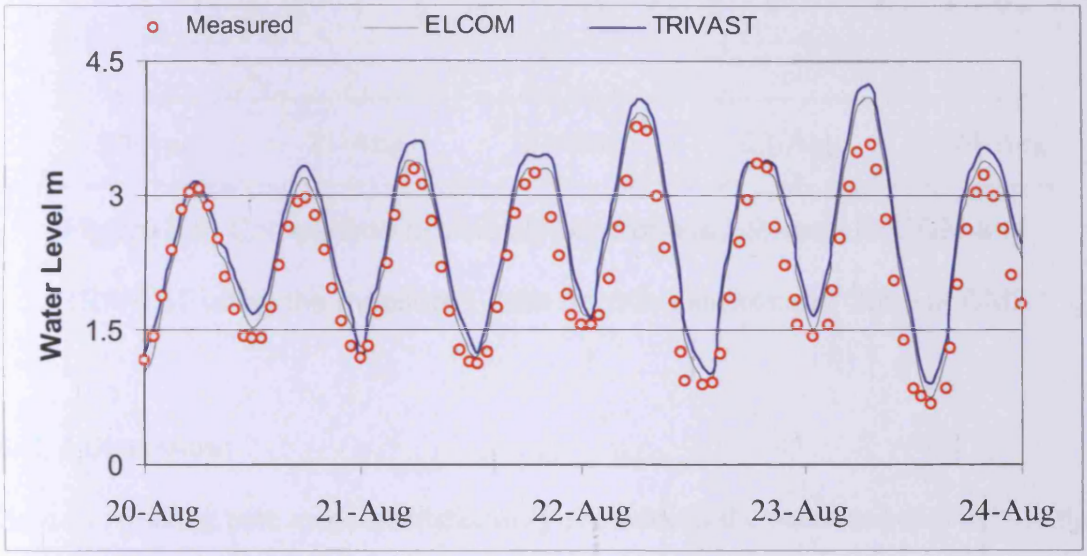

Figure 8.5: Comparison of water level predictions between ELCOM and TRIVAST using the measured data for the summer of 2005 at CM2

8. 2. 2. 2 Velocity:

As with the water levels in the Bay, both models were able to represent the collected data at CM2. Unlike the Gulf predictions, however, both models were able to replicate low velocities, where the lowest mean value was 0.15 m/s at CM2.

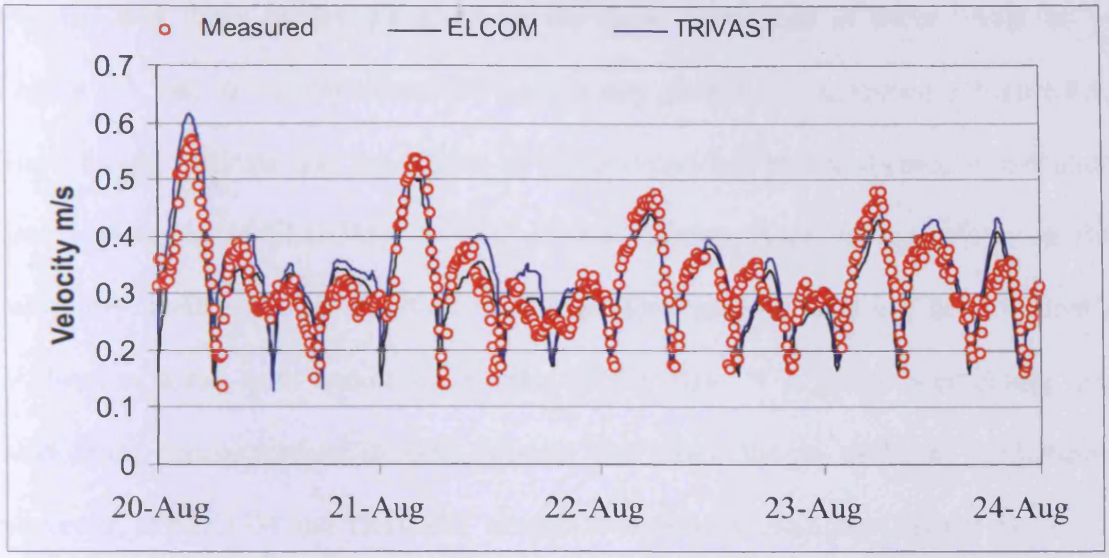

Figure 8.6: Comparison of velocity predictions between ELCOM and TRIVAST using the measured data from the summer of 2005 at CM2

8. 2. 3 Discussion:

Broadly speaking both models satisfactorily reproduced the measured data in both the Gulf and the Bay as explained in sections 8.2.1 and 8.2.2. However better predictions were achieved for the Gulf by ELCOM (see Figures 8.2 and 8.3) compared to TRIVAST. This may well be attributed to the momentum equation representations in both models. In ELCOM, tidal forces were calculated from the gravitational potential which was included in the momentum equation (for more details see [*Cartwright and Tayler*, 1971]), while such effects were not included in TRIVAST (for more details see Chapter 4). Also, a deficiency in the TRIVAST predictions rose from a lack in surface-water-heat-input representations, which would be more pronounced in the much larger Gulf model due to the much more substantial losses. Furthermore, the Gulf water can develop stratification during the warm seasons (see Chapter 5), which would have apparent effects on water circulation, particularly with regard to the velocity of water, as shown in Figure 8.3.

For the Bay, both models gave almost the same predictions in water levels, as in Figure 8.5, and to a lesser extent, for the velocity predictions, as shown in Figure 8.6. Such results indicate that the effects of the gravitational potential (used to calculate the tidal forces in ELCOM), as well as stratification, have limited effects on the relatively small and less stratified Bay. Therefore, both models can be sufficiently utilised in areas with conditions similar to the Bay. It is worth mentioning that turbulence representation in both models can give rise to different predictions, however, in ELCOM and TRIVAST similar models were used (see Chapter 4).

It is very important to understand the physical background for each intended modelling study. The gravitational potential effect which is found in ELCOM is very important when considering long water bodies, such as the Gulf and the Red Sea. This has allowed for tidal generation within the estuary, in which the water level fluctuations in numerous locations associated with the lunar semidiurnal tidal response were incorporated particularly for the Gulf predictions. Also, for estuaries where significant stratification occurs due to heat input, models such as TRIVAST should not be considered. However, were models such as theses to be considered, further model developments should be taken into consideration (see Chapter 9 for future work and recommendations).

8. 3 Water quality predictions of phosphorus (P) (ELCOM-CAEDYM and TRIVAST):

In this section, the main differences in PO_4 predictions between ELCOM-CAEDYM and TRIVAST are investigated. As mentioned earlier both models are based on different source and sink terms (see Chapter 4), and therefore potentially lead to

different predictions. In general, more detailed processes are included in the P cycle in CAEDYM (see Table 4.1 in Chapter 4), while in TRIVAST less detailed processes are included. In this section the development model of TRIVAST will be investigated, which includes PO_4 adsorption effects. Due to limited data, the investigations were carried only out for the Bay, and during the summer months.

8. 3. 1 Model setup and prediction results:

In modelling P in the Bay, settings similar to those of Chapter 7 were utilised (see section 7.3.2, Table 7.5) and both models had the same forcing boundary conditions. It is worth mentioning that other detailed parameters related to P in CAEDYM were not included in TRIVAST (see Table 7.5 in Chapter 7). In this investigation Z1 was considered, which is located in the northern area of the Bay, as shown in Figure 8.4.

As can be seen in Figure 8.7, good predictions were achieved in both models. However, more accurate predictions were achieved with TRIVAST than with ELCOM-CAEDYM, although the ELCOM-CAEDYM predictions were smoother. TRIVAST predictions were particularly accurate during July 2005 when most adsorption occurred. Furthermore, ELCOM-CAEDYM predictions show an increase of at least 0.004 mg/l in PO_4 compared to TRIVAST for the same period. An explanation of such predictions will be given in the following section.

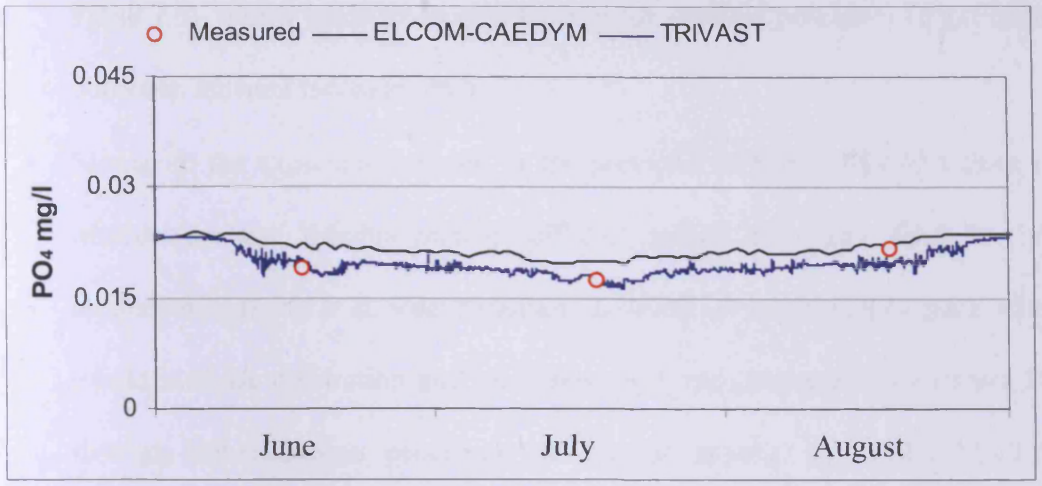

Figure 8.7: Comparison of PO_4 predictions between ELCOM-CAEDYM and TRIVAST using the measured data from the summer of 2005 at Z1

8. 3. 2 Discussion:

Although ELCOM-CAEDYM is more a sophisticated model (see Chapter 4 for more details), TRIVAST predictions were more accurate in representing the measured data at Z1 for the summer of 2005. This does not necessarily indicate that ELCOM-CAEDYM is a less reliable model in such conditions due to the following:

- The developed TRIVAST model, suggests that most PO_4 reduction occurred due to adsorption processes. In ELCOM-CAEDYM, additional sources increased the PO_4 predictions rose from organic matter and the PO_4 sediment flux which is a function of temperature, DO and pH. Such processes are not modelled in TRIVAST. Therefore, detailed water quality data is crucial to identifying the most suitable model for studying the Bay.
- The representation of the biological uptake of PO_4 in TRIVAST is summarised in three parameters (see equation 4.39 in Chapter 4), where as in ELCOM-CAEDYM more than three terms are involved in such representations. This includes nutrient representations in each algal group (see

Table 7.5), which leads to an explanation for detailed processes (e.g. limiting nutrients, nutrient increases etc).

- Similar to the explanation given in the previous section, TRIVAST does not include surface thermodynamic effects, which normally lead to high temperatures rising from solar radiation. In terms of water quality, such effects would increase respiration and mortality rates and consequently increase PO_4 through mineralisation processes of organic matter, as in the ELCOM-CAEDYM predictions (see Figure 8.7).

In terms of the computational aspects of both models, TRIVAST is a relatively faster model than ELCOM-CAEDYM. As for the predictions shown in Figure 8.7, a time of approximately 6 days was needed to complete the simulation using TRIVAST, while roughly 19 days were needed in a typical ELCOM-CAEDYM test. Consequently, a smaller computational memory is needed when using TRIVAST (typically around 2 GB), compared to ELCOM-CAEDYM (more than 20 GB). This is mainly due to the sophisticated modelling processes included in CAEDYM.

Similar to hydrodynamic modelling, in water quality modelling it is important to understand the fundamental chemical and biological background of the intended modelling region. Based on this requirement, the modeller should consider which is the best model to utilise for the relevant case. As shown in this chapter, TRIVAST is a relatively good model to consider for the Gulf and, in particular, for the Bay. However, for sophisticated physical, chemical and biological case studies, ELCOM-CAEDYM is a better option. Unlike sophisticated models, such as ELCOM-

CAEDYM, simpler models, such as TRIVAST, are often computationally less expensive.

8. 4 Summary:

Although most models are based on solving similar set of governing equations, different results may be achieved based on the techniques used to solve theses equations. In this chapter the main differences between TRIVAST and ELCOM-CAEDYM have been investigated by means of comparing hydrodynamic and water quality predictions (PO_4). The study was implemented for the Gulf and in the Bay, and in general both models show acceptable results. The hydrodynamic results of both models showed that the effects of gravitational potential, included in ELCOM, give good predictions in relatively large water bodies such as the Gulf. In addition, thermodynamics is an important factor to include when considering warm seasons in large water bodies such as the Gulf. Such an effect is not so significant in the Bay, due to the structure being well mixed throughout the year. Hence, TRIVAST is the equally reliable in smaller and less stratified water bodies.

In terms of water quality, PO_4 was taken into consideration in the Bay. Again both models gave good predictions during the summer, however, better predictions were achieved by TRIVAST due to adsorption representations in the model. In ELCOM-CAEDYM, additional sources have over estimated the PO_4 concentrations in this model. This leads to the fact that adsorption processes are an important factor when considering PO_4 fluxes in the Bay. In addition, detailed water quality data is a crucial factor that enables the selection of an appropriate model. Computationally, ELCOM-CAEDYM has been shown to be a more expensive model –computationally- due to

the detailed water quality parameterisation involved, as well as the larger range of parameters and processes.

Chapter 9

Conclusions and Recommendations

9.1 Summary and conclusions:

Estuaries and coastal areas are generally considered to be highly productive systems, as they frequently contain reasonable amounts of algae, phytoplankton and sea grass biomass. Thus, they normally support large bird and fish populations, which are essential for the community. This high population of living plants and animals implies that the biota and seabed sediments embody important nutrient pools that are necessary for the productivity of estuaries and coastal areas and these are mainly controlled by the water flow. Therefore, the hydrodynamics of such water bodies are an essential factor that provide a fundamental understanding of the water mixing processes and the accumulation of biodiversity. Unlike rivers, estuaries and coastal areas seas are more complex systems, since the flow is usually driven by the slope of the water surface, wind stresses and also internal density variations that may exist in some rivers, however, oscillating flow adds a further complexity to the coastal system.

In this study, the Arabian Gulf and Kuwait Bay were considered for further investigations and an analysis of the physical and chemical aspects of these water bodies were undertaken by means of numerical modelling. The Gulf is a relatively shallow semi-enclosed water body located in the Middle East, which is detached from the Gulf of Oman by the Strait of Hormuz. The Bay is an elliptically shaped embayment that extends in a westward direction from the extreme north of the Gulf.

In recent decades, and especially during the last few years, coastal developments in the Gulf countries have accelerated enormously, due to the major increase in oil related income and economic diversification schemes. The rapid expansion of

industrial complexes, an exceptional rise in private real estate investment, tourism and service industries, including high birth rates and the entry of foreign labour, accompanied by prospering economies, have all resulted in a massive human population growth along the Gulf's coastal waters. Such effects have raised concerns in the Gulf countries about the marine ecology, since the coastal zone serves as a resource for fishing, recreation, urban development, oil transportation and perhaps, most importantly, a major source of fresh water via desalination plants. Furthermore, natural phenomenal issues related to climate change have been considered to act as a source of pollution that includes flash floods and dust storms and perhaps requires further scientific investigation. This has all led to numerous environmental issues in the region, with one of most frequent being eutrophication and red tides, mainly due to nutrient increases.

Recently, numerical models have been widely used to resolve many hydro-environmental issues related to anthropogenic activities and waterfront developments such as those found in the Gulf, such as Dubai in the United Arab Emirates. Furthermore, they play an important role in a number of political and economical fields by means of decision-making. Numerical models are based upon fundamental physical, chemical, and biological principles that illustrate the spatial and temporal variations of a marine system. Due to the environmental complexity of estuaries, and to a lesser extent computational cost, there has been no such model, or what may possibly be called a 'Global Model', able to present all of the key physical and chemical aspects of all estuaries. Therefore, numerical models attempt to integrate only those aspects of the problem that are most relevant. Otherwise, further developments to models are essential in tackling a particular problem.

The main conclusions and outcomes achieved in this study in modelling the Gulf and Bay, can be summarised as follows:

- Dispersion processes are of fundamental importance to marine life in the Gulf, which are affected by extensive anthropogenic activities. Traditionally, the Gulf countries have relied on the dispersion of effluents once they entered coastal waters so that, once diluted, biological breakdown renders them harmless. However, such practices have been extensively used and have led to various environmental impacts in the region. Therefore, the main goal achieved in this study is determining the geographic dispersion of numerical tracers and flushing characteristics, in terms of residence time, of the Gulf. That, in turn, has provided a crucial guide for new engineering developments. This was achieved by incorporating ELCOM and most importantly, validating the model using 1992 Mt Mitchell data from the summer and winter. Excellent model validation was achieved and utilised to conduct various sensitivity analyses on the forcing boundaries, in particular winds and tides. The study has revealed that dispersion of numerical tracers is chiefly controlled by tides. Winds had limited effects on dispersing the numerical tracers in the Gulf, particularly during the summer. The highest dispersion coefficient was calculated near Qatar during the early stages of tracer injection in the winter (141 m^2/s), in which coastal areas have enhanced tracer spreading due to shear effects. The horizontal dispersion of other tracers in the estuary varied from 60 to 90 m^2/s, which were mainly affected by shear forces produced by tides. Although, such results were based on the 1992 forcing data, dispersion coefficients obtained in this study can be considered as typical

values for the Gulf, since wind did not affect the results significantly. Therefore, applying 2011 forcing data, for example, would give similar results.

- Residence times are generally measures used to calculate the retention time of water or scalar quantities transported by water. In the Gulf such measures are of particular importance in understanding the formation and accumulation of biodiversity. The residence time in the Gulf was calculated to be almost 3 years using ELCOM. The residence time being the longest for the waters along the Arabian, vis-à-vis the Iranian, coast of the Gulf. In particular, near Kuwait Bay, Qatar and the UAE coast the residence times values reached 858 days. Obviously the residence time near the Strait of Hormuz was lowest (2 days) due to the open boundary effects in the region.
- Water flow is an essential mechanism that controls a major amount of the variability of water quality in estuaries [*McCutcheon*, 1989]. Any fundamental study of water quality including modelling studies, requires a knowledge of the circulation patterns of the water mass within the basin. In practical terms, the first step in any water quality modelling investigation is to determine 'where the water departs' and how water circulation affects the accumulation of suspended and dissolved materials. Hence, Kuwait Bay was investigated in terms of hydrodynamics using ELCOM before conducting water quality modelling studies. The model was first validated with the 2005 measured data for water levels, velocity and velocity direction, obtained from KISR. Similar to the Gulf, investigations showed that the Bay is chiefly driven by tides and to a lesser extent by winds, particularly near coastal regions. Simulations have shown the water velocity to be highest near the mouth of the Bay, typically 0.8

m/s during flood tides, which create a fairly mixed structure throughout the year, while low velocity fields were obvious in the coastal areas of the Bay, particularly at Sulaibikhst Bay (typically 0.1 m/s). Detailed studies of the temperature, using the same model, showed that temperature varied seasonally in the Bay with the highest value being predicted during the summer with 34 °C and the lowest during the winter with 15 °C. Furthermore, stratification was slightly raised near coastal regions during the summer due to the heat from solar radiation effects. In terms of salinity, investigations have shown that the Shatt Al Arab has an apparent effect on the Bay's salinity, particularly in the northern areas, while desalination plants have local effects such as at the Al Doha desalination station.

- Studies using tracer injection at the mouth of the Bay showed that the circulation of the Bay is characterised mainly by two gyres produced by tides; the first is slightly larger than the second and acts in a clockwise direction, while the second acts in a counter clockwise direction. Such forces are mainly responsible for the mixing process in the main channel of the Bay, while wind effects are predominant in the far north of the Bay and in the southern areas near Sulaibikhat Bay. The maximum residence time of the Bay was calculated to be 57 days near al Jahra using ELCOM. Such studies provided important information for water quality modelling.
- Water quality represents the physical, chemical, and biological characteristics of water and measures the capability of a marine system to sustain its beneficial use to society. For the Bay water quality parameters were investigated using ELCOM-CAEDYM and TRIVAST. ELCOM-CAEDYM was used to predict DO, NH_4, NO_3 and PO_4 during 2005. In general, good

agreement was obtained between the model results and the model showed reasonable agreement with the measured data.

- DO predictions varied seasonally, with the highest values achieved during the winter 8.5 mg/l and the lowest during the summer 5.8 mg/l. High DO is attributed to the fresh water input from the open boundary (mainly from the Shatt Al Arab). While low DO concentrations during the summer are mainly due to biological respiration and mineralisation processes. N levels in the Bay are mainly supplied from the open boundary and have been shown to be in sufficient levels for biological activity. NH_4 concentrations generally ranged from 0.02 to 0.12 mg/l throughout 2005 with the highest values occurring during the winter. Similarly, NO_3 values ranged from 0.02 to 0.14 mg/l. PO_4 predictions have agreed reasonably well with the measured data during the winter, but were less accurate during the summer. Unlike N, PO_4 levels did not show large temporal variations during 2005 but did have noticeable spatial variations. PO_4 levels had comparatively lower concentrations than N, which ranged from 0.023 to 0.03 mg/l in the middle of the Bay. Such results implied that PO_4 is the main the limiting nutrient for biological activity for during most of the year.
- Investigations on the main contributors to PO_4 levels show that most PO_4 entered the Bay from the Gulf, while anthropogenic activities had similar contributions. OP was found to have larger concentrations than PO_4 and therefore the mineralisation rate was an important factor when considering PO_4 modelling in the Bay.
- The main model developments were undertaken on the PO_4 source and sink terms in TRIVAST. Such developments were associated with PO_4 sorption

processes to sediment particles. Seasonal predictions from the developed model (TRIVAST) showed that the adsorption of PO_4 had a critical influence on the removal of PO_4 from the Bay during the summer, which supported PO_4 to be the limiting nutrient, particularly during high suspended sediment level events. Therefore, such developments gave crucial understanding to the phosphorus behaviour in the Bay.

- Although model developments of phosphorus adsorption were based on experimental work conducted on sediments obtained for the Loughor Estuary, U.K., it was found that such effects could successfully be applied to analysing the phosphorus-sediment interaction behaviour in Kuwait Bay.
- As mentioned earlier, numerical models do not purport to represent all the features of an actual complex marine environment, but merely attempt to integrate only those aspects of the problem that are most relevant. In this study two models were considered, ELCOM-CAEDYM and TRIVAST, which have various and notable dissimilarities in their numerical aspects based on solving the governing equations. Investigations into the model differences were undertaken by conducting various hydrodynamic and water quality analyses in the Gulf and the Bay. Due to limited data the Gulf was only investigated in terms of the hydrodynamics. In general, the study showed that better predictions were achieved using ELCOM than TRIVAST in the Gulf and Bay. This was due to the additional term of tidal forces that were calculated from the gravitational potential in ELCOM. It is crucial when modelling such long domains to consider such forces in the model. In comparison, such effects have been shown to be minor in the Bay predictions using ELCOM, leading to very similar predictions in both models. PO_4 predictions in ELCOM-

CAEDYM and TRIVAST showed that adsorption processes of PO_4 are a vital factor to consider when modelling PO_4 in the Bay. This was apparent in the prediction of the developed model TRIVAST in which a reasonable amount of PO_4 was removed from the Bay waters through adsorption to SS.

9.2 Recommendations for further study:

This research project has led to several key conclusions and the outcome of the work has also led to a number of primary recommendations for additional study. These recommendations can be summarised as follows:

- Although good results were achieved in identifying the dispersion coefficient in the Gulf, it is worth investigating and comparing the results with actual dye release studies, such as those conducted by *Hetling and O'Connell*, [1966].
- In modelling the Bay it is necessary to include the new fresh water input, originating from the Shatt Al Arab, in the modelling domain as it appears to have apparent effects on the water salinity. Hence, obtaining detailed data of the various physical water parameters of fresh water inflow are essential for accurate Bay modelling studies.
- As for the hydrodynamic studies, when considering water quality modelling studies in the Bay, it is important to include the Shatt Al Arab in the modelling domain, as it appears to have a direct effect on nutrient levels, in particular N. This would also need detailed data for the modelling applications of various water quality parameters originating from upstream of the Euphrates and Tigris rivers.
- Due to the high level of organic matter in the Bay, further investigation on the mineralisation rate of organic matter would be highly beneficial in terms of

understanding the amount of nutrients rising from this source. Several studies have suggested that factors such as DO and temperature have a direct influence on the mineralisation rate [*Middelbrug et al.,* 1993], and therefore should be further investigated when modelling the Bay.

- Obtaining detailed data of various water quality parameters originating from wastewater outfalls have crucial implications in understanding the accumulation of nutrients in the southern areas of the Bay, and consequently would give a better understanding of the ecological composition and variations within the Bay. In terms of modelling, this would allow further refinements to the ecological aspects of the models.
- The position of phytoplankton in the food web, and the undesirable effects of phytoplankton blooms on the water quality and biota of coastal seas denote that understanding their dynamics is crucial in managing eutrophication [*Paerl,* 1988; *Reynolds et al.,* 2000]. Therefore, detailed data and further investigation of phytoplankton is an essential requirement to understanding eutrophication in the Gulf and Bay.
- Mathematical representations of atmospheric deposition of dust/sand particles should be taken into consideration when modelling PO_4 in the Bay, in particular when studying adsorption processes in the Bay.
- Suspended sediment data originating from the Shatt Al Arab has crucial importance when studying sorption processes in the Bay, with detailed data, including SS levels from wastewater outfall, providing improved information for more accurate model applications.
- Similar to PO_4, N has a sorption capacity to SS [*Ji, 2008*], however, this was not studied in the Bay. Further investigations and model refinements on

sorption processes, similar to PO_4, would give a better understanding to N levels in the Bay particularly during high SS events.

- Although the grid used in modelling the Bay was 150 m and showed relatively good results, it is worth reducing the grid resolution to include the mud flats of the Bay, since such areas can possibly act as a nutrient source arising from sediment-water interactions [*Abdel Aziz,* 1997; *Al-Zaidan et al.,* 2006].
- Due to frequent dust storms, further investigations should be carried out on the dry sediment chemical composition in order to investigate the dominant nutrient sources for the estuary arising from this phenomenon, and therefore allowing for further refinements to the model.
- The inclusion of thermodynamic effects and better tidal force representations in the TRIVAST model is an important required refinement, particularly for modelling partially stratified long estuaries or coastal seas, such as the Gulf during summer months.

References:

Abaychi J. K., Darmian S. A. and Dou Abul A. A. Z. (1988), *The Shatt Al-Arab River: a nutrient salt and organic matter source to the Arabian Gulf,* Hydrobiologia, 166, 217-224.

Abdelrahman M. and Ahmad F. (1995), *A note on the residual currents in the Arabian Gulf,* Continental Shelf Research, 15, 1015-1022.

Abdel Aziz S. R. (1997), *Coastal geomorphology and environmental assessment of Sulaibikhat Bay, Kuwait,* MSc thesis, Kuwait University.

Abdel-Jawad M. and Al-Tabtabaei M. (1999), *Impact of current power generation and water desalination activities on Kuwaiti marine environment,* Proceedings of IDA World Congress on desalination and water reuse, San Diego, 3, 231-240.

Abouseida M. M. and Alsarawi M. A. (1990), *Utilization and management of coastal areas in Kuwait,* Coastal Management, 18, 385-401.

Ahmad F. and Sultan S. A. R. (1991), *Annual mean surface heat fluxes in the Arabian Gulf and the net heat transport through the Strait of Hormuz,* Atmosphere-Ocean, 29, 54-61.

Altinbilek, D. (2004), *Development and management of the Euphrates-Tigris basin,* Water Resources Development, 20, 15-33.

Ali M. and Riley J. (1986), *The distribution of halomethanes in the coastal waters of Kuwait,* Marine Pollution Bulletin, 17, 409-414.

Al-Asfour T. (1981), *The study of and a contribution to the geomorphology of the Arabian Gulf,* Change and development in the Middle East, 173-188.

Al-Enezi E., Alosairi Y., Bockelmann-Evans B. N. and Falconer, R. A. (2010), *Modelling of phosphorus adsorption in estuarine sediment,* in Christodoulou G. C. et al. (Eds.), Proceedings of the 6th Internationa Symposium on Environmental Hydraulics, Athens, 2, 759-764.

Al-Enezi E. (2010), Private Communications.

Al-Enezi E. (2011), *Modelling of phosphorus adsorption processes in estuarine and coastal waters,* PhD Thesis, Cardiff University, (submitted).

Al-Fahed S., Al-Hawaj O. and Chakroun W. (1997), *The recent air temperature rise in Kuwait,* Renewable Energy, 12, 83-90.

Al-Gahtani A. and Maslehuddin M. (2002), *Characteristics of the Arabian Gulf environment and its impact on concentrate durability - An overview.* The 6th Saudi Engineering Dhahran, Saudi Arabia King Fahd University of Petroleum and Minerals, Dhahran.

Al-Ghadban A. N. (2002), *Geological oceanography of the Arabian Gulf,* in Khan N. et al. (Eds.), The Gulf ecosystem, health and sustainability, Leiden, 23-40.

Al-Ghadban A. N., Abdali F. and Massoud M. S. (1998), *Sedimentation rate and bioturbation in the Arabian Gulf,* Environment International, 24, 23-31.

Al-Ghadban A. N. and El-Sammak A. (2005), *Source, distribution and composition of the suspended sediments, Kuwait Bay, Northern Arabian Gulf,* Journal of Arid Environments, 60, 647-661.

Al-Ghadban A. N., Saeed T., Al-Dousari A. M., Al-Shemmari H., and Al-Mutairi M. (1999), *Preliminary assessment of the impact of drainage of Iraqi marches on Kuwait's northern marine environment,* Water Science Technology, 40 (4), 75–87.

Al-Haddad S. (2009), *The direct behind the dust,* Kuwait Times Electronic Newspaper, Kuwait, Available via dialog: http://www.kuwaittimes.net/read_news.php?newsid=MTA4NTU4MzgzOA.

Al-Hajri K., (1990), *The Circulation of the Arabian (Persian) Gulf: A Model Study of its Dynamics*, PhD Thesis, The Catholic University of America.

Al-Hassan L. A. J. and Hussain N. J. (1985), *Hydrological parameters influencing the penetration of Arabian Gulf fishes into the Shatt Al-Arab River, Iraq*, Cybium, 9 (1), 7-16.

Al-Muzaini S., Beg M. U. and Ali L. N. (1997), *Microtox assay for assessment of marine pollution in industrial discharge zone of Kuwait*, Kuwait Institute for Scientific Research, Environmental Sciences, 109-115.

Al-Qabandi A. (2010), *Dust remain several days in summer 2010,* Al-Watan Electronic Newspaper, Kuwait, Available via dialog: http://watanpdf.alwatan.com.kw/alwatanPDF/2010-05-25/2010-05-25.pdf.

Al-Rashid O. and Al-Mikaimi M. (2010), *Records of high temperature puts the electricity crisis in the interface,* Al-Jarida Electronic Newspaper, Kuwait, Available via dialog: http://www.aljarida.com/AlJarida/Resources/PdfPages/AlJarida/16-06-2010/P02_eruio.pdf.

Al-Rashidi T. B. (2009), *An analysis of drivers of seawater temperature in Kuwait Bay, Arabian Gulf*, PhD Thesis, University of Southampton.

Al-Saadi H. A., Hadi R. A. M., Schiewer U. and Al Mousawi A. H. (1989), *On the influence of the sewage drainage from Basrah City on the phytoplankton and related nutrients in the Shatt al-Arab estuary, Iraq*, Archiv fuer Molluskenkunde, 114 (3), 443-452.

Alsharhan, M. (2009), *The days of dust will be more than quarter of the year*, Al-Qabas Electronic Newspaper, Kuwait, Available via dialog: http://www.alqabas.com.kw/Temp/Pages/2009/03/22/09_page.pdf.

Al-Taiee T. M. (1990), *The influence of a dam on the downstream degradation of a river bed: case study of the Tigris River,* Hydrology in mountainous regions, artificial reservoirs: water and slopes, Proceeding of two Lausanne Symposia, 194.

Al-Yamani F. (2008), *Importance of the Freshwater Influx from the Shatt-Al-Arab River on the Gulf Marine Environment*, in Abuzinada A. H. et al., (Eds.), Protecting the Gulf's Marine Ecosystems from Pollution, Birkhauser, Berlin, 207-222.

Al-Yamani F. Y., Bishop J. M., Al-Rifaie K. and Ismail W. (2007), *The effects of the river diversion, Mesopotamian marsh drainage and restoration, and river damming on the marine environment of the northwestern Arabian Gulf*, Aquatic Ecosystem Health and Management, 10, 277-289.

Al-Yamani F.Y., Bishop J. M., Ramadhan E., Al-Husaini M., and Al-Ghadban A. (2004), *Oceanographic Atlas of Kuwait's Waters*, Kuwait Institute for Scientific Research,Kuwait, 202.

Al-Yamani F., Subba Rao D. V., Mharazi A., Ismail W. and Al-Rifaie K. (2006), *Primary production off Kuwait, an arid zone environment, Arabian Gulf*, International Journal of Oceans and Oceanography, 1(1), 67-85.

Al-Zaidan A. S., Kennedy H., Jones D. A. and Al-Mohanna S. Y. (2006), *Role of microbial mats in Sulaibikhat Bay (Kuwait) mudflat food webs: evidence from delta C-13 analysis*, Marine Ecology-Progress Series, 308, 27-36.

Amorocho J. and Devries J. J. (1980), *A new evaluation of the wind stress coefficient over water surfaces*, Journal of Geophysical Research., 85, 433-442.

Anderlini V. C., Jacob J. C. and Lee, J. W. (1982), *Atlas of physical and chemical oceanographic characteristics of Kuwait Bay*, Final report of the oceanographic data project, Kuwait Institute for Scientific Research, KISR704, 15-66.

Aqrawi A. A. M. (1994), *Petrography and mineral content of sea-floor sediments of the Tigris-Euphrates Delta, North-west Arabian Gulf, Iraq,* Estuarine and Coastal Shelf Science, 38 (6), 569-582.

Aref, H. (1984), *Stirring by chaotic advection*, Journal of Fluid Mechanics, 143, 1-21.

Attrill M. J. and Power M. (2002), *Climate influence on a marine fish assemblage,* Nature, 417, 275-278.

Basson P. W., Burchard J. E., Hardy J. T. and Price A. R. G. (1977), *Biotopes of the Western Arabian Gulf,* ARAMCO, Dhahran, 284.

Becacos-Kontos T. (1977), *Primary production and environmental factors in an oligotrophic biome in the Aegean Sea,* Marine Biology, 42, 93-98

Biggs B. J. F. (1996), *Patterns in periphyton of streams*, in Stevenson R. J. et al. (Eds.), Algal ecology: Freshwater benthic ecosystems, Academic, 31-56.

Biggs B. J. F. and Smith R. A. (2002), *Taxonomic richness of stream benthic algae: effects of flood disturbance and nutrients,* Limnology and Oceanography, 47(4), 1175-1186.

Bleninger T. and Jirka G. H. (2010), *Environmental planning, prediction and management of brine discharges from desalination plants*, Middle East Desalination Research Centre, Sultanate of Oman, MEDRC Project: 07-AS-003

Blumberg, A. F. and Mellor G. L. (1987), *A description of a three-dimensional coastal ocean circulation model*, in Heaps N. S. (Eds.), Three-dimensional coastal ocean models, American Geophysical Union, 1-16.

Borowitska L. J. (1981), *The microflora: adaptation to life in extremely saline lakes,* Hydrobiologia, 81, 33-46.

Bouvier T. C. and del Giorgio P. A. (2002), *Compositional changes in free-living bacterial communitics along a salinity gradient in two temperate estuaries,* Limnology and Oceanography, 47, 453-470.

Bou-Olyan A. A. and Al-Sarawi A. M. (1993), *Inorganic and organic pollutant measurements at the Kuwait waterfront project,* Water, Air, and Soil Pollution, 69, 301-308.

Bowden K. F. (1963), *The mixing processes in a tidal estuary,* International Journal of Air and Water Pollution, 7, 343-356.

Bowden K. F. (1967), *Circulation and diffusion,* in Lauff G. H. (Eds.), Estuaries, American Association for the Advancement of Science, 85, 15-36.

Bowden, K. F. (1965), *Horizontal mixing in the sea due to a shearing current.* Journal of Fluid Mechanics, 21, 83-95.

Bowie G. L., Mills W. B., Porcella D. B., Campbell C. L., Pagenkopt J. R., Rupp G. L., Johnson K. M., Chan P. W. H. and Gherini S. A. (1985), *Rates, constants, and kinetics formulations in surface water quality modelling*, Environmental protection agency, U.S., EPA/600/3-85/040.

Boyland P. L., Aref H. and Stremler M. A. (2000), *Topological fluid mechanics of stirring*, Journal of Fluid Mechanics, 403, 277-304.

Boynton W. R., Garber J. H., Summers R. and Kemp W. M. (1995), *Input, transformations, ad transport of nitrogen and phosphorus in Chesapeake Bay and selected tributaries*, Estuaries, 18, 285-314.

Brewer P. G. and Dyrssen D. (1985), *Chemical Oceanography of the Persian Gulf.*, Progress in Oceanography, 14, 41-55.

Bryant E. (2005), *Natural Hazards,* Cambridge University Press, U.S.A, 312.

Burger J. and Gochfeld M. (2002), *Effects of chemicals and pollution on seabirds*, in Schreiber E. A. and Burger J. (Eds.), Biology of marine birds, CRC press, Florida, 485-525.

Cartwright D. E. and Tayler R. J. (1971), *New computations of the tide-generating potential*, Geophysical Journal Royal Astronomical Society, 23, 45-74.

Casulli V. and Cattani F. C. (1994), *Stability, accuracy and efficiency of a semi-implicit method for three-dimensional shallow water flow*, Computers & Mathematics with Applications, 27, 99-112.

Casulli V. and Cheng R. T. (1992), *Semi-implicit finite difference methods for three dimensional shallow water flow*, International Journal for Numerical Methods in Fluids, 15, 629-648.

Chan T. U., Hamilton D. P., Robson B. J., Hodges B. R. and Dallimore C. (2002), *Impacts of hydrological changes on phytoplankton succession in the Swan River, Western Australia*, Estuaries, 25, 1406-1415.

Chanson H. (2004), *The hydraulics of open channel flow: an introduction,* Elsevier Ltd, China, 585.

Chapra S. C. (1997), *Surface Water-Quality Modelling*, McGraw Hill, New York, 844.

Chen Z. and Sheng P. (2005), *Three-dimensional modelling of sediment and phosphorus dynamics in lake Okeechobee, Florida: spring 1989 simulation,* Journal of Environmental Engineering, 131 (3), 359-374.

Clausen B. and Biggs B. J. F. (1997), *Relationships between benthic biota and hydrological indices in New Zealand streams*, Freshwater Biology, 38, 327-342.

Cloern J. E., (2001), *Our evolving conceptual model of the coastal eutrophication problem,* Marine Ecology Progress Series, 210, 223-253.

Cox G. C. and Macola A. M. (1967), *Predicting salinity in an estuary*, American Society of Civil Engineering, USA, 433.

Crowder D. W. and Diplas P. (2006), *Applying spatial hydraulic principles to quantify stream habitat,* River Research and Applications, 22, 79-89.

Dooley H. D. and Steele J. H. (1969), *Wind driven currents near coast,* Ocean Dynamics, 22(5), 213-223.

Dronkers J. and Zimmerman J. T. F. (1982), *Some principles of mixing in tidal Lagoons*, Proceedings International Symposium on Coastal Lagoons, France, 107-117

El-Sabh M. I., Aung T. H. and Murty T. S. (1997), *Physical processes in reverse estuarine systems*, Oceanography and Marine Biology, 35, 1-69.

Elsayed M. and Albakri D. (1994), *Geomerphology and sedimentary/ biosedimentary structures of the intertidal environment along the coast of Kuwait, north-western Arabian Gulf*, Geologische Rundschau, 83, 1773-1788.

Elshorbagy W. (2005), *Overview of marine pollution in the Arabian Gulf with emphasis on pollutant transport modeling,* 1st international conference and exhibition on coastal zone management and engineering in the Middle East, Dubai.

Elshorbagy W., Azam M. H. and Taguchi K. (2006), *Hydrodynamic Characterisation and Modelling of the Arabian Gulf*, Journal of Waterway, 132(1), 47-56.

EPA (1999), *Understanding variation in partition coefficient, K_d, values*, United States Environmental Protection Agency, EPA 420-R-99-004A.

Facey R. (2008), *Pollution from sea based sources*, in Abuzinada A. H. et al. (Eds.), Protecting the Gulfs Marine Ecosystems from pollution, Birkhauser, Berlin, 163-189.

Fadllalah Y. H., Allen K. W. and Estudillo R. A. (1995), *Damage to shallow roof corals in the Gulf caused by periodic exposure to air during extreme low tides and low water temperatures (Tarut bay, eastern Saudi Arabia)*, in Ginsburg R. N. (Eds), Proceedings of the Colloquium on Global Aspects of Coral Reefs, Health, and History 1993, Miami, 371-377.

Falconer R. A. (1993), *An introduction to nearly horizontal flows*, in Abbott M. B. and Price W. A. (Eds.), Coastal Estuarial and Harbour Engineers, London: E and F.N. Spon Ltd, 27-36.

Falconer R. A. and Chen Y. (1996), *Modeling sediment transport and water quality processes on tidal floodplains*, in Anderson M. G. et al, Floodplain processes Wiley, Chichester, 361-398.

Falconer R. A. and Lin B. (1997), *Three-dimensional modelling of water quality in the Humber Estuary*, Water Research, 31(5), 1092-1102.

Falconer, R. A., Lin B., Harris E. and Kashefipour S. M (2001), *DIVAST Model: Reference Manual*, Cardiff University, Hydro-Environmental Research Centre, 32.

Falconer R. A., Lin B. and Kashefipour S. M. (2005), *Modelling Water Quality Processes in Estuaries*, in Bates et al., (Eds), Computational fluid dynamics: applications in environmental hydraulics, John Wiley & Sons Ltd, New York, 305-328.

Falconer, R. A. and Owens, P. H. (1987), *Numerical simulation of flooding and drying in a depth averaged tidal flow model*, Proceedings of the Institution of Civil Engineers, 83(2), 161-180.

Fischer H. B. (1973), *Longitudinal dispersion and turbulent mixing in open channel flow*, Annual Review of Fluid Mechanics, 5, 59-78.

Fischer H. B., List E. J., Koh R. C. Y., Imberger J., and Brooks N. H. (1979), *Mixing in inland and coastal waters*, Academic Press, New York, 483.

Froelich P. N. (1988), *Kinetic control of dissolved phosphate in natural rivers and estuaries: a primer on the phosphate buffer mechanism*, Limnology and Oceanography, 33, 649-668.

French R. (1986), *Open-Channel Hydraulics*, McGraw-Hill Book Company, New York, 638.

Frihy O. E., Hassan A. N., El Sayed W. R., Iskander M. M. and Sherif M. Y. (2006), *A review of methods for constructing coastal recreational facilities in Egypt (Red Sea)*, Ecological Engineering, 27 (1), 1-12.

Geyer W. R. and Signel R. P. (1992), *A reassessment of the role of tidal dispersion in estuaries and bays*, Estuaries, 15(2), 97-108.

del Giorgio P. A. and Bouvier T. C. (2002), *Linking the physiologic and phylogenetic successions in free-living bacterial communities along an estuarine salinity gradientm* Limnology and Oceanography, 47, 471-486.

Glibert P. M. (2007), *Eutrophication and harmful algal blooms: a complex global issue, examples from the Arabian sea including Kuwait bay, and an introduction to the global ecology and oceanography of harmful algal blooms (GEOHAB) programme,* Internationa Journal of Oceans and Oceanography, 2(1), 157-211.

Glibert P. M, Landsberg J. H., Evans J. J., Al-Sarawi M. A., Faraj M., Al-Jarallah M. A., Haywood A., Ibrahem S., Klesius P., Powell C. and Shoemaker C. (2002), *A fish kill of massive proportion in Kuwait Bay, Arabian Gulf, 2001: the roles of bacterial disease, harmful algae, and eutrophication*, Harmful Algae, 1, 215-231.

Goldstein S. (1938), *Modern Development in Fluid Dynamics*, Oxford University Press, Oxford, 680.

Gopalakrishnan T. C. and Muralidhar M. A. (1989), *Residual currents and flushing in Kuwait Bay-A numerical modelling study*, Kuwait Institute of Scientific Research, Project EES-144, KISR 3262.

Habib K. and Fakhral-Deen A. (2001), *Risk assessment and evaluation of materials commonly used in desalination plants subjected to pollution impact of the oil spill and oil fires in marine environment*, Desalination, 139, 249-253.

Hakimzadeh H. and Falconer R. A. (2007), *Layer integrated modeling of three-dimensional recirculating flows in model tidal basins*, Journal of Waterway, Port, Coastal, and Ocean Engineering, 133 (5), 324-333.

Hall P. (1987), *The numerical modelling of wind-induced lake circulation*, PhD Thesis, University of Birmingham.

Harahsheh H., Essa S., Shiobarac M., Nishidaid T. and Onumad T. (2004), *Operational satellite monitoring and detection for oil spill offshore of United Arab Emirates*, Proceedings XXth ISPRS Congress Geo-Imagery Bridging Continents, Istanbul, 658-663.

Harleman D. R. F. (1966), *Diffusion process in stratified flow*, in Ippen A. T. (Eds.), Estuary and Coastline Hydrodynamics, McGraw Hill Book Co. Inc, New York, 575-597

Harrison S. P., Kohfeld K. E., Roelandt C. and Clanquin T. (2001), *The role of dust in climate change today, at the last glacial maximum and in the future*, Earth-Science Reviews, 54, 43-80.

Hartmann M., Lang H., Seibold E. and Walger E. (1971), *Surface sedimentation in the Persian Gulf and the Gulf of Oman. I. Geological-hydrological conditions and preliminary sedimentological results*, Meteor-Froschungsergebn, C4, 181-194.

Hecky R. E. and Kilham P. (1988), *Nutrient limitation of phytoplankton in freshwater and marine environments: A review of recent evidence on the effects of enrichment,* Limnology and Oceanogrophy, 33(4 part 2), 796-822.

Heil C. A., Glibert P. M., Al-Sarawi M. A., Faraj M., Behbehani M. and Husian M. (2001), *First record of a fish-killing Gymnodinium sp. bloom in Kuwait bay, Arabian sea: chronology and potential causes*, Marine Ecology Progress Series, 214, 15-23.

Henderson F.M. (1966), *Open channel flow*, Macmillan Co. Ltd, USA, 522.

Herut B., Collier R. and Krom M. D. (2002), *The role of dust in supplying nitrogen and phosphorus to the southeast Mediterranean,* Limnology and Oceanography, 47 (3), 870-878.

Hetling L. J. and O'Connell R. L. (1966), *A study of tidal dispersion in the Potomac River*, Water Resources Research, 2, 825-841.

Hipsey M. R., Romero J. R., Antenucci J. P. and Hamilton D. (2006), *Computational Aquatic Ecosystem Dynamics Model: CAEDYM v2,* v2.3 Science Manual, Centre for Water Research, 102.

Hipsey M. R., Antenucci J. P. and Brookes J. D. (2008), *A generic, process-based model of microbial pollution in aquatic system*, Water Resources Research, 44, 1-26.

Hodges B. R., Imberger J., Saggio A. and Winters K. B. (2000), *Modeling basin-scale internal waves in a stratified lake*, Limnology and Oceanography, 45, 1603-1620.

Hoepner T. and Lattemann S. (2003), *Chemical impacts from seawater desalination plants - a case study of the northern Red Sea*, Desalination, 152, 133-140.

Hughes P. (1956), *A determination of the relation between wind and sea surface drift*, Quarterly Journal of the Royal Meteorological Society, 82, 494-502.

Hughes P. and Hunter J. R. (1979), *A proposal for a physical oceanography program and numerical modeling of the KAP region*, UNESCO, Division of Marine Science,, Paris, MARIN, 27.

Hunter J. R. (1983), *A review of the residual circulation and mixing processes in the KAP region, with reference to applicable modeling techniques*, Oceanographic modeling of Kuwait Action Plan (KAP), UNESCO reports in marine science, 28, 37-45.

IDA (2006), *IDA Worldwide desalting plant inventory,* 19, Media Analytics Ltd., Oxford, U K.

Imberger J., Mamouni E. A. D., Anderson J., Ng M. L., Nicol S. and Veale A. (2007), *The index of sustainable functionality: a new adaptive, multicriteria measurement of sustainability-application to Western Australia*, International Journal of Environment and Sustainable Development, 6, 323-355.

Imberger J. and Patterson J. C. (1981), *A dynamic reservoir simulation model-DYRESM 5*, in Fischer H. (Eds.), Transport models for inland and coastal waters, Academic Press., 310–361.

Inoue M. and Wiseman W. J. (2000), *Transport, stirring and mixing processes in a Louisiana Estuary: A model study*, Estuarine, Coastal and Shelf Science, 50, 449-466.

IPCC, (2007): Climate Change 2007: *The Physical science basis*, Contribution of working Group I to the Fourth Assessment Report of the Intergovernmental Panel on Climate Change, in Solomon S. et al., (Eds.), Cambridge University Press, Cambridge, 996.

Ismail W. A., Al-Yamani F. Y. and Al-Rifaie K. S. (2007), *Field surveys and a perturbation experiment in testing the role of eutrophication in initiating red tides in Kuwait Bay*, International Journal of Oceans and Oceanography, 2(1), 187-211.

Jacquet J. (1983), *Simulation of the thermal regime of rivers*, in Orlob G. T. (Eds.), Mathematical modelling of water quality: Streams, lakes and reservoirs, Wiley-Interscience.

Ji Z. (2008), *Hydrodynamics and water quality modeling rivers, Lakes, and estuaries*, John Wiley & Sons, Canada, 676.

Jin X. C., Wang S. R., Pang Y., Zhao H. Z., and Zhou X. N. (2005), *The adsorption of phosphate on different trophic lake sediments*, Colloid and Surfaces A: Physicochem Engineering Aspects, 254, 241-248.

Johns W. E., Yao F., Olson D. B., Josey S. A., Grist J. P. and Smeed D. A. (2003), *Observations of seasonal exchange through the Straits of Hormuz and the inferred freshwater budgets of the Persian Gulf*, Journal of Geophysical Research, 108 (C12), 3391.

Jones C., Sultan M., Yan E., Milewski A., Hussein M., Al-Dousari A., Al-Kaisy S. and Becker R. (2008a), *Hydrologic impact of engineering projects on the Tigris-Euphrates system and its marshlands*, Journal of Hydrology, 353, 59-75.

Jones D. A., Hayes M., Krupp F., Sabatini G., Watt I. and Weishar L. (2008b), *The impact of the Gulf War (1990-91) oil release upon the intertidal Gulf coast line of Saudi Arabia and subsequent recover,* in Abuzinada A. H. et al. (Eds.), Protecting the Gulfs Marine Ecosystems from pollution, Birkhauser, Berlin, 237-254.

Karim H. H. and Salman H. H. (1987), *Estimation of sediment rate and the fate of hydrocarbon residues of Shatt Al-Arab River sediments, northwest Arabian Gulf,* Marina Mesopotamica, 2, 103-115.

Khalaf F. I., Al-Kadi A. and Al-Saleh, S. (1985), *Mineralogical composition and potential sources of dust fallout deposits in Kuwait, Northern Arabian Gulf*, Sedimentary Geology, 42, 255-278.

Khordagui H. (2002), *Environmental impacts of power-desalination on the gulf marine ecosystem,* in Khan et al. (Eds), The Gulf Ecosystem: Health and Sustainability, Backhuys, 173-191.

King I. P. (1988), *A finite element model for three dimensional hydrodynamic systems*, report prepared by Resource Management Associate, Lafayette California, for U.S Army Crops of Engineers, Waterways Experiment Station, Vicksburg, Mississippi.

Klotz R. L. (1988), *Sediment control of soluble reactive phosphorus in Hoxie Gorge Creek*, Canadian Journal of Fisheries and Aquatic Sciences, 45, 2026-2034.

Krupp F. (1998), *Coral reefs in the Red Sea and Gulf of Aden threatened by bleaching and mortality,* Al-Sambouk, 8, 9-11.

Krone R. B. (1962), *Flume studies of the transport of sediment in estuarial processes*, Hydraulic Engineering Laboratory and Sanitary Engineering Research Laboratory, University of California, Berkeley.

Krupp F. and Anegay K. (1993), *Habitats and species composition in subtidal areas north of Abu Ali, Saudi Arabia,* Final report of the scientific workshop on results of the R/V Mt. Mitchell cruise in the ROPME sea area, Kuwait, 2, 174-184.

Krupp F. and Symens P. (1994), *Gulf Sanctuary,* Arabian Wildlife, 1(1), 18-20

Lattemann S. and Hopner T. (2008), *Impacts of seawater desalination plants on the marine environment of the Gulf,* in Abuzinada A. H. et al. (Eds), Protecting the Gulfs Marine Ecosystems from pollution, Birkhauser, Berlin, 192-205.

Laval B. E., Hodges B. R. and Imberger J. (2003), *Numerical Diffusion in 3D, Hydrostatic, Z-Level, Lake Models*, Journal of Hydraulic Engineering, 129(3), 215-224.

Lawrence G. A., Ashley K. I., Yonemitsu N. and Ellis J. R. (1995), *Natural dispersion in a small lake*, Limnology and Oceanography, 40(8), 1519-1526.

Lehr W. J. (1984), *A brief survey of oceanographic modelling and oil spill studies in the KAP region*, in El-Sabh M. I. (Eds), Oceanographic Modeling of the Kuwait Action Plan (KAP) Region,UNESCO reports in Marine Science, Paris, 28, 4-11.

Leonard B. P. (1991), *The ULTIMATE conservative difference scheme applied to unsteady one-dimensional advection*, Computer Methods in Applied Mechanics and Engineering, 88, 17-74.

Lewis R. E. (1997), *Dispersion in Estuaries and Coastal Waters*, John Wiley & Sons, Chichester, 312.

Liang D., Falconer R. A. and Lin B. (2006), *Comparison between TVD-MacCormack and ADI-type solvers of the shallow water equations*, Advances in Water Resources, 29 (12), 1833-1845.

Liang D., Lin B. and Falconer R. A. (2007), *Simulation of rapidly varying flow using an efficient TVD-MacCormack scheme*, International Journal for Numerical Methods in Fluids, 53, 811-826.

Lin B. and Falconer R. A. (1997), *Three-dimensional layer-integrated ,modelling of estuarine flows with flooding and drying*, Journal of Estuarine, Coastal and Shelf Science, 44, 737-751.

Lin B. and Falconer R. A. (1996), *Numerical modelling of three-dimensional suspended sediment for estuarine and coastal waters,*, Journal of Hydraulic Research, 34 (4), 435-455.

MacIsaac J. J. and Dugdale (1972), *Interaction of light and inorganic nitrogen in controlling nitrogen uptake in the sea,* Deep Sea Research, 19, 202-232.

McCutcheon S. C. (1989), *Water quality modelling,* Vol. I, *Transport and Surface Exchange in Rivers*, CRC Press, Boca Raton, 208.

Mehta A. J., Hayter E. J., Parker R. W., Krone R. B. and Teeter A. M. (1989), *Cohesive Sediment Transport. I: Process Description*, Journal of Hydraulic Engineering, 115 (8), 1076-1093.

Meinesz A., Lefevre J. R. and Astier J. M. (1991), *Impact of coastal development on the infralittoral zone along the southeastern Mediterranean shore of continental France*, Marine Pollution Bulletin, 23, 343-347.

Menesguen A. (1990), *Eutrophication along the French coasts*, in Barth H. and Fegan L. (Eds.), Eutrophication-related phenomena in the Adriatic sea and in the Mediterranean coastal zones, Water Pollution Report, 16, 63-82.

Meshal A. H. and Hassan, H. M. (1986), *Evaporation from the Coastal Waters of the Central Part of the Gulf*, Arab Gulf Journal of Scientific Research, 4(2), 649-655.

Middelburg J. J., Vlug T. and van der Nat F. J. W. A. (1993), *Organic matter mineralization in marine systems*, Global and Planetary Change, 8, 47-58.

Monsen N. E., Cloern J. E., Lucas L. V. and Monismith S. G. (2002), *A comment on the use of flushing time, residence time, and age as transport time scales*, Limnology and Oceanography., 47(5), 1545-1553.

Murray S., Conlon D., Siripong A., and Santoro J. (1975), *Circulation and salinity distribution in the Rio Guayas estuary, Ecuador*, in Cronin G. G. (Eds.), Estuarine Research. Academic Press, New York, 345-363.

Nasrallah H. A., Nieplova E. and Ramadan E. (2004), *Warm seaon extreme temperature events in Kuwait,* Journal of Arid Environments, 56, 357-371.

Newhouse S. and Pignataro T., (1993), *On the estimation of topological entropy,* Journal of Statistical Physics, 72, 1331–1351.

Newton A., Icely J. D., Falcao M., Nobre A., Nunes J. P., Ferreira J. G. and Vale C. (2003), *Evaluation of eutrophication in the Ria Formosa coastal lagoon, Portugal,* Continental Shelf Research, 23, 1945-1961.

Okely P., Imberger J. and Shimizu K. (2010), *Particle dispersal due to interplay of motions in the surface layer of a small reservoir,* Limnology and Oceanography., 55(2), 589-603.

Okubo A. (1971), *Oceanic diffusion diagrams,* Deep-Sea Research, 18, 779–802.

Okubo A. (1974), *Some speculations on oceanic diffusion diagrams,* Rapp. Proc. Verb. Cons. Int. Explor. Mer., 167, 77-85.

Paerl H., (1988), *Nuisance phytoplankton blooms in coastal, estuarine, and inland waters,* Limnology and Oceanography, 33, 823-847.

Partheniades E. (1965), *Erosion and deposition of cohesive soils,* Journal of the Hydraulic Devision, American Society of Civil Engineers, 91 (HY1), 105-139.

Patterson J. C., Hamblin P. F. and Imberger J. (1984), *Classification and dynamic simulation of the vertical density structure of lakes,* Limnology and Oceanography, 29 (4), 845-861.

Paulson R. (1969), *The longitudinal diffusion coefficient in the Delaware river estuary as determined from a steady state model,* Water Resources Research., 5, 59-67.

Paytan A. and McLaughlin K. (2007), *The Oceanic phosphorus cycle,* Chemical Reveiws, 107, 563-576.

Perrone T. J. (1981), *Winter shamal in the Persian Gulf,* Naval environmental prediction research facility, Monterey D A, I.R.-79-06.

Perry A. L., Low P. L., Ellis J. R. and Reynolds J. D. (2005), *Climate change and distribution shifts in marine fishes,* Science, 308(5730), 1912-1915.

Pritchard D. W. (1967), *What is an estuary?: physical viewpoint,* in Lauff G. S. (Eds.), Estuaries, American Association for the Advancement of Science, 85, 3-5.

Privett D. W. (1959), *Monthly charts of evaporation from the North Indian Ocean, including the Red Sea and the Persian Gulf,* Quarterly Journal of the Royal Meteorological Society, 85, 424-428.

Purcell J. E. (2005), *Climate effects on formation of jellyfish and ctenophore blooms: a review*, Journal of the Marine Biological Association of the UK, 85, 461-476.

Rakha K. A., Al-Banaa K. and Al-Hulail F. (2009), *Flushing of Kuwait Bay north of the Arabian Gulf*, Proceedings of international conference in Ocean Engineering, Madras.

Rakha K., Al-Banaa K., Al-Ragum A., Al-Hulail F. (2007a), *Hydrodynamic model for Kuwait Bay*, Coastal and Air Pollution Department of Engineering, Kuwait Institute for Scientific Research, Kuwait.

Rakha K., Al-Salem K. and Neelamani, S. (2007b), *Hydrodynamic Atlas for the Arabian Gulf*, Journal of Coastal Research, 50, 550-554.

Reynolds C. S., Dokulil M. and Padisak J. (2000), *Understanding the assembly of phytoplankton in relation to the trophic spectrum: where are we now?*, Hydrobiologia, 424, 147-152.

Reynolds R. M. (1992a), *Report of activities-Leg I of the Mt. Mitchell Expedition*, National Oceanographic and Atmospheric Administration, Seattle, USA, HMRAD 92-99.

Reynolds R. M. (1992b), *Report of activities-Leg VI, A/B of the Mt. Mitchell Expedition*, National Oceanographic and Atmospheric Administration, Seattle, USA,HMRAD 92-100.

Reynolds R. M. (1993), *Physical Oceanography of the Gulf, Strait of Hormuz, and the Gulf of Oman-Results from the Mt Mitchell Expedition*, Marine Pollution Bulletin, 27, 35-59.

Richardson L. F. (1926), *Atmospheric diffusion shown on a distance-neighbour graph*, Proceedings of the Royal Society, 110, 709-737.

Richlen M. L., Morton S. L., Jamali E. A., Rajan A., Anderson D. M. (2010), *The catastrophic 2008–2009 red tide in the Arabian Gulf region, with observations on the identification and phylogeny of the fish-killing dinoflagellate Cochlodinium polykrikoides*, Harmful Algae, 9(2), 163-172.

Robinson A. and Brink K. (2006), *The global coastal ocean, Interdisciplinary regional studies and syntheses. The sea: Ideas and observation on progress in the study of the seas*, Harvard University Press, USA, 1375-1385.

Robson B. J. and Hamilton D. P. (2004), *Three-dimensional modelling of a microcystis bloom event in the Swan River estuary, Western Australia*, Ecological Modelling, 174, 203-222.

Rodi, W. (2000), *Turbulence models and their application in hydraulics*, International Association for Hydraulics Research, Delft, Netherlands, 104.

Romero J. R., Dallimore C. J., Antenucci J. P., Hamilton D. P., Imberger J., Horn D. A. and Deen A. (2002), *Application of 1 D and 3D hydrodynamic models coupled to an ecological model to two water supply reservoirs*, in Rozzoli A. E. and Jakeman A. J. (Eds.), Internationa Environmental Modelling and Software Society, 2, 307-312.

Ruttenberg K. C. (1992), *Development of a sequential extraction method for different forms of phosphorus in marine sediments*, Limnology and Oceanography, 37, 1460-1482.

Saad H. R. and Al-Azmi D. (2002), *Radioactivity concentrations in sediments and their correlation from space: Some new perspectives*, Applied Radiation and Isotopes, 56, 991-997.

Sadrinasab M. and Kämpf J. (2004), *Three-dimensional flushing times of the Persian Gulf*, Geophysical Research Letters., 31, L24301.

Shams El Din A., Arain R. and Hammoud A. (2000), *On the chlorination of seawater,* Desalination, 129, 53-62.

Sharpley A. N., Kleinman P. J. A., McDowell R. W., Gitau M. and Bryant R. B. (2002), *Modeling phosphorus transport in agricultural watersheds: processes and possibilities,* Jouranl of Soil and Water Conservation, 57, 425-439.

Sheppard C. R. C. (2000), *Coral Reefs of the Western Indian Ocean : an Overview,* in McClanahan T. et al (Eds), Coral reefs of the Western Indian Ocean: Ecology and conservation, Oxford University Press, Oxford, 3-38.

Simonson R. W. (1995), *Airborne dust and its significance to soils,* Geoderma, 65, 1-43.

Smith R. A., Schwarz G. E. and Alexander R. B. (1997), *Regional interpretation of water-quality monitoring data,* Water Resources Research, 33 (12), 2781-2798.

Sotiropoulos F. (2005), *Introduction to statistical turbulence modelling for hydraulic engineering flows*, in Bates et al., (Eds), Computational Fluid Dynamics: Applications in Environmental Hydraulics, John Wiley & Sons Ltd, U.K., 531

Spigel R. H., Imberger J. and Rayner K. N. (1986), *Modeling the diurnal mixed layer*, Limnology and Oceanography., 31, 533-556.

Stocker R. and Imberger J. (2003), *Horizontal transport and dispersion in the surface layer of a medium-sized lake*, Limnolology and Oceanography, 48(3), 971-982.

Stommel H. (1953), *Computation of pollution in a vertically mixed estuary*, Sewage and Industrial Wastes, 25, 1065-1071.

Stutter M. I. and Lumsdon D. G. (2008), *Interactions of land use and dynamic river conditions on sorption equilibria between benthic sediments and river soluble reactive phosphorus concentrations,* Water Research, 42, 4249-4260.

Subba Rao D. V., Al-Yamani F., (1998), *Phytoplankton ecology in the water between Shatt Al-Arab and the Straits of Hormuz, Arabian Gulf: a review*, Plankton Biology and Ecology, 45, 101-116.

Subba Rao D. V. and Al-Yamani F., (1999), *Analysis of the relationship between phytoplankton biomass and the euphotic layer off Kuwait, Arabian Gulf*, Indian Journal of Marine Sciences, 28, 416-423.

Sultan S. A. R. and Ahmad F. (1994), *Heat budget of the coastal water of Kuwait: A preliminary study*, Estuarine, Coastal and Shelf Science, 38, 319-325.

Sultan S. A. R., Ahmad F., El-Ghribi N. M. and Al-Subhi A. M. (1995), *An analysis of the Arabian Gulf monthly mean sea level*, Continental Shelf Research, 15(11/12), 1471-1482.

Talling J. F. (1980), *Water Characteristics*, in Rzoska J. (Eds.), Euphrates and Tigris: Mesopotamian Ecology and Density, Monographiae Bilogicae, 38: 63-86.

Tannehill J. C., Anderson D. A. and Pletcher R. H. (1997), *Computational Fluid Mechanics and Heat Transfer*, Taylor & Francis, USA, 792.

Taylor G. I. (1954), *The dispersion of matter in turbulent flow through a pipe*, Proceedings of the Royal Society of London, 223(1155), 446-468.

Taylor A. W. and Kuinishi H. M. (1971), *Phosphate equilibria on stream sediment and soil in a watershed draining an agricultural region*, Journal of Agricultural and Food Chemistry, 19, 827-831.

Thatcher M. L. and Harleman D. R. F. (1972), *A Mathematical model for the prediction of unsteady salinity intrusion in estuaries*, Ralph M. Parsons Laboratory, MIT, 144.

UNEP (1999), *Overview on land-based sources and activities affecting the marine environment in the ROPME sea area*, 168, UNEP/GPA Coordination office, P.O. Box 16227 2500 BE The Hague, The Netherlands and Regional Organization for the Protection of the Marine Environment (ROPME), Box 26388, Safat 13124, Kuwait, 127.

Van Rijn L. C. (1984a), *Sediment Transport, Part I: Bed Load Transport*, Journal of Hydraulic Engineering, 110 (10), 1431-1457.

Van Rijn L. C. (1984b), *Sediment Transport, Part II: Suspended Load Transport*, Journal of Hydraulic Engineering, 110 (11), 1613-1641.

Van Rijn, L. C. (1993), *Principles of Sediment Transport in Rivers, Estuaries and Coastal Seas*, Aqua Publications, Netherlands.

Vieira J. K. (1993), *Dispersive processes in two-dimensional models*, in Abbott et al. (Eds), Coastal, Estuarial and Harbour Engineers, E.&F.N. Spon Ltd., London, 179-190.

Vreugdenhil C. B. (1994), *Numerical methods for shallow-water flow*, Kluwer Academic Publications, 261.

Wondzell S. M. (2006), *Effect of morphology and discharge on hyporheic exchange flows in two small streams in the Cascade Mountains of Oregon,* Hydrological Process, 20, 267-287.

Wilkinson C., Linden O., Hodgson H., Cesar J., Rubens J. and Strong A. (1999), *Ecological and socio-economic impacts of 1998 coral mortality in the Indian Ocean: an ENSO (El Nino/Southern Oscillation) impact and a warning of future change?,* Ambio, 28, 188-196.

Winterwerp J. C. and Van Kesteren W. G. M. (2004), *Introduction to the Physics of Cohesive Sediment in the Marine Environment*, Elsevier B.V., Amesterdam, 466.

Wu J., (1969), *Wind stress and surface roughness at air-sea interface*, Journal of Geophysical Research, 74, 444-455.

Wu Y. and Falconer R. A. (2000), *A mass conservative 3-D numerical model for predicting solute fluxes in estuarine waters*, Advances in Water Resources, 23, 531-543.

Appendix

JOURNAL OF GEOPHYSICAL RESEARCH, VOL. 116, C03029, doi:10.1029/2010JC006769, 2011

Mixing and flushing in the Persian Gulf (Arabian Gulf)

Yousef Alosairi,[1] Jörg Imberger,[2] and Roger A. Falconer[1]

Received 27 October 2010; revised 25 December 2010; accepted 18 January 2011; published 31 March 2011.

[1] The assimilative capacities of estuaries and coastal seas for effluent discharges are predominantly determined by the rates at which pollutant-bearing effluents are first dispersed and then flushed from the coastal region into the open ocean. The dispersion coefficients and flushing, as measured by the water residence time in the Persian Gulf (Arabian Gulf), were investigated using the three-dimensional numerical model Estuary, Lake and Coastal Ocean Model (ELCOM). The model was first validated using the R/V *Mt. Mitchell* expedition profile data, collected from 27 January to 26 February 1992 and from 13 May to 12 June 1992. The validated model was then used to compute the geographic variability of the horizontal dispersion coefficients K_x throughout the gulf. Model results revealed that dispersion was principally driven by the shear associated with the tides, but along the Arabian coast, wind was an additional significant energy source for dispersion. The water residence time was found to be more than 3 years along the Arabian coast, but shorter along the Iranian coast.

Citation: Alosairi, Y., J. Imberger, and R. A. Falconer (2011), Mixing and flushing in the Persian Gulf (Arabian Gulf), *J. Geophys. Res.*, *116*, C03029, doi:10.1029/2010JC006769.

1. Introduction

[2] The Persian Gulf (Arabian Gulf, hereinafter called the gulf), shown in Figure 1, is a relatively shallow coastal basinthat extends between 22° and 30° north and between 48° and 56° east and is surrounded by eight countries, namely: Kuwait, Saudi Arabia, Bahrain, Qatar, United Arab Emirates, Oman, Iran and Iraq. The gulf has a maximum width of 338 km, a length of about 1000 km, a mean depth of 36 m and a volume of around 900 km^3. It is separated from the Gulf of Oman by the Strait of Hormuz which, at its narrowest point is only 56 km wide. From the strait seaward toward the Indian Ocean the depth gradually increases from 100 m to 2000 m. River inflows occur mostly in the northern end of the gulf, primarily on the Iranian side, with the largest being the Shatt Al Arab-a river formed by convergence of the Tigris, Euphrates, and Karun rivers (Figure 1). This river has an average annual flow of around 1456 m^3/s. Other key rivers are the Hendijan (203 m^3/s), the Hilleh (444 m^3/s), and the Mand (1387 m^3/s) (see Figure 1) [*Reynolds*, 1993].

[3] The gulf is generally bowl-shaped, with very shallow depths along the Arabian coastline, with particularly shallow waters occurring around the western coastline adjacent to Kuwait, Qatar, and United Arab Emirates, ranging from 10 to 15 m. Rapid coastal development in these gulf countries has caused considerable ecological stress in the shallow coastal regions, with increasing levels of effluent discharges from oil production, exploration and transportation, as well as from municipal and petrochemical activities, and red tides having been noted along various parts of the Arabian coast [*Richlen et al.*, 2010].

[4] Traditionally, coastal communities have relied on dispersion of effluents once they entered coastal waters so that, once diluted, biological breakdown has rendered them harmless. Here we define the "assimilative capacity" as that loading, which properly dispersed throughout the receiving domain, can be rendered harmless without jeopardizing the health of the ecosystem. Clearly, three distinct sets of processes combine to determine whether a domain has the assimilative capacity to accept an additional effluent loading. First, the near and intermediate rates of dispersal must be sufficiently fast to dilute the effluent to a level sufficiently low, that when added to the background concentration, it does not kill components of the ecosystem impacting on the functioning of the ecosystem [*Imberger et al.*, 2007]. Second, the transport or flushing must remove the by-products of the effluent breakdown processes sufficiently rapidly such that there is no long-term build up in the domain as a whole. In simple terms the flushing must prevent the domain from filling up with harmful products, implying that the criterion of whether a discharge is acceptable or not may depend on an event in the future. Third, the ecosystem must have the biochemical capacity necessary to ensure the breakdown of those pollutants that may be harmful to the rest of the original food chain. In the present paper we concern ourselves with only the first two, the physics of dispersion and flushing in the gulf. In particular, our objective is to determine the geographic dispersion and flushing characteristics of the gulf, in terms of residence time, to provide

[1]Cardiff School of Engineering, Cardiff University, Cardiff, UK.
[2]Centre for Water Research, University of Western Australia, Crawley, Western Australia, Australia.

0148-0227/11/2010JC006769

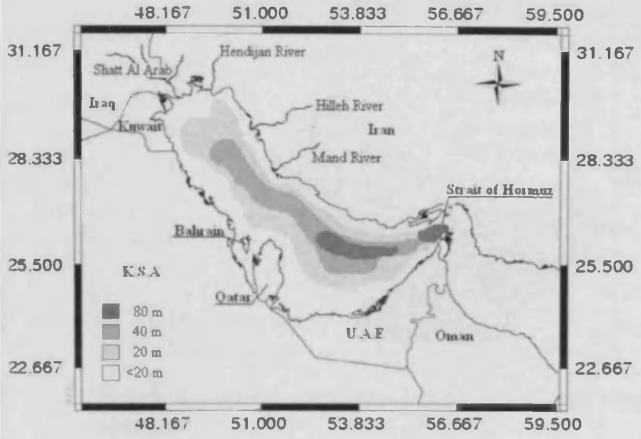

Figure 1. Persian Gulf (Arabian Gulf) physical characteristics. Source: National Geophysical Data Centre (http://www.ngdc.noaa.gov).

a guide for new engineering developments and their environmental management.

2. Horizontal Dispersion Mechanisms

2.1. Mixing Regimes

[5] Dispersion is achieved by the following three mechanisms [*Fischer et al.*, 1979]:

[6] 1. Turbulent near field dispersion, where the dispersion is energized by the turbulent kinetic energy from the discharge itself.

[7] 2. The region following the near field, called the intermediate field, where the mixing switches from being discharge energized to mixing that is energized by the turbulence of the ambient fluid flow. When the effluent density differs from that of the receiving water, the intermediate region can be quite significant in extent because the added buoyancy must be overcome by energy from the receiving water flow.

[8] 3. The far field, where the pollutant is dispersed by mechanisms inherent in the ambient flow conditions.

2.2. Far Field Mixing

2.2.1. Turbulent Dispersion

[9] After initial dispersion in the near field, effluents disperse by turbulent mixing until the effluent cloud has reached a size comparable to the scale of the velocity field. Once it is as large as the scale of the shear, the mean background velocity field distorts the effluent cloud and shear and transverse mixing combine to yield an enhanced dispersion (see section 2.2.2). For effluent clouds smaller than the scale of the background shear, turbulence disperses the effluent cloud and *Richardson* [1926] showed that the dispersion may be modeled by the "4/3 law," which accounts for the rate of increase of dispersion as the effluent cloud intersects ever increasing scales of turbulence as the cloud grows.

2.2.2. Shear Dispersion

[10] Longitudinal shear dispersion occurs when the distortion of a concentration field by a vertical or horizontal shear flow is balanced by vertical or transverse turbulent mixing [*Fischer et al.*, 1979]. Once balance is achieved the rate of dispersion may be modeled [see *Fischer et al.*, 1979] by a simple diffusion equation with a horizontal dispersion coefficient

$$K_x = \phi \frac{U^2 l^2}{K_z}.$$

Here ϕ is a constant dependent on the velocity and transverse diffusivity profile, l is the length scale of the velocity straining the concentration field, U is the velocity scale and K_z is the vertical diffusivity. As demonstrated by *Fischer et al.* [1979] for a simple plane flow with a vertical turbulent velocity profile, $l = h$, where h is the depth, U is the discharge velocity, and $K_z = 0.07hU^*$, where U^* is the bottom shear velocity. By contrast, in a wide river with a transverse velocity profile, l becomes the width of the channel and U is the discharge velocity. The coefficient ϕ depends on the vertical structure of the velocity and diffusivity. For constant diffusivity, *Fischer et al.* [1979] showed that $\phi = 0.008$ for a linear velocity profile and *Bowden* [1965] showed that $\phi = 0.001$ for a logarithmic profile resulting from bottom friction, $\phi = 0.019$ for the density current profile, and $\phi = 0.005$–0.008 for wind drift profiles.

[11] Clearly, dispersion due to the balance of transverse mixing and longitudinal straining will always be much larger than that due to vertical mixing in shallow estuaries. However, the validity of this statement depends on the time available for mixing. It is well known [see *Fischer et al.*, 1979] that a balance between distortion due to velocity shear and that due to transverse mixing can be achieved only after there has been sufficient time for transverse mixing to take place, a time of $O\left(\frac{l^2}{K}\right)$ where K is the horizontal (or vertical) diffusion coefficient. Shear dispersion via vertical shear with, typically a depth of 10 m and a vertical diffusion coefficient of around 10^{-4} m^2/s leads to a set up time O(12) days and a horizontal dispersion coefficient of around 6 m^2/s, assuming a value of $\phi = 0.01$ and $U = 0.025$ m/s. If the water velocity is around 0.5 m/s, then shear dispersion would become relevant only after 500 km, which is already half of the studied domain. By contrast, if we assume a coastal current with a transverse scale of 1 km and a transverse diffusion coefficient of 1 m^2/s, then the horizontal dispersion coefficient for transverse mixing and longitudinal strain balance would be around 2500 m^2/s and the time required to reach such a balance would again be O(12) days. So we see that the larger the length scale, the larger the horizontal dispersion. However, again the distance required for this estimate to become valid would be comparable to, or larger than, the dimensions of the gulf itself [*Lewis*, 1997; *Dooley and Steele*, 1969].

[12] Dispersion of a coastal effluent discharge occurs in several stages. First, in the near field the mean kinetic energy of the discharge generates turbulence that mixes or stirs the discharge into the receiving water. Second, in the absence of a buoyancy flux the diluted effluent is mixed with the receiving water turbulence until the cloud reaches a scale comparable to the scale of the ambient velocity field. Once this happens the mean velocity shear distorts the cloud, rather than simply transporting it, and this distortion

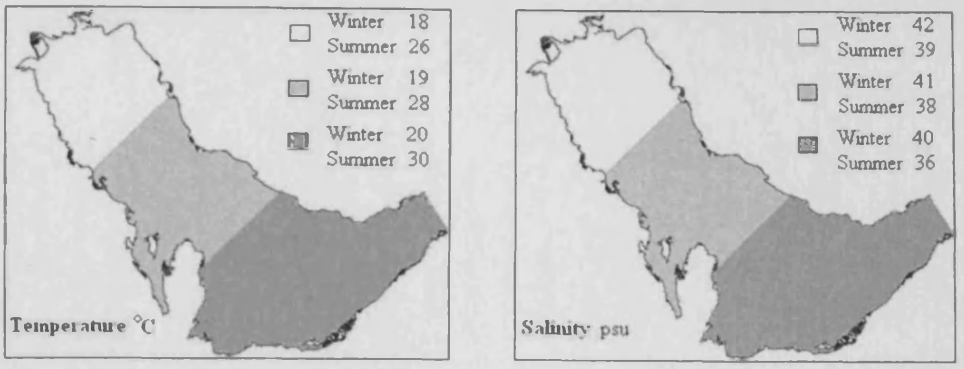

Figure 2. Initial condition configurations of temperature and salinity in ELCOM during winter and summer.

may interact with the ambient turbulent mixing to produce shear dispersion and/or stagnation point dispersion as with *Okely et al.* [2010], or it may interact with particular kinematic flow forms to produce kinematic chaos or ghost rod dispersion [*Aref*, 1984; *Stocker and Imberger*, 2003; *Boyland et al.*, 2000; *Newhouse and Pignataro*, 1993]. Although the last three forms of dispersion were not specifically investigated in the present study, as this would require an extensive field survey to identify individual processes, it is likely that each contributes to the dispersion evaluated numerically with the 3-D model.

[13] Here we first validate a 3-D model of the flow dispersion in the gulf by showing that the model reproduces the dispersion of the salinity field originating from the Strait of Hormuz and river inflows. The salinity differences were low enough not to influence the buoyancy, with salinity acting simply as a tracer in the upper reaches of the gulf. Once validated, the 3-D model was used to ascertain the degree of dispersion of tracers as a function of geographic location, the processes sustaining the simulated dispersion and the net flushing or residence time resulting from this dispersion.

3. ELCOM

3.1. Brief Description of Model

[14] The Estuary Lake Coastal Ocean Model (ELCOM) applied to the gulf solves the 3-D, hydrostatic, Boussinesq, Reynolds-averaged Navier-Stokes, and scalar transport equations, to model velocity, temperature and salinity distributions in space and time [*Hodges et al.*, 2000]. The model utilizes a fixed, Z coordinate finite difference mesh with Euler-Lagrangian approach for momentum advection, Ultimate-Quickest scheme for advection of scalars and a kinematic boundary condition for the free surface evolution [*Casulli and Cheng*, 1992; *Leonard*, 1991; *Casulli and Cattani*, 1994]. Scalars and momentum are mixed vertically according to the excess of turbulent kinetic energy available from wind stirring and shear production throughout the water column over the potential energy inherent in the ambient stratification [*Spigel et al.*, 1986; *Laval et al.*, 2003]. A new component to allow for tidal generation as a body force was incorporated in the model, necessary because of the relatively long length of the gulf, associated with a lunar semidiurnal tidal response and its effect in dispersing tracers. Following *Cartwright and Tayler* [1971], tidal forces were calculated from the gravitational potential and included in the momentum-transport equation in ELCOM.

3.2. Model Setup

[15] The modeling approach adopted in this study involved a uniform grid of 5000 m in both X and Y directions. Twenty layers in the Z direction at increments of 4 m for the first top 11 layers and 4.5 m for the remaining layers were adopted leading to a total of 104,056 wet cells discretizing the domain, and a Neumann boundary condition was applied at the open boundary. A computational time step of 300 s was utilized in the model. The bathymetric information was obtained from a map digitiser at the Hydro-Environmental Research Centre of Cardiff University that interpolated the depth at each grid point from a map obtained from the United Kingdom Hydrographic Office. The sea surface elevation due to semidiurnal tide is prescribed at the open boundary at the Strait of Hormuz using the KGULF model developed by Al-Salem (Kuwait Institute of Scientific Research, 2009) for the 1992 period (available on Coastal Information System www.hceatkuwait.net). The salinity and temperature data acquired by the R/V *Mt. Mitchell* cruise [*Reynolds*, 1993] were used as initial conditions for the model. Also, temperature-salinity data gathered in a recent study in the southern part of the gulf [*Elshorbagy et al.*, 2006] were used to define three main subdomains for the model initial conditions, as shown in Figure 2. Discharges from the rivers were assumed to remain constant throughout the simulation, based on the values given by *Reynolds* [1993], and as explained in the introduction. Horizontal diffusivity, κ, is an input parameter in Estuary, Lake and Coastal Ocean Model (ELCOM) representing turbulent sub grid diffusion in the model transport equations (more details provided by *Hodges et al.* [2000]) and was set to 1 m^2/s, but the effect of 5 and 10 m^2/s on the horizontal dispersion of numerical tracers was also investigated, as described in section 5 and discussed in section 6. A bottom drag coefficient of 0.005 was assigned to the whole domain to take account of bed friction. A light extinction coefficient of 0.25 was used for light attenuation.

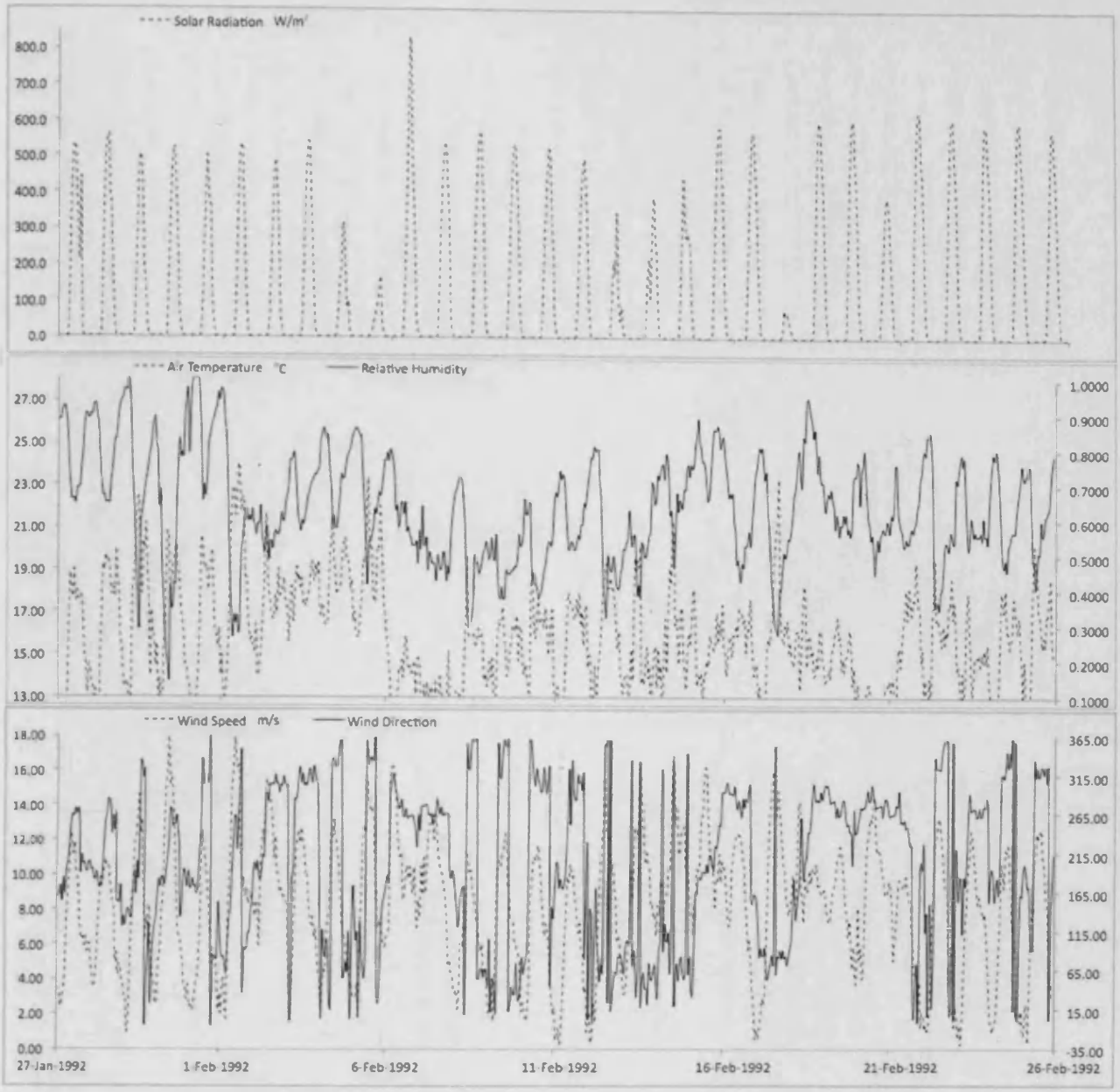

Figure 3. Winter meteorological conditions.

Meteorological forcing, shown in Figures 3 and 4, was applied at 8 m above sea level.

4. Model Validation Using 1992 Field Data

4.1. Meteorological Data

[16] Meteorological effects over the estuary during 1992 were included in the model and were obtained from the Dubai Meteorological Services (DMS), located at the far south of the gulf in Dubai and the Kuwait Institute for Scientific Research (KISR), located at the far north of the gulf, near Kuwait Bay. The differences in meteorological parameters outlined in Figures 3 and 4 between the stations were insignificant from 27 January to 26 February 1992 and from 13 May to 7 June 1992, in particular for wind speeds as shown in Figures 5 and 6. Not surprisingly, other parameters such as air temperature are seen to vary seasonally at both stations, with values ranging from 15 to 40°C in winter and summer, respectively. Humidity variations were similar to air temperature variations, but in the opposite sense (see Figures 3 and 4) at both stations. Records of solar radiation at both stations showed the same maximum mean values of 550 w/m^2 during January and February 1992 and 900 w/m^2 during May and June 1992, probably as a result of the similar geographic locations of the two stations. KISR data for 1992 (Figures 3 and 4) were assumed to be adequate for

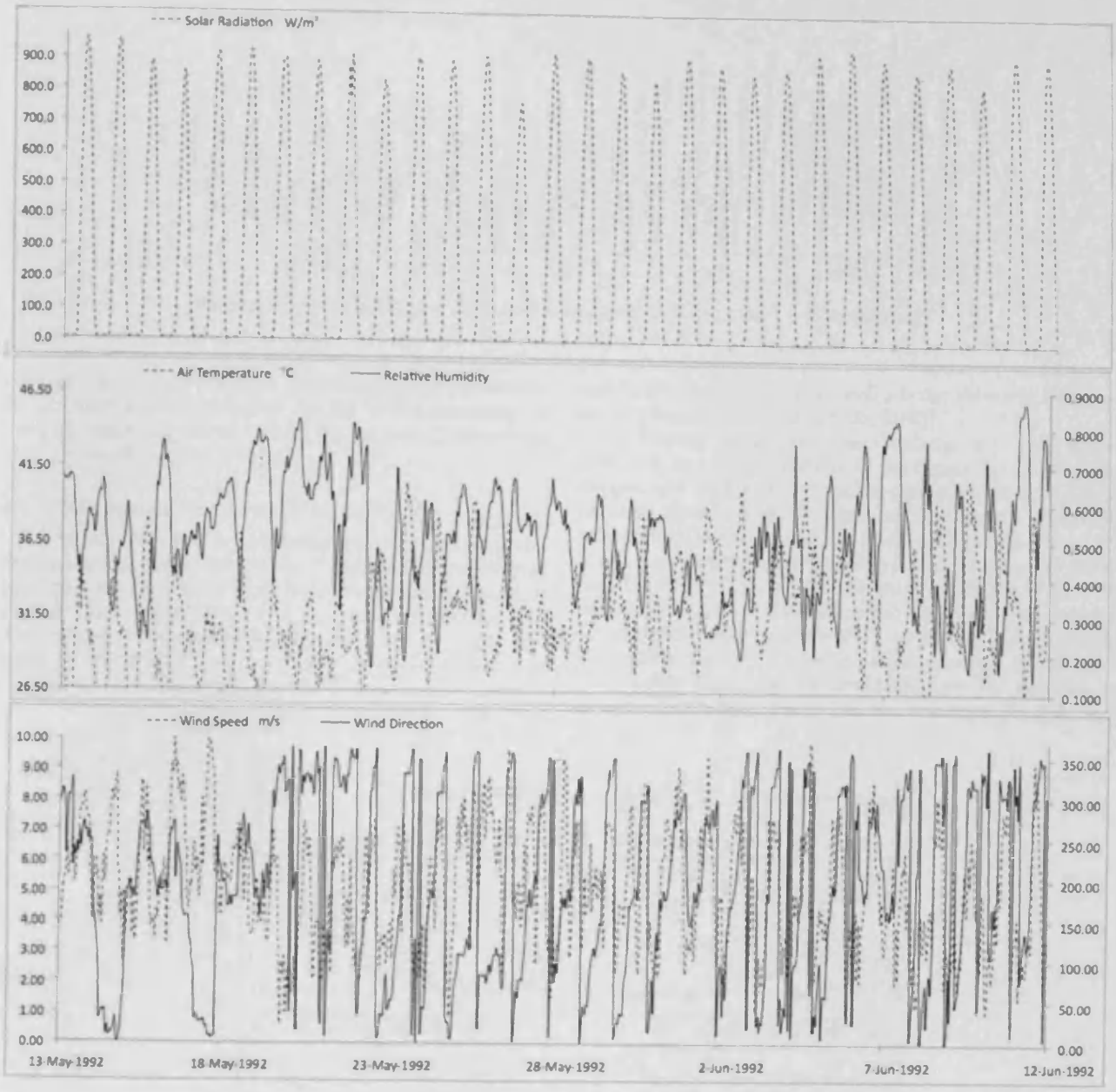

Figure 4. Summer meteorological conditions.

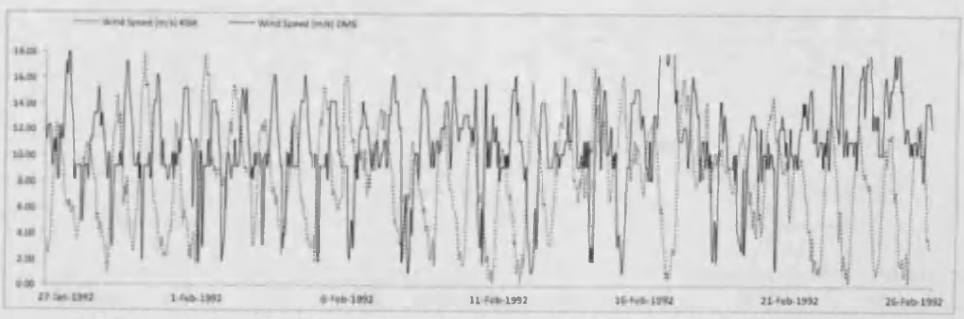

Figure 5. Comparison of wind speed between at KISR and DMS in winter.

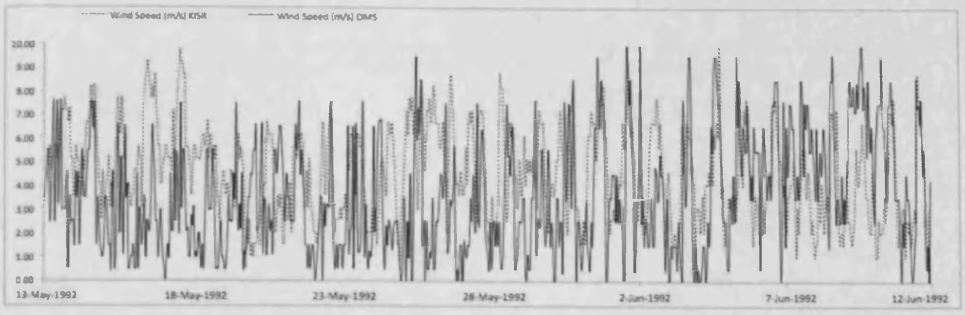

Figure 6. Comparison of wind speed between at KISR and DMS in summer.

our study, as minor differences in meteorological parameters do not have a great influence on the water dynamics of the gulf, which are driven chiefly by the tides [*Elshorbagy et al.*, 2006; *Reynolds*, 1993].

4.2. Salinity and Temperature in the Gulf

[17] In late 1991 a joint monitoring program was set up by the Regional Organization for the Protection of the Marine Environment (ROPME), the Intergovernmental Oceanographic Commission (IOC) and the National Oceanic and Atmospheric Administration (NOAA) with a vessel supplied by NOAA. A broad, multidisciplinary survey was carried out over six periods for 100 days between February and June 1992, the relevant results being shown in Figures 7 and 8 [*Reynolds*, 1992a, 1992b, 1993].

[18] During winter the water column was well mixed vertically to a depth of about 70 m (Figure 7a) and both the temperature and salinity varied gradually along the gulf between Kuwait and the Strait of Hormuz, in which the temperature increased and the salinity decreased toward the strait. Together these variations resulted in a density difference of about 2 kg/m^3 over a distance of 500 km (Figure 7a, bottom). In summer, the surface mixing penetrated to a depth of only about 30 m and the 25°C isotherm (Figure 7b, top) was almost horizontal over the whole domain. More saline and cooler water was observed (Figure 7b, middle), its location between 100 and 700 km southeast Kuwait, sug-

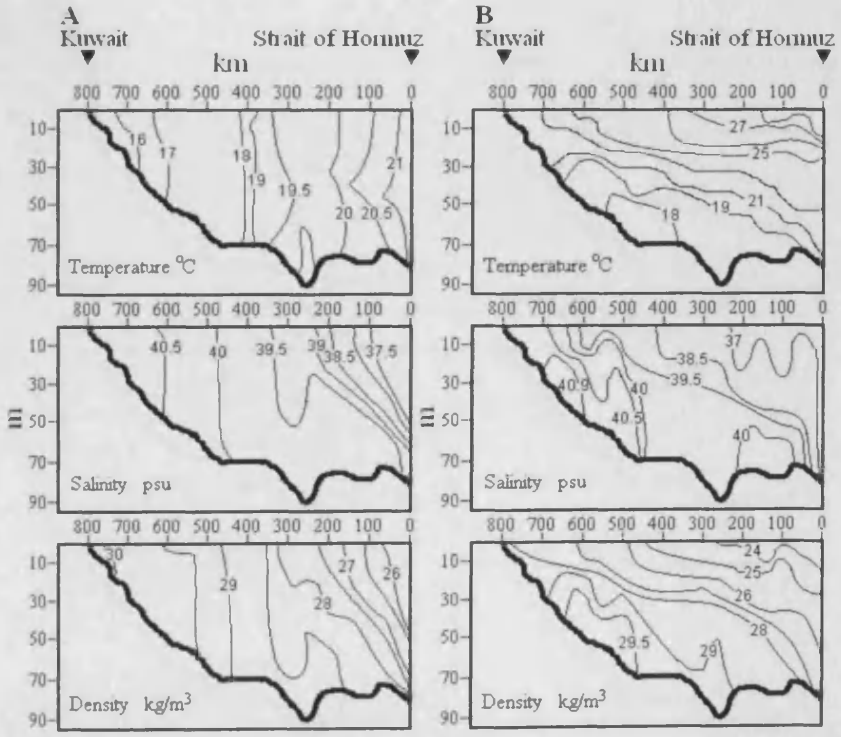

Figure 7. (a) Vertical variation of temperature, salinity, and density along the gulf (from the Strait of Hormuz to Kuwait) during winter; starting 26 February 1992 [*Reynolds*, 1993]. (b) Vertical variation of temperature, salinity, and density along the gulf (from the Strait of Hormuz to Kuwait) during summer; starting 12 June 1992 [*Reynolds*, 1993].

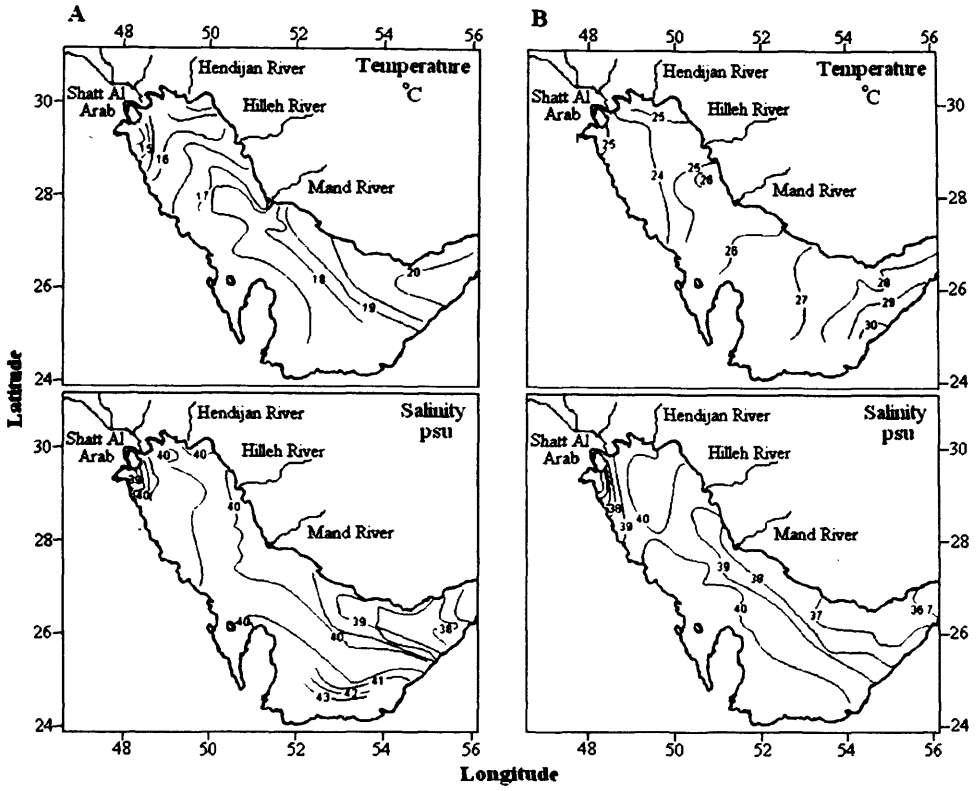

Figure 8. Surface field data variation of temperature and salinity of the gulf during (a) winter, starting 26 February 1992 [*Reynolds*, 1993], and (b) summer, starting 12 June 1992 [*Reynolds*, 1993].

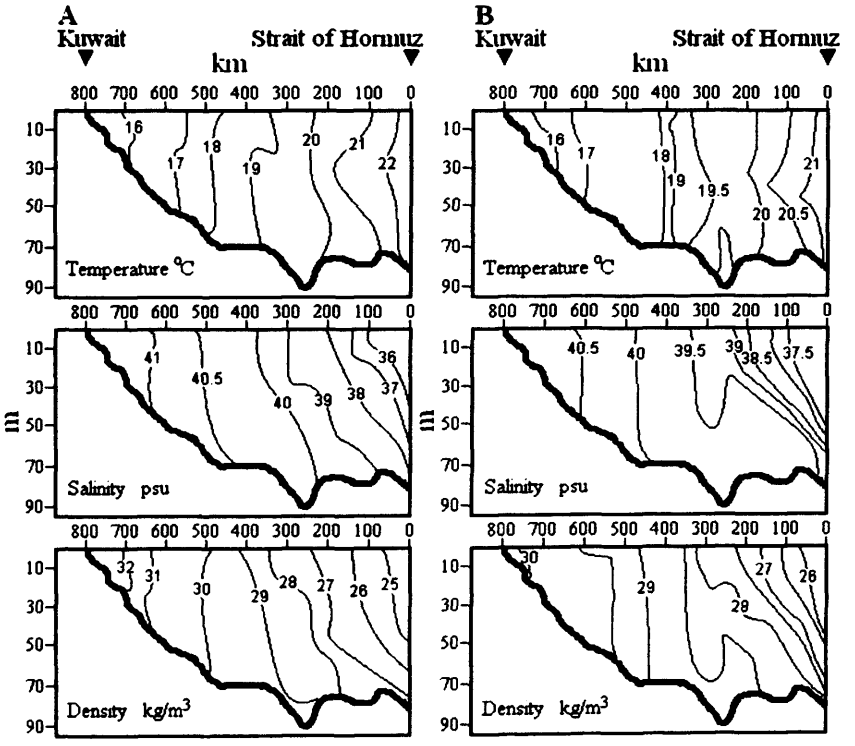

Figure 9. (a) Simulated vertical variation of temperature, salinity, and density along the gulf (from the Strait of Hormuz to Kuwait) during winter (1992). (b) Field data variation of temperature, salinity, and density along the gulf (from the Strait of Hormuz to Kuwait) during winter (1992).

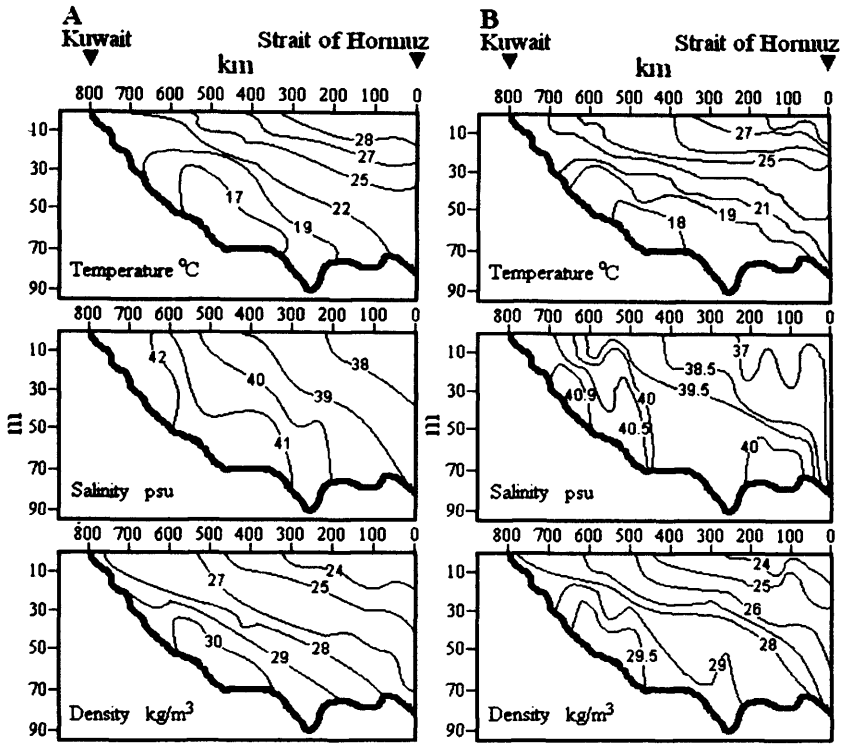

Figure 10. (a) Simulated vertical variation of temperature, salinity, and density along the gulf (from the Strait of Hormuz to Kuwait) during summer (1992). (b) Field data variation of temperature, salinity, and density along the gulf (from the Strait of Hormuz to Kuwait) during summer (1992).

gesting an origin not in the Strait of Hormuz, as the salinity maximum lies over 100 km away from the strait. Furthermore, as seen from Figure 7b (bottom), the isopycnols showed a distinct slope downward toward the strait, the origin of this water column therefore most likely being the gulf perimeter, where evaporation over shallow water would increase salinity. The Strait of Hormuz acts as a hydraulic control for the exchange between the Persian Gulf (Arabian Gulf) and the Gulf of Oman, the upper layer of fresher water transferring from the Gulf of Oman to replace water lost by evaporation, and the lower, higher saline water exiting to complete the reverse estuarine circulation [*Reynolds*, 1993]. More details of the temperature, salinity and density cross sections across the estuary between Kuwait and Iran, Qatar and Iran, and across the Strait of Hormuz are given by *Reynolds* [1993]. The surface inflow from the Gulf of Oman into the Persian Gulf (Arabian Gulf) occurs year-round, but extends deeper along the northern boundary into the gulf in the summer, as seen in Figures 7 and 8.

[19] River inflows do not contribute significantly to the water structure in the gulf, but local effects are apparent during both seasons, particularly during winter at Shatt Al Arab, north of the gulf (Figure 8). In addition, records show that precipitation during 1992 was very low in the gulf, so the relatively small fresh water inflow and the short period considered in this study (i.e., around 30 days each season) suggest that this is not likely to have had a significant impact on the dispersion mechanisms considered in this study.

4.3. Model Validation and Estimation of the Shear Scale

[20] The above information provided an excellent data set for the validation of the model hydrodynamics and associated dispersion. To optimize the test we carried out a 30 day simulation for both winter and summer configurations, with initial values as stated in Figure 2 (i.e., 13 May to 12 June 1992 and 27 January to 26 February 1992). The simulations were required to model first the hydraulic control across the Strait of Hormuz and fresh water input from the rivers, and then the dispersal of the salinity across the gulf, as observed in Figures 7 and 8. Evaluation of both temperature (mainly at the water surface) and salinity (mainly through the strait and rivers) provided the validation.

[21] The purpose of the validation simulations was to see whether ELCOM could reproduce the three-dimensional summer and winter temperature and salinity structures when forced with the data shown in Figures 3 and 4 and initialized with uniform water columns having values given as shown in Figure 2. The results from these simulations are shown here for the winter (Figures 9 and 11) and summer (Figures 10 and 12) periods; the agreement between the simulation results and the field data are generally excellent (Figures 9–12).

[22] During winter, relatively fresh water entered the gulf through the Strait of Hormuz, making its way to the comparatively deeper Iranian coast. In contrast, higher water densities were noticed all around the basin, particularly around the area surrounding Qatar and the UAE (Figure 9a, bottom). These results support the predominant control of

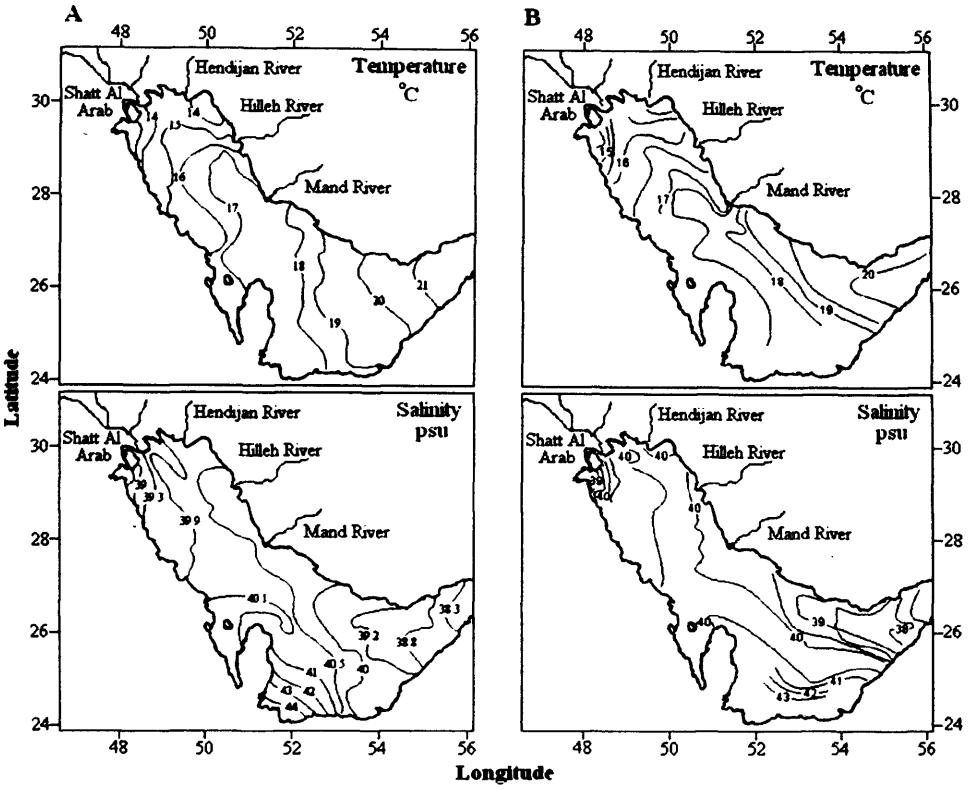

Figure 11. (a) Simulated surface variation of temperature and salinity of the gulf during winter. (b) Field data of temperature and salinity of the gulf during winter.

density by the salinity distribution (Figure 11a). This pattern is consistent with the broad circulation in the gulf where the Coriolis force deflects the surface inflow toward Iran and the subsurface outflow toward the Arabian coastline [*Sultan et al.*, 1995]. The salinity increased from 36 psu near the strait to 41 psu near Kuwait (Figures 9a, middle and 11), while the temperature fell from 22 to approximately 14°C, as shown in Figures 9a (top) and 11, at the same location. In the shallower waters of the gulf higher salinity levels are obvious, reaching 44 psu near the UAE coastal waters (Figure 11), resulting in an increase in the surface density and consequent vertical sinking (Figure 9a, bottom). This generally agreed with the findings of *Reynolds* [1993]. The simulations revealed that the gulf water is mostly mixed vertically along its main axis during 1992 winter conditions.

[23] Summer simulations exposed a more stratified structure in the estuary but with horizontal trends of both temperature and salinity similar to those of winter (Figures 10a, top and 10a, middle). A significant rise in water temperature of the estuary was evident parallel to the coastal areas of the gulf, as indicated in Figures 10a (top) and 12, reaching 31°C near the UAE. This sharp rise in temperature was due to the continuous heat input through the air-sea interface as indicated in Figure 4, leading to a rather lower surface water density than winter, ranging between 24 and 30 kg/m^3 (Figure 10a, bottom). The contour plot in Figure 12 and the vertical plot in Figure 10 A imply that relatively cold, saline and dense gulf water is found beneath the warmer, less saline and lighter surface inflow from the Gulf of Oman.

[24] As for the collected data, fresh water inflow from rivers did not significantly affect the flow characteristics of the basin as a whole for both seasons, but local effects were apparent, particularly at the far north of the gulf near Kuwait, where the Shatt Al Arab meets the hypersaline water (Figures 11 and 12). Also, during winter, at 650 km off the strait predictions in Figure 9a (middle) show salinity values (41 psu) lower than the summer 42 psu (Figure 10a, middle), suggesting that the river buoyancy effect is apparent in this region of the gulf.

[25] The scale of motion in the domain is shown in Figure 13, where the depth-averaged velocity of the spring flood tide at the Strait of Hormuz is depicted. Clearly the scale of the velocity field is considerably larger than the grid resolution of 5000 × 5000 m.

5. Geographic Distribution of Dispersion

5.1. Geographic Distribution of Dispersion Intensity

[26] Horizontal dispersion coefficients K_x were derived following *Taylor* [1954], *Okubo* [1971], and *Lawrence et al.* [1995] using

$$K_x = \frac{1}{4}\frac{\sigma^2}{t} \text{ and } \sigma^2 = \frac{A_{90}}{7.23}.$$

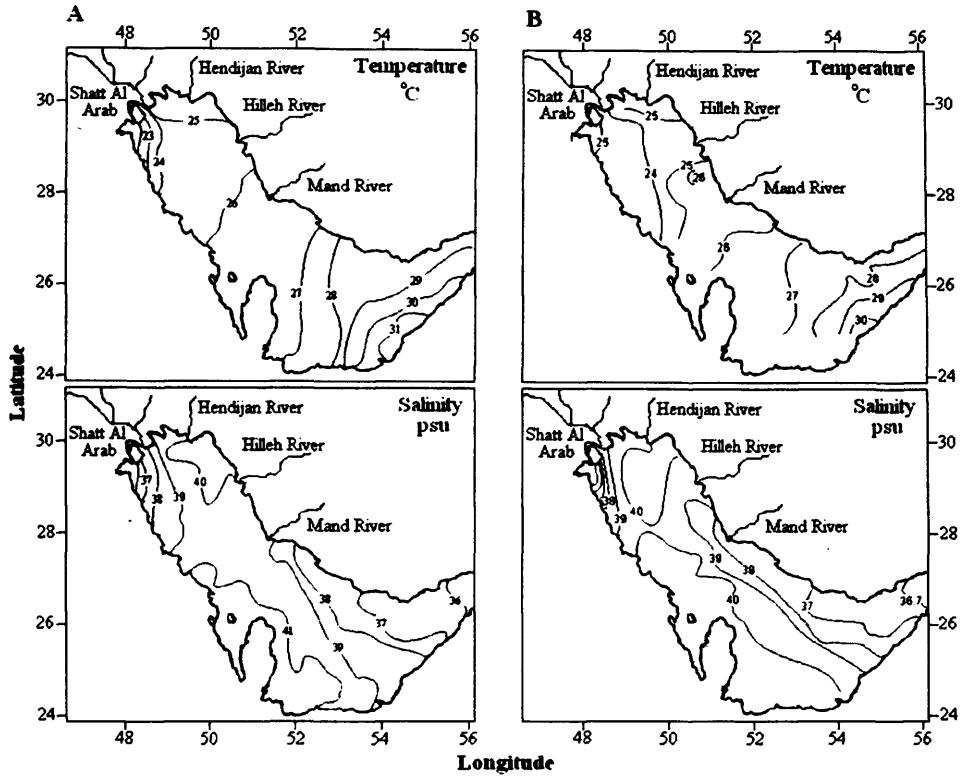

Figure 12. (a) Simulated surface variation of temperature and salinity of the gulf during summer. (b) Field data of temperature and salinity of the gulf during summer.

Here t is time (5, 20, and 40 days) and A_{90} is the horizontal area containing 90% of the tracer mass. The time for vertical mixing t_v can be estimated by arranging the above equation to give

$$t_v = \frac{\sigma_z^2}{4K_z}.$$

It is usual to assume that vertical mixing is complete when the standard deviation equates to $0.8h$ [*Lewis*, 1997], where h is the total depth, and hence the mixing time is given by

$$t_v = \frac{(0.8h)^2}{4K_z} = \frac{0.32h^2}{K_z}.$$

For a well-mixed estuary, a typical value of K_z would be 0.01 m^2/s [*Lewis*, 1997], so that for a water depth of typically 36 m deep, such as the gulf, the above equations imply that t_v = 5.75 h for a complete mix scenario over the depth. *Fischer et al.* [1979] estimated the vertical mixing time scale to be

$$t_v = \frac{h^2}{10K_z}.$$

Using similar values of K_z in the above equation, t_v is estimated to be 3.6 h.

[27] Horizontal dispersion coefficients were determined by observing the horizontal spread of four numerical tracers and utilizing the above equations. The numerical tracers were introduced uniformly over the depth at various locations as shown in Figure 14, namely at stations T6, T7, T8, and T9. It is worth mentioning that the initial size of the patch was 5000 × 5000 m, which equates to the size of a grid cell. The length scale was obtained by calculating A_{90}/7.23 using MATLAB, and the horizontal dispersion coef-

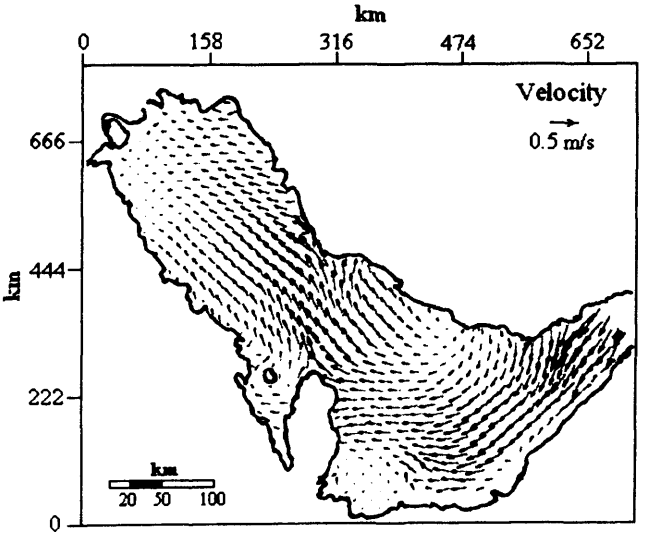

Figure 13. Depth-averaged velocity for spring flood tide during winter 1992 at the Strait of Hormuz.

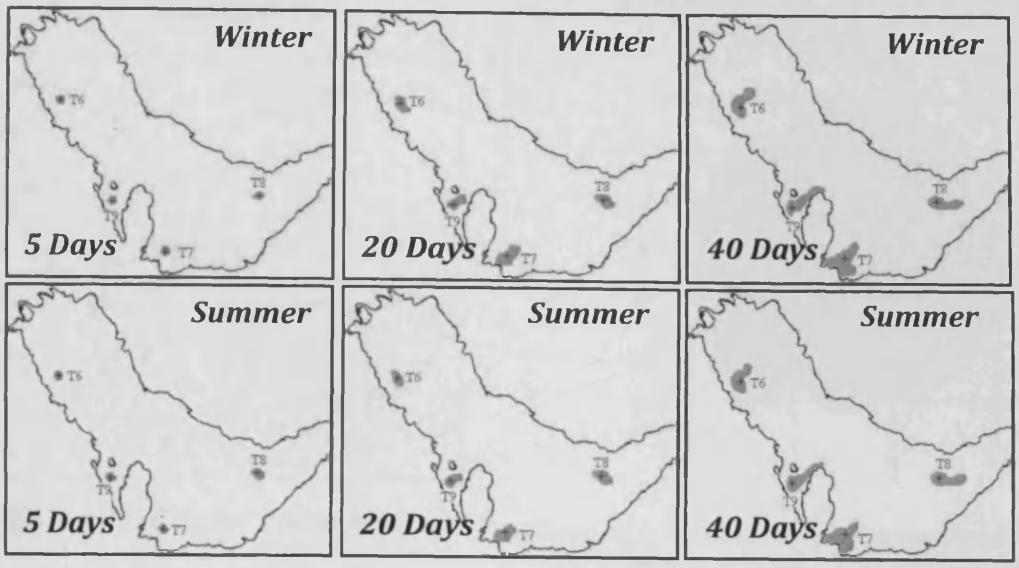

Figure 14. Tracer spread after 5, 20, and 40 days during summer and winter 1992, using meteorological effects from 18 January to 26 February for winter simulations and from 8 May to 12 June for summer simulations. Crosses indicate the release points.

ficient was calculated after 5, 20, and 40 days of continuous tracer release, starting from the validation period as in Table 1.

[28] In general, higher values were apparent near the Arabian coast. The highest dispersion coefficient occurred during winter, with a value of 141 m^2/s at T9, during the early days of tracer release; similar values were achieved during summer. It is clear that even with higher horizontal diffusivities of 5 and 10 m^2/s, the dispersion coefficients remained almost the same as in Table 1. In the model validation section it was obvious that the effect of rivers was significant only locally, and buoyancy related to fresh water inflows would only be substantial in the long run. Hence the effect of rivers may be neglected since all locations of injections were far enough away from the fresh water inputs.

5.2. Residence Time

[29] Flushing time, age, and residence time are the commonly used measures for calculating retention characteristics of water or scalar quantities transported by the flow. *Boynton et al.* [1995] argued that the residence time is a vital element that should be the basis of comparative analyses of ecosystem nutrient budgets. In practice, different approaches may lead to different time scales, even for the same domain [*Monsen et al.*, 2002].

[30] *Dronkers and Zimmerman* [1982] defined the residence time as the time taken for a whole water parcel to leave the lagoon through its outlet to the sea. In this study special attention was given to the residence time of the water in the whole estuary, since flushing time is an integrative system measure, whereas both residence time and age are local measures. In the case of the gulf, the circulation in and out of the Strait of Hormuz has been poorly defined in the past, resulting in estimates of the residence times varying widely from 2 to 5 years [*Hughes and Hunter*, 1979; *Hunter*, 1983]. *Sadrinasab and Kämpf* [2004] studied the flushing time of the gulf and found that 95% flushing times of surface waters ranged from 1 to 3 years along the Iranian coast, while larger values of more than 5 years were obtained along the Arabian coast.

Table 1. Dispersion Coefficients K_x (m^2/s) During Summer and Winter 1992[a]

	5 Days			20 Days			40 Days		
	κ = 1.0	κ = 5.0	κ = 10.0	κ = 1.0	κ = 5.0	κ = 10.0	κ = 1.0	κ = 5.0	κ = 10.0
				Winter					
T6	103	103	104	73	73	73	77	78	78
T7	99	99	100	86	86	86	90	90	90
T8	127	128	128	61	62	62	80	80	80
T9	140	141	141	87	88	88	83	83	83
				Summer					
T6	100	100	100	70	71	71	75	75	76
T7	95	95	95	81	81	82	87	87	88
T8	126	127	127	60	61	61	83	83	83
T9	137	138	138	83	84	84	81	82	82

[a]Using meteorological effects from 18 January to 26 February for winter simulations and 8 May to 12 June for summer simulations, with κ = 1, 5, and 10 m^2/s.

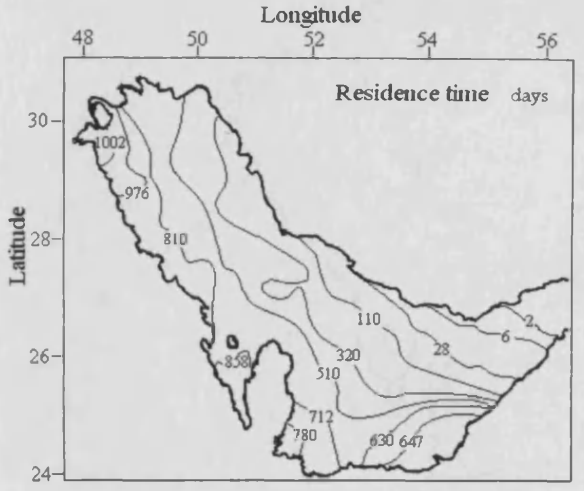

Figure 15. Residence time of the gulf in days.

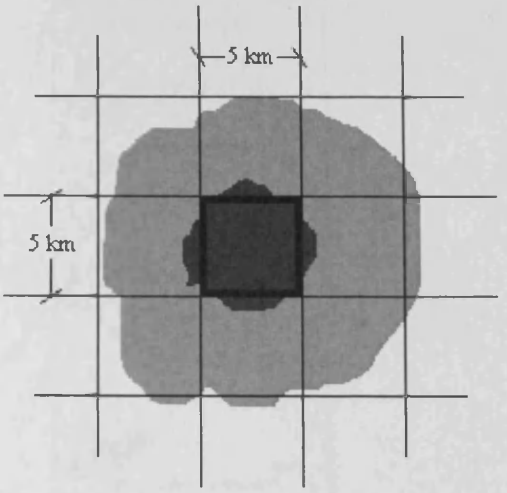

Figure 16. Injection of tracer at a representative cell, with a scale of 5000 × 5000 m, would typically take 30 days to spread 5000 m.

[31] In modeling the residence time of the gulf using ELCOM, forcing model data of 1992 (January-December) were adopted and repeated for successive years. It was assumed that initially each cell contained water with a residence time of zero. The flushing time was defined as the residence time of the water as it left the domain (i.e., the time taken for the water to leave the domain). The model revealed that the residence time in the gulf was almost 3 years, as shown in Figure 15, the residence time being the longest time for water packages to remain along the Arabian coast of the gulf. In particular, near Kuwait Bay, Qatar and the UAE coast values reached 858 days. Obviously the residence time at the Strait of Hormuz was lowest (2 days), due to the open boundary effects in the region.

6. Discussion

[32] To determine the main drivers of the horizontal dispersion of the tracers various forcing scenarios were implemented for the sensitivity analysis. All the simulations were carried out using a selection of the above summer and winter forcing data from 1992, as detailed in Table 2.

[33] These simulations enabled a sensitive analysis to be undertaken for the various forcing mechanisms. As seen from Table 2, tidal forcing accounted for about two thirds of the total tracer dispersion at T6 and T7, almost 90% at T8 and 75% at T9 during summer and winter.

[34] Justification for using a 5000 m grid and the chosen horizontal diffusivity value is necessary before analyzing the results obtained in this study. Previously, observations by *Lawrence et al.* [1995] suggested diffusivity values of O (10^{-1}) m^2/s for length scale of 500 m; also *Stocker and Imberger* [2003] computed turbulent diffusivities of O (10^0) m^2/s in Lake Kinneret. *Okely et al.* [2010] for Victoria Lake revealed that a horizontal diffusivity in ELCOM of less than 1 m^2/s was appropriate. In this study, an initial horizontal diffusivity of 1 m^2/s was utilized in the model, selected on the basis of *Okubo*'s [1974] findings, in which a length scale of 5000 m corresponds to 1 m^2/s. By analogy, 1 m^2/s would take account of horizontal dispersion at scales smaller than the model grid resolution as shown in Figure 16, in which this value is fixed throughout the simulation period. To ensure adequacy of the value chosen, the horizontal diffusivity was altered to 5 m^2/s and then to 10 m^2/s in the model, confirming that this did not significantly influence the horizontal dispersion of the tracers, as shown in Table 1. Therefore, Table 1 shows that as time progress the tracer at each station forms a circular patch during the first days after injection that eventually progresses into an oval shape along the mean flow direction due to turbulent diffusion, as shown in Figures 17a and 17b. However, as the patch size evolves due to further injection the oval shape is distorted and stretched, forming a random shape dependent on the direction of shear force effects and, to a smaller extent, large or small eddies. Shear effects playing the main role in expanding the patch size after 30 days will be explained in the following paragraph. It is worth mentioning that by using the *Okubo* [1974] K versus l graph to calculate K_x from the corresponding length scales of T6, T7, T8, and T9 during 20 days (shown in Table 1), values of 68, 78, 62, and 83 m^2/s were obtained, with these values being similar to the respective computed values cited in Table 1.

Table 2. Diffusion Coefficients (m^2/s) Due to Various Effects After 40 Days of Release

Experiment	Season	Tide	Wind	T6 (K_x)	T7 (K_x)	T8 (K_x)	T9 (K_x)
ELCOM1	Winter	Yes	No	49	60	69	60
ELCOM2	Winter	No	Yes	24	27	10	20
ELCOM3	Summer	Yes	No	53	60	72	60
ELCOM4	Summer	No	Yes	20	25	8	19

[35] Scenarios adopted in this study and shown in Table 2 revealed that the gulf is mainly driven by tidal forces during both seasons and therefore tides are the main drivers in creating the shear forces that play key roles in dispersing the numerical tracers in both summer and winter. Although T8

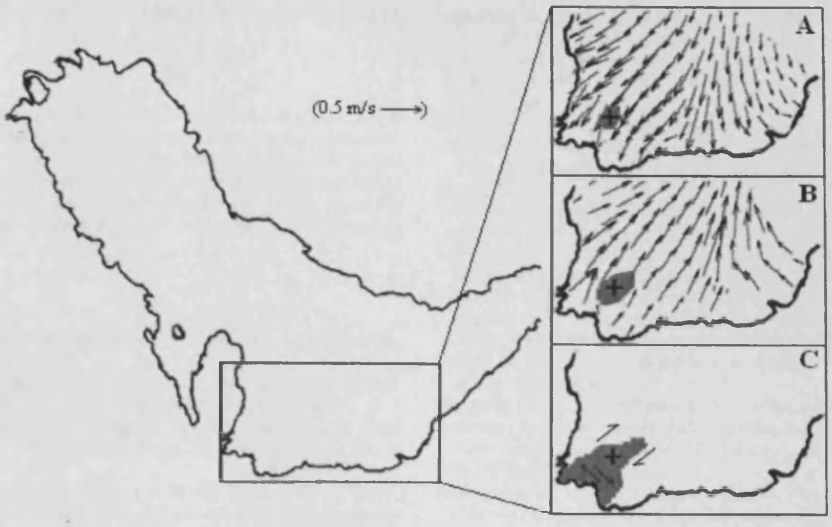

Figure 17. (a) Flood tide effect at T7 (5 days), (b) ebb tide effect at T7 (10 days), and (c) shear force effect in spreading the tracer at T7 (45 days).

was located at a site with a comparatively greater depth, the simulation suggests a dispersion coefficient similar to that at the shallower T6 site due to the uniform currents, since tracers spread out in both directions away from the release point, similar to the spread shown at T7 in Figures 17a and 17b. Furthermore, higher currents and consequently larger shear forces generated by tides are distinguishable and played a key role in dispersing the tracer at T8. Similarly, but to a smaller extent at T6, shear generated by wind speeds of approximately 15 m/s in a direction across the mean flow, combined with large eddies and Coriolis forces, enhanced dispersion by more than 15% along the estuary and deflected the patch in a seaward direction with dispersion coefficients comparable to values obtained at T8. Analogously, conditions at T9 are significantly affected by wind shear, but the topography at this location caused dispersion coefficients to be increased due to bed friction. This elongated the patch toward the north Qatar coastline, and eventually it became vulnerable to large eddies (e.g., Figure 13) as it developed toward the estuary main channel.

[36] At T7 the great contribution of tides in stretching the patch away from the release point toward the coast of the UAE and Qatar is indicated by its increase in size and developing a most random shape, as shown in Figure 17c. This can be explained by the combination of wind, tides, an irregular topography and coastal interaction that enhanced shear forces. Moreover, as the patch evolved, it interacted with the coastline, comprising of smaller bays and headlands that dramatically increased the dispersion coefficients after 40 days, giving rise to "Coastal Trapping" [*Inoue and Wiseman*, 2000] and making mixing efficient and chaotic (Figure 17c). Although the mixing processes appear to be considerable at T7, the residence time in Figure 15 suggests that the patch would prevail for about 750 days.

[37] Horizontal turbulent diffusion played a minor role because dispersion coefficients varied only slightly for different horizontal diffusivities (shown in Table 1). Bottom and internal shear, as observed in the velocity profiles in the top center of the gulf, also contributed to vertical mixing of the water column particularly during summer due to minor stratification developing in the upper layer (Figure 10). Shear components of horizontal velocity along the Arabian coastline were greater both near the surface and near the bed, due to wind drift and bottom friction, respectively.

[38] The dispersion mechanisms affecting the gulf have a fundamental influence on the estuary ecology. Furthermore, spatial variability in the horizontal mixing and dispersion coefficients has several implications for water quality within the gulf. Due to the nature of the gulf, high nutrient values normally result in high rates of oxygen consumption, particularly in the relatively shallow Arabian shoreline [*Brewer and Dyrssen*, 1985], so dispersion processes arising from wind along this region would significantly influence the nutrient levels along the coast. *Brewer and Dyrssen* [1985] found high surface phosphorus levels that may be attributed to the vertical dispersion mechanism in such regions. Moreover, nutrient concentrations in the gulf have often been concentrated in the north of the gulf, in Kuwait Bay and in the region around the outfall of Shatt Al Arab, and they have been cited as the cause of a number of eutrophication incidents, mostly during summer. For example, a major red tide and an associated fish kill occurred in 1999 [*Heil et al.*, 2001].

[39] An estimate of the fluid residence time, i.e., the average time a water particle spends within a region [*Geyer and Signel*, 1992], is given as

$$t_R = \frac{l^2}{K_x},$$

where $t_R \approx 200$ days for an average dispersion coefficient of 90 m^2/s and $l = 40$ km, an estimated length scale for the assemblage localities. This relatively long time scale allows the ecological niches to exist and promotes spatial hetero-

geneity of biochemical material, in particular in the northern part of the gulf.

[40] **Acknowledgments.** The first author would like to thank CWR for financial support in enabling him to stay at the centre for 2 months. The authors would also like to acknowledge the Kuwait Institute of Scientific Research and Dubai Meteorological Office for providing meteorological data essential for this study. The manuscript benefited greatly from the editing of Allan Barton. This article represents Centre for Water Research reference ED 2318 YA.

References

Aref, H. (1984), Stirring by chaotic advection, *J. Fluid Mech., 143*, 1–21, doi:10.1017/S0022112084001233.

Bowden, K. F. (1965), Horizontal mixing in the sea due to a shearing current, *J. Fluid Mech., 21*, 83–95, doi:10.1017/S0022112065000058.

Boyland, P. L., H. Aref, and M. A. Stremler (2000), Topological fluid mechanics of stirring, *J. Fluid Mech., 403*, 277–304, doi:10.1017/S0022112099007107.

Boynton, W. R., J. H. Garber, R. Summers, and W. M. Kemp (1995), Input, transformations, ad transport of nitrogen and phosphorus in Chesapeake Bay and selected tributaries, *Estuaries, 18*, 285–314, doi:10.2307/1352640.

Brewer, P. G., and D. Dyrssen (1985), Chemical oceanography of the Persian Gulf, *Prog. Oceanogr., 14*, 41–55, doi:10.1016/0079-6611(85)90004-7.

Cartwright, D. E., and R. J. Tayler (1971), New computations of the tide-generating potential, *Geophys. J. R. Astron. Soc., 23*, 45–73, doi:10.1111/j.1365-246X.1971.tb01803.x.

Casulli, V., and E. Cattani (1994), Stability, accuracy and efficiency of a semi-implicit method for three-dimensional shallow water flow, *Comput. Math. Appl., 27*, 99–112, doi:10.1016/0898-1221(94)90059-0.

Casulli, V., and R. T. Cheng (1992), Semi-implicit finite difference methods for three dimensional shallow water flow, *Int. J. Numer. Methods Fluids, 15*, 629–648, doi:10.1002/fld.1650150602.

Dooley, H. D., and J. H. Steele (1969), Wind driven currents near coast, *Ocean Dyn., 22*, 213–223, doi:10.1007/BF02225162.

Dronkers, J., and J. T. F. Zimmerman (1982), Some principles of mixing in tidal lagoons, *Oceanol. Acta, 4*, suppl., 107–117.

Elshorbagy, W., M. H. Azam, and K. Taguchi (2006), Hydrodynamic characterization and modelling of the Arabian Gulf, *J. Waterw. Harbors Coastal Eng. Div. Am. Soc. Civ. Eng., 132*, 47–56.

Fischer, H. B., E. J. List, R. C. Y. Koh, J. Imberger, and N. H. Brooks (1979), *Mixing in Inland and Coastal Waters*, Academic, San Diego, Calif.

Geyer, W. R., and R. P. Signel (1992), A reassessment of the role of tidal dispersion in estuaries and bays, *Estuaries, 15*, 97–108, doi:10.2307/1352684.

Heil, C. A., P. M. Glibert, M. A. Al-Sarawi, M. Faraj, M. Behbehani, and M. Husain (2001), First record of a fish-killing *Gymnodinium* sp. bloom in Kuwait Bay, Arabian Sea: Chronology and potential causes, *Mar. Ecol. Prog. Ser., 214*, 15–23, doi:10.3354/meps214015.

Hodges, B. R., J. Imberger, A. Saggio, and K. B. Winters (2000), Modeling basin scale internal waves in a stratified lake, *Limnol. Oceanogr., 45*, 1603–1620, doi:10.4319/lo.2000.45.7.1603.

Hughes, P., and J. R. Hunter (1979), A proposal for a physical oceanography program and numerical modeling of the KAP region, *UNESCO Rep. Mar. Sci. 27*, Paris.

Hunter, J. R. (1983), A review of the residual circulation and mixing processes in the KAP region, with reference to applicable modeling techniques, Oceanographic modeling of Kuwait Action Plan (KAP), *UNESCO Rep. Mar. Sci. 28*, Paris.

Imberger, J., E. A. D. Mamouni, J. Anderson, M. L. Ng, S. Nicol, and A. Veale (2007), The index of sustainable functionality: A new adaptive, multicriteria measurement of sustainability—Application to Western Australia, *Int. J. Environ. Sustainable Dev., 6*, 323–355, doi:10.1504/IJESD.2007.015309.

Inoue, M., and W. J. Wiseman (2000), Transport, stirring and mixing processes in a Louisiana estuary: A model study, *Estuarine Coastal Shelf Sci., 50*, 449–466, doi:10.1006/ecss.2000.0587.

Laval, B. J., J. Imberger, B. R. Hodges, and R. Stocker (2003), Modeling circulation in lakes: Spatial and temporal variations, *Limnol. Oceanogr., 48*, 983–994, doi:10.4319/lo.2003.48.3.0983.

Lawrence, G. A., K. I. Ashley, N. Yonemitsu and J. R. Ellis (1995), Natural dispersion in a small lake, *Limnol. Oceanogr., 40*, 1519–1526.

Leonard, B. P. (1991), The ULTIMATE conservative difference scheme applied to unsteady one-dimensional advection, *Comput. Method. Appl. Mech. Eng., 88*, 17–74, doi:10.1016/0045-7825(91)90232-U.

Lewis, R. E. (1997), *Dispersion in Estuaries and Coastal Waters*, John Wiley, Chichester, U. K.

Monsen, N. E., J. E. Cloern, L. V. Lucas, and S. G. Monismith (2002), A comment on the use of flushing time, residence time, and age as transport time scales, *Limnol. Oceanogr., 47*, 1545–1553, doi:10.4319/lo.2002.47.5.1545.

Newhouse, S., and T. Pignataro (1993), On the estimation of topological entropy, *J. Stat. Phys., 72*, 1331–1351, doi:10.1007/BF01048189.

Okely, P., J. Imberger, and K. Shimizu (2010), Particle dispersal due to interplay of motions in the surface layer of a small reservoir, *Limnol. Oceanogr., 55*, 589–603, doi:10.4319/lo.2009.55.2.0589.

Okubo, A. (1971), Oceanic diffusion diagrams, *Deep Sea Res., 18*, 779–802.

Okubo, A. (1974), Some speculations on oceanic diffusion diagrams, *Rapp. P.-V. Reun. Cons. Int. Explor. Mer, 167*, 77–85.

Reynolds, R. M. (1992a), Report of activities-Leg I of the *Mt. Mitchell* Expedition, *Rep. HMRAD 92–9*, NOAA, Seattle, Wash.

Reynolds, R. M. (1992b), Report of activities-Leg VI, A/B of the *Mt. Mitchell* Expedition, *Rep. HMRAD 92–10*, NOAA, Seattle, Wash.

Reynolds, R. M. (1993), Physical oceanography of the gulf, Strait of Hormuz, and the Gulf of Oman—Results from *Mt. Mitchell* expedition, *Mar. Pollut. Bull., 27*, 35–59, doi:10.1016/0025-326X(93)90007-7.

Richardson, L. F. (1926), Atmospheric diffusion shown on a distance-neighbour graph, *Proc. R. Soc. London A, 110*, 709–737, doi:10.1098/rspa.1926.0043.

Richlen, M. L., et al. (2010), The catastrophic 2008–2009 red tide in the Arabian Gulf region, with observations on the identification and phylogeny of the fish-killing dinoflagellate *Cochlodinium polykrikoides*, *Harmful Algae, 9*, 163–172, doi:10.1016/j.hal.2009.08.013.

Sadrinasab, M., and J. Kämpf (2004), Three-dimensional flushing times of the Persian Gulf, *Geophys. Res. Lett., 31*, L24301, doi:10.1029/2004GL020425.

Spigel, R. H., J. Imberger, and K. N. Rayner (1986), Modeling the diurnal mixed layer, *Limnol. Oceanogr., 31*, 533–556, doi:10.4319/lo.1986.31.3.0533.

Stocker, R., and J. Imberger (2003), Horizontal transport and dispersion in the surface layer of a medium-sized lake, *Limnol. Oceanogr., 48*, 971–982, doi:10.4319/lo.2003.48.3.0971.

Sultan, S. A. R., F. Ahmad, N. M. El-Ghribi, and A. M. Al-Subhi (1995), An analysis of the Arabian Gulf monthly mean sea level, *Cont. Shelf Res., 15*, 1471–1482, doi:10.1016/0278-4343(94)00081-W.

Taylor, G. I. (1954), The dispersion of matter in turbulent flow through a pipe, *Proc. R. Soc. London A, 223*, 446–468.

Y. Alosairi and R. A. Falconer, Cardiff School of Engineering, Cardiff University, Queen's Building, The Parade, Cardiff CF24 3AA, UK. (alosairiy@cf.ac.uk)

J. Imberger, Centre for Water Research, University of Western Australia, M023, 35 Stirling Hwy., Crawley, WA 6009, Australia.